IntechOpen

New Perspectives on Electric Vehicles

Edited by Marian Găiceanu

New Perspectives on Electric Vehicles

Edited by Marian Găiceanu

IntechOpen

Supporting open minds since 2005

We are IntechOpen,
the world's leading publisher of Open Access books
Built by scientists, for scientists

5,700+
Open access books available

140,000+
International authors and editors

175M+
Downloads

156
Countries delivered to

Our authors are among the
Top 1%
most cited scientists

12.2%
Contributors from top 500 universities

Interested in publishing with us?
Contact book.department@intechopen.com

Numbers displayed above are based on latest data collected.
For more information visit www.intechopen.com

Meet the editor

Prof. Dr. Marian Gaiceanu graduated from the Naval and Electrical Engineering Faculty, Dunarea de Jos University of Galati, Romania, in 1997. He received a Ph.D. (Magna Cum Laude) in Electrical Engineering in 2002. Since 2017, Dr. Gaiceanu has been a Ph.D. supervisor for students in Electrical Engineering. He has been employed at Dunarea de Jos University of Galati since 1996, where he is currently a professor. Dr. Gaiceanu is a member of the National Council for Attesting Titles, Diplomas and Certificates, an expert of the Executive Agency for Higher Education, Research Funding, and a member of the Senate of the Dunarea de Jos University of Galati. He has been the head of the Integrated Energy Conversion Systems and Advanced Control of Complex Processes Research Center, Romania, since 2016. He has conducted several projects in power converter systems for electrical drives, power quality, PEM and SOFC fuel cell power converters for utilities, electric vehicles, and marine applications with the Department of Regulation and Control, SIEI S.pA. (2002–2004) and the Polytechnic University of Turin, Italy (2002–2004, 2006–2007). He is a member of the *Institute of Electrical and Electronics Engineers* (IEEE) and cofounder-member of the IEEE Power Electronics Romanian Chapter. He is a guest editor at *Energies* and an academic book editor for IntechOpen. He is also a member of the editorial boards of the *Journal of Electrical Engineering, Electronics, Control and Computer Science* and *Sustainability*. Dr. Gaiceanu has been General Chairman of the IEEE International Symposium on Electrical and Electronics Engineering in the last six editions.

Contents

Preface

Due to greenhouse gas (GHG) emissions, climate change and air pollution, the world's political instruments, as well as the spread of means of transport, the replacement of polluting means of transport (diesel or gasoline engines) with non-polluting ones (electric vehicles, plug-in hybrid electric vehicles) has become a global urgency. This book aims to find possible answers related to the new-coming era of transport. The authors share their research experience regarding the main barriers to electric vehicle implementation, their thoughts on electric vehicle modelling and control, and network communication challenges. The book is structured in four sections.

The introductory chapter discusses specific EU initiatives and regulations to attain climate neutrality by 2050. It highlights the main barriers to purchasing electric vehicles and future electric vehicle development. It examines existing charging modes as well as a revolutionary technology that allows for charging an electric vehicle battery in five minutes. Hydrogen vehicles are mentioned, but the importance of lithium-ion batteries is also marked, the discovery of which was rewarded in 2019 with the Nobel Prize in Chemistry, making possible a society without fossil fuels.

Chapter 2, "Strategies for Electric Vehicle Infrastructure of Cities: Benefits and Challenges" presents the future priorities of urban life: the balancing of demand in the electricity distribution network, charging schedules, dynamic prices, and the different types of charging stations. This cannot be done without a strategic city plan that includes transportation infrastructure. The chapter outlines the fundamental components of a strategic plan for both electric vehicles and the infrastructure needed for a smart city, such as a requirement's analysis, business planning, and education of electric vehicle owners, all of which facilitate a smooth transition from gasoline vehicles to electric vehicles. To maximize the total benefits and easily overcome challenges, experiences must be shared.

Chapter 3, "Fast-Charging Infrastructure Planning Model for Urban Electric Vehicles" presents a solution for implementing the strategic plan mentioned in the previous chapter. The optimal location of the charging station plays an important role during the transition to electric vehicles. This chapter develops a model for planning the fast-charging infrastructure of electric vehicles, at the urban level, considering both the vehicle's own influencing factors, such as battery degradation and vehicle heterogeneity in the driving range, but also external conditions like traffic congestion and vehicle traffic flow conditions, user loading costs, daily journeys, and loading behavior against the constraints of the distribution network, to determine the optimal locations for the network of fast-charging stations.

Chapter 4, "A Review of Hybrid Electric Architectures in Construction, Handling and Agriculture Machines" provides architectural solutions for high-power propulsion. It discusses how, for heavy loads, the limitations of the current state of the art of batteries leads to the choice of a hybrid solution for vehicles. It shows how the

requirements of each specific field strongly affect the design of an optimal hybrid electrical architecture. Moreover, the integration of electric vehicles in the automotive field has both advantages and weaknesses of the current level of technology. Battery charging time is the main obstacle in implementing the high-power electric solution. Another reason is the additional cost generated by the cumulative delays, which is not acceptable for companies that will use these new vehicles. Thus, for heavy vehicles, the best solution is to pursue a hybrid solution with a low-power diesel engine supported by an energy storage system-based electrical system. For low-power machines and other special cases (depending on the specific duty cycle), fully electric solutions are perfectly possible.

Chapter 5, "High Power Very Low Voltage Electric Motor for Electric Vehicle" presents a variety of very low-voltage motor solutions with a required power of up to 100 kW. Although, from an energy point of view, it is recommended to use a high voltage level for electric car-based electric propulsion, for low power propulsions (battery voltage up to 700 V, less than 30 kW per motor), sizing the system at very low voltage (less than 60V) may be more beneficial. This approach allows many constraining safety requirements to be overcome and the use of available components (motor controllers, connectors, etc.) that are more readily available on the market for this voltage range. There are also many regulatory provisions that may require you to stay within this voltage limit.

The communications infrastructure of an intelligent transport system has a special role in ensuring stability and controllability. The important role of the communication system is described in Chapter 6, "Improving Communication System for Vehicle-to-Everything Networks by Using 5G Technology". For high-speed transport systems (air or rail) the solution of ubiquitous coverage is given by wireless communication systems (5G infrastructure).

Chapter 7, "Advanced Driving Assistance System for an Electric Vehicle Based on Deep Learning", deals with the design of a new method of speed control using artificial intelligence techniques applied to an autonomous electric vehicle. The deep learning, image processing, and nonlinear autoregressive moving average level-2 model (NARMA-L2) controllers have been successfully developed and simulated using MATLAB to control the speed of a brushless direct current motor by recognizing traffic sign images.

The authors of chapter 8, "Revisiting Olivine Phosphate and Blend Cathodes in Lithium Ion Batteries for Electric Vehicles", propose one solution to improve the safety feature of lithium-Ion batteries for electric vehicles, based on olivine phosphate, which has an excellent safety performance, being favorable for the realization of new cathodic materials. In addition, the authors present a solution to improve energy density and power.

Chapter 9, "Design, Simulation and Analysis of the Propulsion and Control System for an Electric Vehicle", presents the multi-converter/multi-machine (MCMMS) electric propulsion system. The speed and torque of two reluctance synchronous motors (SynRM) that drive the two rear wheels of the reluctance synchronous motors-based electric vehicle are controlled by using three different PID controller strategies. The PSO algorithm was used as an optimization technique to find the optimal PID parameter to improve the performance of the electric drive system.

The linear speed of the vehicle is controlled by an electronic differential controller that provides the reference speed for each drive wheel, which depends on the driver's reference speed and the steering angle.

The last chapter, "Powerful Multilevel Simulation Tool for HiL Analysis of Urban Electric Vehicle's Propulsion Systems", presents the main assemblies of the traction system of an urban electric vehicle, its modelling being based on Macroscopic Energy Representation (EMR). The use of EMR facilitates the transition to hardware-in-the-loop (HiL) implementation, replacing the simulated ensemble with the real one by using the communication between two professional software tools through National Instruments VeriStand software for real-time test applications. In this way, the analysis of advanced operation simulations of the propulsion unit of urban electric vehicles can be performed in real-time.

The book is a useful resource for students, researchers, and professionals in electrical engineering.

I wish to thank all the contributing authors as well as the staff at IntechOpen, particularly Author Service Manager Ms. Marina Dusevic, for all their support.

Prof.dr.habil. Marian Găiceanu
Department of Automatic Control and Electrical Engineering,
"Dunărea de Jos" University of Galati,
Galati, Romania

Section 1

Electric Vehicles Infrastructures

Introductory Chapter: Towards 2050 NZE Pathway - Electric Transportation

Marian Gaiceanu

1. Introduction

If there are some dilemmas which type of green vehicle to choose, the consumers should take into account some aspects: autonomy, infrastructure availability, time to battery charge, cost, safety, efficiency, electric vehicle development in the medium and long-term. There are pros and contra for both types of source vehicles: fuel cells, lithium-ion battery or both. With the use of fuel cells combined with the cogeneration technology, all the necessary sources for electric vehicle operation are available: electric, and thermal (for any season) [1–3]. The maximum energy efficiency of the fuel cell-based vehicle is lower than that of the battery-powered electric vehicle [4]. Recently (2019), the award of the remarkable Nobel Prize for the greenway opened by the use of Li-Ion battery comes as a reward for the effects of its use in global applications, an important step being its application as a primary source for electric transport.

2. Path to achieve zero net CO_2 emissions by 2050

In order to ensure the path to Net Zero Emissions (NZE) by 2050, as European Union stated, the use of renewable energy sources and energy efficiency should be increased, as well as the air quality improving by reducing greenhouse gas emissions should be performed [5]. There are four factors that contribute to the NZE: consumer affection adaptation, governmental policies, the strategy of the traditional original equipment manufacturers (OEMs), corporate companies [6].

The energy consumptions prediction is based on four scenarios, developed by the World Energy Outlook 2021 (WEO-2021) based on the World Energy Model (WE): Net Zero Emissions by 2050 Scenario (NZE, stated as a normative in order to obtain the specific outcomes), the Announced Policies Scenario (APS, stated as exploratory, deliver the market dynamics or other relevant outputs based on the defined set of starting conditions inputs applied to the WEM), the Stated Policies Scenario (STEPS, stated as exploratory), and the Sustainable Development Scenario (SDS, stated as normative to fulfill the Paris Agreement).

In order to highlight the paths to achieve zero net CO_2 emissions by 2050, in the global and industrial energy sector by specific actors, there is the Net Zero Emissions by 2050 Scenario. In order to achieve the long-term goals agreed in Paris in 2015 to limit global warming to 1.5°C, the Announced Policies Scenario highlights

the difference between the target and the current state of energy and climate policies to achieve the above-mentioned goal through all the climate commitments made by governments around the world, but also through their own national contributions. This scenario ensures that all assumed zero net targets are met on time (Announced Policies Scenario).

The Stated Policies Scenario provides a baseline picture of the achievements and developments of energy and climate policies undertaken by governments around the world through their evaluation.

The Sustainable Development Scenario is used to achieve the goals set out in the Paris Agreement on Climate Change and to take effective measures to significantly reduce air pollution by 2030, by ensuring universal access to modern energy services (**Figure 1**) [7].

The rise of the sales appears on one hand due to the subsidies inclusion in the pandemic resilient plans in certain European countries), on the other hand, due to the European Union's policy to ban the sale of polluting vehicles (petrol, gas, or diesel) in 2030. Only in one year (2019–2020), in the Covid-19 pandemic evolution, the EV and PHEV sales have been tripled in EU-27, Iceland, Norway, and the United Kingdom increasing from 3.5% in 2019 to 11.41% in 2020.

The main barriers to purchasing electric vehicles are hierarchal ordered: price, autonomy, charging time [8].

The increase in sales in 2021 is due on the one hand to the introduction of subsidies in certain European countries (following the pandemic recovery plan), on the other hand, due to the European Union's policy to ban the sale of polluting vehicles (petrol, gas or diesel) in 2030. The main barriers to purchasing electric vehicles are price, autonomy, charging time. Electric vehicles are at risk of being powered by a single power supply.

The EU has seen 2020 the largest increase in sales of electric vehicles in 2020. The best-selling electric cars (including batteries and plug-in hybrid) were registered in Germany, the Nordic countries, and the Netherlands (**Figure 2**) [9].

According to Regulation (EU) 2019/631, the CO_2 emissions from the new passenger cars should be registered with specific details.

In terms of carbon emissions, the new Environment, Climate, Safety and Security Standard, called the Worldwide Harmonized Light Vehicle Test Procedure (WLTP), came into force in 2021. This standard replaces the New European Driving
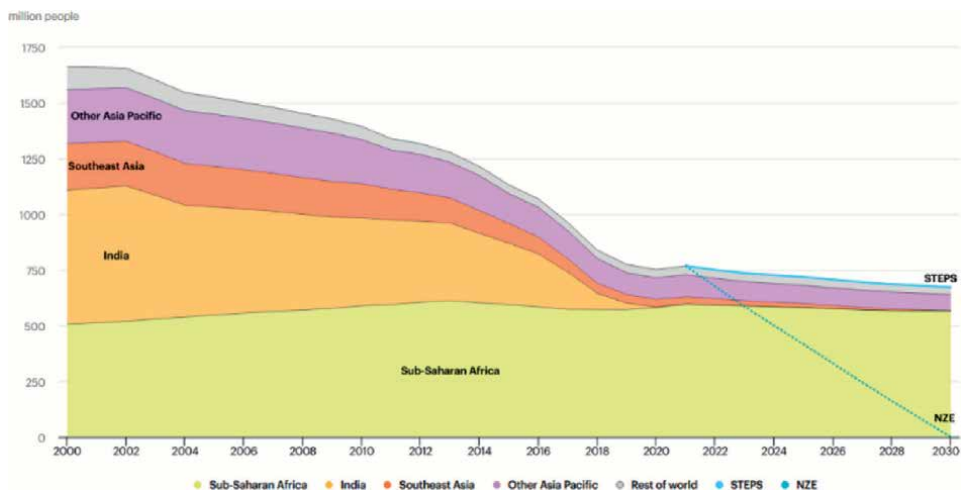
Figure 1.
The development progress scenario of the population accessing to the electricity [7].
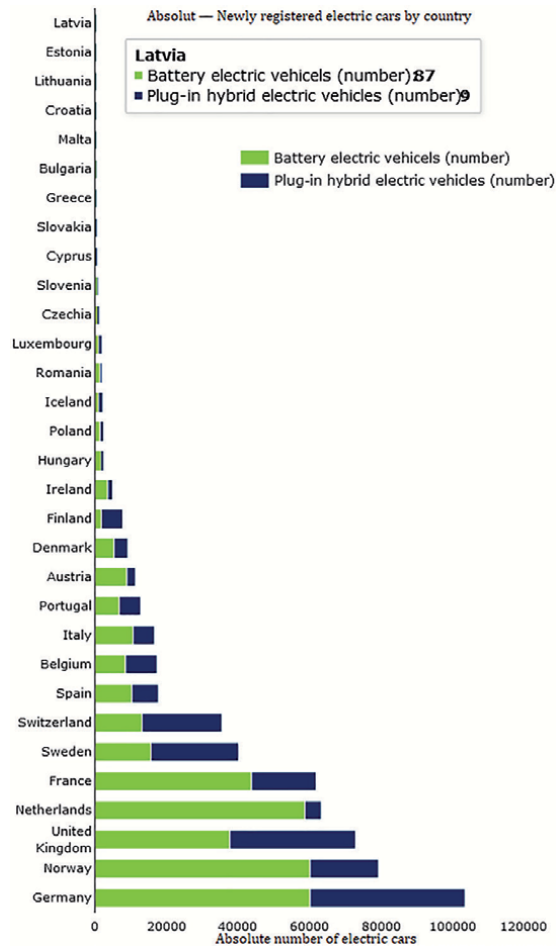
Figure 2.
The electric vehicle market in EU by countries: absolute newly registered electric cars [9].

Cycle (NEDC) standard, being closer to the real driving conditions. In this way, each EU country has to register each vehicle on the basis of a data set that characterizes the vehicle (name of the manufacturer, specific emissions of CO_2, mass, type of fuel, engine capacity, and engine power) (**Figures 3** and **4**).

Figure 5 includes the historical greenhouse gas emissions (GHGE) in the domestic transport sector of the European Union Member States, the future path of GHGE by taking the stipulated measures of the European Parliament, and the future path without additional measures. Taking into account the reference year of 1990, in 2030 it is expected a reduction of GHGE by 6% with existing additional measures. Without any additional measures case, the GHGE would be increased, the maximum registering in 2025, before changing the gradient sign; thereafter, in 2030 the GHGE would be 10% above the 1990 level. Due to the Covid-19 pandemic, the GHGE decreases by 12.7% at the 2020 level.

The most GHGE production after road transport (72%) are aviation (13.1%-international and domestic) and navigation (13%) at the 2014 level [11], as is shown in **Figure 6a**.

GHGE distribution in the transport sector by mode in 2014 [11] is reflected in **Figure 6a**. At the 2019 level (**Figure 6b**), the EU greenhouse emissions in the road transport sector by mode decrease to 71.1%, in aviation increases to13.4%, and in total navigation slowly increase to 14.1%, according to [12].
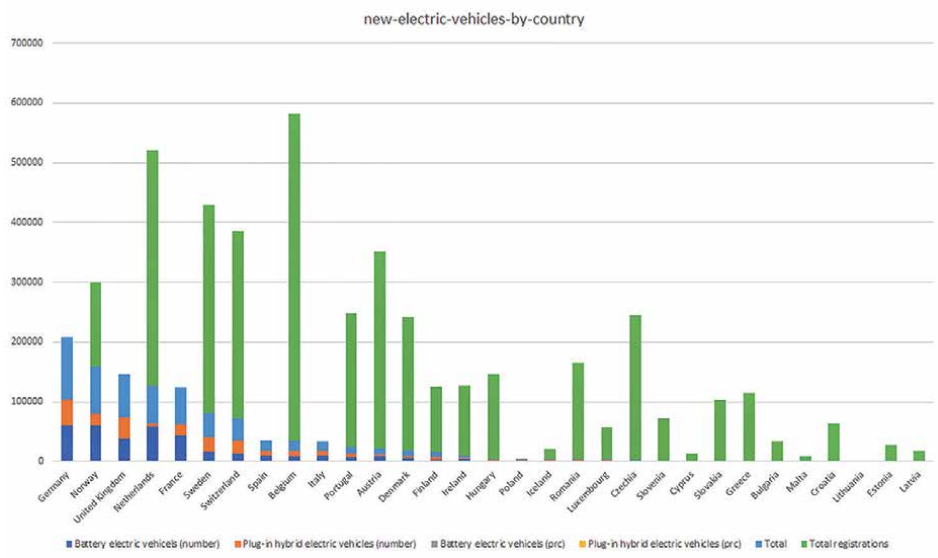
Figure 3.
The number of light vehicles registration by country [9].
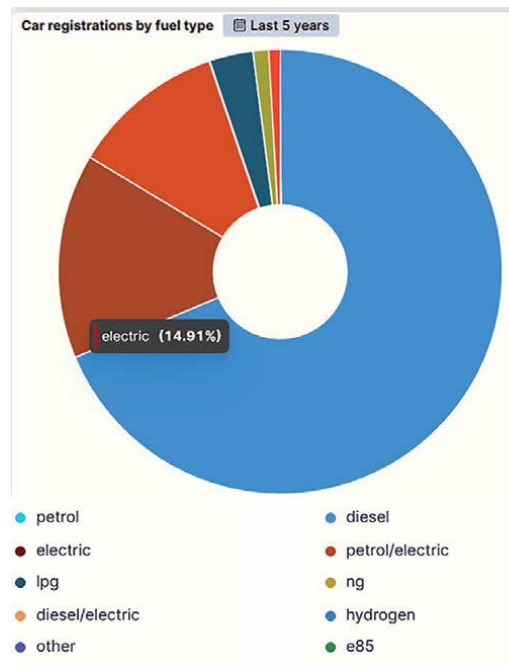
Figure 4.
The weight of each type of vehicle depending on the used fuel type [9].

At the worldwide level, **Figure 7** shows the subsector GHGE distribution from the transport domain in 2020 (**Figure 8**) [13].

In addition to domestic transport, the international aviation and shipping sectors contribute to the total GHG, which is up from the 1990 reference level.
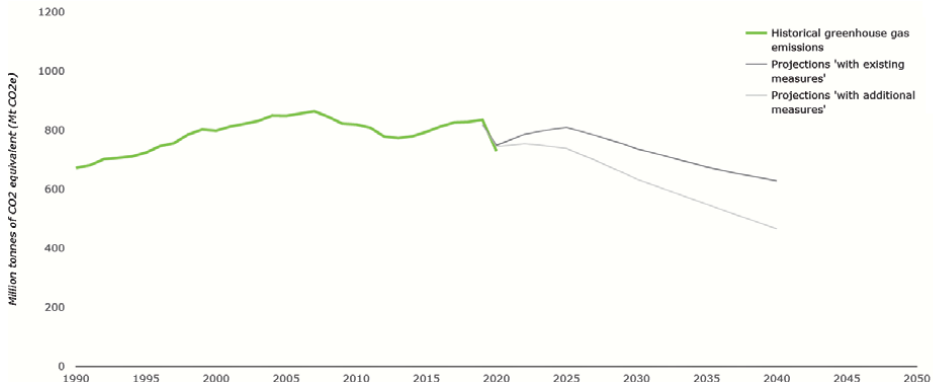
Figure 5.
The historical, present, and the predicted greenhouse gas emissions from the transport sector in European Union [10].
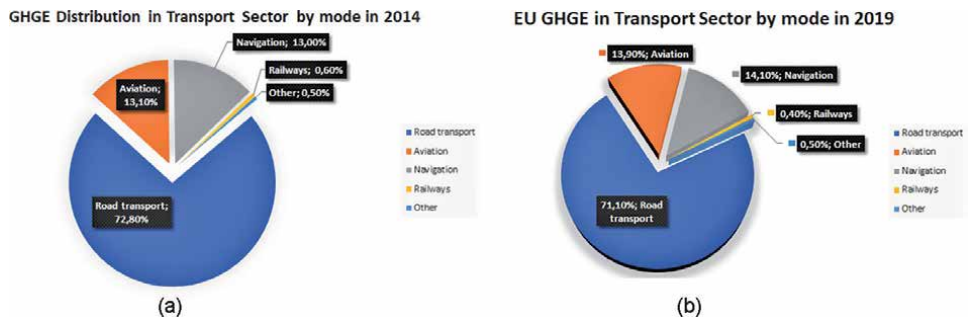
Figure 6.
EU GHGE distribution in transport sector by mode in 2014 (a) [11] and 2029 (b) [12].
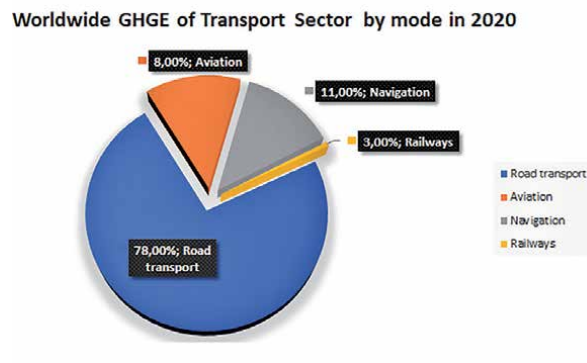
Figure 7.
Worldwide GHGE distribution in transport sector by mode in 2020 [13].

The largest share of CO_2 emissions comes from transport belongs to the road (72% in 2019). Therefore, most of the measures to reduce emissions are dedicated to road transport. The effect will be to reduce this share in 2030 but to increase other modes of transport (e.g. aviation).
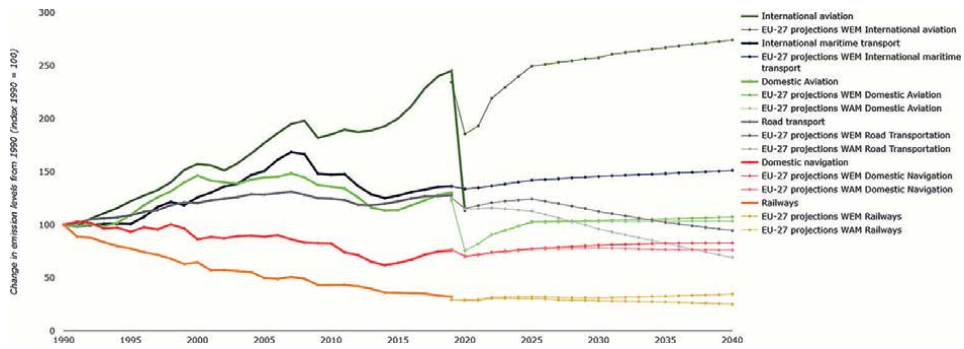
Figure 8.
The greenhouse emissions by category: past, present, future [14].

The Covid-19 pandemic has led to a sharp drop in emissions, especially in the aviation sector, following an increase in the coming years.

3. EU green transition

The EU's strategy for reducing emissions is based on 3 main pillars: increasing transport efficiency, accelerating the development of low-emission energy alternatives in the field of transport, moving to zero-emission vehicles.

The European Commission implements the green objectives (to reduce CO_2 or noxe emissions, at the same time with the use of fossil fuels going through net-zero emissions by 2050) rely on the National Recovery and Resilience Plans to counteract the economic effects of the Covid pandemic, that must be implemented by every European country. EU has imposed one ambitious target to decrease by 55% the CO_2 emission up to 2030. This is an intermediate step to achieve zero greenhouse gas emissions by 2050. To achieve its goal, the European Union combine the European Environment Agreement, with the European Climate Law. In July 2021, the European Commission proposed CO_2 emissions reduction of new cars to zero from 2035. The process of implementing the infrastructure needed for electric vehicles will lead the EU to one of the most advanced continents for the delivery of electric vehicles in the coming years. In this respect, the new goal of the International Energy Agency is to deliver the first energy sector roadmap [15].

One of the EU instruments is "Fit for 55" plan. At the same time, a number of proposals can be found in "Fit for 55".

Fit for 55 Plan has the main objective the emission reduction by 55% up to 2030 [16]. The major objective of the EU is to attain climate neutrality up to 2050, as it is stipulated in the European Green Deal, through the European Climate Law as the use instrument. The legislative revision related to this plan arise "Fit for 55 package" [17].

According to **Figure 9**, 31 countries have electrification targets or Internal Combustion Engine bans for cars. The European Union, along with 8 countries have announced zero net emissions commitments.

The main category of vehicles that are supposed to be developed is the light-duty vehicle (LDV). The spread of the light-duty vehicle (LDV) will be twill be the most used road vehicle. Even the trucks category type of road vehicles is reduced (5% of the total), the pollution with CO_2 reaches 30% of total emissions. Therefore, the EU takes into account the trucks category as the second road vehicle to downward the emission to zero net in 2050.
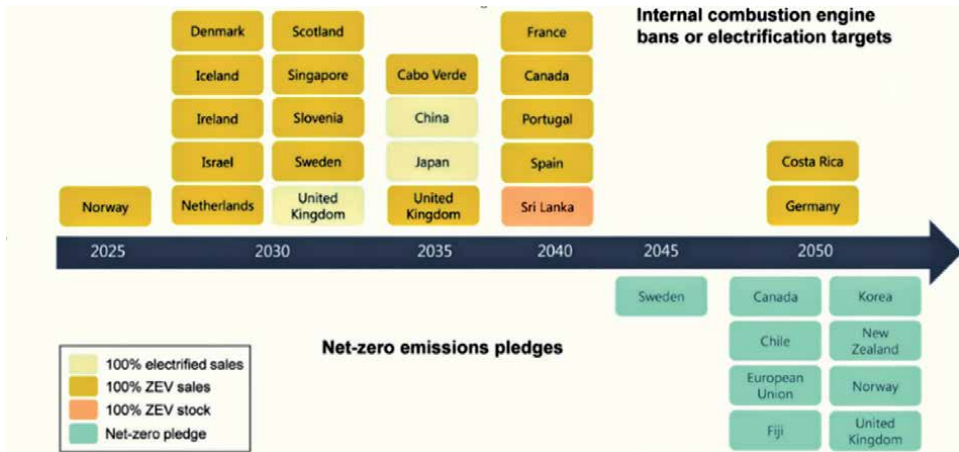
Figure 9.
Timeline for bans of ICE for EU and different countries [18].

The gradual transition to electric vehicles (BEV and PHEV) by 2030 is based on four factors: consumer affection adaptation, governmental policies, the strategy of the traditional original equipment manufacturers (OEMs), and corporate companies' participation [18].

The fundamental path to achieve net-zero emissions by 2050 is to impose further EV mobility.

It could be noted that the passenger light-duty vehicles (PLDVs) are the most spreader in the transport sector and will increased the penetration of them due to the European measures in both Stated Policies Scenario, and Sustainable Development Scenario [19, 20].

4. Electric transport mode: enabling technologies

There are some barriers to accelerate sales in EV transport. According to the opinion poll, the future EV buyers' concerns are related to autonomy, fuel cost, charging time, charging infrastructure, safety regarding battery technology [21, 22].

The experts estimate that EVs will be cheaper than those on fuel by 2027, cheaper car manufacturers—such as Dacia—have also entered this market, and charging infrastructures could be accelerated through governmental programs and European governments [23, 24].

Data intelligence still must be part of the infrastructure around the EV [24].

The electric vehicle available infrastructure is an important milestone in the EV integration process. At the same time, the standards in the field along with the infrastructure availability take part from the sustainability of the global emissions reduction challenges.

The battery recharging time is a key point in infrastructure implementation.

Challenges to large spread the EV adoption are charger compatibility, charging infrastructure availability, renewable energy, and climate mitigation, network capacity, vehicle costs, charging behavior, sales outlook, charging station financing, and ownership, prices [25].

Many challenges come from reducing the charging time for battery-powered EVs. These include the amount of available power at the charging station, the cable

carrying the power from the charging station to the vehicle, and the charging subsystem within the vehicle itself [25].

From the perspective of charging time, there are currently three standardized charging levels: voltage level 1–120 [V] AC with slow charging time (up to 20 h), voltage level 2 of 240 [V] AC with time 8-h charging (this type of charging is used by domestic consumers, and level 3—fast charging in direct current (40 min charging time of a car battery for a light vehicle) Output Voltage: 200–500 V DC for 60 kW charging station output power [26], Output voltage: 300–1000 V DC for the 120 kW charging station output power.

At the laboratory level, by analyzing and implementing the advanced fluid-based cooling system, researchers increased the current capacity of an electric-vehicle charging-station cable by a factor of four of various EV chargers available worldwide. According to this, the maximum current through charging wires is experiment at 2.4 kA. In this way, the charging time is reduced up to 5 min [27–30].

The maritime transport reveals the first full-electric container navy: Yara Birkeland from the Yara International, Norway [31].

The 6.7 MWh Leclanché Marine Rack System (MRS) contains a high-energy lithium-ion battery. MRS ensures optimal temperature control through integrated liquid cooling. The MRS system also contains an integrated fire protection system specially designed and certified for maritime requirements. The container ship has a service speed of approximately 6 knots, with a maximum speed of 13 knots. The sizes of the total electric navy are 80 m long, 15 m wide, with 3120 tons weight. The battery system (6.7 MWh) of the Yara Birkeland, manufactured in Switzerland, Europe, and the battery life is at least 10 years (**Figure 10**).

For commercial purposes, the vertical take-off and landing Sikorsky Autonomous Research Aircraft (SARA), a full electric helicopter based on the Matrix Technology autonomy system, is a reference for new standards in the field and for logistic development (different kinds of services: routes, and helipads as the infrastructure, and air traffic control) (**Figure 11**).

The new type of vehicles will incorporate the new Artificial Intelligence (AI) Technology, taking into account the recent DARPA Programmes: Explainable AI (XAI) [34] 2017–2021, and Lifelong Learning Machines (L2M). The XAI program is considered as the 3rd wave of AI systems [34, 35].

Figure 10.
The Norway (Yara Birkeland) first autonomous and total electric container ship [32].

Figure 11.
Sikorsky autonomous research aircraft (SARA) [33].

The L2M program has in view to create the new Artificial Intelligence types of architectures and Machine Learning systems being capable to learn continuously during execution tasks, not separated as the actual AI architectures [36, 37].

5. Conclusion

The content of this chapter is structured within four Sections. The first section, there is an introduction with justified path towards the electric transport. The second section includes a path to achieve zero net CO_2 emissions by 2050, with justified statistics in the field. The third section, the EU Green transition, includes the justified European Union actions. The last section, Electric Transport Mode. Enabling Technologies presents the main types of the Electric Transport Modes with some high-performance examples in the Electric Transport sector, to achieve Net Zero Emissions by 2050.

Acknowledgements

Author details

Marian Gaiceanu[1,2]

1 Dunarea de Jos University of Galati, Romania

2 Integrated Energy Conversion Systems and Advanced Control of Complex Processes Research Center, Romania

*Address all correspondence to: marian.gaiceanu@ugal.ro

IntechOpen

References

[1] Glandorf J. On the Move: Unpacking the Challenges and Opportunities of Electric Vehicles; November 5, 2020; USA

[2] Available from: https://ourworldindata.org/co2-emissions-from-transport [Accessed: September 18, 2021]

[3] Available from: https://www.eea.europa.eu/data-and-maps/data/data-viewers/greenhouse-gases-viewer [Accessed: September 14, 2021]

[4] Available from: https://www.volkswagenag.com/en/news/stories/2019/08/hydrogen-or-battery--that-is-the-question.html; https://www.nobelprize.org/prizes/chemistry/2019/press-release/ [Accessed: October 11, 2021]

[5] Available from: https://www2.deloitte.com/uk/en/insights/focus/future-of-mobility/electric-vehicle-trends-2030.html [Accessed: October 12, 2021]

[6] Available from: https://www.iea.org/data-and-statistics/charts/population-without-access-to-electricity-in-the-stated-policies-and-net-zero-by-2050-scenarios-2000-2030 [Accessed: October 12, 2021]

[7] IEA. Population without access to electricity in the Stated Policies and Net Zero by 2050 scenarios, 2000-2030. Paris: IEA. Available from: https://www.iea.org/data-and-statistics/charts/population-without-access-to-electricity-in-the-stated-policies-and-net-zero-by-2050-scenarios-2000-2030 [Accessed: October 12, 2021]

[8] Available from: https://www.agerpres.ro/economic-extern/2021/06/29/vanzarile-de-masini-electrice-au-crescut-in-europa-in-urma-inaspririi-obiectivelor-privind-emisiile--739760 [Accessed: October 23, 2021]

[9] Available from: https://www.eea.europa.eu/data-and-maps/daviz/new-electric-vehicles-by-country-3#tab-dashboard-01 [Accessed: October 23, 2021]

[10] Available from: https://www.eea.europa.eu/ims/greenhouse-gas-emissions-from-transport [Accessed: November 01, 2021]

[11] Available from: https://ec.europa.eu/clima/eu-action/transport-emissions_en [Accessed: November 03, 2021]

[12] Distribution of transportation greenhouse gas emissions in the European Union in 2019, by mode. Available from: https://www.statista.com/statistics/1237597/transport-greenhouse-gas-emissions-by-mode-eu/ [Accessed: December 17, 2021]

[13] Available from: https://www.statista.com/statistics/1185535/transport-carbon-dioxide-emissions-breakdown [Accessed: December 17, 2021]

[14] Available from: https://www.eea.europa.eu/data-and-maps/daviz/greenhouse-gas-emissions-from-transport-3#tab-chart_1 [Accessed: September 14, 2021]

[15] Available from: https://www.iea.org/news/iea-to-produce-world-s-first-comprehensive-roadmap-to-net-zero-emissions-by-2050 [Accessed: August 18, 2021]

[16] Available from: https://www.consilium.europa.eu/en/policies/green-deal/eu-plan-for-a-green-transition/ [Accessed: August 15, 2021]

[17] Available from: https://www.consilium.europa.eu/en/policies/green-deal/eu-plan-for-a-green-transition/ [Accessed: August 18, 2021]

[18] Available from: https://www2. deloitte.com/uk/en/insights/focus/ future-of-mobility/electric-vehicle- trends-2030.html [Accessed: September 18, 2021]

[19] Available from: https://www.iea. org/data-and-statistics/charts/global- ev-stock-by-mode-in-the-stated- policies-scenario-2020-2030 [Accessed: October 05, 2021]

[20] Available from: https://www.iea. org/data-and-statistics/charts/global- ev-stock-by-mode-in-the-sustainable- development-scenario-2020-2030 [Accessed: October 05, 2021]

[21] Available from: https://www2. deloitte.com/uk/en/insights/focus/ future-of-mobility/electric-vehicle- trends-2030.html [Accessed: August 20, 2021]

[22] Available from: https://www.eesi. org/articles/view/on-the-move- unpacking-the-challenges-and- opportunities-of-electric-vehicles [Accessed: November 22, 2021]

[23] Available from: https://www. dw.com/ro/spotmediaro-v%C3% A2nz%C4%83rile-de-ma%C8%99ini- electrice-%C8%99i-hibride-s-au- dublat-%C3%AEn-ultimii-doi-ani- %C3%AEn-rom%C3%A2nia-topul- celor-mai-populare-modele/a-58987547 [Accessed: November 22, 2021]

[24] Mühlon F, Palazzo G. The future of EV charging infrastructure: Executive perspectives. Available from: https:// www.mckinsey.com/business- functions/operations/our-insights/ the-future-of-ev-charging- infrastructure-executive-perspectives [Accessed: November 20, 2021]

[25] Available from: https://www.forbes. com/wheels/advice/ev-charging-levels/ [Accessed: November 19, 2021]

[26] Available from: https://www. en-plustech.com/60kw-3in1-fast- charging-station.html [Accessed: December 01, 2021]

[27] Devahdhanush VS, Lee S, Mudawar I. Experimental investigation of subcooled flow boiling in annuli with reference to thermal management of ultra-fast electric vehicle charging cables. International Journal of Heat and Mass Transfer. 2021;**172**:121176. DOI: 10.1016/j.ijheatmasstransfer

[28] Devahdhanush VS, Lee S, Mudawar I. Consolidated theoretical/ empirical predictive method for subcooled flow boiling in annuli with reference to thermal management of ultra-fast electric vehicle charging cables. International Journal of Heat and Mass Transfer. 2021;**175**:121224. DOI: 10.1016/j.ijheatmasstransf]

[29] Available from: https://www. purdue.edu/newsroom/releases/2021/ Q4/electric-vehicles-could-fully- recharge-in-under-5-minutes-with- new-charging-station-cable-design. html [Accessed: December 15, 2021]

[30] Fluid-Cooled Cable Quadruples EV Charging-Current Capacity. Available from: https://www.electronicdesign.com/ markets/automotive/article/21183308/ electronic-design-fluidcooled-cable- quadruples-ev-chargingcurrent- capacity?utm_source=EG%20ED%20 Analog%20%26%20Power%20 Source&utm_medium=email&utm_ campaign=CPS211201076&o_ eid=3588C5978523C5X&rdx.ident%5Bpu ll%5D=omeda%7C3588C5978523C5X& oly_enc_id=3588C5978523C5X [Accessed: December 08, 2021]

[31] Available from: https://www. powersystemsdesign.com/articles/ the-worlds-first-100-electric-and- autonomous-e-container-ship/8/18529 [Accessed: December 10, 2021]

[32] Available from: https://www.
powersystemsdesign.com/images/
articles/1639102696-e2d0e24d-4b63-
4e89-9d49-25c33d40f274.jpeg
[Accessed: December 10, 2021]

[33] Available from: https://www.
youtube.com/watch?v=xhZy8rJMFxE
[Accessed: December 10, 2021]

[34] Defense Advanced Research
Projects Agency, DARPA. Available
from: https://www.darpa.mil/program/
explainable-artificial-intelligence
[Accessed: December 10, 2021]

[35] Gunning D, Vorm E, Wang Y, et al.
DARPA's Explainable AI (XAI) program:
A retrospective. Applied AI Letters.
2021;**2**(4). Available from: https://
onlinelibrary.wiley.com/doi/full/
10.1002/ail2.61

[36] 2017 First announcement. Available
from: https://www.darpa.mil/program/
lifelong-learning-machines [Accessed:
December 10, 2021]

[37] Available from: https://idstch.com/
technology/ict/darpa-l2m-program-
progress-seen-lifelong-learning-
machines/[Accessed: December 10, 2021]

Strategies for Electric Vehicle Infrastructure of Cities: Benefits and Challenges

Murat Furat, İsra Karabiber and Senem Kocaoğlu

Abstract

The emerging technology, electric vehicles (EVs), has gained more attention due to the greenhouse gas (GHG) emission, climate change, and air pollution in the cities. The rising demand for EVs brings new benefits and challenges to the city life of citizens. Balancing the demand in the electrical energy distribution grid, charging scheduling, dynamic pricing, and different types of charging stations change the priorities of city life. In order to manage the new requirements and perform the permanent transition from gasoline-powered vehicles to EVs, a strategic plan must be prepared by the city authorities. Currently, a number of cities in different countries have published their strategic plans for the sense of perspective about reaching a 30% sales share for EVs by 2030. These plans focus on the solutions to maximize the benefits of EVs and the awareness of the citizens. In the present study, fundamental components of a strategic plan for both EVs and necessary infrastructure are outlined with different aspects.

Keywords: Electric vehicles, infrastructure, strategic plan, charge scheduling, grid management

1. Introduction

Different technologies and structural changes are coming to city life with EVs. The number of EVs has increased exponentially in the last decade because there are many benefits that EVs bring to their owners and the environment. According to the Electric Vehicles Initiative (EVI), the fourteen member countries have accelerated the development of EVs. Also, the EV30@30 Campaign was launched by the members of EVI to increase the EV market by 30% of the total of all vehicles until 2030 [1]. In addition to the countries, several companies have also supported the Campaign [2].

On the other hand, the cities and the citizens must be ready for the requirements of the emerging technologies [3]. Getting cities ready for the basic infrastructure of EVs will determine the permanent transition times of EVs from gasoline-powered vehicles. Therefore, understanding EVs and their infrastructure are crucial [4].

In order to make ready a city for EVs, a strategy must be determined which includes the following indicators:

- Education of citizens about EVs, their benefits and associated technologies,

- Optimum planning of the location and installing the charging/swapping stations,

- Planning necessary energy resources for charging stations,

- Establishing the essential infrastructure and maintenance,

- Establishing the essential communication networks of electric vehicles and charging stations,

- Defining the roles of the federal government, the city authorities, energy providers and EV users to collaborate with other cities to share experiences.

Obviously, a strategic plan can be shaped not only at the city level but also at the federal level with a host of incentives and initiatives [2, 3]. Also, the goals of the plan must be realistic and flexible to change for unpredictable future requirements. The strategic plans of many cities, published recently, have been considered within this framework. In addition, many countries have announced their roadmap for EVs and highlighted key policies [5]. Because EVs are not only electric cars. The EV term covers all transportation vehicles from bikes to busses, from heavy-duty vehicles to ships and aircrafts which are powered electrical energy. Therefore, a wide range of vehicles is about to transform into electrically powered vehicles.

In this chapter, information is given about the way to be followed to create the electric vehicle infrastructure of a city within the scope of these plans. There are several benefits and challenges for cities and citizens to be ready for them. In the next section, EVs are introduced. Then, a necessary strategic plan is outlined. Finally, the conclusion is provided.

2. Motivation

Electric vehicles are not an invention of today's technology. The first EV was seen in the 1800s. From the first EV to today's modern EVs, the evaluation of EV technology can be summarized as in **Figure 1** [6].

In the beginning, electric-powered vehicles were popular since they were quiet, easy to drive especially for women. Later, as gasoline stations available everywhere, the interest in gasoline-powered vehicles was increased. When the price of gasoline has risen, EVs were retaken into account. However, their small range and long charging time were still the main barriers in front of EVs. Whenever the ranges are increased and necessary infrastructures are constructed, the popularity of electric vehicles has gained more attention [7, 8]. According to [2, 9], it is clearly seen that the direction in the vehicle preference has been towards to EVs. In **Figure 2**, annual EV market growth is given [10].

According to [1], worldwide EV sales in 2017 was over 1 million and then two years later, it surpassed the 2 million mark in 2019. Technical improvements on EVs
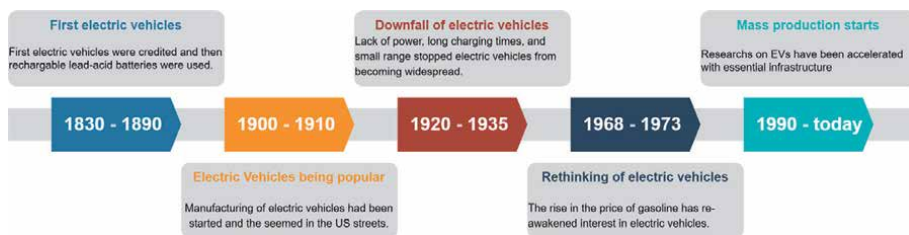
Figure 1.
Timeline of the EVs.
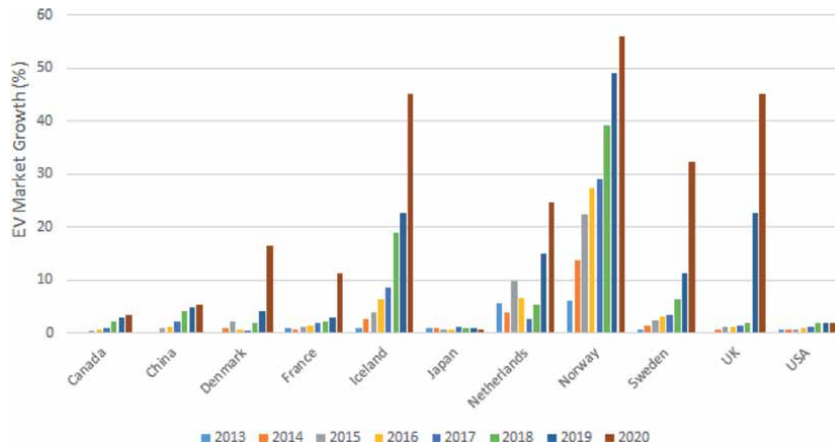
Figure 2.
Annual EV market growth (%) by country from 2013 to 2020.

have been increased to the attractiveness of EVs. The demand for EVs is further increased if the cost of EVs is reduced and the travel range is increased. By the end of 2020, the number of electric vehicles worldwide, in the light-duty segment, exceeded 10 million [2]. Among the countries, the largest number of ELDVs was registered in China, with 4.5 million. China was followed by European countries with 1.4 million registered ELDVs. In addition, a number of EV manufacturers, such as Volvo, Ford, General Motors, announced that they only sell EVs from 2030 [2].

Not only in ELDV sales but also in EHDT and electric bus sales, China is the dominant country all over the world. In 2020, the number of electric busses was 600 thousand and the number of EHDT was 31 thousand [2]. According to the IEA, the global prediction on the number of EVs are summarized with the following **Table 1** [11].

Today, many governments around the world have focused on making all current vehicles electrified at a specific time in the near future. In addition, studies on the necessary infrastructure and the adoption of citizens are carried out within the framework of strategic plans.

A strategic plan should include a training section in which EVs' terminology and basic infrastructures are introduced. Therefore, in the present section, the fundamental information is given.

2.1 Classification of EVs

EVs do not have a unique structure. Depending on the energy source, EVs are classified as follows:

- *Battery Electric vehicles (BEVs) or all-electric vehicles (AEVs)* are vehicles powered only by electrical energy. The electrical energy is stored in the battery utilized in the vehicle. The battery is charged from the electrical energy distribution grid and partly from a regenerative braking system which recovers the lost energy when braking. The range of this type of vehicle is between 150 and 500 km. But, many manufacturers continue to improve the driving range.

- *Plug-in hybrid electric vehicles (PHEVs) or extended-range electric vehicles (EREVs)* use electrical energy for short driving ranges and turn into an internal combustion engine when the vehicle's battery is depleted. The range of this type of vehicle with only electrical power is between 25 and 85 km.

- *Hydrogen Fuel Cell Electric Vehicles (FCEVs)* are currently under development since their electrical energy is obtained from hydrogen. It is presently difficult to storage and refuels the hydrogen. A limited number of FCEVs are available between 500 and 600 km driving range.

2.2 Charging methods

Another classification can be performed for the Electric Vehicle Supply Equipment (EVSE) which is the charging facilities of the EVs as shown in **Figure 3**.

In order to charge an EV at home or at the office, Level 1 type charging stations are suitable since they can be used with home electricity provided by a standard AC wall outlet. It is ideal for EV owners who generally preferred to charge their vehicles at home [12]. Level 1 cord set is generally provided with most EVs.

Level 2 type charging stations provides faster charging and are commonly installed for public usage in car parks and supermarkets. 3 or 4 EVs can be charged a day by using this type of charging station [12].

Level 3 type charging stations uses 3-phase supply voltage for fast charge. It is suitable for EV owners who need quick charges such as commercial vehicles and taxis [12].

Level 4 charging stations, namely developed by Tesla, enable rapid charge for larger battery-powered EVs [12].

Induction charging or wireless charging is an emerging technology based on power transfer by an electromagnetic field [13, 14]. The efficient power transmission can be performed by a small space between the EV and inductive coils mounted on the ground. However, the space is directly related to the load on the vehicle and the clearance of the ground [15]. Protected connections without any cable and low infection risk are the main advantages of induction charging, while slower and inefficient charging makes it more expensive. The main benefit of induction charging can be seen on public transportation vehicles since charging the vehicle on the road reduces the total size of the battery for the trip. Therefore, wireless energy transfer to EVs is currently under development [16].

Pantograph is another solution for EVs especially commercial vehicles such as busses and trucks. More than 150 kW DC power can be supplied by a conductive charging system mounted at the top of the busses or trucks [17].

A patented approach to supply power to EVs is swapping batteries at battery swapping stations (BSS) [18, 19]. Consumer acceptance, non-standard batteries and technical challenges on SoC of the batteries are the main barriers to battery swapping.

2.3 Charging modes

Another technical detail of the EV charging is the charging modes which is defined by the reference standard is IEC 61851–1. There are four different charging modes as shown in **Figure 4**.

Scenario/Year	2025	2030
Stated Policies Scenario	BEV ~ 30 million PHEV ~16 million FCEV ~233 thousand	BEV ~ 80 million PHEV ~44 million FCEV ~1.15 million
Sustainable Development Scenario	BEV ~ 41.5 million PHEV ~21 million FCEV ~830 thousand	BEV ~ 138 million PHEV ~61 million FCEV ~5 million

Table 1.
Global predictions of EVs with different scenarios.
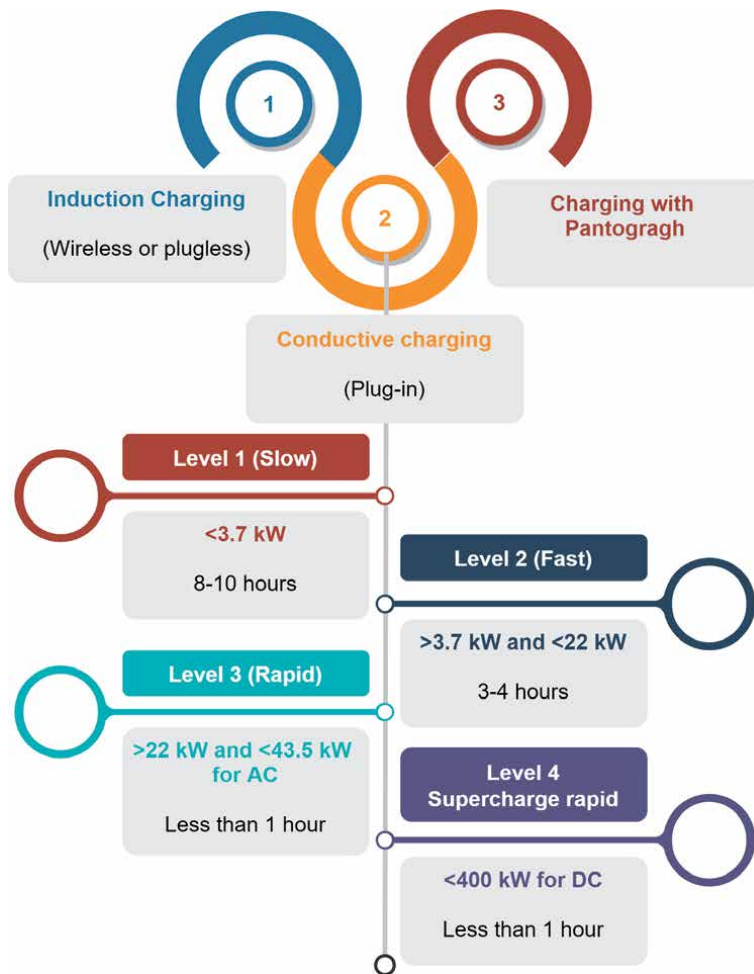
Figure 3.
Charging facilities of the EVs.

Mode 1: This charging mode (Schuko mode) is generally used in two-wheel vehicles such as electric bikes and scooters. The household outlet is directly connected to the vehicles by an extended cable without any safety device. This is currently unpopular and also no longer used for EVs.

Mode 2: The electrical energy from the household outlet to the vehicle is transmitted over a control box which is also known as a portable EV charger. In order to fully charge a battery, the EV must be connected for up to 16 hours.

Mode 3: An AC power supply directly connected to the electric distribution network is used in this type of charging mode. The power supply is generally mounted a wall and is used in both public areas and residences. The typical charging duration in this mode is between 4 and 9 hours, depending on the battery size of the EV.

Mode 4: It is generally used in public areas due to its high cost. The charging station provides faster charging over an AC-to-DC converter mounted in the station. It takes less than 1 hour to charge an EV to 80%.

2.4 Essential energy phenomenon

As the battery capacity is increased to extend the range of electric vehicles, the required energy to charge the battery in a short time interval will pose a problem for
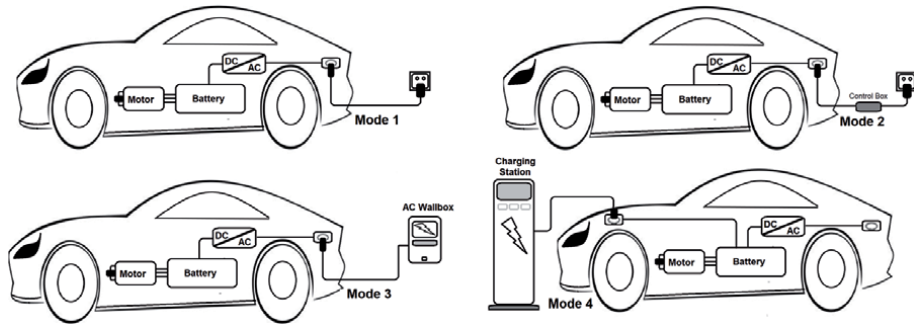
Figure 4.
Charging modes of the EVs.

the electrical energy distribution grid of the cities. In addition, the waiting time to charge EVs and waiting time for the available charging stations will be the problems of EV owners as the number of EVs on the roads increases [20].

In recent years, different solutions have been proposed for the rising problems. Scheduling of charging [21, 22], placement of charging stations [23], different pricing methodologies [24] and also integrating the renewable energy sources [25] are frequently studied to supply energy to the vehicles. These solutions also bring new habits the citizens. At the same time, it brings great responsibilities to local governments in the implementation of these solutions. In this sense, sharing experiences among the cities becomes more important to find appropriate policies, financial supports and also the adoption of citizens to the new technology. More than 100 cities come together for an initial period of 5 years in order to build a network for The Electric Vehicles Initiative Global EV Pilot City Programme (EVI-PCP) [26].

The necessary number of charging stations, either home type or publicly accessible, are installed proportionally to the number of EVs on the roads. Especially Level 3 and Level 4 charging stations play an important role in the amount of load on the electrical energy distribution grid. According to [2], these charging stations are increasingly installed in all regions. Necessary infrastructure for the charging station to provide parking areas and necessary electrification have to be planned. In order to meet the energy needs of electric vehicles continuously, a target has been set by Alternative Fuel Infrastructure Directive (AFID) which is 1 public charging station per 10 EVs [27]. There are also several patent studies to overcome the charging scheduling phenomenon of EVs [25–34].

In addition, renewable energies are also studied for this purpose [8, 35]. Although the main target is to provide sufficient public charging stations, electric busses and electric heavy-duty trucks, medium freight trucks (MFTs) and heavy freight trucks (HFTs) have also been on the roads. Therefore, the needed energy supply equipment for HFTs and necessary energy sources may be a big problem in cities with heavy commercial transport. This problem brings a new solution with megachargers of 1 MW which satisfies the need for HFTs [2]. A project on the clean transit corridor used by heavy commercial trucks started by West Coast Clean Transit Corridor Initiative to reduce the greenhouse gas (GHG) emission by the diesel trucks. Another project scope is the required amount of space to install EVSE for the heavy commercial trucks since these vehicles may need to be charged frequently [36].

Electric vehicles are considered not only for road transport but also for sea and air transport. In order to contribute to the reduction of GHG emission, shipping and flying vehicles are planned to power with electrical energy [37–41].

2.5 Reduction of greenhouse gases emission

Globally, over 20% of total GHG has been emitted by transportation vehicles [27, 42]. It is partially true that all types of EVs are considered a significant solution for reducing GHG emissions. EVs themselves do not emit GHG. Therefore, their contribution to air quality is undoubtedly in cities with heavy traffic. However, the required electrical energy is generated in power plants that emit GHG. All vehicles emit GHG in their lifecycle. But, the generated GHG by power plants for EVs is lower than the total amount of GHG emitted by gasoline-powered vehicles [43, 44]. A higher ratio of the electrical energy generated by renewable energy sources results in a further reduction in GHG emissions [42] which is the main reason to obtain zero-emission transportation.

2.6 New habits and routines of citizens

Living with EVs will be different than living with gasoline-powered vehicles. As described above, EVs will bring new regulations to city life. In order to use EVs without any interruption, charging of the vehicles in any location might be predefined to the owners. The charging decision of an EV owner depends on the battery status of the EV. The battery power, driving characteristics, environmental and geographic conditions plays a significant role on the frequency of the charging EV. Meanwhile, the selection of charging type, duration and time is decided by the owner [45]. Driving and driver behaviors in the big data perspective were also discussed in the literature [46].

In the literature, different methods have been proposed to overcome the charging problems, such as waiting for a charging station and waiting for charging of the EV [21]. In order to maximize the benefits of EVs, the owners may need to follow new regulations [47]. Therefore, new habits and new routines get into the city life which the governments may previously explain. Currently, many cities and countries have implemented the necessary regulations and practices for electric vehicles. In order to permanent transition in a phased manner, a number of strategic reports are published by the governments [3, 12, 48–54].

2.7 Obstacles to the strategic plan

In the development stages of the vehicles, either gasoline-powered or electric-powered, there were different obstacles to both vehicles. Although EVs are technologically advanced, the infrastructure to fully replace gasoline-powered vehicles is not ready in many cities. There are obstacles that cities have to overcome in order to have the infrastructure [55]. A well-designed strategic report will play an important role in overcoming the following obstacles in front of the city authorities:

- Introduction of electric vehicles in all aspects

- Determining the necessary infrastructure

- Financial resources to cover the cost of infrastructure

- Determining the policies and their implementation the city life

EVs are still under development stage and each city has its own characteristics to adopt the EVs essentials. Because of this reason, currently, there is no specific result that describes the whole experience of a strategic plan. According to [55], the primary obstacles can be divided into sub-obstacles.

3. Methodology of strategic plan

The framework for a strategy report has been drawn in the previous section to overcome the multidimensional preparation problem that arises with the spread of electric vehicles. The critical sections in the structure of a strategic plan to prepare a city and its citizens determine how well perform a flawless transition to EVs (**Figure 5**).

The first section of a strategic plan is designed for the citizens unfamiliar with EV technology to motivate the citizens to have EVs. Therefore, the following topics can take place in this section:

- How an EV works?

- Charging of battery

- Environmental benefits of EVs

- Economic advantages

  ○ Taxation policy of the government

  ○ Running costs of EVs

- Local, federal and global trends in the EVs market
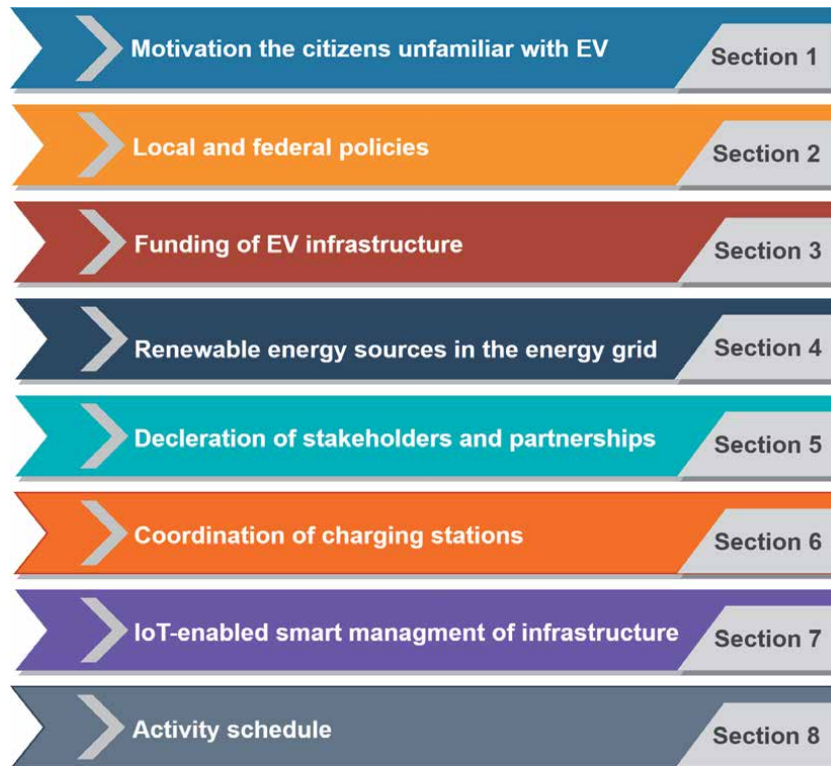
Figure 5.
Critical sections of a strategic plan.

- The objectives of the strategic plan

  ○ Future predictions about number of EVs

  ○ Rate of reduction in GHG emission

  ○ Increase the awareness of EVs by social media

The framework of the local and federal policies on EVs and their structure can be considered with the density of the population and their geographical characteristics of the cities. In the second section, the following related subsections can be given:

- Local and federal health policy

- Local and federal air quality policy

- Future plans to ban gasoline-powered vehicles

- Zero-emission policy for GHG

Funding of necessary infrastructure is a financial problem in front of the governments. The strategy that will be followed for deploying charging stations, charging parks, organization and also providing vital electrical energy can be explained in the third section as follows:

- Free or reduced cost of parking EVs

- Cost of infrastructure for electric busses

- Cost of installing renewable energy sources

- Running cost of EVSE

- Methods to increase cost recovery time

Supporting the installation of renewable energy sources significantly contributes the zero-emission target. Therefore, necessary plans should be put forward to research the city's renewable energy sources and add them to the electrical energy distribution grid. The steps to be taken in this regard should be included in a strategic plan as follows:

- Identifying the city's renewable energy sources

- Possibilities of integrating the renewable energy sources into the grid

- Feeding of charging stations from these sources

- Encouraging the EV owners to use private renewable energy sources

Another critical topic is the declaration of external stakeholders and strategic partnerships. Many countries and cities have come together to share their experiences. In order to inform the citizens, these partners can be explained in a section as follows:

- Working with EV manufacturers

- Coordination with energy providers

- Collaboration between the cities and countries around the world, such as EVI

Although the rapid chargers are developed, at least 30 minutes waiting time is required to charge an average ELDV. This problem will increase proportionally to the number of EVs in a city. A limited solution is to direct EV owners to charge their vehicles at home. As stated above, it does not fit EV owners who need quick charges such as commercial vehicles, taxis and HDTs. Coordination of charging stations to minimize waiting time, different methods have been proposed in the literature. Within the framework of a city's possibilities, the goal of coordination can be put forward with a strategy as follows:

- Collect all EV owner data in a database with the information of their EVs and charging characteristics

- Design a recommender system for the EV owners so that the system

  ○ Keeps the load balancing of the electrical distribution network

  ○ Follows the SoC of EVs

  ○ Recommends charging/swapping using a dynamic pricing methodology

  ○ Gets charging demand by a developed mobile phone application

- Determine optimal locations for additional charging stations in the light of collected data.

IoT-enabled smart applications for reducing the running cost of EVs have taken place from a daily life perspective of smart cities. As mobile communication devices are used widespread, smart EV and its infrastructure management systems have gained a great interest in the sense of IoT. Because of this reason, a section can be designed for the management of EV infrastructure with the following properties:

- Centralized load management of the electrical energy distribution grid

- Predicting and managing of charging operations of large-scale EVs

- Controlling the direction of energy flow in the grid

- Creating digital twins of EV owners (DToEVO)

- Performing different benchmark scenarios on the infrastructure by DToEVO

There are different approaches to model a real system to simulate. A DToEVO is a dynamically updated model of both EV and its owner. Therefore, data-driven modeling is appropriate to create and update DToEVO with the following properties:

- Model and age of EV

- Battery capacity of EV

- Charge frequency of EV

- Preferred SoC to charge the battery

- Average velocity per travel

- Maximum velocity per travel

- Travel duration and routes

- Resting duration and location

Finally, a section has been prepared for the activity schedule in order to realize the goals of the strategic plan in a phased manner [49].

Obviously, as the technological development on the EVs and essential infrastructure, these plans must be revised. There is no standard plan to fit all cities [56]. Every city has its own characteristics. In this sense, a collaboration between the cities increases the total benefits.

4. Conclusion

EV technology brings structural changes in city life. Therefore, city authorities and governments have important duties. In the present study, the outline of a city-scale strategic plan is explained. It is open to improvement since each city has its own specific requirements in the sense of EVs and their essential infrastructure. Analyzing the requirements, planning the activities and educating the EV owners result in an easy transition from gasoline-powered vehicles to EVs. In order to maximize the total benefits and overcome the challenges easily, experiences must be shared between the cities.

Conflict of interest

The authors declare no conflict of interest.

Nomenclature

AC	Alternating Current
AEV	All-Electric Vehicle
AFID	Alternative Fuel Infrastructure Directive
BEV	Battery Electric Vehicle
BSS	Battery Swapping Stations
DC	Direct Current
DToEVO	Digital Twin of Electric Vehicle Owner
EHDT	Electric Heavy-duty Truck
ELDV	Electric Light-duty Vehicle
EREV	Extended-range Electric Vehicle

EV	Electric Vehicle
EVI	Electric Vehicles Initiative
EVSE	Electric Vehicle Supply Equipment
FCEV	Hydrogen Fuel Cell Electric Vehicle
GHG	Greenhouse Gas
HFT	Heavy Freight Trucks
IEA	International Energy Agency
MFT	Medium Freight Trucks
PHEV	Plug-in Hybrid Electric Vehicle
SoC	State of Charge

Author details

Murat Furat*, İsra Karabiber and Senem Kocaoğlu
İskenderun Technical University, Hatay, Turkey

*Address all correspondence to: murat.furat@iste.edu.tr

IntechOpen

References

[1] "Global EV Outlook 2020," *Glob. EV Outlook 2020*, 2020, doi: 10.1787/d394399e-en.

[2] "Global EV Outlook 2021," *Glob. EV Outlook 2020*, 2020, doi: 10.1787/d394399e-en.

[3] D. Garas, G. O. Collantes, and M. A. Nicholas, "City of Vancouver EV infrastructure strategy report," no. December, 2016, [Online]. Available: https://escholarship.org/content/qt0w90c61t/qt0w90c61t.pdf.

[4] H. S. Das, M. M. Rahman, S. Li, and C. W. Tan, "Electric vehicles standards, charging infrastructure, and impact on grid integration: A technological review," *Renew. Sustain. Energy Rev.*, vol. 120, no. November 2019, 2020, doi: 10.1016/j.rser.2019.109618.

[5] International Energy Agency, "Global EV Policy Explorer," 2021.

[6] "Timeline: History of the Electric Car | Department of Energy." https://www.energy.gov/timeline/timeline-history-electric-car (accessed May 25, 2021).

[7] F. J. Soares, D. Rua, C. Gouveia, B. D. Tavares, A. M. Coelho, and J. A. P. Lopes, "Electric Vehicles Charging: Management and Control Strategies," *IEEE Veh. Technol. Mag.*, vol. 13, no. 1, pp. 130-139, 2018, doi: 10.1109/MVT.2017.2781538.

[8] J. A. Peças Lopes, F. J. Soares, P. M. Almeida, and M. Moreira Da Silva, "Smart charging strategies for electric vehicles: Enhancing grid performance and maximizing the use of variable renewable energy resources," *24th Int. Batter. Hybrid Fuel Cell Electr. Veh. Symp. Exhib. 2009, EVS 24*, vol. 4, no. February 2014, pp. 2680-2690, 2009.

[9] M. Muratori *et al.*, "The rise of electric vehicles—2020 status and future expectations," *Prog. Energy*, vol. 3, no. 2, p. 022002, 2021, doi: 10.1088/2516-1083/abe0ad.

[10] J. A. Sanguesa, V. Torres-Sanz, P. Garrido, F. J. Martinez, and J. M. Marquez-Barja, "A Review on Electric Vehicles: Technologies and Challenges," *Smart Cities*, vol. 4, no. 1, pp. 372-404, 2021, doi: 10.3390/smartcities4010022.

[11] "Global EV Data Explorer – Analysis - IEA." https://www.iea.org/articles/global-ev-data-explorer (accessed Jun. 11, 2021).

[12] Warwickshire County Council, "Electric Vehicle Charging Infrastructure Strategy 2017-2026," no. November, 2017, [Online]. Available: https://api.warwickshire.gov.uk/documents/WCCC-930-349.

[13] X. Lu, *P. Wang*, D. Niyato, D. I. Kim, and Z. Han, "Wireless Charging Technologies: Fundamentals, Standards, and Network Applications," *IEEE Commun. Surv. Tutorials*, vol. 18, no. 2, pp. 1413-1452, 2016, doi: 10.1109/COMST.2015.2499783.

[14] A. Zakerian, S. Vaez-Zadeh, and A. Babaki, "Efficiency Maximization Control and Voltage Regulation for Dynamic Wireless EV Charging Systems with Mutual Induction Estimation," *IECON Proc. (Industrial Electron. Conf.*, vol. 2019-Octob, pp. 4298-4303, 2019, doi: 10.1109/IECON.2019.8926940.

[15] A. Marinescu *et al.*, "The way to engineering EV wireless charging: DACIA electron," *2017 Electr. Veh. Int. Conf. EV 2017*, vol. 2017-Janua, pp. 1-6, 2017, doi: 10.1109/EV.2017.8242094.

[16] S. Sharma, "China is the New Hub for Wireless Charging Technology."

https://www.ipwatchdog.com/2020/07/06/china-new-hub-wireless-charging-technology/id=123032/ (accessed May 23, 2021).

[17] "OppCharge - Fast charging of electric vehicles." https://www.oppcharge.org/ (accessed May 23, 2021).

[18] F. Adegbohun, A. von Jouanne, and K. Y. Lee, "Autonomous battery swapping system and methodologies of electric vehicles," *Energies*, vol. 12, no. 4, pp. 1-14, 2019, doi: 10.3390/en12040667.

[19] I. J. R. Dahn, T. Van, and N. Westminster, "United States Patent [191 [11] Patent Number : US5998963A," vol. 2, no. 19, pp. 1-7, 1990.

[20] T. S. Bryden, G. Hilton, B. Dimitrov, C. Ponce De León, and A. Cruden, "Rating a Stationary Energy Storage System Within a Fast Electric Vehicle Charging Station Considering User Waiting Times," *IEEE Trans. Transp. Electrif.*, vol. 5, no. 4, pp. 879-889, 2019, doi: 10.1109/TTE.2019.2910401.

[21] W. Jiang and Y. Zhen, "A Real-Time EV Charging Scheduling for Parking Lots with PV System and Energy Store System," *IEEE Access*, vol. 7, pp. 86184-86193, 2019, doi: 10.1109/ACCESS.2019.2925559.

[22] Z. Moghaddam, I. Ahmad, D. Habibi, and Q. V. Phung, "Smart Charging Strategy for Electric Vehicle Charging Stations," *IEEE Trans. Transp. Electrif.*, vol. 4, no. 1, pp. 76-88, 2017, doi: 10.1109/TTE.2017.2753403.

[23] C. Luo, Y. F. Huang, and V. Gupta, "Placement of EV charging stations-balancing benefits among multiple entities," *arXiv*, pp. 1-10, 2018.

[24] Z. Moghaddam, I. Ahmad, D. Habibi, and M. A. S. Masoum, "A coordinated dynamic pricing model for electric vehicle charging stations," *IEEE Trans. Transp. Electrif.*, vol. 5, no. 1,

pp. 226-238, 2019, doi: 10.1109/TTE.2019.2897087.

[25] P. Mesarić and S. Krajcar, "Home demand side management integrated with electric vehicles and renewable energy sources," *Energy Build.*, vol. 108, pp. 1-9, 2015, doi: 10.1016/j.enbuild.2015.09.001.

[26] "EVI Global EV Pilot City Programme – Programmes and partnerships - IEA." https://www.iea.org/areas-of-work/programmes-and-partnerships/evi-global-ev-pilot-city-programme (accessed May 25, 2021).

[27] "DIRECTIVE 2014/94/EU OF THE EUROPEAN PARLIAMENT AND OF THE COUNCIL of 22 October 2014 on the deployment of alternative fuels infrastructure." https://eur-lex.europa.eu/legal-content/EN/TXT/HTML/?uri=CELEX:32014L0094&from=en (accessed May 26, 2021).

[28] A. Deshpande and P. Murali, "Managing Electric Vehicle (EV) Charging Station Usage Pub. No.: US 2015/0032516 A1," *Patent*, vol. 1, no. 19, 2015.

[29] S. Kawano *et al.*, "Charging Management System Pub. No.: US 2015 / 0158393 A1," *Patent*, vol. 1, no. 19, 2015.

[30] T. K. Paul and H. Aisu, "Electric Vehicle Charging Scheduling System Pub. No: US 9,112,382 B2," *Patent*, vol. 2, no. 12, 2015.

[31] M. Ramezani, H. Vogt, and H. Braun, "Vehicle Electric Charging Schedule Selection and Evolution Based on Multiple Weighted Charging Objectives Pub. No.: US 2013/0054045 A1," *Patent*, vol. 1, no. 19, 2013.

[32] S. B. Pllack and W. Bridges, "Systems and Methodsfor Smart Charging Techniques, Value and Guarantee Pub . No.: US 2013 / 0184886 A1," *Patent*, vol. 1, no. 19, 2013.

[33] E. D. Tate and S. A. Tarnowsky, "Electric Charging Station Reservation System and Method Pub . No .: US 2012 / 0233077 A1," *Patent*, vol. 1, no. 19, 2012.

[34] S. Smullin, M. J. Stefik, D. E. Schwartz, and D. H. Greene, "Computer - Implemented System and Method for Managing Interchangeable EV Charging - Capable Parking Spaces Patent No . : US 9 , 779 , 365 B2," *Patent*, vol. 2, 2017.

[35] C. Goeltner, "Solar Powered, Grid Independent EV Charging System Pub. No.: US 2010/0181957 A1," *Patent*, vol. 1, no. 19, 2010.

[36] "West Coast Clean Transit Corridor Initiative." https://westcoastcleantransit.com/ (accessed May 27, 2021).

[37] N. Shakeri, M. Zadeh, and J. Bremnes Nielsen, "Hydrogen Fuel Cells for Ship Electric Propulsion: Moving Toward Greener Ships," *IEEE Electrif. Mag.*, vol. 8, no. 2, pp. 27-43, 2020, doi: 10.1109/MELE.2020.2985484.

[38] H. Liu, Y. Wang, and D. Gao, "Research on control strategy of hybrid electric ship based on minimum equivalent fuel consumption," *IOP Conf. Ser. Earth Environ. Sci.*, vol. 632, no. 3, 2021, doi: 10.1088/1755-1315/632/3/032029.

[39] M. Macdonald, J. Rheaume, Y. Khakpour, and C. Lents, "Transient cooling approach for a mhr class hybrid electric propulsion system battery pack," *AIAA Scitech 2020 Forum*, vol. 1 PartF, no. January, pp. 1-7, 2020, doi: 10.2514/6.2020-0120.

[40] M. Crittenden, "Ultralight batteries for electric airplanes," *IEEE Spectr.*, vol. 57, no. 9, pp. 44-49, 2020, doi: 10.1109/MSPEC.2020.9173903.

[41] "Electric ships: the world's top five projects by battery capacity." https://www.ship-technology.com/features/electric-ships-the-world-top-five-projects-by-battery-capacity/ (accessed May 27, 2021).

[42] K. J. Dillman, Á. Árnadóttir, J. Heinonen, M. Czepkiewicz, and B. Davíðsdóttir, "Review and meta-analysis of EVs: Embodied emissions and environmental breakeven," *Sustain.*, vol. 12, no. 22, pp. 1-32, 2020, doi: 10.3390/su12229390.

[43] "Reducing Pollution with Electric Vehicles." https://www.energy.gov/eere/electricvehicles/reducing-pollution-electric-vehicles (accessed May 28, 2021).

[44] "Alternative Fuels Data Center: Emissions from Hybrid and Plug-In Electric Vehicles." https://afdc.energy.gov/vehicles/electric_emissions.html (accessed May 28, 2021).

[45] J. C. Spoelstra, "Charging behaviour of Dutch EV drivers," *MSc. Thesis*, 2014, [Online]. Available: https://dspace.library.uu.nl/handle/1874/297327.

[46] R. Terzi, S. Sagiroglu, and M. U. Demirezen, "Big Data Perspective for Driver/Driving Behavior," *IEEE Intell. Transp. Syst. Mag.*, vol. 12, no. 2, pp. 20-35, 2020, doi: 10.1109/MITS.2018.2879220.

[47] Z. Le Hong and N. Zimmerman, "Air quality and greenhouse gas implications of autonomous vehicles in Vancouver, Canada," *Transp. Res. Part D Transp. Environ.*, vol. 90, no. December 2020, p. 102676, 2021, doi: 10.1016/j.trd.2020.102676.

[48] City of Vancouver, "Vancouver's EV Ecosystem Strategy," no. November, pp. 1-78, 2016, [Online]. Available: https://vancouver.ca/files/cov/EV-Ecosystem-Strategy.pdf.

[49] "Calgary ' s Electric and Low-Emissions Vehicles Strategy," [Online]. Available: https://solaralberta.ca/wp-content/uploads/2020/10/Calgarys-Electric-Low-Emission-Vehicle-Strategy_0.pdf.

[50] Cidade de Edmonton, "Edmonton's Electric Vehicle Strategy," no. September, 2018, [Online]. Available: https://www.edmonton.ca/city_ government/documents/PDF/ EdmontonElectricVehicleStrategy.pdf.

[51] "Tompkins County Plug-in Electric Vehicle Infrastructure Plan: Charging Station Implementation Strategies," 2017.

[52] London Borough of Richmond-upon-Thames, "Electric Vehicle Recharging Strategy 2016-2026," no. December, pp. 1-23, 2016.

[53] T. Council, "Town of San Anselmo Electric Vehicle Strategy," pp. 1-11, 2018, [Online]. Available: https://www. townofsananselmo.org/ DocumentCenter/View/23894/ San-Anselmo-EV-Strategy.

[54] W. E. Forum, "EV-Ready India Part 1 : Value Chain Analysis of State EV Policies," no. October, 2019, [Online]. Available: http://www3.weforum.org/ docs/WEF_EV_Ready_India.pdf.

[55] P. K. Tarei, P. Chand, and H. Gupta, "Barriers to the adoption of electric vehicles: Evidence from India," *J. Clean. Prod.*, vol. 291, p. 125847, 2021, doi: 10.1016/j.jclepro.2021.125847.

[56] J. Gardner, "Creating Ev-Ready Towns and Cities: a Guide To Planning and Policy Tools Electric Vehicle Supply Equipment Support Study," no. November, 2012, [Online]. Available: https://www.transportationandclimate. org/sites/default/files/EVSE_Planning_ and_Policy_Tool_Guide.pdf.

Chapter 3

Fast-Charging Infrastructure Planning Model for Urban Electric Vehicles

Tran Van Hung

Abstract

Electric vehicles have become a trend as a replacement to gasoline-powered vehicles and will be a sustainable substitution to conventional vehicles. As the number of electric vehicles in cities increases, the charging demand has surged. The optimal location of the charging station plays an important role in the electric vehicle transit system. This chapter discusses the planning of electric vehicle charging infrastructure for urban. The purpose of this work develops an electric vehicle fast-charging facility planning model by considering battery degradation and vehicle heterogeneity in driving range, and considering various influencing factors such as traffic conditions, user charging costs, daily travel, charging behavior, and distribution network constraints. This work identifies optimal fast-charging stations to minimize the total cost of the transit system for deploying fast-charging networks. Besides, this chapter also analyzes some optimization modeling approach for the fast charging location planning, and point out future research directions.

Keywords: Fast-charging station, charging network, charging station planning, electric vehicles, EVs traffic flow

1. Introduction

Global environmental and energy problems are becoming more and more serious, and one of the main causes is fossil fuel-consuming transportation. Electric vehicles have obvious advantages in energy saving and emission reduction (such as reducing gas emissions, air pollution especially PM2.5 fine dust and noise, reducing dependence on fossil fuels, promoting industrial development and using renewable energy), so they are growing rapidly. Electric vehicles are the most promising solution for a green and clean environment when the world is more dependent on renewable energy sources. At the same time, they have also become an alternative to gasoline-powered vehicles and are promoted by policymakers worldwide as a solution to combat environmental problems and stimulate the economy. Electric vehicles are considered an extremely effective and urgent solution in the electrification of the transportation sector, and it will be an indispensable means of transportation in the future. Electric vehicles have been proven as a tool to reduce the negative effects of petroleum extraction, importation, refining and combustion. However, electric vehicles face many disadvantages compared to conventional gasoline and diesel-powered vehicles, including high initial investment costs, limited

driving range and especially a scarcity of available stations for recharging them. The popularity of electric vehicles in the future, more or less depends on the development of the infrastructure to serve this type of vehicle. Demand for electric vehicles is expected to increase over the next few years, it is still constrained by many factors especially battery cost and availability of charging station infrastructure. Investors are willing to invest in charging station infrastructure if and only if there is a sufficiently large number of electric vehicles in the network.

To attract consumers to purchase and use electric vehicles, charging station infrastructure must be deployed in convenient locations that are coordinated with each other. A power battery is one of the most important components of electric vehicles and the fundamental challenge for electric vehicles is to ensure a suitable energy storage device capable of supporting high range, fast charging and efficient driving. With an increasing number of electric vehicles on the road, the implementation of an efficient and well-planned charging infrastructure is highly desirable. In order to gradually replace traditional means of transport and put electric vehicles into use on a large scales, the construction of electric vehicle charging facilities has received strong support from governments around the world and has been focused on by scientists. As the number of electric vehicles in the city increases, the optimal location of the charging station plays an important role in ensuring the efficient operation of electric vehicles. To solve this problem, there are many design parameters related to charging stations available in the electric vehicle network that need to be considered. These parameters need to be involved to determine the optimal electric vehicle fast-charging station infrastructure. These parameters typically include: location, level, size and capacity of charging stations.

There are typically two different types of charging station configurations for electric vehicles: inter-city charging stations and intra-city charging stations. With inter-city charging stations required for electric vehicles to travel long distances, the electric vehicle will charge during the electric vehicle's journey. In contrast, for intra-city or urban charging stations with short distance travels, the electric vehicle's charging can be done when the electric vehicle finishes its journey. Different charging station locating approaches should be applied to the different charging demands.

2. Literature review

Battery electric vehicles have enjoyed fast-growing adoption in recent year, however a number of factors are restricting the development of electric vehicles [1]. One of the typical limitations is that electric vehicles take a long time to charge. DC fast charging requires around half an hour to fill up to 80% of the battery capacity, whereas AC slow charging may take 6–8 h to fully recharge the battery [2]. In addition, electric vehicle charging piles are considered to be inconvenient and insufficient in number at present [3]. Fang He et al. [4] have proposed how to optimally locate public charging stations for electric vehicles on the road network, considering drivers' spontaneous adjustments and interactions of travel and recharging decisions. This paper adopts a tour-based approach to analyze the complete tour of the driver that may consist of several trips in a pre-determined order, and assume that their drivers simultaneously decide tour paths and recharging plans to minimize the travel and recharging times while ensuring not running out of charge before completing their tours.

The location model based on flow demand was first proposed by Hodgson, who developed a Flow-Capture Location Model (FCLM) based on the maximum coverage. On this basis, Kuby considered the driving range of the vehicle and proposed

the Flow-Refueling Location Model (FRLM) [5, 6], Capacitated Fow Refueling Location Model (CFRLM) that considers capacity constraints [7] and Deviation-Fow Refueling Location Model (DFRLM) [8]. Patrick Jochem et al. [9] were extended the flow-refueling location model (FRLM) to the German autobahn, this model extension comprehends mainly the inclusion of the access distance for traffic participants to their closest network node. Traditionally, the FRLM has been formulated using a two-stage approach: the first stage generates combinations of locations capable of serving the round trip on each route, and then a mixed-integer programming is used to locate p facilities to maximize the flow refueled given the feasible combinations created in the first stage. Ismail Capar et al. [10] presented a Mixed-Binary-Integer Programming (MBIP) formula, which is an improvement of FRLM. The FRLM and flexible reformulation FRLM (FRFRLM) is used by Cheng Wang et al. [11] to solve the large-scale transportation network problem within a reasonable time.

Travel demand is the indispensable component to generate the travel routes of EVs, which provide the basic geographic information to locate charging stations. Several studies conducted the planning of EV charging stations with assumed traffic flow and network [12–14]. Jianmin Jia et al. [15] presents the approach to locate charging stations utilizing the reconstructed EVs trajectory derived from the Cellular Signaling Data, investigated the large-scale CSD and illustrated the method to generate the 24-hour travel demand for each EV. With the development of information technology, researchers started to explore the trajectory data in the locating problems of charging station on the basis of the floating vehicles, such as taxis, with Global Positioning System (GPS) devices [16]. The travel demand model can provide quick estimation of EV trips, while the trajectory data, such as the taxi GPS data, would better represent the real-world travel patterns of EVs. For locating fast-charging stations, in [17] Csaba Csiszár was presented an arc-based location optimisation method realized by using a geographic information system and greedy algorithm.

3. Charging station model description and method

From the point of view of modern city planning, the location of EVs charging stations must meet the requirements of the city transportation network layout. While from the perspective of power system planning, the location of EVs charging stations should be in accordance with the current situation in short-term as well as long-term planning of the distribution system involved. EVs charging stations must be close to load centers and respect constraints on load balance, power quality, and power supply reliability of urban. From the perspective of EVs' owners, the sites of EV charging stations should be in locations which are convenient for EV's owners and near the charging demands. Furthermore, other factors, such as the location adaptability and land price, should also be considered. Thus, the initial candidate sites of EV charging stations can be determined with the aforementioned factors properly considered.

3.1 Illustrative example and electric vehicle data collection

We first use a simple illustrative example to highlight the importance of considering the trip sequence in describing the travel and charging behaviors in a common use case of electric vehicles. In **Figure 1**, assuming network nodes (1), (2), (3), (4) and (5) are candidate locations for charging station placement. Node 1 was set as origin and node (5) was set as destination. The distance of each link are also shown
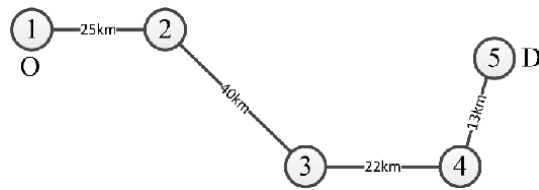
Figure 1.
An example network with a single O-D.

in the Figure. A full journey would be (1,2), (2,3), (3,4), (4,5) to reach the destination, and then back (5.4), (4, 3), (3,2), (2,1) to return to the original position. We first assume that the vehicle battery range R ¡40 km when the tour starts, there is no chance for vehicles to complete the trip between the O-D pair because vehicles cannot complete the trip (2,3). When R = 40, the charging station can choose one of two alternatives with (1,2,3,4) or (1,2,3,5). Under both solutions, electric vehicles will be charged at nodes (1), (2) and (3). If at (4) is placed a charging station, vehicles charged at (4) can reach the destination and return to (4). Next, after being fully charged at (4), the vehicle can return to the origin by charging again at (3) and (2). Similarly, we can see that when R = 50, it does not need to place the charging station at (1) anymore because a fully charged vehicale at (2) (while returning from the destination) can reach the origin and have enough electric capacity to travel to (2) when a new trip is next start. When R = 200 km, a single charging station at any node is sufficient to charge the entire journey because even after a full charge at (1), the vehicles will have enough battery capacity to reach (5) and go back to (1).

Through the above simple example, we see that the range of battery electric vehicle plays a decisive role in the distribution of charging stations on the traffic network in the city. First, if there is no charging station built at the origin then there should be at least one charging station was built within the R/2 distance to the origin node. Second, if there is a charging station was built at a location, the next charging station should be within the range R. Finally, if the vehicle range is greater than or equal to two times the path length, a single charging station at any node can provide electrical power whole journey. Thus, if there is a charging station at the origin node, the model will start the round trip with a fully charged state (State of Charge - SoC = 100%). If there is no charging station at the origin node, vehicles will start with the remaining battery SoC observed at the end of the previous trip. With the assumption of constant energy consumption and roundtrips it is secured that each trip will at least start with SoC of 50%.

The problem of placing charging stations for electric vehicles involves finding the optimal location of charging stations in the transport network so that the operating parameters of the vehicle network are least affected. Real-world vehicle travel patterns, especially for electric vehicles, provide abundant information to investigate charging demand. Nevertheless, it is impractical to adopt the travel information from all private vehicles. Therefore, GPS location data and vehicle's trace collection was considered to provide the travel information.

Besides the commute trips, the other purpose trips were also considered in this model. The purpose of activity locations was determined by the time of day. For instance, the "home" location is defined as the place with the most visits between 8 pm and 8 am for each day during the observation period, while the "work" location is defined as the place with the most visits on weekdays between 8 am and 8 pm during the observation period. The rest of the locations are regarded as the "other", such as shopping and recreation. With the activity location and purpose inferred from the vehicle's traces, the 24-hour travel demand for the electric vehicle is able to generate based on the time sequence of each activity.

3.2 Charging station model descriptions

We focus on the urban electric vehicle fast charging infrastructure planning model and investigate the positioning aspects of fast charging stations in the dense residential areas road network. It supports city trips, where charging infrastructure and BEVs both play an important role in optimizing electric vehicle charging station locations. Consider a metropolitan road network where all vehicles in the network are assumed to be battery electric vehicles. This assumption is not necessarily restrictive as the model proposed below can be easily extended to accommodate both electric and regular vehicles. Let G(N,A) be a transportation network of the electric vehicles system, where N is the set of nodes (i.e., origins, destination, junctions) and A is the set of directed links (arcs). While all nodes in N are eligible candidate sites for stations, the set of O-D nodes can be a subset of N. Thus, an unpopulated road junction can be included as a candidate site but need not be included as an O-D node. Next, given a set of O-D pairs (Q) with a nonnegative traffic flow (fq), the set of nodes visited while traveling on path q (Nq), and vehicle range (R), the FRLM is defined as the problem of locating p facilities on the network G(N,A) to maximize the total traffic flow refueled. Traffic flow between an O-D pair q is considered as refueled only when vehicles leaving the origin can reach the destination and return back to the origin without running out of fuel. Before presenting the problem defini-tion, we discuss related assumptions and present additional notation, subsequently. It is assumed that the traffic and path between the O-D pairs are known in advance. Traffic assigned a unique path is usually the shortest path determined by the Disktra algorithm [18]. From a problem formulation perspective, the proposed model can easily be extended to multiple avenues; therefore, this assumption is not restrictive. Although in some cases flow information may not be available, it can be obtained from the traffic demand matrix or through O-D estimation methods. Therefore, it is also reasonable to assume that the traffic volume is known in advance.

This work applied and extended the flow-refueling location model (FRLM) developed by Capar et al. (2013) [19, 20] as a basis. The formulation of the problem is as follows.

$$Max \left[\sum_{q \in Q} f_q y_q \right] \tag{1}$$

Subject to:

$$\sum_{i \in K^q_{j,k}} z_i \geq y_q \, \forall q \in Q, a_{j,k} \in A_q \tag{2}$$

$$\sum_{i \in N} z_i = p \tag{3}$$

$$z_i, y_q \in \{0, 1\} \forall q \in Q, i \in N \tag{4}$$

Where,

f_q: Traffic volumes on the shortest path between O-D pair q.

$a_{j,k}$: A directional arc starting from node j and ending at the node k.

A_q: Set of directional arcs on path q, sorted from origin to destination and back to origin.

$K^q_{j,k}$: Set of candidate nodes, which can refuel the directional arc $a_{j,k}$ in A_q.

M: Set of O-D nodes where $M \in N$.

N: Set of nodes which constitute the network, $N = \{1, 2, \ldots, n\}$.

p: The number of stations to be located.

q: Index of O-D pairs.

Q: Set of O-D pairs.

y_q and z_i are decision variables. =1 if the flow on path q is recharged (and feasible), and equal 0 if not; z_i =1 if a service station is built at node i, and z_i =0 if not.

$i; j; k$: Indexes for potential facilities at nodes.

The set of candidate sites accessible from the mth candidate site on a path q can be calculated from [10]:

$$
K^q_{j,k} = \begin{cases} \left[N_q \big| d^q_{j,r} \leq R, r > j \right] & \forall q \in Q, j = 1, 2, \ldots, M_q, k = 1 \\ \left[N_q \big| d^q_{j,r} < R, r > j \right] & \forall q \in Q, j = 2, \ldots, M_q, k = 0 \\ \left[N_q \big| d^q_{j,r} \leq R/2, r > j \right] & \forall q \in Q, j = 1, k = 0 \end{cases} \tag{5}
$$

Where,

$K^q_{j,k}$: is the set of candidate sites accessible from the mth candidate site on a path q.

N_q: is the set of candidate sites on a path q, now sorted in sequential order from origin to destination.

M_q: the number of candidate sites on path q beyond the origin but not within half the range R of the destination of path q, that is, in the distance interval $(0, D_q - R/2)$ on path q; if $(D_q - R/2 \leq 0)$ then M_q =0, with D_q is the length of the shortest path of an O-D pair q.

R: the range of electric vehicle.

The battery range of an EV trip represents the maximum length an EV can travel without charging, which is imposed by the battery technology. Here, "charging" is used to broadly represent battery recharge, battery exchange, or any other option to obtain a fully charged battery for the EV to continue its travel. To develop a widely applicable fast-charging station location optimisation method that considers the several relevant variables of the electromobility systems, which are as follows: trafic flow volume, the usual range of battery electric vehicle, general user demand, and especially taking into account the effect of traffic congestion; however, trafic flow volume, range of electric vehicle, and the number of EVs are the most critical parameters. The outlined method first computes static ranking variables based on statistics and spatial relations (getting and summing close attribute values). Then the selection of those candidate sites that fit the scenario goals was performed by GIS scripting.

In fast-charging infrastructure location optimization method, the set of candidate sites $K^q_{j,k}$ (Eq. (5)) was combined with the vehicle traffic data from the EV trajectory was grouped into charging demand clusters through clustering analysis to determine the optimal locations for charging stations.

3.3 Traffic congestion coefficient

The energy consumption of an electric vehicle depends not only on the distance it travels, but also on the density of vehicle traffic on the road. Traffic congestion at different times of the day plays an important part in the energy consumption of an electric vehicle. We use a traffic congestion coefficient [21] to analyze the interlink

between traffic and energy consumption. This coefficient is calculated as the ratio of actual energy consumed by an electric vehicle to cover a certain distance during particular hour of the day, to the energy consumed by it during the same period to cover the same distance on an empty road under ideal conditions. The coefficient varies between 0 to 1, with 1 reflecting an empty road condition and 0 being standstill traffic. This traffic congestion coefficient might vary from place to place. This coefficient takes into consideration the energy loss due to frequent breaking and accelerating and extra energy consumed during vehicle ignition. All other minor inefficiencies are included in this coefficient.

$$\tau = \frac{d_{act}}{d_{idc}} \qquad (6)$$

Where,

τ: Traffic congestion coefficient.

d_{act}: Actual distance travelled by an electric vehicle.

d_{idc}: Distance travelled by an electric vehicle under ideal condition.

Before scheduling the next trip for EV, its state of charge has to be assessed to evaluate whether the remaining battery level is sufficient enough to take the next trip or to travel to the nearest charging station. A general equation for the distance that an EV can travel during a certain hour of the day can be derived as [22]:

$$D = \sum_{i}^{i+1} (I_{SoC_i} - SoC_{\min}) \times R \times \tau_i \qquad (7)$$

Where,

D: Distance traveled over the operating period per day, (km).

I_{SoC_i}: Initial State of Charge of the Battery at the start of an hour, (%).

$SoC_{\min}$: Minimum State of Charge of the battery, (%).

R: Range of an electric vehicle under ideal conditions, with low traffic and no obstacles, in a single charge, (km).

τ: Traffic Congestion Coefficient.

4. Application: a case study

The geographical information of the transport system was extracted from OpenStreetMap [23]. The survey area is in Cau Giay district, Hanoi city (Vietnam). It is comprised of 166 nodes (geographical points) and approximately 500 sections of roads (straight lines connecting two nodes) with lengths ranging from a few meters up to 10 km. Office/work hours are based on the Vietnam legislation are from 8 am to 17 pm. This information is used to create the vehicles' plans.

This network has 363 arcs and 166 junctions (vertices), each of which serves as a candidate site. The OD flow of electric vehicles and the distance between the OD points in Cau Giay district during a working day are provided. There are 166 candidate sites and 5000 O-D pairs were tested in a working day. Note that because the model ensures that the return trip is rechargeable, by extension so are the round trips starting at either end. For illustration purposes, **Figure 2** shows, the transportation system indicating roads, as bold lines. In the transportation network shown in **Figure 2**, there are 166 candidate sites for the fast-charging station. These were locations where fast-charging stations can be deployed, highlighted in green, and numbered from 1 to 166. However, not all of them have been selected for
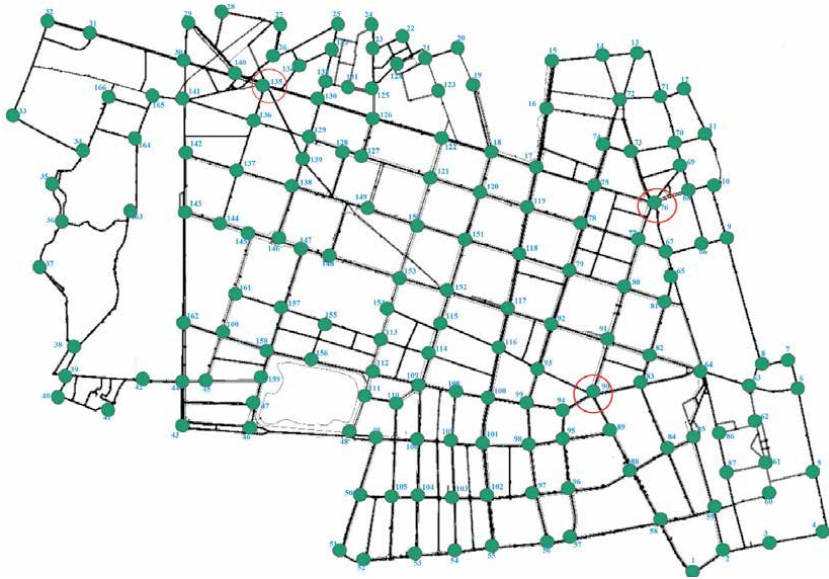
Figure 2.
Transportation network in Cau Giay District, Hanoi, Vietnam.

fast-charging station deployment. The selection depends on the vehicles traffic flow through the candidate sites' locations. Therefore, the vehicle traffic flows through nodes were evaluated, the node with high traffic will be prioritized for selection to deploy the fast-charging station. The three candidate nodes circled in red in **Figure 2** (nodes 76, 90, and 135) are nodes with high media flow as assessed through simulation. These nodes are located on arterial traffic routes which vehicles from outside enter the center and vice versa. The traffic flow profiles for nodes 76, 90, and 135 of intense vehicle movement, surveyed during the average 1-day period, was shown in **Figure 5**.

Before the traffic flow simulation, the routes of each vehicle must be defined, i.e. the shortest path between the points in their plans (Dijkstra's algorithm [18]). After each traffic flow simulation, vehicles facing traffic jams have their routes recalculated. The travel time of each vehicle depends on the length of the section of road belonging to its route and the actual velocity. All vehicles perform their routes concurrently. This process is repeated for a pre-defined number of iterations to reduce the travel times individually [24].

It can be noted from **Figure 3** that most of the trips are shorter than 35 km. Generally, the travel modes of trips consist of walking, riding a bicycle, using public transit, and using a private car. The walk and bicycle travel modes have short trip lengths mainly under 10 km. Therefore, the daily trips whose length is over 20 km are assumed to be EV trips in this survey, and these trips were used to generate basic travel demand.

The hourly travel demand was imported into SUMO (Simulation of Urban Mobility) [25] for vehicle traffic flow analysis to generate the trajectory of the EVs. Since the EVs may have multiple trips in a day, the time sequenced trajectories between different activity locations for one EV were merged to reconstruct the complete daily trip. **Figure 4** illustrates an EV trajectory example, trajectory 1 illustrates the route from home to work, while trajectory 2 illustrates a different route since the EV traveled to other purpose activity place during the trip from work to home. Both trajectory 1 and trajectory 2 make up the complete daily trip for one EV.
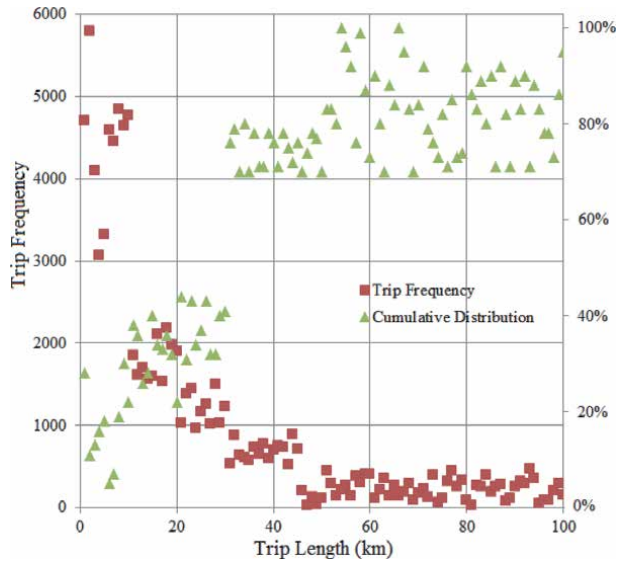
Figure 3.
Distribution of trip frequencies by cumulative trip length.

Figure 4.
An example of EV trajectory with other purpose trip.

In traffic flow analysis, we applied to the 166 nodes in the traffic network, one O-D flow contains the information about how many vehicles are driving from O to D and back in a day, a week or a certain period of time. The set of locations of nodes with high traffic is determined through simulation data analysis which are preferred locations in the fast-charging station selection.

Table 1 shows an exemplary O-D pair from node (76) to node (90). The distance from node (76) to node (90) is 32 km. The path of this O-D flow shown in the table starts at node (76) and continues all the way crossing nodes (77), (80), and (91) until it reaches node (90) and come back. Traffic flow through all nodes are evaluated. The high traffic flow sections of roads are considered to be potential fast charging stations locations. The traffic flow profiles of nodes locations (76), (90) and (135) are plotted on **Figure 5**. Each profile is unique, consequence of vehicles

From node (O)	To node (D)	Flow volumne (trips/day)	Distance (km)	Shortest path (via nodes)	Distances between nodes (76–77/77–80/80–91/91–90)
76	90	124	32	76–77–80–91–90–91–80–77-76	7/8/8/9

Table 1.
Table entries for the O-D pair 76–90.

Figure 5.
Traffic flow profiles for three roads of intense vehicle movement.

flowing towards city centre in the morning and the other way around after work. High and thin peaks indicate possible traffic jams.
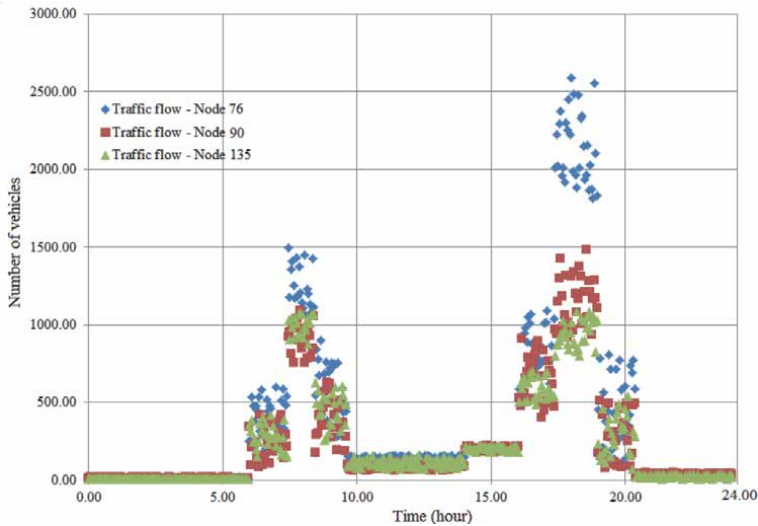
Characteristics of electric vehicles used in this survey are shown in **Table 2**. Fast-charging stations are assumed to be immediately available to EVs that arrive for charging, i.e. EVs do not wait to charge.

The travel times of EVs can be translated into cost. Thus, initially, fast-charging stations locations are selected using the most used routes of regular vehicles based on traffic flows. So, the selected fast-charging stations locations might be suitable for some EVs, it will not necessarily be aligned with the routes of all EVs. Several EVs go to charge in this fast charging stations causing traffic jams, leads to larger travel times within the region. This highlights the importance of evaluating the selected locations. Besides, traffic congestion is quite a serious problem in developing cities, especially with mixed traffic characteristics like in Hanoi. Traffic congestion affects the distance traveled by EVs, and this must be taken into account when planning electric vehicle charging stations. **Figure 6** shows the variations in the traffic congestion coefficient over the day, calculated using the Eq. (6). Survey time is from 7 am to 10 pm.

From all candidate sites, the top 18 busiest sections of roads are considered to be potential fast-charging station locations (red circle in **Figure 7**). Most of these fast-charging station locations are outside the city centre, on the northern and western areas due to the population distribution. With the fast-charging station locations identified, the traffic flow analysis is performed for each of the fast-charging station cases: from one to 18 fast-charging station locations.

Variable	Value
Battery Capacity	280 Ah
Technology	Lithium-ion
Battery on-board power	15.4 kWh
Driving Range	140 Km
Charging point power demand	50 kW
SoC_{crit}	40%

Table 2.
Characteristics (average) of EVs [26].
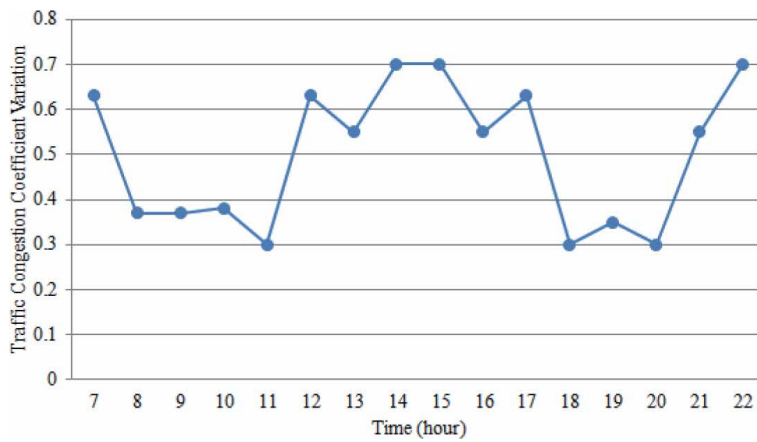
Figure 6.
Traffic congestion coefficient variation.
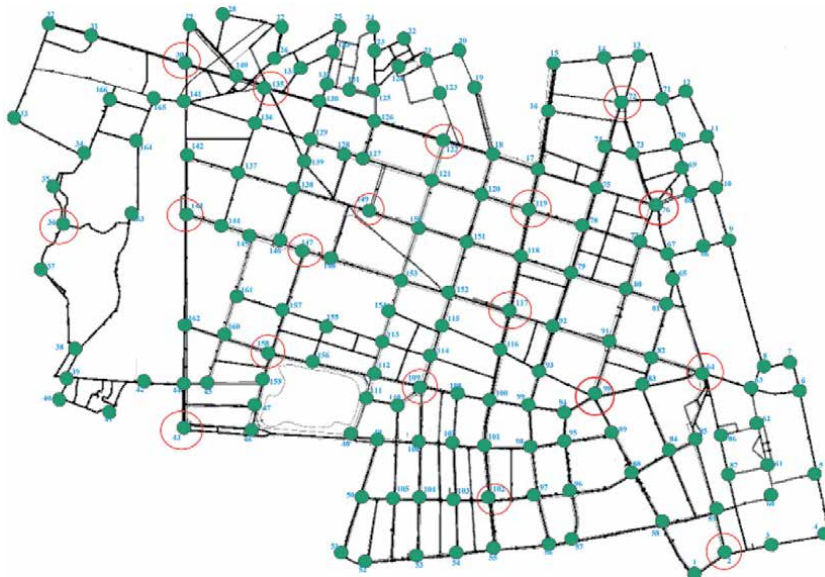
Figure 7.
Potential fast-charging station locations with high traffic flow of EVs.

5. Conclusions

The daily increase in the number of EVs brings in a big challenge for the planning of charging stations. In order to deal with the placement issues of EV charging stations, this chapter presents an optimized model for locating fast-charging stations using the EV trajectories reconstructed from simulation. In this model, battery degradation, the range of electric vehicle, traffic congestion conditions and especially vehicles traffic flow have considered to determine the optimal locations for the fast-charging station network. This is a quick and efficient way to solve the location problem of fast-charging stations. However, this approach is based on the assumption that the EVs will take the route derived from the simulation, which can be veriï¬ed. under the connected vehicle environment in the future. It can also be further improved if more research can be carried out to investigate the deployment of the local institutional and spatial settings.

Author details

Tran Van Hung
University of Transport and Communications, Hanoi, Vietnam

*Address all correspondence to: hungtv_ktdt@utc.edu.vn

IntechOpen

References

[1] Chung, S.H.; Kwon, C. Multi-period planning for electric car charging station ocations: A case of Korean Expressways. Eur. J. Oper. Res. 2015, 242, 677–687.

[2] Wu, F.; Sioshansi, R. A stochastic flow-capturing model to optimize the location of fast-charging stations with uncertain electric vehicle flows. Transp. Res. Part D Transp. Environ. 2017, 53, 354–376.

[3] Explore The Difference between Fast Charging and Slow Charging Based on the Principle of Lithium Batteries. Available online: http://www.juda.cn/news/22476.html

[4] Fang He, Yafeng Yin, Jing Zhou. Deploying public charging stations for electric vehicles on urban road networks. Transportation Research Part C 60 (2015) 227–240.

[5] Kuby, M.; Lim, S. Location of Alternative-Fuel Stations Using the Flow-Refueling Location Model and Dispersion of candidate Sites on Arcs. Netw. Spat. Econ. 2007, 7, 129–152.

[6] Upchurch, C.; Kuby, M.; Lim, S. A Model for Location of Capacitated Alternative-Fuel Stations. Geogr. Anal. 2009, 41, 85–106.

[7] Kim, J.G.; Kuby, M. The deviation-flow refueling location model for optimizing a network of refueling stations. Int. J. Hydrogen Energy 2012, 37, 5406–5420.

[8] Kim, J.G.; Kuby, M. A network transformation heuristic approach for the deviation flow refueling location model. Comput. Oper. Res. 2013, 40, 1122–1131.

[9] Patrick Jochem et al. Optimizing the allocation of fast charging infrastructure along the German autobahn. Springer-Verlag Berlin Heidelberg 2015, J Bus Econ (2016) 86:513–535. DOI 10.1007/s11573-015-0781-5

[10] Ismail Capar, Michael J. Kuby: An Efficient Formulation of the Flow Refueling Location Model for Alternative Fuel Stations. DOI: 10.1080/0740817X.2011.635175

[11] Cheng Wang et al. Electric Vehicle Charging Facility Planning Based on Flow Demand—A Case Study. https://doi.org/10.3390/su13094952. 2021

[12] Kou, L.F.; Liu, Z.F.; Zhou, H. Modeling algorithm of charging station planning for regional electric vehicle. Mod. Electr. Power 2010, 27, 44–48.

[13] Ge, S.Y.; Liang, F.E.; Hong, L.; Long, W.A. The planning of electric vehicle charging stations in the urban area.In Proceedings of the Electric Mechanical Engineering and Information Technology (EMEIT) Conference, Yichang, China, 16–18 September 2011.

[14] Wu, C.Y.; Li, C.B.; Du, L.; Cao, Y.J. A method for electric Charging infrastructure planning. Autom. Electr. Power Syst. 2010, 34, 36–39.

[15] Jianmin Jia, Chenhui Liu and Tao Wan. Planning of the Charging Station for Electric Vehicles Utilizing Cellular Signaling Data. Sustainability 2019, 11, 643; doi:10.3390/su11030643

[16] Zhang, H.; Shi, B.; Zhuge, C.; Wang, W. Detecting Taxi Travel Patterns using GPS Trajectory Data: A Case Study of Beijing. KSCE J. Civ. Eng. 2019, 1–9.

[17] Csaba Csiszár et al. Location optimisation method for fast-charging stations along national roads. https://doi.org/10.1016/j.jtrangeo.2020.102833

[18] Dijkstra, E.W.: 'A note in two problems in connexion with graphs', Numer. Math., 1959, 1, (1), pp. 269–271

[19] Capar, I., Kuby, M., Leon, V.J., Tsai, Y.-J., 2013. An arc cover–path-cover formulation and strategic analysis of alternative-fuel station locations. Eur. J. Operat. Res.227 (1), 142–151. https://doi. org/10.1016/j.ejor.2012.11.033.

[20] Treiber, M., Kesting, A.: 'Traffic flow dynamics: data, models and simulation' (Springer, Berlin, 2013)

[21] Ameya Ulhas Ghodke et al. Intra-city EV charging optimization based on vehicle usage pattern and traffic congestion analysis. 2nd International Conference on Large Scale Grid Integration of Renewable Energy, India, July 2019.

[22] Ameya Ulhas Ghodke et al. Intra-city EV charging optimization based on vehicle usage pattern and traffic congestion analysis. 2nd International Conference on Large-Scale Grid Integration of Renewable Energy, 2019.

[23] 'Map data copyrighted by OpenStreetMap contributors'. Available at https://www.openstreetmap.org, accessed 26 November 2019

[24] Treiber, M., Kesting, A.: â'Traffic flow dynamics: data, models and simulation' (Springer, Berlin, 2013)

[25] D. Krajzewicz, "Traffic simulation with SUMO–simulation of urban mobility," in Fundamentals of traffic simulation, Springer, 2010, pp. 269–293.

[26] Recargo Inc.: 'Compare Electric Cars and Plug-in Hybrids by Features, Price, Range'. Available at http://www. plugincars.com/cars, accessed 26 November 2019

Section 2

Architectures of the Electric Vehicles

A Review of Hybrid Electric Architectures in Construction, Handling and Agriculture Machines

Francesco Mocera and Aurelio Somà

Abstract

Recent regulations on pollutant emissions have pushed working machines manufacturers towards research and development efforts to meet the strict limits imposed. For a long time, the use of gas aftertreatment systems have been the most widely accepted solution to reduce the amount of pollutants produced per unit of work done. However, lower emissions limits lead to larger systems and consequently higher difficulties in vehicle integration. Thus, alternative solutions have been studied in the last years to solve the emissions problem using wisely the on-board space. Hybrid electric technologies represent a valuable alternative in this direction. In this work, a review of the current state of the art in the adoption of hybrid and electric technologies on working vehicles is proposed. Due to the high amount of application fields and concepts for special applications, the analysis focused on the three major fields which however includes most of the working machines: Construction, Handling and Agriculture. This work highlights how the requirements of each specific field, strongly affects the design of an optimal hybrid electric architectures.

Keywords: Construction machinery, Handling machinery, Agriculture machinery, Hybrid electric systems, Energy saving

1. Introduction

Worldwide, air quality is now recognized to be affected at different levels by each human activity field [1–4]. The transportation field is generally addressed as one of the major contributors to air pollution. However, residential and commercial heating as well as industrial processes [5, 6], play an important role when it comes to CO_2, NOx and particulate matter production.

Transportation covers a wide range of vehicles categories, from light/heavy duty road transport up to railway, maritime or aviation transport of people or goods. Each of them affects in a different way the total production of some pollutant elements. This is the reason why regulations have been imposed in the last years to force vehicle manufacturers to satisfy certain quality standards in terms of pollutants production. Passenger cars and light duty vehicles have now emissions levels way lower than two decades ago [7] but there is still room for further improvements. New technologies have been developed to properly treat exhaust gas and to

increase the overall vehicle efficiency. In this direction, hybrid and electric vehicles have demonstrated to be a realistic alternative solution for the near future. Lower footprints on CO2 emissions have been measured in Real Driving Scenarios with Portable Emissions Measurement Systems (PEMSs) [8] but still open is the discussion on the production of other pollutants like NOx and Particulate Matter (PM) [9]. However, proper control strategies of a hybrid power unit can reduce the overall emissions with respect to traditional thermal engine powered architectures [10].

If on one hand the electrification process is a well-established trend in automotive, there are also other fields of application where this technology is demonstrating its capabilities as alternative propulsion system for traditional powertrains. This is the case of Non-Road Mobile Machineries (NRMM), vehicles which can be used both for transportation and for heavy industrial works. According to the definition given by the EU regulations [11–15], machines can be classified as NRMMs if they are used in construction, handling, agriculture and farming, forestry and gardening. However, also railcars, locomotives and inland waterway vessels fall within the given definition, although they represent a totally different segment of vehicles. Several studies have shown that due to the high level of resources invested to improve road transports' emissions, NRMM are becoming a not negligible source of pollutants [16–18]. Historically, these machines have been equipped with high power Diesel engines known for their high efficiency, durability and reliability. However, despite of the high performance over total cost of ownership (TCO) ratio for this type of propulsion technology, diesel engines have been addressed by many researchers and non-academic authorities as one of the greatest contributors to air pollution [19, 20]. Exhaust gas aftertreatment systems have been widely used by OEM engine manufacturers to meet international emissions regulations and adopted by NRMMs' companies which use these systems to power their machines. However, the stricter regulations have become, the higher the volume required by aftertreatment systems to properly filter the exhaust gas stream from dangerous pollutant elements [21, 22]. The on-board volume required to install these filters is space dedicated only to exhaust gas elaboration. This space can be considered as a dead volume from the productivity point of view, in terms of space used to add functionalities to the machine. This is one of the reasons why several NRMM manufacturers are looking for proper alternatives to standard Diesel-based propulsion systems. Hybrid electric architectures represent a viable solution to increase the overall efficiency of the machine [23]. The hybridization level of the architecture [24, 25] optimized to the specific working cycle helps in reducing the amount of pollutant produced per Unit of Work performed [26, 27]. At the same time, the more sophisticated technology involved in these architectures allows to add extra functionalities to the machine, opening new working scenarios to the same machines.

This work aims to give an overview about the electrification process that is involving the field of working off road machines. Starting from the definition of the basic architectural topologies and their comparison within the scope of off-road heavy-duty applications, an analysis of the proposed concepts and products during the last two decades is shown. Since the NRMM classification cover a wide range of working fields, this review focused the attention on the three major working fields: Construction, Handling and Agriculture. All the considerations developed for these fields of application can be extended to other specific projects.

2. Basic hybrid and electric architectures

Vehicle electrification involves the adoption of electric and electronic components within a mechanical system to provide power as a primary source or together

with other power units [28–32]. Combining properly these components, many powertrain topologies can be obtained allowing for a high level of performance optimization. This characteristic is crucial when it comes to NRMMs, where each field of application requires special custom solutions. Thus, the knowledge of the load characteristics and of the working cycle of each type of machine is mandatory to design an optimal architectural solution [33, 34]. Looking closer at the structure of all the possible electric topologies, three basic functional schemes can be identified: full electric, series hybrid and parallel hybrid [35–39].

2.1 Battery electric vehicles

From a system point of view, a full electric architecture is the simplest solution when it comes to powertrain electrification. As shown in **Figure 1**, a full electric architecture consists of a single power source used to drive all the possible mechanical loads applied to the vehicle: the driveline, the hydraulic system and all the PTOs (Power -Take-Off s) are electrically driven. By means of an electronic converter, the electric energy previously stored in a battery pack (DC voltage and current) is regulated to provide alternate voltage and current (AC) to the installed electric motor (EM) [40, 41]. One or more electric machines can be used to optimize performance of the specific machine [42, 43].

The lower number of moving parts involved in electric machines increases the powertrain mechanical reliability when compared to Internal Combustion Engines (ICE) [44, 45]. Nowadays, power converters represent a well consolidated technology. If temperatures are well managed with proper cooling solutions, aging mechanisms related to thermal cycles can be mitigated leading to good reliability over the entire life of the vehicle [46–48]. Full electric architectures would probably replace all modern powertrains solutions if the available energy storage systems (ESSs) would perform better under different aspects [49, 50]. The most developed and promising ESSs for vehicle applications are based on Lithium-Ion Batteries (LiB) [51–54]. In terms of energy density, the ratio between 1 liter of Diesel fuel ($\approx$10.9 kWh) and 1 liter of LiB ($\approx$0.25 kWh) is currently 44. Considering an average conversion efficiency of an ICE ($\approx$30%) and of an electric system composed by an electric motor and its power converter ($\approx$85%), the gap reduces to 15 times, still too shifted in favor of thermal engines. If a proper battery pack design can satisfy the energy needs of a machine typical working cycle, still precautions are required to safely use the stored electric energy. LiB manufacturers prescribe a Safe operating Area (SoA) [55–58] in terms of temperature ranges and power limits where the chemical stability of each single cell is usually guaranteed. To operate in the SoA, a proper cooling system must be considered to avoid undesired thermal runaway phenomena which could damage permanently the entire battery pack [59–64]. Moreover, a proper Battery Management System must be designed to continuously monitor cells behavior, to avoid them to work outside their voltage limits both during charging and discharging [65–67]. This approach is necessary both for short and
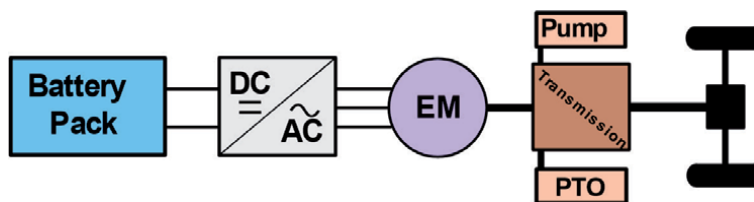

Figure 1.
Full electric architecture for a working vehicle.

long term performance analysis based on the State of Charge (SoC) [68–72] and State of Health [73–77] estimation using different modeling technique and specific testing activities [78–81]. If proper care of the battery pack working conditions is guaranteed, chemical aging mechanisms can be stemmed achieving a total life of thousands of cycles depending on the specific battery chemistry [82–84].

Battery electric vehicles represent today a promising alternative to traditional thermal powertrains. The actual state of the art LiB technology suggests that with proper design strategies this solution could be a suitable choice to propel also NRMMs. However, the actual cost [85–88] of the commercially available LiB solutions prevent from the widespread adoption of this type of architecture. New battery chemistries promise to increase the average LiB energy and power densities which could place this architectural solution closer to traditional powertrains.

2.2 Parallel hybrid electric vehicles

In a parallel hybrid electric vehicle, the power coming from an ICE and from an EM is mechanically combined to satisfy the power demand from all the different mechanical loads. This architectural solution allows to satisfy the same peak power demand of a traditional powertrain with a smaller ICE. This is called engine downsizing [89, 90] and is particularly useful when the average power demand is consistently lower than the peak power capability of the thermal engine. This is a very common problem especially in NRMMs where their multipurpose nature prescribes high power engines to satisfy all the possible loading scenario the machine might face during its operating life. Thus, the oversized engines usually work far from their nominal working conditions leading to higher fuel consumption. Using an electric machine coupled to a smaller engine, it is possible to cover the average power demand with the thermal unit and the peak power with the boost given by the electric system (**Figure 2**).

The parallel hybrid topology increases the overall efficiency of the vehicle requiring less amount of fuel per unit of work performed [91–93]. Moreover, the use of an EM and the fast response of the electronic units allow to quickly accommodate rapid variations in the external mechanical load. On the other hand, the topology intrinsically reduces the level of optimization on the ICE operating point. The mechanical connection between the engine and the external load does not allow it to work in the most efficient conditions. The rotational speed required by the application is intrinsically related to the actual engine speed so if the load requires a specific operating speed due to the limited amount of gear ratios of the transmission, the engine will rotate at a speed different from the optimal one. Thus, on this type of architecture, at least one clutch and a gearbox are required. The presence of these components increases the efforts required to integrate an external electric system on an existing vehicle layout.
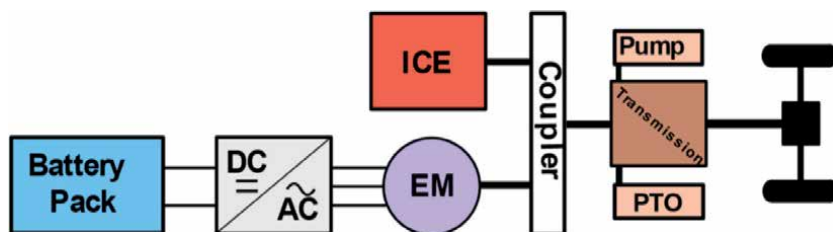

Figure 2.
Parallel hybrid architecture for a working vehicle.

2.3 Series hybrid electric vehicles

Most of the drawbacks of a parallel hybrid architecture are related to the mechanical connection between the ICE and the mechanical loads. The series hybrid topology shown in **Figure 3** addresses this problem, decoupling the ICE from the driveline. An electric generator (EG) attached to the engine is used to convert its mechanical power into electricity which can be used to charge the battery pack, to propel the vehicle using the electric motor attached to the driveline or both [94, 95]. Being mechanically free to rotate at its own speed, the engine can deliver power in its most efficient working points, most of the time in steady state conditions. This allows a high level of optimization in terms of fuel consumption depending on the specific working cycle [96–99]. A series hybrid configuration can work in different operating modes: full hybrid if all the power produced by the ICE is used to propel the vehicle (the presence of a battery pack may not be necessary); full electric if the engine is shut down and the installed battery pack is the only source of energy going into the driveline or other services (hydraulic systems, PTOs, etc.); mixed modes when both the ICE and the battery pack are involved. The last case is particularly interesting because the engine can be used both to propel the vehicle and to charge the battery pack when the power demand is lower than the current production. At the same time, the combined use of both the engine and the battery pack increases the power availability. This is the reason why the proper design of this architecture allows a higher level of engine downsizing compared to a parallel hybrid topology. As in the NRMM case, most of the time engines are oversized with respect of their standard working cycles. Thus, the availability of another source of energy allows to size the ICE for the average power demand covering the peaks with the electric system. The greater flexibility of this hybrid configuration comes at the price of a higher number of components, thus more on-board space is required. As shown in the following sections, this architecture well fit to machines where the power produced by the engine cannot be mechanically transferred by a shaft to the driveline because of the engine location inside the vehicle. Traditionally, this problem was faced using hydrostatic transmissions, which however are not very efficient if compared to electric power transmission [100–102].

2.4 Power split

Electric systems well perform when it comes to power transfer between machines that are not mechanically coupled together. This characteristic can be used to design power-split drivelines where power can be taken from a point of the transmission and used in another point with a different combination of torque and speed using combining mechanisms like planetary gear sets [103–105]. As
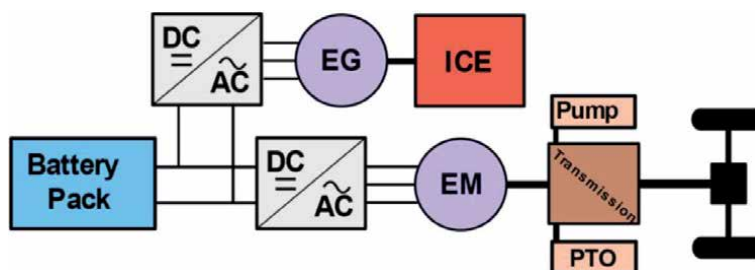

Figure 3.
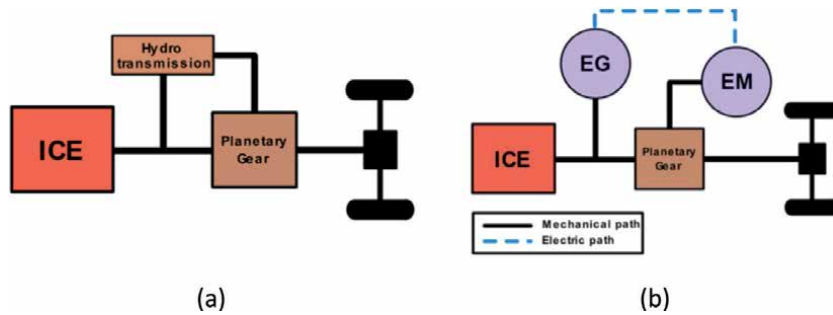*Series hybrid architecture for a working vehicle.*

Figure 4.
Hydraulic (a) and hybrid electric (b) power split configuration.

shown in **Figure 4**, this approach is not an exclusive feature of electric systems. Hydraulic power-split configurations have been widely used in the past on NRMMs achieving good performance in terms of controllability and power density. The main drawback is related to the low efficiency (60–70%) which characterize power transfer by mean of a hydraulic path. Depending on the vehicle layout thus on the distance between the pump and the hydraulic motor, the energy loss can increase consistently requiring a high-power engine to achieve the desired performance at the wheel or PTO. The same power-split capabilities can be achieved using an "Electric transmission". An electric machine actuated as a generator (EG) can take power from a certain point of the transmission (usually directly from the ICE) and transfer it by means of a DC Bus to the electric motor (EM). The higher transmission efficiency (>85%) and its stability over time allows to consider highly optimized ICE, thus better performance of the overall driveline in terms of liters of fuel per unit of work.

2.5 Hybridization factor for NRMM

The high number of possible configurations achievable with the combination of an ICE and one or more electric machines makes it difficult to classify them. Several years ago [26, 106], the definition of a Hybridization Factor (HF) given in Eq. 1 was thought to classify different hybrid solution in automotive applications.

$$HF = \frac{P_{em}}{P_{ICE} + P_{em}} \tag{1}$$

Where:
P_{em} represents the power delivered by the electric motor/motors to propel the vehicle

P_{ICE} is the nominal power of the thermal unit.

With this definition, the lower the HF value, the lower is the contribution of the electric system to the overall power output of the driveline. In **Table 1**, the typical HF classification proposed for hybrid powertrains is shown. The lower and upper bound of this classification are of course the traditional thermal powered architecture (HF = 0) where the power demand is covered by the ICE and the full electric powertrain (HF = 1) where electricity is the only on-board source of power. In between, there are all the possible combination. Micro hybrid indicates those vehicles with small electric systems (usually 12–48 V) used to help the ICE mainly

Electrification class	HF
Micro Hybrid	< 5%
Mild Hybrid	5–10%
Full Hybrid	10–50%
Parallel	50–75%
Series	
Full Electric	100%

Table 1.
Typical HF classification for automotive powertrains.

in start/stop conditions. Mild hybrid are systems with high voltage battery systems (200 V) with the aim to help the engine mainly during transient working conditions. Full hybrid configurations have high voltage electric systems (>400 V) to power the vehicle together with downsized ICE. Some battery packs have enough stored energy to propel the vehicle in full electric mode for small periods if the driveline is designed to allow it.

In the field of NRMMs, the classification problem is a more challenging task due to the large differences among the categories included in the same class. The very first problem to face when dealing with the classification of these machines is the presence of different power path and users inside the same vehicles. In a car, the power coming from the engine will be mainly used to propel the vehicle. The power required by the auxiliaries is usually a very small fraction of the engine delivery. Thus, the hybridization level of the main power user (the driveline) coincides with the one of the entire vehicle. On the other hand, in NRMMs different power path and users can usually coexists with similar power needs. Thus, the Hybridization Factor definition must consider the level of hybridization of each power user within the same machine. This is the reason why Somà et al. proposed in [24, 107] a new formulation of the Hybridization Factor (Eq. 2) specifically defined for working machines. In this definition, there is a clear distinction between the two main functions of this class of vehicles: the driving (HF_{Drive}) and working ($HF_{Loading}$) paths. Considering telescopic handlers as main case study, the authors proposed an equal distribution of the overall power demand scenario which translated into a weight factor of 0.5 to be applied to each path.

$$HF_{WM} = \frac{1}{2}\left(HF_{Drive} + HF_{Loading}\right) \qquad (2)$$

This definition overcomes the standard approach proposed in the automotive field introducing a clear distinction between what can be described as the wheel path and the other ones (hydraulic tools, implements, etc.) which instead characterize and distinguish each NRMM. If no specific information about the machine working cycle are available, it is possible to assume that on average both the driveline and the other mechanical loads have the same weight in terms of power demand for the engine.

3. Overview on powertrain electrification for NRMM

International regulations about vehicle emissions are pushing the industry and the scientific community into the investigation of new alternative powertrain

solutions for NRMM. Requirements are clearly stated in those documents and the main outcome is the same in all the categories grouped under the NRMM definition: more efficient and less pollutant machines are mandatory. Manufacturers from the construction field were already the pioneers in the electrification process back in the early 2000s. Later on, several other segments started to consider electric powertrains in all their different topologies to improve their products performance. In the following sections an overview on the actual state of the art of hybrid and electric NRMM is presented, considering both prototype concepts and production machines where available. Due to the wide range of machines falling within the EU definition, the authors propose an analysis focused on the three main categories of industrial working machines: Construction, Handling and Agriculture. These three fields will be explored in this order also because of the historical evolution that involved the electrification process. As already stated, in the construction field the first movements started back in the early 2000s. Then, several solutions were proposed in the handling field which can be considered also in between the needs that come both from the construction and agriculture field. Nowadays, also several manufacturers from the agriculture field are experiencing new electric solution which both allow to meet emissions regulations and to increase the overall productivity with the adoption of a higher level of automation.

3.1 Construction

The first scouting attempts on the real capabilities of electric powertrains in industrial vehicles were performed in the construction field as discussed in [108, 109]. First excavators [110–112], then wheel loaders and bulldozers were electrified with different hybridization levels [113–115]. Nowadays, several manufacturers are already at a mature development stage and propose to the market electrified version of their top line products. In the following sections, a review of the most mature hybrid technologies in the construction field is given.

3.1.1 Excavator

Nowadays, the most relevant excavators' manufacturers propose to the market electric and hybrid solution as alternative solution to traditional powertrains demonstrating the maturity of this technology on this specific segment. The most widely adopted architecture for this type of machines consists in a series–parallel configuration like the one shown in **Figure 5**. The ICE is coupled with an electric motor/generator machine which can supply/take power to/from the mechanical path depending on the actual working condition. The electric system usually consists also of an ESS in charge of exchanging electric power with the electric machine which actuate the swing mechanism of the machine. During the acceleration phase of the swing movement, both the ESS and the motor generator attached to the ICE can provide power to improve performance. Vice versa, during deceleration the ESS can recover the electric energy coming from the swing machine actuated as a braking element.

If on one hand the architecture is more or less the same among different players as shown in **Table 2**, the structure of the ESS is a strategic point and several solutions are available today. Manufacturers like Komatsu [115] and Hitachi [117] use Ultracapacitor based ESS in favor of a higher power capability. Other manufacturers like Kobelco [118] prefer to use LiB based ESS in favor of their higher energy density. These two solutions affect the ICE sizing at the design stage as well as the control strategy which is in charge of optimizing power delivery and fuel consumption. Currently, the tracks, the arm, the boom and the bucket are still hydraulically actuated using the fluid coming from the pump mechanically coupled to the hybrid
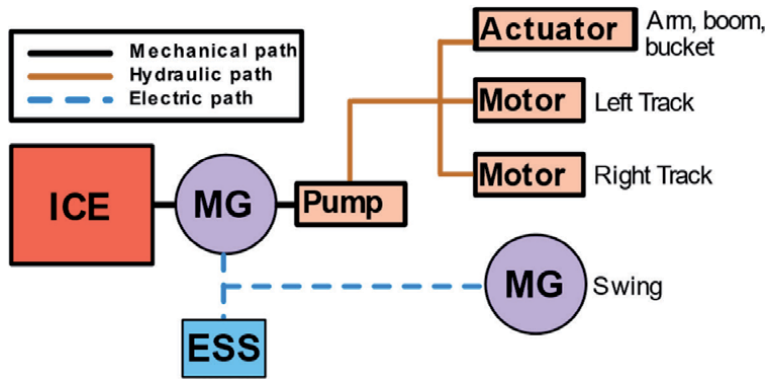
Figure 5.
Common hybrid architecture for hybrid excavators.

Manufacturer	Model	Year	Operative weight (t)	Architecture Drive-Load	ESS
Bobcat	E10e	2019	1.2	Full Electric	Li-Ion
Caterpillar	323F ZLine	2019	25.7	Full Electric	Li-Ion
Hitachi [116]	ZH210 5	2014	22	Parallel–Series	Supercapacitor
	ZH210 6	2017	22	Parallel–Series	Li-Ion
	ZE85	2019	8.5	Full Electric	Li-Ion
	ZE19	2019	1.9	Full Electric	Li-Ion
Kobelco [117]	SK210 H	2017	21	Parallel–Series	Li-Ion
	SK17SR-3E	2019	1.7	Full Electric	Li-Ion
Komatsu [115]	HB215LC-3	2018	21.5	Parallel–Series	Supercapacitor
	HB365LC-3	2016	36.5	Parallel–Series	Supercapacitor
	Mini Excavator	2019	4.7	Full Electric	Li-Ion
Volvo	EX2	2017	2.5	Full Electric	Li-Ion
	ECR25	2019	2.5	Full Electric	Li-Ion
Wacker Neuson	EZ17e	2019	1.7	Full Electric	Li-Ion
	EZ26e	2019	2.6	Full Electric	Li-Ion

Table 2.
Hybrid electric excavators.

power unit. Since no mechanical connection is present between the ICE and the mechanical loads, this architecture allows the design of energy optimization strategies focused on finding the most efficient engine working point to meet the actual power demand. It is also interesting to note how several manufacturers proposed full electric solutions for small excavators in the last years (**Table 2**). One of the main reasons for this trend is the possibility to use these full electric machines in urban area with low emission restrictions for public health reasons.

3.1.2 Wheel loaders

Among wheel loaders manufacturers', Caterpillar, Hitachi, John Deere and Volvo have demonstrated to be fully involved in the electrification process of their products (**Table 3**). Compared to excavators, the different vehicle architecture of these

Manufacturer	Model	Year	Operative weight (t)	Architecture Drive-Load	ESS
Atlas Weyhausen	AR65	2010	6.5	Parallel–Parallel	Li-Ion
Caterpillar	988 K XE	2017	52.7	Series-N/A	N/A
	906	2019	5.6	Full Electric	Li-Ion
Hitachi [119]	ZW220HYB-5B	2015	18.8	Series–Parallel	Supercapacitor
John Deere [120]	944 K	2013	54.2	Series-N/A	N/A
Kramer [121]	5055e	2016	4.1	Full Electric	Lead Acid
Mecalac	12MTX	2009	11.4	Parallel–Parallel	Li-Ion
	e12	2018	11.4	Full Electric	Li-Ion
Volvo [122–124]	L220F	2008	31	Parallel–Parallel	Li-Ion
	LX1	2017	21	Series–Parallel	Li-Ion
	LX2	2017	4.9	Full Electric	Li-Ion
	L25	2019	5	Full Electric	Li-Ion

Table 3.
Hybrid electric wheel loaders.

machines well fit with different hybrid electric solutions. As the example shown in **Figure 6a**, Hitachi used a series architecture for its ZW220HYB-5 [119]. In this architectural solution, the hybrid power unit obtained by the mechanical coupling between an ICE and an electric generator is responsible of the electric energy production that is transferred to the two electric motors installed on the front and rear axle to propel the vehicle. The adoption of two independent electric machine for the driveline allows for better traction management and energy recovery during braking. An ultra-capacitor based ESS is in charge of providing a power boost to the two electric machines attached to the driveline as well as of recovering the energy during regenerative breaking. Moreover, the extra power can help the ICE during transient conditions and in case of stationary operations.

Other interesting solution have been developed by Volvo in the last years. The Volvo L220F Hybrid was the first result of the electrification research and development program of this company [122]. The architecture developed for this machine is shown in **Figure 6b**. It was a parallel hybrid configuration with an electric motor/generator mechanically coupled to the engine shaft. The main goal of this structure was to help the engine during transient operations providing the required extra power and to allow frequent and responsive start & stop operations thanks to the higher power capabilities of the installed electric motor compared to usual engine starters. The adoption of an ultra-capacitors based ESS allowed for fast power boost during transient operations as well as for energy recovery during braking. In this case, the power unit was mechanically connected to the driveline by mean of a gearbox which split the mechanical power between the front and rear axle. Thus, the engine working point was intrinsically related to the load characteristics, limiting the degrees of freedom in energy management and optimization.

Two hybrid and electric vehicle derived from L220F Hybrid project: the LX1 (**Figure 6c**) [123] and the LX2 [124]. The former is a series hybrid configuration with no mechanical driveline. Four electric motor/generators are directly connected
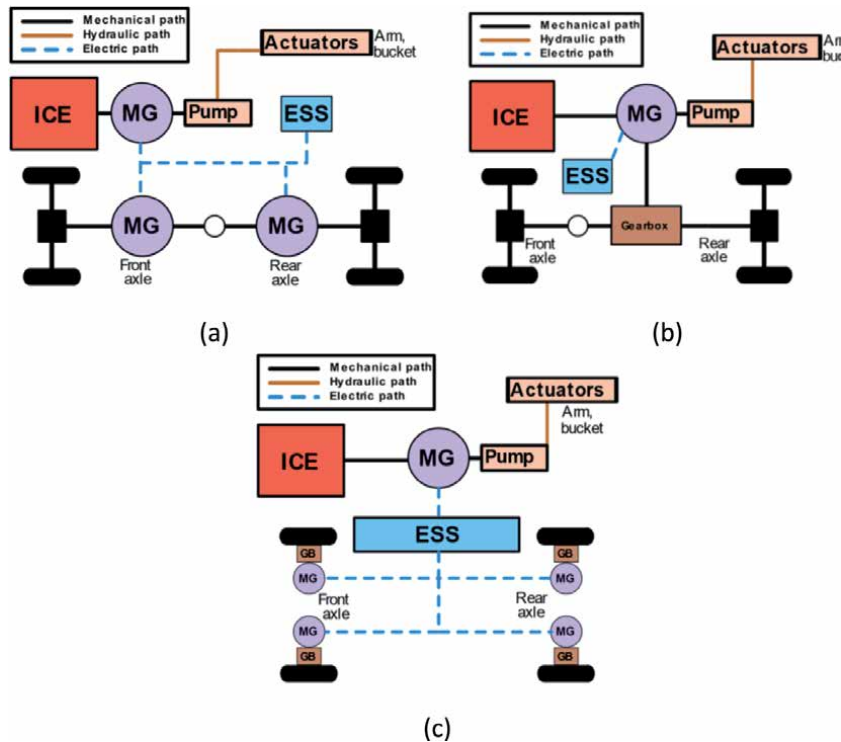
Figure 6.
Common hybrid architecture for hybrid wheel loaders: a) Hitachi ZW220HYB-5, b) Volvo L220F, c) Volvo LX1.

to each wheel and use the power coming from the hybrid power unit with the ICE coupled to an electric motor/generator. The system can rely also on a battery based ESS which guarantees a certain full electric capability to this machine. This configuration comes with a downsized Diesel engine to cover the average power demand of the working cycle using the electric system to supply extra power for the instantaneous peaks. The combination of a smaller Diesel engine and an overall higher efficiency of the driveline allows to achieve lower fuel consumption as demonstrated by the field tests performed by Volvo. On the other side, the LX2 project is a small full electric autonomous dumper designed to work for a full day without any local emission.

Another interesting solution was proposed by John Deere with the 944 K Hybrid Wheel Loader [120]. The loader proposed by John Deere is a series hybrid configuration with four electric drives, one for each wheel and a motor/generator mechanically coupled with the ICE. The main difference between this architecture and the one proposed by Volvo (LX1) is the absence of an ESS on board. The hybrid power unit (ICE+MG) is responsible for the overall electric energy production, thus for the power going to the wheels to propel the vehicle. The use of high-power brake resistors is mandatory to preserve the high voltage DC bus when the four motors must provide braking power. To regulate the overall vehicle speed during downhill, the four electric machines must provide braking torque, thus must work as generators. The electric energy coming from the vehicle kinetic energy can be dissipated as heat into the brake resistors without permanently damaging the High Voltage Bus. A controlled braking torque allows to achieve constant speed during downhill increasing productivity and reducing the operator efforts (**Figure 7**).

Other manufacturers developed hybrid wheel loaders prototypes as shown in **Table 3**. However, as demonstrated also in other NRMM segments, the
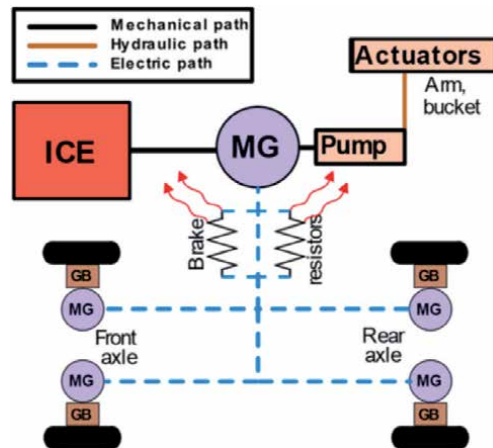
Figure 7.
Hybrid architecture: John Deere 944 K wheel loader.

improvements in LiB ESS and their lower costs are pushing manufacturers towards full electric architectures, especially for small loaders used primary in closed environments (Low Emissions Zone). Kramer, with its 5055e [121] wheel loader is the perfect example of this trend.

3.2 Handling

Handling machines can be found in several fields of application, from construction to agriculture and more in general in all freight movements between different places. These machines are characterized by a high level of versatility thanks also to the use of proper external tools. Several studies focused in finding the best way to electrify this class of machines, focusing their attention on the lifting/handling systems as well as on the driveline [24, 25, 125].

Among the manufacturers involved in the development of hybrid electric solutions for telehandlers, the Italian manufacturer Merlo was the first in proposing a hybrid electric architecture. In 2010 at Bauma (one of the most worldwide known fairs about construction machines) the company presented their first hybrid electric prototype of a telescopic handler, the P25.5. However, the project grew both technologically and architecturally leading to the gold medal received at the Agritechnica fair in 2013 thanks to the hybrid electric turbo-farmer TF40.7 [24, 25]. As shown in **Figure 8**, a series–parallel configuration was chosen to provide power both to the driveline and to the hydraulic system which actuates the telescopic boom. Looking closely the architecture, the driveline is a traditional series hybrid topology, with an electric motor/generator directly connected to the input of the gearbox which then split the power between the front and rear axles. This electric machine can receive power from the hybrid power unit (ICE+MG) designed with a smaller diesel engine or from a LiB based ESS which could also allow for some full electric operations in Low Emissions Zones. The hydraulic path is supplied by the hybrid power unit to which the pump is mechanically connected. Moreover, a specific design of the mechanical architecture allows to move the telescopic in full electric operations without the need to power on the ICE [126].

In 2018, two different manufacturers proposed two hybrid electric telescopic handlers projects: the Liebherr TL 432–7 and the Manitou MT1135. A common denominator can be found between these two projects. Both are powered by the E-Deutz power unit [127]. Deutz is an OEM manufacturer focused on diesel engines
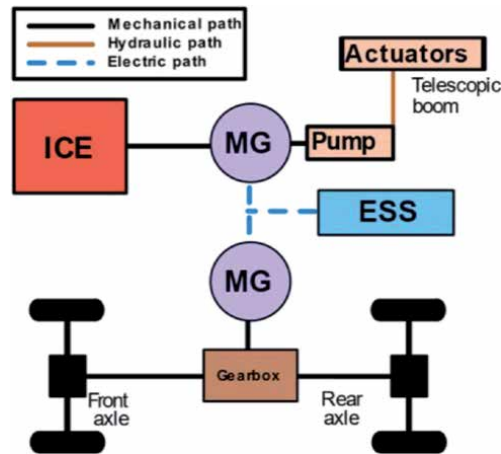
Figure 8.
Hybrid architecture: Merlo TF 40.7 telescopic handler.

for off-road applications. The E-Deutz system consists of an electric drive mechanically coupled to a diesel engine through a mechanical transmission able to disengage the connection when necessary. Like in a traditional parallel hybrid power unit, the electric motor can provide extra power to the engine during transient heavy operations using the energy stored in a LiB based ESS. The key point of this solution is the electric characteristics of the system. The ESS and the DC bus of the power line has a nominal voltage of 48 Volt. Despite the high current required to provide the nominal power of the electric machine ($\approx$20 kW for a total of 400 A), the low voltage electric system is something which also other manufacturers are looking for. Although not explicitly declared, low voltage electric systems may represent a clear trend for the near future. To the authors opinion, the higher safety level against electric shock of a low voltage system could be the key to disrupt the skepticism of the final user against the adoption of electrified technologies. However, it is clear that low voltage systems are possible only in low power application due to the high currents that could be involved in heavy duty tasks.

As shown in **Table 4**, several other interesting applications can be found in the literature as well as in some commercial product. The trend is to move towards full electric configurations which greatly simplify an architecture which is already very complex due to the high number of tasks these machines can be called to perform. Within the E-Deutz project, Liebherr and Manitou recently presented two full electric prototypes characterized by a high voltage battery pack (about 400 V). On the other hand, Manitou is developing another electrification project called Oxygen [128], a series of electric and hybrid handlers presented at Bauma fair in 2019. Small telescopic handlers have a real possibility to be fully electrified thanks to their relatively less demanding use. These machines usually operate in limited areas where the availability of charging point can reduce the range anxiety regarding full electric solutions.

Talking about small machines, the Italian manufacturer Galizia proposed a small telescopic handler the Multi 636 electric several years ago. This machine was powered by a 48 V system demonstrating that the limited amount of power which characterizes its typical workload could be satisfied by a low voltage system. Recently, also another Italian manufacturer Faresin proposed the 6.26 [129], a small full electric telehandler.

Other interesting application of electric technologies in the handling field can be found in port container handlers. Konecranes is the pioneer manufacturer in this

Manufacturer	Model	Year	Operative weight (t)	Architecture Drive-Load	ESS
Merlo [24, 25]	P41.7	2010	6.7	Series–Parallel	Li-Ion
	TF40.7	2013	7.5	Series–Parallel	Li-Ion
	Roto 45.35 S	2016	15.4	Series–Parallel	Li-Ion
Liebherr (E-Deutz) [127]	TL 432–7	2018	7	Parallel–Parallel	Li-Ion
	TL 432–7	2018	7	Full Electric	Li-Ion
Manitou (E-Deutz) [127]	MT1135	2018	8.9	Parallel–Parallel	Li-Ion
	MT1135	2018	8.9	Full Electric	Li-Ion
Manitou Oxygen [128]	MRT 2550 h	2019	18.9	Series–Parallel	Li-Ion
	MT 625 e	2019	4.7	Full Electric	Li-Ion
Faresin [129]	6.26	2018	2.6	Full Electric	Li-Ion
Galizia [130]	Multi 636	2014	6.4	Full Electric	Lead Acid
Konecranes [131]	SMV 4531 TB5 HLT	2013	45	Series–Parallel	Supercapacitor
CSV Ferrari [132]	HY-LIFT	2017	38.5	Series-Electric	Supercapacitor
XCMG	XCS45-EV	2018	45	Full Electric	Li-Ion

Table 4.
Hybrid electric handlers.

sector. The company presented in 2013 the SMV 4531 TB5 HLT reach stacker [131]. This machine consists of a series–parallel configuration where the hybrid power unit provide power both to electric driveline and to the electro-hydraulic lifting system. The adoption of an ultra-capacitors based ESS well fit to the application due to the frequent lifting operation from which is possible to recover a good amount of energy. Similarly to Konecranes, the Italian manufacturer CSV-Ferrari developed a hybrid ultra-capacitor based container handler called HY-Lift [132] which uses two electric motors to power the driveline.

3.3 Agriculture

There is a large number of machines designed to increase the mechanization level of agricultural or farming tasks. However, this variety can be simplified if the analysis is performed looking at the common needs of a farmer. The most used machines to pull and move objects as well as to transfer power to external devices are tractors. In few cases, depending on the size of the machine and on how often it needs to be used, it may be convenient to install a dedicated power unit which can be used for self-propulsion. There are several machines which can be identified in this category but the number of electric or hybrid configuration is still very small. Thus, for the purpose of this analysis agricultural machines will be divided in tractors and other agriculture machines.

3.3.1 Tractors

In a farm, tractors can be seen as a multipurpose machine able to pull trailers or external tools (properly called implements) and/or provide power to other machines or implements which do not have their own power unit. As shown in **Table 5**, the electrification process in agriculture started in the early 2000s [140–142] but, for a long time, nothing more than sporadic projects can be found. The first official concept was presented by Belarus at Agritechnica 2009: it was the Belarus/RuselProm 3022e [133, 143]. As shown in **Figure 9**, it was a full series hybrid with no external ESS. Thus, the power required to propel the vehicle and, eventually, external auxiliaries came always from the ICE. There are pros and cons to this architectural solution. The series configuration allows to disconnect the ICE from the driveline, giving higher freedom in energy management. Moreover, the adoption of an electric drive which can operate also at low rpm (down to 0) without the need of external gear reductions allows to reduce and simplify the overall layout of the gearbox. This is a big advantage especially for tractors which are well known

| Manufacturer	Model	Year	Operative weight (t)	Architecture Drive-Load	ESS
Belarus/RuselProm [133]	3022e	2009	11	Series–Parallel	N/A
Claas [134]	Arion 650	2015	6.8	N/A-Series	Li-Ion
Carraro [135]	Ibrido	2018	2.7	Parallel–Parallel	Li-Ion
Fendt [136]	e100 Vario	2017	3	Full Electric	Li-Ion
John Deere [137, 138]	6210 RE	2013	7.3	N/A-Series	N/A
	6R SESAM	2016	7.3	Full Electric	Li-Ion
RigiTrac [139]	EWD 120	2011	8	Series–Series/ NA	Li-Ion
	SK50	2018	2.4	Full Electric	Li-Ion

Table 5.
Hybrid electric tractor.
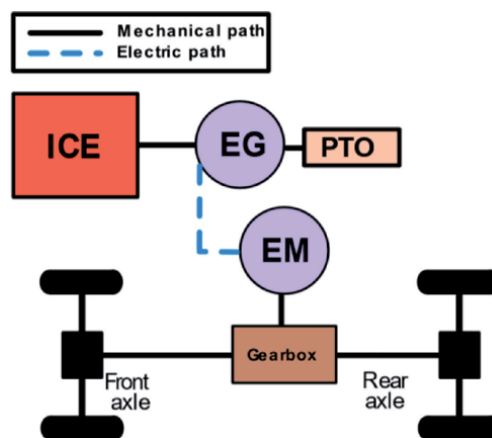
Figure 9.
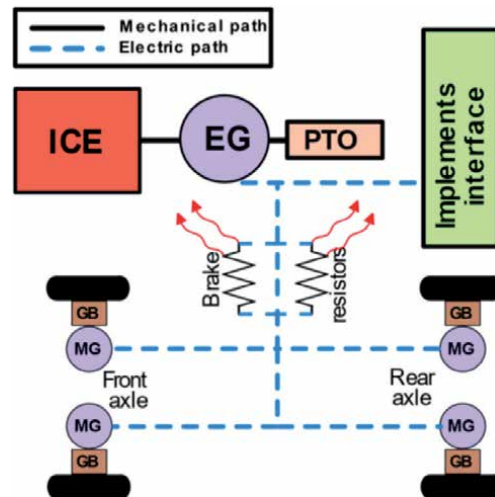*Hybrid architecture: Belarus 3022e tractor.*

Figure 10.
Hybrid architecture: RigiTrac EWD 120 tractor.

for having a large number of gear ratio to cover all the possible working needs of the user. However, some cons can be identified in this architectural solution. The absence of an external ESS does not allow any engine downsizing in favor of fuel consumption optimization. The ICE must be able to cover the peak power requirements of the traditional power unit. Moreover, the physical connection with the PTO forces the engine to rotate at fixed rotational speeds prescribed for this standard connection (usually 540 and 1000 rpm). Thus, when powering external tools, the energy management strategy cannot pursue the optimal working point for the ICE.

In 2011, the company RigiTrac presented the EWD 120 at Agritechnica 2011 [139]. As shown in **Figure 10**, the architecture proposed by the Swiss company consisted of a full series architecture where the hybrid power unit was in charge of producing the electric energy required to propel the four in-wheel motors. This was the true innovation introduced with respect of the previous concepts. In-wheel electric motors well fit to machines which have to properly transmit torque to the ground to maximize traction. The fine controllability obtainable with this driveline solution allows to achieve better performance in traction force. However, the major innovation introduced with this prototype, which is also in accordance with the most recent trends in this field, is related to the adoption of an electric interface to transfer electric power to external implements [134–137, 144]. Implements are usually powered mechanically through the PTO and/or hydraulically using the power taken by a hydraulic pump from the ICE (usually low power applications). The mechanical connection of the load to the PTO shaft, force the engine to rotate to the standard speeds discussed before. Moreover, within the implement the PTO power is split by means of complex mechanisms which convert the rotational motion to the most convenient form for the final implement users. This process is highly inefficient and usually does not guarantee a high precision in the motion transmission, especially in the long term due to wear of mechanical components. This is becoming a strong drawback now more than ever because of the need for highly accurate implements required in the framework of precision farming. The availability of an electric power source (the hybrid unit) and the possibility to easily transfer this power to electrically driven devices on the implements were the major breakthroughs of this prototype.

Following the RigiTrac example, John Deere (2013) and Claas (2015) presented two implement oriented electrified tractors. The John Deere 6210 RE [137] and the Claas Arion 650 Hybrid [134] tractor architectures can be schematically described as shown in **Figure 11a** and **b**. They consist of an electric generator connected to the ICE which convert its mechanical energy into electric energy for the high voltage implement interface. Thus, this configuration can be thought as a series configuration from the implement point of view and a traditional mechanical architecture for the driveline which is powered by the ICE.

In this architecture, the role of the energy management controllers is crucial. It is clear that an intelligent controller must be developed also on the implement side to evaluate what is the actual power demand which must be provided by the control unit on the tractor side. However, the adoption of advanced controllers on the implement is an already started process which will bring high precision tools in the next years.

More recently, full electric tractors have been presented by several manufacturers. In 2016 John Deere presented at SIMA a full electric prototype of the 6R SESAM [138], the first modern battery powered tractor. It is equipped with two electric machines which propel the transmission and the PTO. The on-board battery pack is claimed to reach 4 hours of mixed work or 55 km of transportation.

On year later, in 2017 Fendt presented the e100 Vario [136] at Agritechnica 2017, the first full electric specialized tractor. A single electric motor is used to propel both the rear and front axle (when the 4WD is required). The system is powered by a 100 kWh battery pack claimed by the manufacturer to accomplish an entire working day with a single charge.

In 2018, Carraro presented the first hybrid electric orchard tractor "Carraro Ibrido" [135] at EIMA fair. This interesting concept considered a pure parallel architecture with a motor generator coupled to a downsized ICE to provide extra power when needed. A small battery pack was considered to store the required electric energy.

At the end of 2018, John Deere presented another electric project: A full electric, cable powered, autonomous tractor [145]. There are traces of similar solutions designed in the Soviet Union when the tractor was directly connected to the grid. At that time the benefits of the technological solution were not enough to justify it. Now, with the increasing need of more efficient vehicles and with the possibility to fully automize some field operations thanks to autonomous technologies, this idea
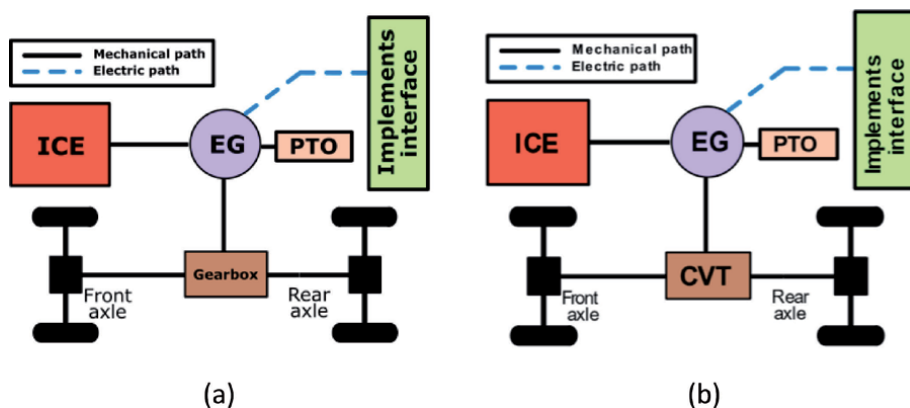

Figure 11.
Hybrid architecture: (a) John Deere 6210 RE, (b) Claas Arion 650 hybrid tractor.

Manufacturer	Model	Year	Operative weight (t)	Architecture Drive-Load	ESS
Supertino [33]	Electra 21	2017	11.9	Full Electric	Li-Ion
Siloking [147]	TruckLine e.0	2016	3.5	Full Electric	—
Kremer [150]	T4E	2013	—	Full Electric	Li-Ion
Schaeffer [148]	23-e	2017	2.3	Full Electric	Li-Ion

Table 6.
Other electric machines in agriculture.

could regain interest. The solution could increase productivity, allowing for 24/7 operations without the need of refuel the tank nor recharge the battery pack.

3.3.2 Others

Although electrification is a well-established trend on the tractor side, there are some relevant applications also on other fields of application too. Generally speaking, these machines are self-propelled machines which have been electrified to reduce emissions with respect to their traditional Diesel engine powered versions. One example is surely the vertical feed mixer by the Italian manufacturer Supertino [33, 146]. In this case, the analysis of the working cycle of these types of machines clearly demonstrates the feasibility of a full electric architecture. The limited area where usually these machines operate reduce the range anxiety because the installed power can be used mainly to conclude the cow feeding. Other manufactures have proposed similar machines. One example can be found in the German manufacturer Siloking [147], which proposes a smaller size full electric feed mixer as well.

Other electric examples can be found when looking at all the handling machines used in agriculture. Surely the Merlo TurboFarmer hybrid presented in the previous section falls also into this category. However, there is a large group of manufacturers that are electrifying small handlers and forklifts, traditionally powered by small Diesel engines. Examples in this direction are the Schaeffer 23-e and 24-e [148, 149] small, full electric loaders mainly used in farming and green maintenance applications.

Finally, it is also worth to mention the first full electric straddle tractor from the French company Kremer: the T4E [150], which aim was to reduce as much as possible the vines contamination level related to exhaust emissions and oil losses from hydraulic tools. This aspect is also an interesting point for those who wants to dedicate to biological agriculture since no contaminants will deposit on plants if full electric solutions are adopted (**Table 6**).

4. Discussion and conclusions

Nowadays, the scientific community and NRMMs manufacturers are investing time and efforts to bring electric technologies into several working field to achieve better performance in a more efficient and less pollutant way. The actual state of the art in terms of technology level is compliant with the working scenarios if the hybrid/electric architecture is properly designed according to the specific need of each application. The successful application of electric technology in Construction, Handling and Agriculture, has proved two major aspects: the suitability of electric technologies also for heavy duty tasks as well as for harsh environments and the overall lower Total Cost of Ownership (TCO) of those electrified machines

compared to their equivalent Diesel-powered versions. In the last decade, the agriculture field has demonstrated to be the most conservative and skeptic field of application. However, the advantages deriving from the electrification of traditional powertrain, the robustness of the new technologies and the strict emissions regulations are pushing manufacturers towards these new technologies. During all the fairs where these new prototypes and/or products were presented, the feedback from the respective community of interest has always been positive. This is demonstrated by all the prizes these machines have won as innovation awards. However, the technology still has difficulties when it comes to the widespread acceptance from the market. There is a mismatch between what the new machines offers and what the final user searches to satisfy their need. To the authors opinion, there are two major elements that are preventing the market acknowledgement for these machines:

- The variety of working scenario that each machine can face during its life makes it difficult to design the perfect architecture to fulfill all the requirements.

- The influences deriving from the automotive field which represent a major concern against the adoption of electric technologies in the NRMM field.

Today's design methodologies derive from standard approaches focused on Diesel technologies which do not have the problem of not having enough energy to accomplish the workday. Diesel powered machines usually comes with oversized engines to cover the peak power demands that can be faced during the whole operating life. Depending on the specific machine, these situations may happen very few times during their entire life thus the average fuel consumption would be higher just to have the capability of doing something instead of really doing it. An oversized power unit can be accepted when the re-fueling time is negligible, but it becomes a real concern for those machines where the recharging time is high and must be well programmed during the working day to minimize the costs. Moreover, an oversized electric architecture can increase a lot the final cost of the machine, thus a more optimized design must be pursued. A proper design of the electrified architecture must identify which applications can benefit from a full electric solution from those where hybrid powertrains still represent the best compromise in terms of costs/ benefits between the past and the future. It is not a case that all the major manufacturers choose hybrid solution for high power machines. They offer several advantages but with a faster way to recharge the on-board energy reservoir. Although the advantages of a full electric solution from the architectural point of view, very few cases can now fit with the current limitation of the actual state of the art of battery technologies. Moreover, the diffusion of electric vehicles in the automotive fields is showing both the advantages and the weaknesses of the actual level of technology. The common term range anxiety which addresses the not comfortable feel of the user to accomplish a certain trip with the on-board charge, is inevitably affecting also the use of electric technology in the NRMM field. Not being able to close a working task may translates in additional costs related to cumulative delays and this is not acceptable for companies which will use these new machines. However, the proper design of the HF and of the ESS can solve this problem. The higher the HF, the more the machine will rely on the installed ESS. Thus, for heavy-duty machines the best solution is to pursue a hybrid solution with a downsized Diesel engine supported by an ESS based electric system. For small machines and other special cases (depending on the specific working cycle) Full Electric solutions are perfectly possible as also demonstrated in **Figure 12**, where the trend in the last years is clearly
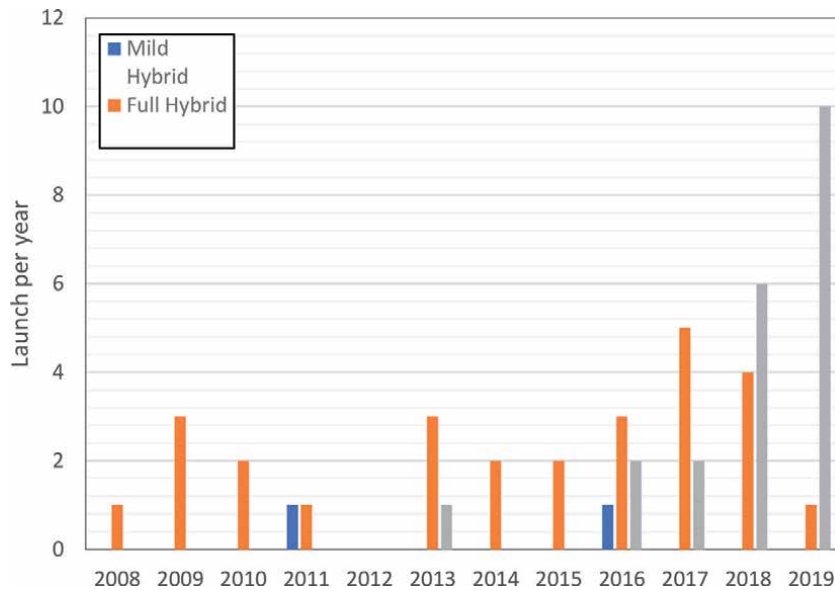
Figure 12.
Overview hybrid electric NRMM launched between 2008 and 2019.

in their favor. Moreover, new LiB technologies with higher energy density or faster charge time are approaching the market and this will solve most of the problem related to the on-board ESS. However, the future of working machines will be more and more closely related to electric technologies and at a some point the final user will have the possibility to choose between electric and non-electric powertrains with no major compromises compared to old traditional ones.

In conclusion, the proposed research review highlighted a clear trend in the scientific and industry community. Electrification is entering, at different growth rates, in different fields of working vehicles, because of the possibility to approach a common problem (reduce emission maintaining the power requirements) with the possibility to improve the technical features of the machine itself. Clearly, electric systems allow to introduce more precise control in any working feature that can translate to productivity increase. Thus, new concepts and solutions can be expected in the next years together with mass production of some consolidated technologies.

Author details

Francesco Mocera* and Aurelio Somà
Department of Mechanical and Aerospace Engineering, Politecnico di Torino, Torino, Italy

*Address all correspondence to: francesco.mocera@polito.it

IntechOpen

References

[1] Y. Van Fan, S. Perry, J. J. Klemeš, and C. T. Lee, "A review on air emissions assessment: Transportation," J. Clean. Prod., vol. 194, pp. 673-684, Sep. 2018.

[2] H. Li et al., "Analyzing the impact of heating emissions on air quality index based on principal component regression," J. Clean. Prod., vol. 171, pp. 1577-1592, Jan. 2018.

[3] E. Giannakis, J. Kushta, D. Giannadaki, G. K. Georgiou, A. Bruggeman, and J. Lelieveld, "Exploring the economy-wide effects of agriculture on air quality and health: Evidence from Europe," Sci. Total Environ., vol. 663, pp. 889-900, May 2019.

[4] Monteiro, M. Russo, C. Gama, and C. Borrego, "How important are maritime emissions for the air quality: At European and national scale," Environ. Pollut., vol. 242, pp. 565-575, Nov. 2018.

[5] Z. Wang, H. Jia, T. Xu, and C. Xu, "Manufacturing industrial structure and pollutant emission: An empirical study of China," J. Clean. Prod., vol. 197, pp. 462-471, Oct. 2018.

[6] P. W. Griffin and G. P. Hammond, "Industrial energy use and carbon emissions reduction in the iron and steel sector: A UK perspective," Appl. Energy, vol. 249, pp. 109-125, Sep. 2019.

[7] N. Hooftman, M. Messagie, J. Van Mierlo, and T. Coosemans, "A review of the European passenger car regulations – Real driving emissions vs local air quality," Renew. Sustain. Energy Rev., vol. 86, pp. 1-21, Apr. 2018.

[8] R. O'Driscoll, M. E. J. Stettler, N. Molden, T. Oxley, and H. M. ApSimon, "Real world CO2 and NOx emissions from 149 Euro 5 and 6 diesel, gasoline and hybrid passenger cars," Sci. Total Environ., vol. 621, pp. 282-290, Apr. 2018.

[9] Y. Huang, N. C. Surawski, B. Organ, J. L. Zhou, O. H. H. Tang, and E. F. C. Chan, "Fuel consumption and emissions performance under real driving: Comparison between hybrid and conventional vehicles," Sci. Total Environ., vol. 659, pp. 275-282, Apr. 2019.

[10] A. García, J. Monsalve-Serrano, R. Sari, N. Dimitrakopoulos, M. Tunér, and P. Tunestål, "Performance and emissions of a series hybrid vehicle powered by a gasoline partially premixed combustion engine," Appl. Therm. Eng., vol. 150, pp. 564-575, Mar. 2019.

[11] European Parliament - Council of the European Union, "Directive 97/68/EC." 1997.

[12] European Parliament - Council of the European Union, "Directive 2004/26/EC." 2004.

[13] European Parliament - Council of the European Union, "Regulation (EU) 2013/167." 2013.

[14] European Parliament - Council of the European Union, "Regulation (EU) 2016/1628." 2016.

[15] European Parliament - Council of the European Union, "Regulation (EU) 2018/985." 2018.

[16] Z. Samaras and K.-H. Zierock, "Off-road vehicles: a comparison of emissions with those from road transport," Sci. Total Environ., vol. 169, no. 1-3, pp. 249-255, Jul. 1995.

[17] L. Pirjola et al., "Exhaust emissions of non-road mobile machine: Real-world and laboratory studies with diesel and HVO fuels," Fuel, vol. 202, pp. 154-164, Aug. 2017.

[18] Muresan et al., "Key factors controlling the real exhaust emissions

from earthwork machines," Transp. Res. Part D Transp. Environ., vol. 41, pp. 271-287, 2015.

[19] İ. A. Reşitoğlu, K. Altinişik, and A. Keskin, "The pollutant emissions from diesel-engine vehicles and exhaust aftertreatment systems," Clean Technol. Environ. Policy, vol. 17, no. 1, pp. 15-27, 2015.

[20] T. Cao et al., "Evaluations of in-use emission factors from off-road construction equipment," Atmos. Environ., vol. 147, pp. 234-245, Dec. 2016.

[21] M. Guo, Z. Fu, D. Ma, N. Ji, C. Song, and Q. Liu, "A Short Review of Treatment Methods of Marine Diesel Engine Exhaust Gases," Procedia Eng., vol. 121, pp. 938-943, Jan. 2015.

[22] Guan, R. Zhan, H. Lin, and Z. Huang, "Review of the state-of-the-art of exhaust particulate filter technology in internal combustion engines," J. Environ. Manage., vol. 154, pp. 225-258, May 2015.

[23] A. Lajunen, P. Sainio, L. Laurila, J. Pippuri-Mäkeläinen, and K. Tammi, "Overview of Powertrain Electrification and Future Scenarios for Non-Road Mobile Machinery," Energies, vol. 11, no. 5, p. 1184, May 2018.

[24] Somà, F. Bruzzese, F. Mocera, and E. Viglietti, "Hybridization Factor and Performance of Hybrid Electric Telehandler Vehicle," IEEE Trans. Ind. Appl., vol. 52, no. 6, pp. 5130-5138, 2016.

[25] Soma', F. Mocera, F. Bruzzese, and E. Viglietti, "Simulation of dynamic performances of electric-hybrid heavy working vehicles," in 2016 Eleventh International Conference on Ecological Vehicles and Renewable Energies (EVER), 2016, pp. 1-8.

[26] T. Katrašnik, "Analytical framework for analyzing the energy conversion

efficiency of different hybrid electric vehicle topologies," Energy Convers. Manag., vol. 50, no. 8, pp. 1924-1938, Aug. 2009.

[27] T. Banjac, F. Trenc, and T. Katrašnik, "Energy conversion efficiency of hybrid electric heavy-duty vehicles operating according to diverse drive cycles," Energy Convers. Manag., vol. 50, no. 12, pp. 2865-2878, Dec. 2009.

[28] A. Emadi, M. Ehsani, and J. M. Miller, Vehicular Electric Power Systems: Land, Sea, Air, and Space Vehicles. Taylor & Francis, 2003.

[29] Emadi, Y.-J. Lee, and K. Rajashekara, "Power Electronics and Motor Drives in Electric, Hybrid Electric, and Plug-In Hybrid Electric Vehicles," IEEE Trans. Ind. Electron., vol. 55, pp. 2237-2245, 2008.

[30] Emadi, Handbook of Automotive Power Electronics and Motor Drives. CRC Press, 2017.

[31] L. Kumar and S. Jain, "Electric propulsion system for electric vehicular technology: A review," Renew. Sustain. Energy Rev., vol. 29, pp. 924-940, Jan. 2014.

[32] G. Rizzoni and H. Peng, "Hybridand and electrified vehicles: The role of dynamics and control," Mechanical Engineering, vol. 135, no. 3, pp. 10-17, 2013.

[33] F. Mocera and A. Somà, "Working Cycle requirements for an electrified architecture of a vertical feed mixer vehicle," Procedia Struct. Integr., vol. 12, pp. 213-223, Jan. 2018.

[34] F. Mocera, A. Somà, "Analysis of a Parallel Hybrid Electric Tractor for Agricultural Applications", Energies, Vol. 13(12), pp. 3055-3072, 2020.

[35] M. A. Hannan, F. A. Azidin, and A. Mohamed, "Hybrid electric vehicles and

their challenges: A review," Renew. Sustain. Energy Rev., vol. 29, pp. 135-150, Jan. 2014.

[36] M. F. M. Sabri, K. A. Danapalasingam, and M. F. Rahmat, "A review on hybrid electric vehicles architecture and energy management strategies," Renew. Sustain. Energy Rev., vol. 53, pp. 1433-1442, Jan. 2016.

[37] W. Enang and C. Bannister, "Modelling and control of hybrid electric vehicles (A comprehensive review)," Renew. Sustain. Energy Rev., vol. 74, pp. 1210-1239, Jul. 2017.

[38] Yi, B. I. Epureanu, S.-K. Hong, T. Ge, and X. G. Yang, "Modeling, control, and performance of a novel architecture of hybrid electric powertrain system," Appl. Energy, vol. 178, pp. 454-467, Sep. 2016.

[39] G. Wu, X. Zhang, and Z. Dong, "Powertrain architectures of electrified vehicles: Review, classification and comparison," J. Franklin Inst., vol. 352, no. 2, pp. 425-448, Feb. 2015.

[40] A. Matallana et al., "Power module electronics in HEV/EV applications: New trends in wide-bandgap semiconductor technologies and design aspects," Renew. Sustain. Energy Rev., vol. 113, p. 109264, Oct. 2019.

[41] G. Zhang, Z. Li, B. Zhang, and W. A. Halang, "Power electronics converters: Past, present and future," Renew. Sustain. Energy Rev., vol. 81, pp. 2028-2044, Jan. 2018.

[42] Z. Li, A. Khajepour, and J. Song, "A comprehensive review of the key technologies for pure electric vehicles," Energy, vol. 182, pp. 824-839, Sep. 2019.

[43] L. S. and L. P. P.S., "Mathematical modeling of Electric vehicles - A survey," Control Eng. Pract., vol. 92, p. 104138, Nov. 2019.

[44] F. H. Gandoman et al., "Status and future perspectives of reliability assessment for electric vehicles," Reliab. Eng. Syst. Saf., vol. 183, pp. 1-16, Mar. 2019.

[45] L. I. Farfan-Cabrera, "Tribology of electric vehicles: A review of critical components, current state and future improvement trends," Tribol. Int., vol. 138, pp. 473-486, Oct. 2019.

[46] K. Ma, U. Choi, and F. Blaabjerg, "Reliability metrics extraction for power electronics converter stressed by thermal cycles," in 2017 IEEE Energy Conversion Congress and Exposition (ECCE), 2017, pp. 3838-3843.

[47] A. Soldati, G. Pietrini, M. Dalboni, and C. Concari, "Electric-vehicle power converters model-based design-for-reliability," CPSS Trans. Power Electron. Appl., vol. 3, no. 2, pp. 102-110, 2018.

[48] Hirschmann, D. Tissen, S. Schroder, and R. W. De Doncker, "Reliability Prediction for Inverters in Hybrid Electrical Vehicles," IEEE Trans. Power Electron., vol. 22, no. 6, pp. 2511-2517, Nov. 2007.

[49] M. A. Hannan, M. M. Hoque, A. Mohamed, and A. Ayob, "Review of energy storage systems for electric vehicle applications: Issues and challenges," Renew. Sustain. Energy Rev., vol. 69, pp. 771-789, Mar. 2017.

[50] Zhang, Y.-L. Wei, P.-F. Cao, and M.-C. Lin, "Energy storage system: Current studies on batteries and power condition system," Renew. Sustain. Energy Rev., vol. 82, pp. 3091-3106, Feb. 2018.

[51] Y. Lu, X. Rong, Y.-S. Hu, H. Li, and L. Chen, "Research and development of advanced battery materials in China," Energy Storage Mater., May 2019.

[52] G. Zubi, R. Dufo-López, M. Carvalho, and G. Pasaoglu, "The

lithium-ion battery: State of the art and future perspectives," Renew. Sustain. Energy Rev., vol. 89, pp. 292-308, Jun. 2018.

[53] Scrosati and J. Garche, "Lithium batteries: Status, prospects and future," J. Power Sources, vol. 195, no. 9, pp. 2419-2430, May 2010.

[54] G. Pollet, I. Staffell, and J. L. Shang, "Current status of hybrid, battery and fuel cell electric vehicles: From electrochemistry to market prospects," Electrochim. Acta, vol. 84, pp. 235-249, Dec. 2012.

[55] M. Berecibar, I. Gandiaga, I. Villarreal, N. Omar, J. Van Mierlo, and P. Van den Bossche, "Critical review of state of health estimation methods of Li-ion batteries for real applications," Renew. Sustain. Energy Rev., vol. 56, pp. 572-587, Apr. 2016.

[56] A. Farmann and D. U. Sauer, "A comprehensive review of on-board State-of-Available-Power prediction techniques for lithium-ion batteries in electric vehicles," J. Power Sources, vol. 329, pp. 123-137, Oct. 2016.

[57] Sun, R. Xiong, and H. He, "Estimation of state-of-charge and state-of-power capability of lithium-ion battery considering varying health conditions," J. Power Sources, vol. 259, pp. 166-176, Aug. 2014.

[58] Cabrera-Castillo, F. Niedermeier, and A. Jossen, "Calculation of the state of safety (SOS) for lithium ion batteries," J. Power Sources, vol. 324, pp. 509-520, Aug. 2016.

[59] S. Ma et al., "Temperature effect and thermal impact in lithium-ion batteries: A review," Prog. Nat. Sci. Mater. Int., vol. 28, no. 6, pp. 653-666, Dec. 2018.

[60] Q. Wang, B. Mao, S. I. Stoliarov, and J. Sun, "A review of lithium ion battery failure mechanisms and fire prevention strategies," Prog. Energy Combust. Sci., vol. 73, pp. 95-131, Jul. 2019.

[61] X. Feng et al., "Investigating the thermal runaway mechanisms of lithium-ion batteries based on thermal analysis database," Appl. Energy, vol. 246, pp. 53-64, Jul. 2019.

[62] Z. Liao, S. Zhang, K. Li, G. Zhang, and T. G. Habetler, "A survey of methods for monitoring and detecting thermal runaway of lithium-ion batteries," J. Power Sources, vol. 436, p. 226879, Oct. 2019.

[63] S. Arora, "Selection of thermal management system for modular battery packs of electric vehicles: A review of existing and emerging technologies," J. Power Sources, vol. 400, pp. 621-640, Oct. 2018.

[64] J. Kim, J. Oh, and H. Lee, "Review on battery thermal management system for electric vehicles," Appl. Therm. Eng., vol. 149, pp. 192-212, Feb. 2019.

[65] R. Xiong, L. Li, and J. Tian, "Towards a smarter battery management system: A critical review on battery state of health monitoring methods," J. Power Sources, vol. 405, pp. 18-29, Nov. 2018.

[66] Q. Lin, J. Wang, R. Xiong, W. Shen, and H. He, "Towards a smarter battery management system: A critical review on optimal charging methods of lithium ion batteries," Energy, vol. 183, pp. 220-234, Sep. 2019.

[67] X. Hu, F. Feng, K. Liu, L. Zhang, J. Xie, and B. Liu, "State estimation for advanced battery management: Key challenges and future trends," Renew. Sustain. Energy Rev., vol. 114, p. 109334, Oct. 2019.

[68] M. A. Hannan, M. S. H. Lipu, A. Hussain, and A. Mohamed, "A review of lithium-ion battery state of charge estimation and management system in

electric vehicle applications: Challenges and recommendations," Renew. Sustain. Energy Rev., vol. 78, pp. 834-854, Oct. 2017.

[69] Y. Wang, Z. Chen, and C. Zhang, "On-line remaining energy prediction: A case study in embedded battery management system," Appl. Energy, vol. 194, pp. 688-695, May 2017.

[70] Z. Li, J. Huang, B. Y. Liaw, and J. Zhang, "On state-of-charge determination for lithium-ion batteries," J. Power Sources, vol. 348, pp. 281-301, Apr. 2017.

[71] V.-H. Duong, H. A. Bastawrous, and K. W. See, "Accurate approach to the temperature effect on state of charge estimation in the LiFePO4 battery under dynamic load operation," Appl. Energy, vol. 204, pp. 560-571, Oct. 2017.

[72] Locorotondo, L. Pugi, L. Berzi, M. Pierini, and G. Lutzemberger, "Online Identification of Thevenin Equivalent Circuit Model Parameters and Estimation State of Charge of Lithium-Ion Batteries," in Proceedings - 2018 IEEE International Conference on Environment and Electrical Engineering and 2018 IEEE Industrial and Commercial Power Systems Europe, EEEIC/I and CPS Europe 2018, 2018.

[73] M. S. H. Lipu et al., "A review of state of health and remaining useful life estimation methods for lithium-ion battery in electric vehicles: Challenges and recommendations," J. Clean. Prod., vol. 205, pp. 115-133, Dec. 2018.

[74] L. Zheng, J. Zhu, D. D.-C. Lu, G. Wang, and T. He, "Incremental capacity analysis and differential voltage analysis based state of charge and capacity estimation for lithium-ion batteries," Energy, vol. 150, pp. 759-769, May 2018.

[75] Z. Wang, S. Zeng, J. Guo, and T. Qin, "State of health estimation of lithium-ion batteries based on the constant

voltage charging curve," Energy, vol. 167, pp. 661-669, Jan. 2019.

[76] Y. Deng et al., "Feature parameter extraction and intelligent estimation of the State-of-Health of lithium-ion batteries," Energy, vol. 176, pp. 91-102, Jun. 2019.

[77] Locorotondo, L. Pugi, L. Berzi, M. Pierini, and A. Pretto, "Online State of Health Estimation of Lithium-Ion Batteries Based on Improved Ampere-Count Method," in Proceedings - 2018 IEEE International Conference on Environment and Electrical Engineering and 2018 IEEE Industrial and Commercial Power Systems Europe, EEEIC/I and CPS Europe 2018, 2018.

[78] Mocera, E. Vergori, and A. Somà, "Battery performance analysis for working vehicles applications," IEEE Trans. Ind. Appl., pp. 1-1, 2019.

[79] Vergori, F. Mocera, and A. Somà, "Battery Modelling and Simulation Using a Programmable Testing Equipment," Computers, vol. 7, no. 2, p. 20, Mar. 2018.

[80] Mocera, E. Vergori, and A. Soma, "Study of battery performance with hardware in the loop simulation of a working vehicle," in 2018 13th International Conference on Ecological Vehicles and Renewable Energies, EVER 2018, 2018.

[81] M. T. Arasu, Q. Ahmed, and G. Rizzoni, "Battery Discharge Strategies for Energy Management in Electrified Truck for Pickup and Delivery Application." 30-Sep-2018.

[82] P. Marques, R. Garcia, L. Kulay, and F. Freire, "Comparative life cycle assessment of lithium-ion batteries for electric vehicles addressing capacity fade," J. Clean. Prod., vol. 229, pp. 787-794, Aug. 2019.

[83] A. Sarkar, P. Shrotriya, A. Chandra, and C. Hu, "Chemo-economic analysis

of battery aging and capacity fade in lithium-ion battery," J. Energy Storage, vol. 25, p. 100911, Oct. 2019.

[84] X.-G. Yang and C.-Y. Wang, "Understanding the trilemma of fast charging, energy density and cycle life of lithium-ion batteries," J. Power Sources, vol. 402, pp. 489-498, Oct. 2018.

[85] J. T. Warner and J. T. Warner, "Overview and comparison of different lithium-ion chemistries," Lithium-Ion Batter. Chem., pp. 79-97, Jan. 2019.

[86] D. L. Wood, J. Li, and C. Daniel, "Prospects for reducing the processing cost of lithium ion batteries," J. Power Sources, vol. 275, pp. 234-242, Feb. 2015.

[87] Berg and M. Zackrisson, "Perspectives on environmental and cost assessment of lithium metal negative electrodes in electric vehicle traction batteries," J. Power Sources, vol. 415, pp. 83-90, Mar. 2019.

[88] R. E. Ciez and J. F. Whitacre, "Comparison between cylindrical and prismatic lithium-ion cell costs using a process based cost model," J. Power Sources, vol. 340, pp. 273-281, Feb. 2017.

[89] T. Katrašnik, "Hybridization of powertrain and downsizing of IC engine – A way to reduce fuel consumption and pollutant emissions – Part 1," Energy Convers. Manag., vol. 48, no. 5, pp. 1411-1423, May 2007.

[90] T. Katrašnik, "Hybridization of powertrain and downsizing of IC engine – Analysis and parametric study – Part 2," Energy Convers. Manag., vol. 48, no. 5, pp. 1424-1434, May 2007.

[91] M. U. Karaoğlan, N. S. Kuralay, and C. O. Colpan, "The effect of gear ratios on the exhaust emissions and fuel consumption of a parallel hybrid vehicle powertrain," J. Clean. Prod., vol. 210, pp. 1033-1041, Feb. 2019.

[92] A. Al-Samari, "Study of emissions and fuel economy for parallel hybrid versus conventional vehicles on real world and standard driving cycles," Alexandria Eng. J., vol. 56, no. 4, pp. 721-726, Dec. 2017.

[93] R. Finesso, E. Spessa, and M. Venditti, "Layout design and energetic analysis of a complex diesel parallel hybrid electric vehicle," Appl. Energy, vol. 134, pp. 573-588, Dec. 2014.

[94] S. Lee and J. Kim, "Implementation methodology of powertrain for series-hybrid military vehicles applications equipped with hybrid energy storage," Energy, vol. 120, pp. 229-240, Feb. 2017.

[95] Strecker, A. Hausmann, and C. Depcik, "Well to wheels energy and emissions analysis of a recycled 1974 VW Super Beetle converted into a plug-in series hybrid electric vehicle," J. Clean. Prod., vol. 68, pp. 93-103, Apr. 2014.

[96] A. Mamun, Z. Liu, D. M. Rizzo, and S. Onori, "An Integrated Design and Control Optimization Framework for Hybrid Military Vehicle Using Lithium-Ion Battery and Supercapacitor as Energy Storage Devices," IEEE Trans. Transp. Electrif., vol. 5, no. 1, pp. 239-251, 2019.

[97] M. Passalacqua, D. Lanzarotto, M. Repetto, L. Vaccaro, A. Bonfiglio, and M. Marchesoni, "Fuel Economy and EMS for a Series Hybrid Vehicle Based on Supercapacitor Storage," IEEE Trans. Power Electron., vol. 34, no. 10, pp. 9966-9977, 2019.

[98] S. Di Cairano, W. Liang, I. V Kolmanovsky, M. L. Kuang, and A. M. Phillips, "Power Smoothing Energy Management and Its Application to a Series Hybrid Powertrain," IEEE Trans. Control Syst. Technol., vol. 21, no. 6, pp. 2091-2103, Nov. 2013.

[99] M. Kim, D. Jung, and K. Min, "Hybrid Thermostat Strategy for

Enhancing Fuel Economy of Series Hybrid Intracity Bus," IEEE Trans. Veh. Technol., vol. 63, no. 8, pp. 3569-3579, 2014.

[100] M. Comellas, J. Pijuan, X. Potau, M. Nogués, and J. Roca, "Analysis of a hydrostatic transmission driveline for its use in off-road multiple axle vehicles," J. Terramechanics, vol. 49, no. 5, pp. 245-254, Oct. 2012.

[101] J.-S. Chen, "Energy Efficiency Comparison between Hydraulic Hybrid and Hybrid Electric Vehicles," Energies, vol. 8, no. 6, pp. 4697-4723, May 2015.

[102] A. Macor, A. Benato, A. Rossetti, and Z. Bettio, "Study and Simulation of a Hydraulic Hybrid Powertrain," Energy Procedia, vol. 126, pp. 1131-1138, Sep. 2017.

[103] W. Wang, R. Song, M. Guo, and S. Liu, "Analysis on compound-split configuration of power-split hybrid electric vehicle," Mech. Mach. Theory, vol. 78, pp. 272-288, Aug. 2014.

[104] W. Yang, J. Liang, J. Yang, and N. Zhang, "Investigation of a Novel Coaxial Power-Split Hybrid Powertrain for Mining Trucks," Energies, vol. 11, no. 1, p. 172, Jan. 2018.

[105] Pei, X. Hu, Y. Yang, X. Tang, C. Hou, and D. Cao, "Configuration optimization for improving fuel efficiency of power split hybrid powertrains with a single planetary gear," Appl. Energy, vol. 214, pp. 103-116, Mar. 2018.

[106] Y. Liao, T. R. Weber, and D. P. Pfaff, "Modelling and analysis of powertrain hybridization on all-wheel-drive sport utility vehicles," Proc. Inst. Mech. Eng. Part D J. Automob. Eng., vol. 218, no. 10, pp. 1125-1134, 2004.

[107] A. Somà, "Trends and Hybridization Factor for Heavy-Duty Working Vehicles," in Hybrid Electric Vehicles, 2017.

[108] X. He and Y. Jiang, "Review of hybrid electric systems for construction machinery," Autom. Constr., vol. 92, pp. 286-296, Aug. 2018.

[109] Wang, Z. Yang, S. Liu, Q. Zhang, and Y. Han, "A comprehensive overview of hybrid construction machinery," Adv. Mech. Eng., vol. 8, no. 3, p. 1687814016636809, 2016.

[110] Q. Chen, T. Lin, and H. Ren, "Parameters optimization and control strategy of power train systems in hybrid hydraulic excavators," Mechatronics, vol. 56, pp. 16-25, Dec. 2018.

[111] Kim, S. Yoo, S. Cho, and K. Yi, "Hybrid control algorithm for fuel consumption of a compound hybrid excavator," Autom. Constr., vol. 68, pp. 1-10, Aug. 2016.

[112] Wang, C. Guan, S. Pan, M. Zhang, and X. Lin, "Performance analysis of hydraulic excavator powertrain hybridization," Autom. Constr., vol. 18, no. 3, pp. 249-257, May 2009.

[113] Oh, H. Kim, K. Ko, P. Kim, and K. Yi, "Integrated wheel loader simulation model for improving performance and energy flow," Autom. Constr., vol. 58, pp. 129-143, Oct. 2015.

[114] X. Zeng, N. Yang, Y. Peng, Y. Zhang, and J. Wang, "Research on energy saving control strategy of parallel hybrid loader," Autom. Constr., vol. 38, pp. 100-108, Mar. 2014.

[115] Wang, L. Liu, G. Zheng, X. Liu, and X. Zhao, "Study of Two-Motor Hybrid Bulldozer," in SAE Technical Paper 2014-01-2376, 2014.

[116] Komatsu, "Komatsu hybrid excavators." [Online]. Available: https://www.komatsu.com.au/innovation/komatsu-hybrid-excavators/.

[117] Hitachi Construction Europe, "Hitachi Hybrid." [Online]. Available: https://www.hitachicm.eu/hybrid/.

[118] Kobelco Construction Machinery Europe, "KOBELCO HYBRID SK210HLC-10." [Online]. Available: https://www.kobelco-europe.com/innovation/hybrid/.

[119] Hitachi Construction Machinery, "Hitachi unveils hybrid wheel loader at Intermat," 2015. [Online]. Available: https://www.hitachicm.eu/press-center/hitachi-unveils-hybrid-wheel-loader-at-intermat/.

[120] John Deere, "John Deere 944K Hybrid Wheel Loader." [Online]. Available: https://www.deere.com/en/loaders/wheel-loaders/944k-wheel-loader/.

[121] Kramer, "The Kramer 5055e - in a vehicle class of its own." [Online]. Available: https://www.kramer-online.com/en/discover-kramer/zero-emission/the-kramer-5055e/?gb=1.

[122] R. Filla, "Alternative system solutions for wheel loaders and other construction equipment," in 1st CTI Forum Alternative, Electric and Hybrid Drive Trains, 2008.

[123] Volvo Construction Equipment, "LX1 prototype hybrid wheel loader delivers around 50% fuel efficiency improvement during customer testing," 2017. [Online]. Available: https://www.volvoce.com/global/en/news-and-events/press-releases/2017/lx1-prototype-hybrid-wheel-loader-delivers-50-percent-fuel-efficiency-improvement/.

[124] Volvo Construction Equipment, "Volvo CE unveils electric compact wheel loader concept," 2018. [Online]. Available: https://www.volvoce.com/global/en/news-and-events/press-releases/2018/volvo-ce-unveils-electric-compact-wheel-loader-concept/.

[125] P. Immonen et al., "Energy saving in working hydraulics of long booms in heavy working vehicles," Autom. Constr., vol. 65, pp. 125-132, May 2016.

[126] A. Somà, G. Renato, and A. Merlo, "Electrohydraulic hybrid work vehicle," US9248731B2, 2011.

[127] DEUTZ, "Fast-forwarding e-competence," 2018. [Online]. Available: https://www.deutz.com/en/e-deutz/.

[128] E. Guide, "Manitou presents electrified solutions across its product lineup," 2019. [Online]. Available: https://www.heavyequipmentguide.ca/article/30595/manitou-presents-electrified-solutions-across-its-product-lineup.

[129] Faresin, "Telehandler 6.26 Full Electric," 2018. [Online]. Available: https://www.faresindustries.com/eng/products/telescopic-handlers/small-range/full-electric/6.26-full-electric.

[130] Galizia, "MULTIS 636 - 6t - electric." [Online]. Available: http://www.galiziagru.com/gru_en.php?id=19.

[131] Konecranes, "Hybrid reach stacker: first in the industry!," 2013.

[132] CSV-Ferrari, "Hy-Lift." [Online]. Available: https://www.cvsferrari.it/products/hybrid-empty-container-handler/.

[133] Wilson, "Belarus goes electric," 2018. [Online]. Available: https://www.farmweekly.com.au/story/5670924/belarus-goes-electric/%0D.

[134] S. Tetzlaff, "Schnittstell enübergreifende Elektrifizierung und Funktionen von Traktor und Anbaugerät," LANDTECHNIK, vol. 70, no. 5, pp. 203-217, 2015.

[135] Carraro, "The Carraro 'Ibrido' tractor has received two awards from FederUnacoma," 2018. [Online].

Available: https://www.carraro.
com/en/media-news/news/post/
il-trattore-carraro-ibrido-premiato-
due-volte-da-federunacoma.

[136] Fendt, "Fendt e100 Vario: The
battery-powered compact tractor," 2017.
[Online]. Available: https://www.fendt.
com/int/fendt-e100-vario.

[137] J. Stoss, J. Sobotzik, B. Shi, and E.
R. Kreis, "Tractor Power for Implement
Operation — Mechanical, Hydraulic,
and Electrical: An Overview," in
Agricultural Equipment Technology
Conference, 2013, pp. 1-25.

[138] AgriLand, "Electric John Deere
tractor runs for 4 hours on a
charge," 2017.

[139] RigiTrac, "RigiTrac EWD 120 -
Diesel Electric." [Online]. Available:
https://tu-dresden.de/ing/
maschinenwesen/int/ast/ressourcen/
dateien/forschung/files/Datenblatt_
Rigitrac.pdf?lang=de.

[140] P. Moreda, M. A. Muñoz-García,
and P. Barreiro, "High voltage
electrification of tractor and
agricultural machinery – A review,"
Energy Convers. Manag., vol. 115,
pp. 117-131, May 2016.

[141] A. Ghobadpour, L. Boulon, H.
Mousazadeh, A. S. Malvajerdi, and S.
Rafiee, "State of the art of autonomous
agricultural off-road vehicles driven by
renewable energy systems," Energy
Procedia, vol. 162, pp. 4-13, Apr. 2019.

[142] Hammar, "Prospects on Diffusion
of Agriculture Hybrid Tractors
Equipped with On Board High Voltage
System," 2015.

[143] S. Florentsev, D. Izosimov, L.
Makarov, S. Baida, and A. Belousov,
"Complete traction electric equipment
sets of electro-mechanical drive trains
for tractors," in 2010 IEEE Region 8
International Conference on

Computational Technologies in
Electrical and Electronics Engineering
(SIBIRCON), 2010, pp. 611-616.

[144] Hahn, "High Voltage Electric
Tractor-Implement Interface," SAE Int.
J. Commer. Veh., vol. 1, no. 1, pp.
20084.01-2660, Oct. 2008.

[145] EXPO, "John Deere develops fully
electric, autonomous tractor," 2019.
[Online]. Available: https://www.
ivtinternational.com/news/agriculture/
john-deere-develops-fully-electric-
autonomous-tractor.html.

[146] Supertino, "ELECTRA carro trincia
miscelatore verticale semovente 100%
elettrico."

[147] Siloking, "Innovation: 100%
electric self-propelled feed mixer with
external loading." [Online]. Available:
https://www.siloking.com/en/
news/51-innovation-100-electric-self-
propelled-feed-mixer-with-
external-loading.

[148] Schäffer, "Schäffer 23e: World's
first yard loader with lithium-ion
battery." [Online]. Available: https://
www.schaeffer-lader.de/en/schaeffer/
news/schaeffer-23e-worlds-first-
yard-loader-lithium-ion-battery/.

[149] Schäffer, "Schäffer 24e: World's
first wheel loader with lithium-ion
battery." [Online]. Available: https://
www.schaeffer-lader.de/en/schaeffer/
news/schaeffer-24e-wheel-loader-
lithium-ion-battery/%0D.

[150] Kremer, "T4E - Straddle Electric
Tractor." [Online]. Available: www.
kremer-energie.fr/en/pages/technical-
specificities-of-t4e.html%0D.

Chapter 5

High Power Very Low Voltage Electric Motor for Electric Vehicle

Daniel Matt, Nadhem Boubaker, Mourad Aitakkache, Philippe Enrici, Jean-Jacques Huselstein and Thierry Martire

Abstract

Electric vehicles are often designed in the same way as their conventional counterparts based on the internal combustion engine, they are heavy machines for comfort and safety reasons, and increasingly powerful. Under these conditions, in order to simplify the motor electrical supply system by reducing the current levels, the voltage chosen for the battery is very high and can go up to 700 V. However, for many applications where the power is relatively low (< 30 kW per motor), it can be more beneficial to size the system at very low voltage (< 60 V). This approach allows to overcome many constraining safety requirements and also to use off-the-shelf components (motor controllers, connectors, etc.) that are more easily available on the market in this voltage range. There are also many regulatory provisions that may require to stay within this voltage limit. This article presents a variety of very low voltage motorisation solutions with a required power up to 100kW. They use two complementary approaches. The first is to implement an original permanent magnet synchronous machine technology with an optimised armature winding for low voltage operation. The second is based on power splitting where the electrical machine being designed to be driven by multiple controllers. Many examples of low-voltage motorised vehicles (sporty vehicle, tractor, re-motorised automobile, etc.) are illustrated in this article.

Keywords: Electric Vehicle, Very Low Voltage, Synchronous Machine, Permanent Magnet, Solid Bar Winding, Power Splitting

1. Introduction

For the sake of safety, the standards and regulations limit the supply voltage level for the electric vehicles drive system. The standards dealing with the very low voltage systems (VLV) provide a general guidance. For example, the 2014/35/UE European Directive for the CE marking fixes the voltage level at 75 V DC, hence, in practice this could be the choice for the battery voltage.

Furthermore, in the automotive realm, the European Regulation R100 concerning the approval of vehicles with regard to specific requirements for the electric powertrain, has even reduced the maximum voltage level to 60 V (Class A). This range of voltage will therefore ease the design constraints and the operational maintenance of the vehicle. The 60 V is generally considered as the reference level of VLV for electric vehicles.

At this low voltage range, there is a large choice of commercially available off-the-shelf components for the power electronics needed to drive the electric motor, regardless its technology, DC motor, synchronous motor or induction motor, though knowing that the permanent magnet synchronous motors are emerging as one of the best candidate to dominate the market of powertrain electrification.

However, at low voltage, when the level of the required electrical power reaches a certain threshold, which is around 30 kW, the availability of the power electronics components becomes considerably limited given the high current level to be handled by the controller, which is greater than 500A at a battery voltage of 60 V. Indeed, this poses very challenging constraints on the design of the power modules where the high current gets closer to the switching capability limit of the transistors available on the market (very low voltage MOS technology). We will be detailing the challenges and the associated solutions related to this topic in a later section of the chapter.

The technology outlined in this chapter, where many validation prototypes are presented, brings some original solutions to the design of very low voltage electric powertrains, even at high power level. Many electric vehicles presented in this chapter involving a power as high as 100 kW.

First of all, we will discuss the design techniques of an electric motor being optimised to operate at very low voltage. Afterwards, several techniques of power distribution have been described, which enables the required total electrical power to be shared between several controllers. Finally, we present an overview of the limits of feasibility of the power electronics that would be required to drive electric motors at very low voltage, based on the current available technologies of the semiconductors components.

2. Very low voltage electric motor

2.1 Solid bar winding

When an electric motor is operating at very low voltage, there is an opportunity to optimise its winding in order to significantly enhance its performance. Conventionally, the windings of electric motors are based on an enamelled round wire (loose random conductors), as illustrated in the **Figure 1b**. In this case, the copper
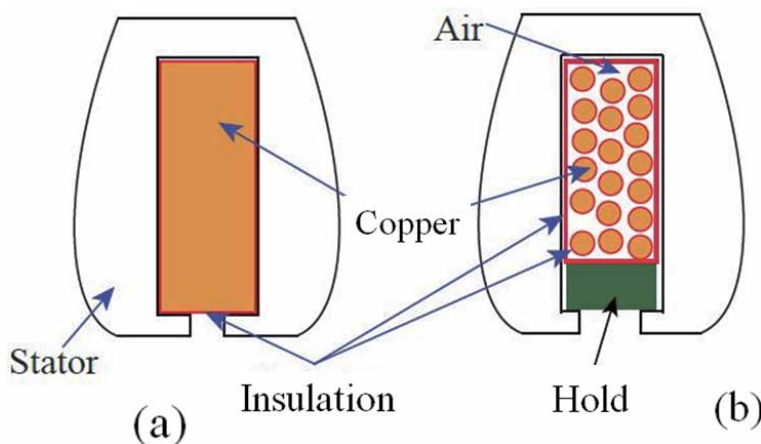

Figure 1.
(a) Solid bar winding vs. (b) Round wire winding.

fill factor inside the stator slot is very poor, where, unless relying on non-conventional manufacturing processes (segmentation, etc.), only around 40% can be achieved in the best case (pure copper CSA/naked slot area), it can be even less than 30% when considering very small size motors with tiny slots.

At very low voltage, the conductors inside the slot are connected in parallel where the number of turns is inherently very low. In the case of a winding design with one turn per slot, which is often the case at VLV, it appears to be more judicious to replace the multi-strand conductor with a single solid copper bar adjusted to the slot dimensions, as illustrated in the **Figure 1a**. In the latter case, the copper fill factor inside the slot can reach approximately 80%, which consequently doubles, even triples, the copper volume for a given motor size.

At a constant copper loss and a given slot cross sectional area, the relationship between the RMS current, I_b, in the solid bar conductor and the total RMS current, I_f, in the equivalent slot wound with multi-strand round conductor is as follows:

$$I_b = I_f.(\sigma_{rb}/\sigma_{rf})^{1/2} \tag{1}$$

The coefficients σ_{rb} and σ_{rf} represent the copper fill factor inside the slot with solid bar conductor and with multi-strand round conductor, respectively. With the 80% fill factor in the first case and 35% in the second one, the current carried by the solid bar conductor is 50% higher, and, consequently, the output torque of the motor increases in the same proportion.

The **Figure 2** illustrates how difficult it is to perform a high quality winding with loose round wire. It can be easily noticed that a non-negligible part of the copper is located outside the active part of the motor (i.e. stator). This bulky copper outside the stator slots increases the volume, the weight and the loss of the machine. All these drawbacks are addressed with the use of a solid bar conductor.

Figure 2.
Electric motor end-windings wound with loose round wires.

Figure 3.
Solid bar winding, distributed winding.

Figure 4.
Solid bar winding, wave concentrated winding.

Figures 3 and **4** illustrate some of our products made using a solid bar winding. It can be easily seen that the useless copper at the end-windings (overshooting the stator core pack) is less bulky and well controlled. These proposed winding techniques are most convenient for low voltage electrical machines.

The distributed winding shown in **Figure 3**, with one slot per pole and per phase, is well suited to medium range power machines (a few tens of kW) operating at few hundreds Hz electric frequency [1–3]. The structure shown in **Figure 4** is more original where the phases are wound around the tooth (wave concentered winding) and grouped in separate sectors [1, 4, 5], without phase overlaps at the end-windings of the machine. This structure is rather well suited for small electrical machines which can then operate at very high frequency (up to 2000 Hz), the resulting winding is very compact.

This technique is not commonly used in practice due to the fact that the solid bars are prone to very high AC copper loss (under alternating regime) which can be much higher than the DC ohmic loss.

Additional losses in massive conductors can be prohibitive, but a detailed study of these phenomena [1, 4] shows that the advantages of the approach largely outweigh the disadvantages if the winding is appropriately designed [1, 3, 4].
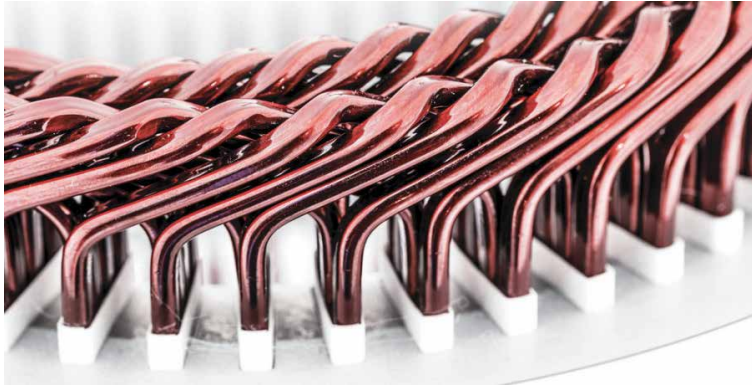
Figure 5.
Hairpin winding (courtesy of special machine tool company).

Paradoxically, the concept can be perfectly applied, as we will see, to high pole count electric motors operating at high frequency, which is the case for all machines with high power density for embedded applications.

Many industrial motor manufacturers, especially for electric vehicles, are using the solid bar copper winding, in particular via the "hairpin" technique consisting in a "pin" forming that can ease the overlapping of conductors at the end-windings (cf. **Figure 5**), but the overall design approach of these machines remains conventional, especially because it uses several conductors per slot. The approach presented in this chapter is distinguished by the use of a single solid bar per slot (one turn per slot), which allows to optimise many parameters and to reach unmatched level of compactness, for high power electric motors operating at very low voltage.

In summary, the main pros in using solid bars are:

- Enhanced copper fill factor (80% filling instead of 40%).

- The iron-copper thermal resistance is reduced.

- The slots opening width can be very small which increases the flux density in the air gap and decreases the cogging torque and eventually the torque ripple.

- The copper overhangs are very compact and controlled.

- The winding manufacturing process is simplified and can be easily automated.

- The machine is more robust and reliable.

And the main cons are:

- Higher copper loss density

- The connection of the copper bars in order to form the whole winding is more complex.

2.2 Additional losses in the solid copper bars

In order to be able to effectively implement the technique of winding with single bar per slot, it is mandatory to fully control the additional copper losses associated with the operation at high electrical frequency.

The different phenomena related to alternating flux density inside the copper yielding to excessive loss are well describes in the literature [6, 7], however we recall here the two main ones.

In order to quantify the loss increase, the k_{AC} coefficient is introduced, which is the ratio of the total AC copper loss, P_{AC}, to the DC copper loss, P_{DC}, in the winding, at given current:

$$k_{AC} = P_{AC}/P_{DC} \qquad (2)$$

The best known phenomenon causing these additional losses is called "skin effect", it appears in any electrical conductor carrying an alternating current. The skin effect tends to push the current back to the periphery of the conductor, as shown in the following **Figure 6**.

The current density, J, in a round conductor, as a function of the distance from the periphery, r, in sinusoidal regime, is expressed by the following relationship:

$$J(r) = J_0 . e^{-\frac{r}{\delta}} . \cos\left(\omega t - \frac{r}{\delta}\right) \qquad (3)$$

where δ represents the skin depth at a conductivity σ of the conductor:

$$\delta = \frac{1}{\sqrt{\sigma \mu_r \mu_0 \pi f}} \qquad (4)$$

The current density at the skin depth is roughly equal to 37% of its value at the surface, while it is only equal to 5% at three times δ.

In the case of a rectangular conductor the relationships of the skin effect are more complex. The following equation [1, 6] is valid for both cases round conductor and rectangular conductor, and allows to precisely quantify the increase in copper loss due to the skin effect:

$$K_{AC} = \sqrt[6]{\left(\frac{3}{4}\right)^6 + \left(\frac{S}{p\delta}\right)^6 + \frac{1}{4}} \qquad (5)$$
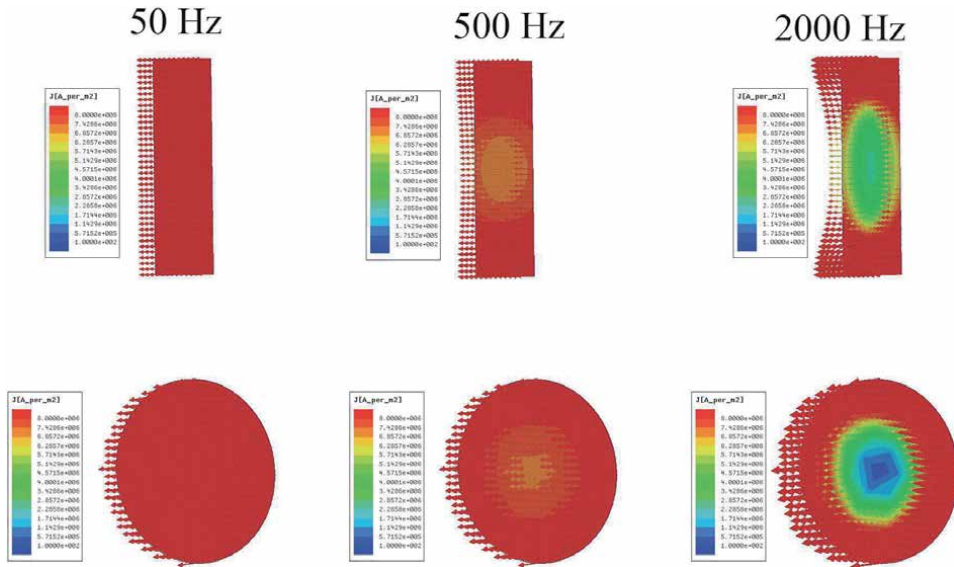
Figure 6.
Current density distribution in two conductors having the same cross-section with round and rectangular shape at different frequencies [1].

S and p respectively represent the cross section area and the perimeter of the conductor.

Table 1 gives the values of K_{AC} for different bar shapes (used in the prototypes presented later) and different frequencies. The dimensions of the bar are defined in **Figure 7**.

According to the **Table 1**, in the worst case scenario, the increase in copper loss due to the skin effect is less than 1%, so this phenomenon is not significant at the considered frequencies.

The second observed phenomenon causing excess copper loss is known as field effect or inductance effect. Unlike the skin effect, it only takes place in the copper volume surrounded by a magnetic circuit (stator). This phenomenon is depicted in **Figure 8**. In this case, the additional loss is due to the transverse flux (slot leakage flux) produced by the armature current, which closes in the slot width (t_{enc}), creating induced currents in the solid bar which will lead to an uneven current density distribution, being much higher in the lower part (near the slot opening) than in the upper part of the solid bar.

The field effect phenomenon is the main cause of increased losses, where the K_{AC} coefficient can be greater than 4 if it is not well controlled, which would cancel out most of the benefits introduced by the use of the solid bar winding.

The coefficient K_{AC} related the field can be precisely calculated using the following analytical relationship [1, 7]:

$$k_{AC} = \frac{h_{bar}}{\delta} \sqrt{\frac{t_{bar}}{t_{enc}}} \qquad (6)$$

#	Dimensions h_{bar} x t_{bar} (mm)	Frequency (Hz)	δ (mm) à 100 °C	K_{AC}
1	4x5	800	2,7	1,003
2	3x5	1666	1,9	1,009
3	8x4	800	2,7	1,009
4	8x3	133	6,6	1

Table 1.
Skin effect for different copper bar dimensions.
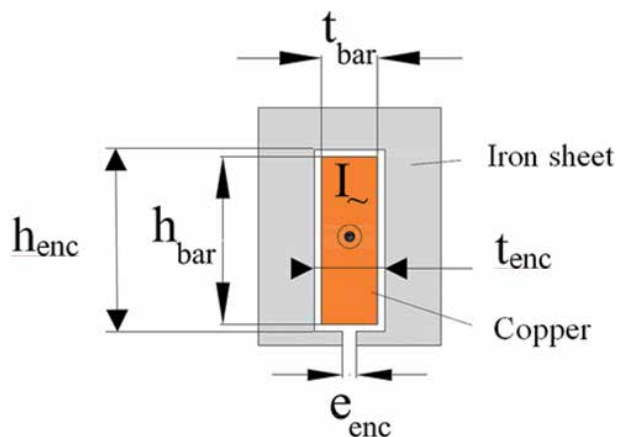
Figure 7.
Main dimensions of the slot and the copper conductor.
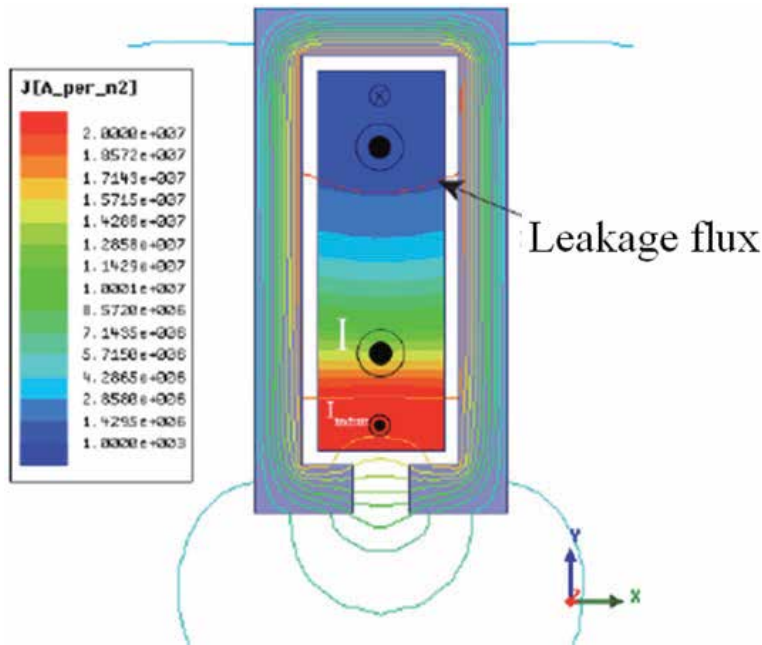
Figure 8.
Illustration of the uneven distribution of the current density inside the conductor due to the slot transverse flux.

#	h_{bar} (mm)	t_{bar}/t_{enc}	Frequency (Hz)	δ (mm) à 100°C	K_{AC}
1	4	0,83	800	2,7	1,35
2	3	0,83	1666	1,9	1,44
3	8	0,8	800	2,7	2,65
4	8	0,75	133	6,6	1,05

Table 2.
Field effect for different copper bar dimensions.

This relationship is only valid when $K_{AC} > 1$. **Table 2** summarises the value of K_{AC} for exactly the same configurations considered in **Table 1**.

According to the results presented in **Table 2**, it can been clearly seen that, as expected, the increase in copper loss due to the use of solid bars is significant, however, the solid bar still beneficial even at high frequencies when considering the overall performance of the machine. Indeed, in order to illustrate this point, we can consider the configuration # 2 operating at a nominal frequency of 1666 Hz. The use of a solid bar would increase the current in the slot, at constant DC losses, by about 50% (cf. relation (1)), while the increase in losses in AC mode would require it to be reduced by 20% ($\sqrt{1,44}$), hence, the overall increase in torque and current is equal to 25%.

The remaining examples of **Table 2** will be analysed when their corresponding products are presented later in this chapter.

3. Low voltage power electronics converter

3.1 Power converter for electric vehicle

In electric vehicles, the electric motors can be fed by one or more power converters depending on one or multiple energy sources. Whether it is an airplane, an

electric vehicle or a boat, several energy sources are available with different characteristics, operating modes and architectures. The most characteristic quantities are the voltage and the current levels requiring the use of specific power and passive components. The architecture design of these converters, whether forward, isolated or segmented, is a first issue that must be specific to the application. Another problem is the integration of static converters in order to increase their compactness (power-to-weight and power-to-volume ratios) because the high power and the low voltage imply very high currents which are not very favourable to a high efficiency and to a volume reduction. Of course, cost constraints are very important in the automotive field and must be integrated from the start of the design process.

The complex power conversion and management functions implemented in the vehicle concern the electric motor, its control electronics, the transmission and management of energy by the charger and the converters used to power the navigation and entertainment systems. All these elements are supplied with very low voltages ranging from 12 V to 48 V, sometimes 60 V, which leads to favouring the use of 100 V components. At the drive train level, it is recommended to stay at low voltage, in order to simplify the control and most important to optimise the efficiency and therefore enhance the autonomy by avoid putting converters in series to adapt the voltage levels (for example, low-voltage battery and high-voltage motor). In other words, it is better to avoid a DC/DC stage between the battery and the inverter and therefore to only have the inverter between the battery and the motor. Furthermore, in order to recover the energy during braking phases, the DC/DC converter has to be reversible which would make its design more complex.
A classical architecture is given in **Figure 9**.

The electrical connection must also be appropriately designed because for a small vehicle, whether it is full electric or micro/mild hybrid type, with for example a power of around 30 kW at 48 V the currents are very high (650A for 48 V). The wiring with a large cross section must therefore be as short as possible and the inverter placed as close as possible to the motor and the battery, ideally in the same compartment and taking advantage of the car structure to dissipate the heat rejection.

Increasing the power of the electric motor quickly becomes a problem if the supply voltage does not increase proportionally because high DC bus and phase currents lead to an unreasonable increase in the number of semiconductor and passive components required. To reach the required switching capability, the surface area of the PCB, the volume of the cooling system and the size of the connectors should be increased accordingly, thus resulting in a weight increase of the
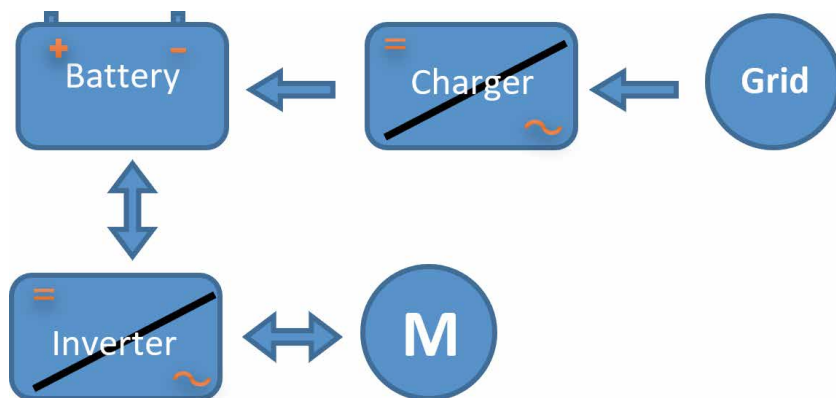

Figure 9.
Example of a drive train with a single power inverter.

electronic system and also a high cost incompatible with the requirements of the automotive field.

Alternatively, when the power becomes too high (at VLV) and therefore the currents are very high (>500A), the solution would be to segment the machine winding into many stars and supply them with several synchronised inverters as shown in **Figure 10**.

In **Figure 10**, the power is shared between two inverters, which mean that there are not too many components in parallel in each inverter arm, and that the inverters are less complex, less cumbersome and easier to build, and, also, that the connections are less bulky with less losses.

3.2 Power components for low-voltage converters

The static converters contains power modules which allow the classical energy conversion functions (AC/DC or DC/AC) and which are generally designed based on two main categories of components, namely the MOSFETs (Metal Oxide Semiconductor Field Effect Transistor) for low voltage inverters or IGBTs (Insulated Gate Bipolar Transistor) for high voltage ones. The field of application and the necessary integration of this static converter make it possible to determine the most suitable components according to several parameters such as power and voltage as well as the switching frequency. **Figure 11** gives a detailed breakdown of the use of these components.

For electric vehicles, the silicon MOSFETs and IGBTs are mainly used. In this field, the battery DC voltage is switched at frequencies ranging from 5 to 20kHz. This switching level is usually achieved by the use of well-adapted control laws. The components required for the DC/AC conversion function are usually packaged in modules. The electric motor of a power train system is three-phase, this implies that the inverter structure must be composed of at least six switches that are bidirectional in current formed by the association of an IGBT with a freewheeling diode or MOSFET in parallel that are naturally bidirectional in current due to their intrinsic integrated diode.
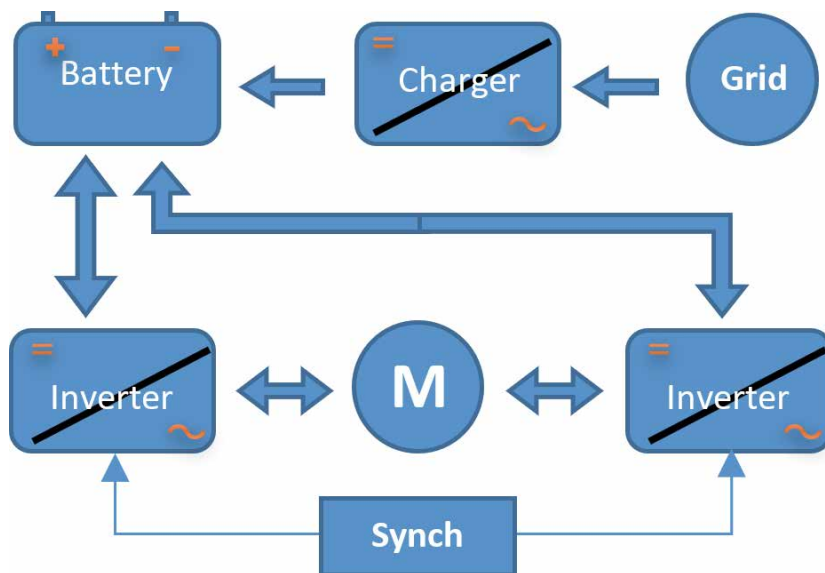
Figure 10.
Distributed system for segmented winding.
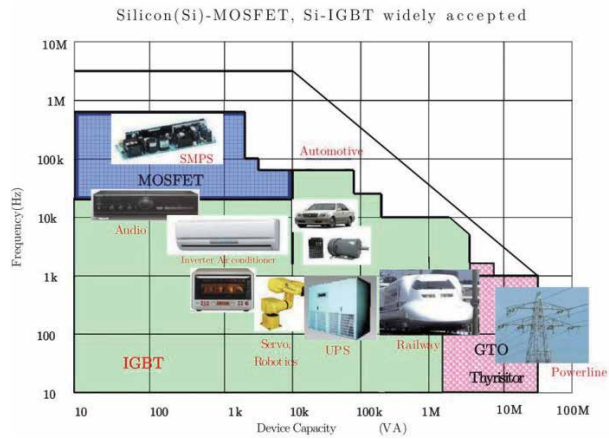
Figure 11.
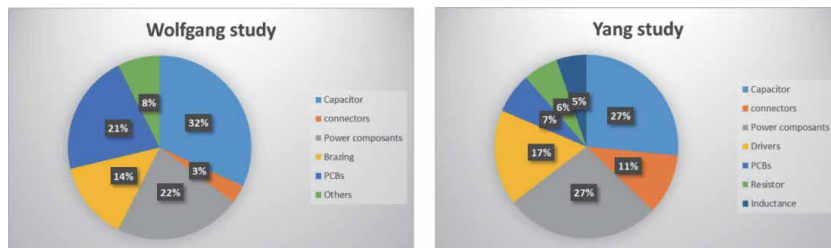*Use of the different types of switchers depending on the application [8].*

Figure 12.
Distribution of failure sources in a power converter [9, 10].

It is also useful to keep in mind that failures can be experienced in a power converter, it is essential that the reliability of this power converter is as high as possible in the case of an electric vehicle for the obvious safety reasons. Several studies show that the power modules can be the most weak part of a converter [9, 10]. The causes of failure are mainly due to temperature (frequent thermal cycling of components and high steady state current), but also to moisture, vibrations and contaminations during the manufacturing process. The **Figure 12** shows the results of two studies carried out on the failure modes of power converters.

The choice of a very low voltage supply, in this case 60 V, allows the use of commercial converters. However, as soon as the required power imposes a current higher than 500 A, it is necessary to design a bespoke power converter or, alternatively, to associate several of them in parallel. The technological constraints and standardisation lead to given silicon chip sizes which are then the building blocks of larger components. The increase in current capacity is thus achieved by combining elementary units in parallel.

Figure 13 shows some examples of power modules used in some conventional electrified vehicles.

We can note here that the semiconductors are associated in parallel in order to be able to switch important currents which depends on the power and the supply voltage of the machine and thus on the range of the EV (low range, high range, commercial vehicle...).

For example, the Tesla Model S has 10 IGBT chips per phase (i.e. 30 per module) to provide the 800 kW needed to power this vehicle whereas a Renault Zoé only needs 12 IGBT chips per module to ensure its nominal operation at 400 V/300 A.
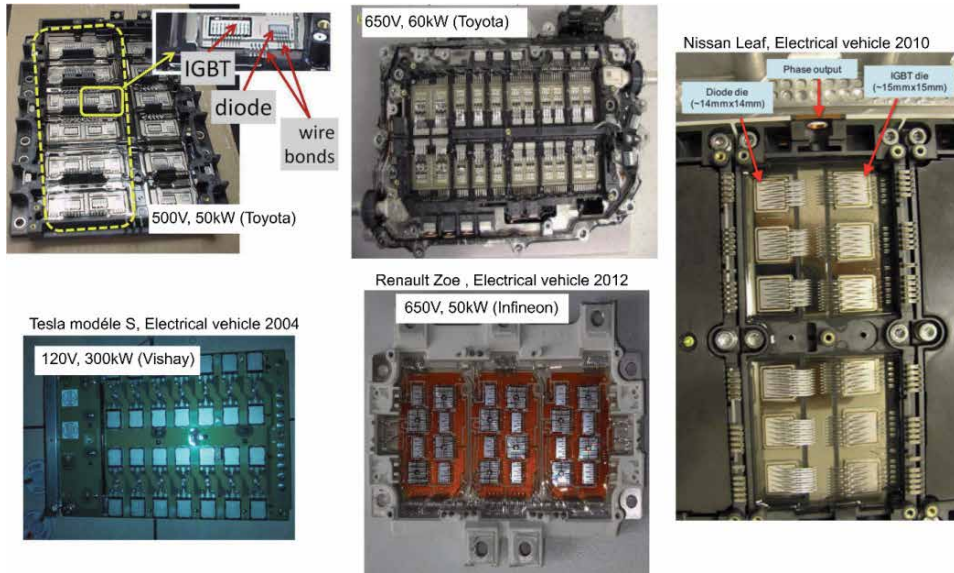
Figure 13.
Examples of inverters in the realm of electric vehicles [11, 12].

The inverter should be compactly designed and should preferably be mounted as close as possible to the motor. The elements that contribute to the performance of the power module and therefore of the inverter are:

- well-balanced current in the parallel MOSFETs,

- low V_{DS} peak at turn-off,

- low R_{dson} when the MOSFETs are turned on,

- low R_{th} of the heat sink.

In addition to conduction losses, switching losses must also be minimised to ensure optimum efficiency and minimal impact on the vehicle autonomy.

The design of the converter must also take into account the control boards, the drivers and the cooling system. **Figure 14** shows the controller and driver circuitry for the Lexus hybrid vehicle.

Nowadays, new materials are emerging to replace silicon such as: silicon carbide (SiC) and Galium nitride (GaN). These materials allow higher switching
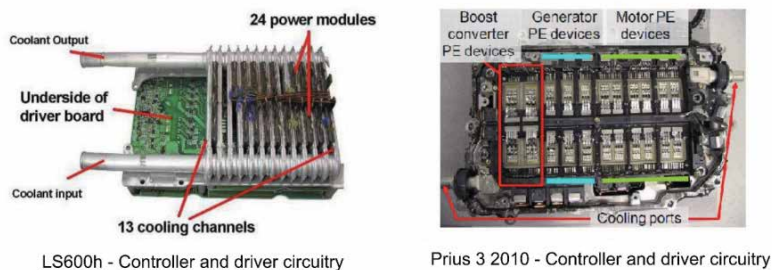
Figure 14.
Examples of controllers and driver circuitry [13].

frequencies, greatly reduced losses and higher operating temperatures resulting in more compact cooling systems, however, they also require a better control of the EMC and the PCB routing.

4. Very low voltage and medium power motorisation for electric vehicles

Many small electric vehicles (boat, kart, motorcycle, quad, cart, utility tricycle, small urban vehicle, unlicensed vehicle…) are equipped with an electrical motorisation with a power ranging from 10 kW to 30 kW. We present in this section a motor architecture optimised to operate at this power level and at very low voltage.

The winding technique for the electric motor is depicted in **Figures 3** and **15**, the slot copper bars are connected to each other at the end-windings via bridges bars located in two planes (crook bar and bow bar). In this case the overhangs are extremely compact. This configuration of the bars corresponds to the case number 1 in **Tables 1** and **2**.

To optimise the manufacturing costs, all motors in this power range will use the same stator laminations, the same number of poles; hence, the number of bars is always the same, only the length of the stator stack is likely to evolve in order to comply with the different specifications, we will be giving two examples.

The motors are assembled in square shaped housing (212x212 mm^2 CSA), as shown in **Figure 16**.
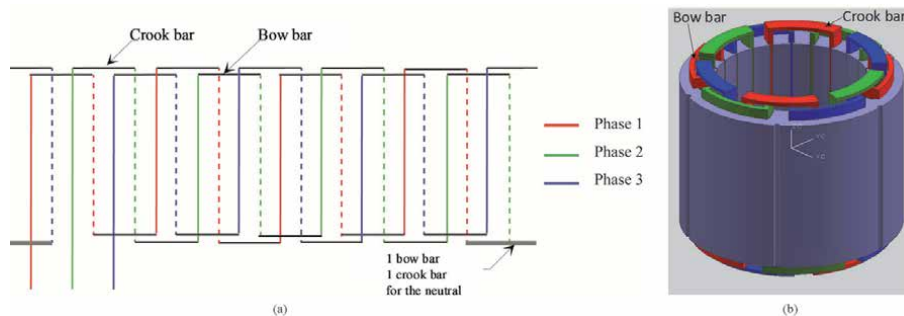
Figure 15.
Winding architecture - 20 kW very low voltage motor. (a) Winding layout, (b) 3D CAD view of the wound stator.

Figure 16.
A motor portfolio with a power ranging from 10 kW to 30 kW, operating at very low voltage (courtesy of SMVE performance SAS).

4.1 Outboard electric motor

The first specification we present is related to a marine outboard motor (electric boat), where the nominal speed of the propeller is 1750 rpm, with a reduction ratio of the transmission angle equal to 2.

The simplified specifications of the motor are as follows:

- Rated power: 10 kW

- Nominal speed: 3500 rpm

- Power supply voltage: 50 VDC

- Efficiency: greater than 90%

There is no need here to detail the EMAG sizing of the motor, which is conventional and does not fit the main purpose of this chapter. The following **Table 3** summarises all the main characteristics of the motor.

This first case of sizing shows that even with a relatively low nominal operating speed, it is possible to reach high specific performances where, in particular, the

Dimensions	
Stator outer diameter	208 mm
Stator inner diameter	172 mm
Magnetic airgap length	1,5 mm
Magnet height	6 mm
Stator stack length	35 mm
Winding bar dimensions (hxw)	4x5 mm
Slot dimensions (hxw)	4,8x5,8 mm
Materials	
Stator corepack	M270-35A
Magnets	N35UH
Electrical parameters	
Pole number	16
Slot number	48
Phase rated current	240A RMS
Phase resistance (AC, K_{AC} = 1,05), 20°C - 100°C	1,3 mΩ - 1,7 mΩ
Torque coefficient kt	0,113 Nm/A
Total weight (including mechanics)	8 kg
Nominal torque-to-weight ratio	3.3 Nm/kg
Joule losses (at 100°C)	300 W
Iron losses + mechanical losses	250 W
Efficiency	95%
Cooling method	Natural convection

Table 3.
Characteristics of the electric boat motor.

power density is higher than 1 kW/kg, without impairing the efficiency. The latter is a key performance in the case of electric boat where the nominal speed corresponds to a permanent operating speed because the vehicle regime is stable during the navigation.

4.2 Kart electric motor

For this second studied case, we use the same motor structure, but considering a much higher power, adapted to the motorisation of a small sport vehicle, a kart for example.

The simplified specifications of the motor are as follows:

- Maximum power: 25 kW

- Maximum speed: 6000 rpm

- Power supply voltage: 60 VDC

- Efficiency: greater than 90%

The following **Table 4** summarises the characteristics of the motor designed for this specification. The laminations are identical to those of the previous case (electric boat Section 4.1).

This sizing case is extreme, because, given the power, we are at the limit of feasibility at VLV, especially if we consider the phase current reaching 500 A. However, contrary to the previous case, the maximum power is transient because the speed of a small sport car is very variable on a winding track, the thermal steady state depends on the nature of the latter.

Even though the efficiency remains good, the losses at maximum power are high, more than 2 kW, but in this vehicle the motor is located outside and will be naturally cooled by a large amount of air flow (**Figure 17**). The maximum speed of the vehicle

Dimensions	
Stator stack length	28 mm
Electrical parameters	
Pole number	16
Slot number	48
Phase rated current	490A RMS
Phase resistance (AC, K_{AC} = 1,35), 20°C - 100°C	1,3 mΩ - 1,7 mΩ
Torque coefficient kt	0,082 Nm/A
Total weight (including mechanics)	7 kg
Nominal torque-to-weight ratio	5,7 Nm/kg
Joule losses (at 100 °C)	1220W
Iron losses + mechanical losses	500 W
Efficiency	94%
Cooling method	Natural convection

Table 4.
Characteristics of the electric kart motor.

Figure 17.
Electric kart.

is well above 100 km/h, a natural convection cooling is sufficient. Furthermore, the heat exchange is improved by the very low copper to iron thermal resistance.

5. High frequency motor for electric airplane

This application illustrates the implementation of the concept for a motor operating at very high electrical frequency for an aeronautical application. It is a laboratory study [1] based on the motorisation specification of one of the first industrial all-electric aircraft, namely the Efan, from AIRBUS (**Figure 18**). The project was

Figure 18.
Prototype Efan (courtesy of AIRBUS).
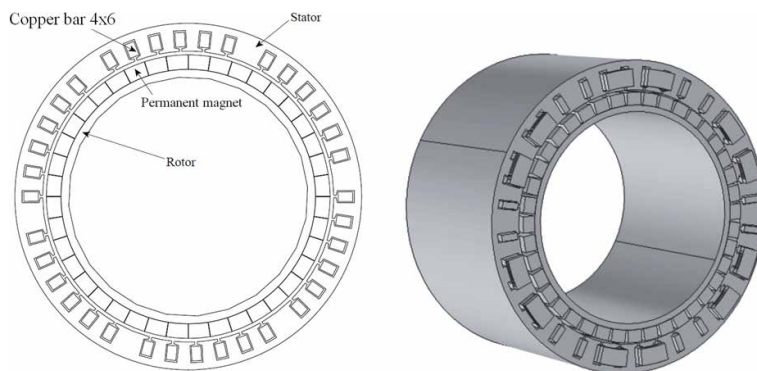
Figure 19.
Structure of the "per group" winding.

quickly abandoned by AIRBUS, but it was taken up by several other companies, and some versions are now offered for sale to the aero clubs.

The power supply voltage of the Efan motor was equal to 300 V, we think that a VLV version would make sense to facilitate the maintenance operations of the aircraft, if it is particularly used in the aero clubs. This approach is all the more interesting as it also allows the search for very high specific performances thanks to the properties of the winding with only one solid bar per slot. The weight of the motor is, of course, one of the first sizing criteria.
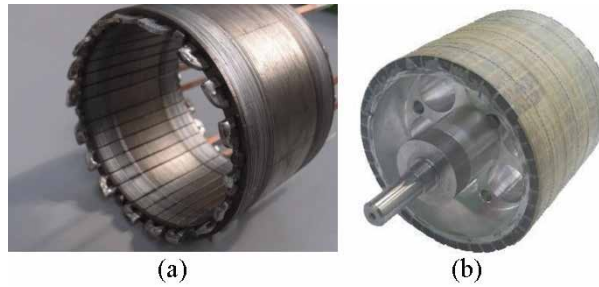
Figure 20.
High frequency electric motor prototype. (a) Wound stator. (b) Rotor assembly.

Dimensions	
Stator outer diameter	137 mm
Stator inner diameter	120mm
Magnetic airgap length	1 mm
Stator stack length	92 mm
Winding bar dimensions (hxw)	3x5 mm
Slot dimensions (hxw)	4x6 mm
Materials	
Stator corepack	Iron-Cobalt, 0,2 mm
Magnets	N35EH
Electrical parameters	
Pole / slot number	40 / 36
Phase rated current	400 A RMS
Phase resistance (AC, K_{AC} = 1,44), 20 °C - 100 °C	1,85 mΩ - 2,44 mΩ
Torque coefficient kt	0,125 Nm/A
Total weight (including mechanics)	6 kg
Nominal torque-to-weight ratio	8.3 Nm/kg
Nominal power-to-weight ratio	4,3 kW/kg
Joule losses (at 100 °C)	1200 W
Iron losses + mechanical losses	400 W
Efficiency	94%
Cooling method	Natural convection

Table 5.
Characteristics of the electric aircraft motor.

To maximise the power-to-weight ratio, we have designed an electric motor operating at high frequency. The winding structure is special [1, 4, 5, 14], where the phases are arranged in six separate sectors, the electrical phase shift is ensured by introducing an intermediate irregular tooth, as illustrated in **Figures 4, 19** and **20**. This winding design allows, on the one hand, to keep a limited number of slots (36 slots), despite the large number of poles (40 poles), and, on the other hand, to avoid the end-windings overlaps, resulting in very short overhangs.

The simplified specifications are as follows:

- Maximum power: 26 kW

- Maximum speed: 5000 rpm

- Power supply voltage: 80 VDC

- Weight: less than 7 kg

- Efficiency: greater than 92%

The **Table 5** shows the main characteristics of the electric motor.

The structure with large number of poles allows to obtain high specific power, more than 4 kW/kg. The VLV winding contributes to this level of performance without compromising the efficiency. The additional loss coefficient, K_{AC}, remains moderate despite operating at a frequency of 1666 Hz. As the motor is placed behind the propulsion propeller, the 1600 W of total losses will be easily evacuated.

6. High power vehicles

When the required power of the vehicle motorisation exceeds the threshold of 30 kW (approximate), it becomes difficult, if not impossible, to supply the motor with a single controller because the phase currents become prohibitive at VLV. The two examples discussed in this paragraph show how to solve this problem using power partitioning.

6.1 Sporty electric vehicle

The first considered case of high power motorisation is that of a rally type sporty vehicle (**Figure 21**).

Figure 21.
Sporty full electric vehicle.

The simplified specifications of the motor are as follows:

- Maximum power: 100 kW

- Maximum speed: 5000 t/mn

- Power supply voltage: 100 VDC

In order to divide the power supplied to the motor, the winding was designed based on the technique described earlier in **Figure 15**, and is split into two electrically isolated stars, as depicted in the following **Figure 22**; each half-winding being fed by a dedicated controller and delivering half of the total required power.

Table 6 summarises all the main characteristics of the electric motor. In this case, we are using the solid bar configuration corresponding to case 3 in **Table 2**.

The losses at simultaneously maximum power and maximum speed are too high, more than 7 kW, particularly due to a high K_{AC} coefficient, but this is only a transient regime occurring during the acceleration phase. Again, here the steady-state thermal behaviour also depends on the nature of the track which cannot be defined a priori, but in all cases the efficiency is high and greater than 95%. However, at low speed acceleration, the copper losses are halved at constant current because the K_{AC} coefficient tends towards 1, the efficiency, therefore, remains high over a wide speed range. The partition of the power on multiple converters makes it possible to reduce the phase current to 650 A during the transient regime. The bar winding has allowed the design of a very compact motor reaching high power density (4 kW / kg in transient regime).

6.2 Utility vehicle

The second example of power partitioning is that of an utility vehicle, an electric tractor for winegrowers (**Figure 23**).

This tractor is equipped with four electrified wheels fully independent. The topology of the motors is very similar to that described in section 4. The solid bars configuration corresponds to line 4 of **Tables 1** and **2**. The four electric motors drive the wheels via a gearbox with a reduction ratio of 1/40.

The simplified specifications of the motors are as follows:

- Maximum power: 40 kW

- Rated power: 5 kW
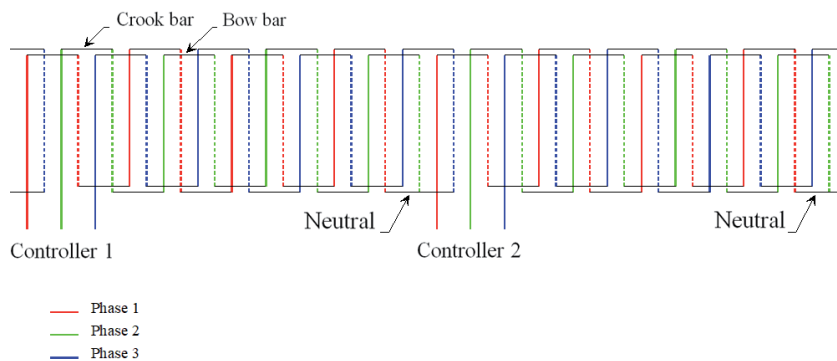
Figure 22.
Dual stars winding layout.

Dimensions	
Stator outer diameter	204 mm
Stator inner diameter	156 mm
Magnetic airgap length	2 mm
Magnet height	5 mm
Stator stack length	175 mm
Winding bar dimensions (hxw)	8x4 mm
Slot dimensions (hxw)	9x5 mm
Materials	
Stator corepack	M270-35A
Magnets	N35UH
Electrical parameters	
Pole number	16
Slot number	48
Phase rated current	650 A RMS
Phase resistance (AC, KAC = 2,39 - 2 x 3 phase), 20 °C - 100 °C	1,85 mΩ - 2,4 mΩ
Torque coefficient kt	0,46 Nm/A
Total weight (including mechanics)	40 kg
Nominal torque-to-weight ratio	7,5 Nm/kg
Joule losses (at 100 °C)	6000 W
Iron losses + mechanical losses	1400 W
Efficiency	95%
Cooling method	Natural convection

Table 6.
Characteristics of the sporty vehicle electric motor.

Figure 23.
Electric tractor.

- Maximum speed: 4000 rpm

- Nominal speed: 1000 rpm

- Power supply voltage: 80 VDC

The nominal operating condition of the electric tractor corresponds to the ploughing phase, where the displacement speed is low and the total required mechanical power does not exceed 20 kW. The tractive force applied on the plough is approximately 16 kN. The sizing was carried out based on the tractor behaviour with a conventional thermal engine.

The power partition, via the use of four electric motors, enables to have a significant power available for the transient mode, approximately 160 kW, thanks to the capacity of over-torque necessary for obstacles clearing and vehicle overspeed during the road trips. During the latter operating conditions, the motors are running without flux weakening. However, this high power is only used very rarely, and only temporarily, in the case of transporting heavy loads on steeply sloping roads.

The efficiency of each electric motor at the nominal conditions, at low speed and at an output torque of 50 Nm per motor, is about 95% and this because the copper losses in the 24 mm^2 solid bars are very low due to the very low electrical frequency (133 Hz).

7. Conclusion

According to the various examples discussed in this chapter, it can be seen that it is possible to design an electric vehicle drive train operating at very low voltage (battery voltage below 120 VDC) and over a wide power range (up to 100 kW). An original, compact and high efficiency motorisation solution using a solid bar winding has been presented. In all the cases, the sizing constraints of the motor controller have been taken into account.

Main symbols and abbreviations

AC	alternating current, alternating voltage
DC	direct current, direct voltage
δ	skin depth in AC mode
EMAG	Electromagnetic
EMC	Electromagnetic Compatibility
h_{bar}	solid bar height
h_{enc}	slot height
IGBT	Insulated Gate Bipolar Transistor
J	current density
k_{AC}	additional loss coefficient AC / DC
MOSFET	Metal Oxide Semiconductor Field Effect Transistor
P_{AC}	Joule AC losses in conductors
P_{DC}	Joule DC losses in conductors
PCB	Printed Circuit Board
R_{dson}	MOSFET drain source electrical resistance
R_{th}	heat sink thermal resistance
σ	copper fill factor
t_{bar}	solid bar width
t_{enc}	slot width
V_{DS}	MOSFET drain source voltage
VLV	Very Low Voltage

Author details

Daniel Matt[1*], Nadhem Boubaker[2], Mourad Aitakkache[1], Philippe Enrici[1], Jean-Jacques Huselstein[1] and Thierry Martire[1]

1 University of Montpellier, Montpellier, France

2 Safran Electrical and Power, Pitstone, UK

*Address all correspondence to: daniel.matt@umontpellier.fr

IntechOpen

References

[1] Boubaker N. Study of atypical losses in high performance permanent-magnet synchronous machines for aircraft applications [thesis]. University of Montpellier; 2016.

[2] Enrici Ph, Boubaker N, Matt D. Bar Winding for the Low-Voltage Motorization of an Electric Tractor. In: Proceedings of the International Conference on Electrical Machines (ICEM); 23-26 August 2020; Gothenburg. Sweden: IEEE; 2005. p. 1711-1717.

[3] Matt D, Boubaker N. Very Low Voltage and High Efficiency Motorisation for Electric Vehicles, "Emerging Electric Machines – Advances, Perspectives and Applications", INTECH ed., ISBN 978-1-83968-732-7

[4] Lorenzo P, Matt D, Gimeno A, Boubaker N. Contribution on AC bar windings losses reduction for a high frequency and high performance machine for aeronautical application. International Symposium on Electromagnetic Fields in Mechatronics, Electrical and Electronic Engineering (ISEF); 29-31 August 2019; Nancy. France: IEEE; 2020. DOI 10.1109/ISEF45929.2019.9097026

[5] Boubaker N, Matt D, Nierlich F. A stator winding arrangement. Patent #WO2020208425A1.

[6] Levasseur A. Nouvelles formules, valables à toutes les fréquences, pour le calcul. Journal de Physique et le Radium. 1930.

[7] Liwschitz M. Calcul des machines électriques. SPES; 1967.

[8] Daou H. Méthodologie de conception numérique d'un module de puissance dédié à l'automobile en vue de l'optimisation des surtensions, des

pertes et des émissions conduites, PhD thesis from the University of Paris-Saclay, 2017.

[9] Wolfgang E. Examples for failures in power electronics systems. ECPE Tutorial Reliability of Power Electronic Systems, April 2007.

[10] Yang S, Bryant A, Mawby P, Xiang D, Ran L, Tavner P. An industry based survey of reliability in power electronic converters. IEEE Transactions on Industry Applications, Vol. 47, no 3, May/June 2011. P 1441-1451.

[11] O'keefe M, Vlahinos A. Impacts of cooling technology on solder fatigue for power modules in electric traction drive vehicles. 5th IEEE Veh. Power Propuls. Conf. VPPC '09, p. 1182-1188, 2009.

[12] Liang Z. Status and trend of automotive power packaging. Int. Symp. Power Semicond. Devices ICs, vol. 1, p. 325-331, 2012.

[13] Olszewski M. Evaluation of the 2008 LEXUS LS 600H "Hybrid Synergy Drive System". US Department of Energy, Washington DC, 2009.

[14] Boubaker N, Matt D, Enrici Ph, Nierlich F, Durand G. Measurements of Iron Loss in PMSM Stator Cores Based on CoFe and SiFe Lamination Sheets and Stemmed From Different Manufacturing Processes. IEEE Transactions on Magnetics, 2018; DOI: 10.1109/TMAG.2018.2877995

Section 3

Technologies of the Electric Vehicles

Chapter 6

Improving Communication System for Vehicle-to-Everything Networks by Using 5G Technology

Tarik Adnan Almohamad, Muhammet Tahir Güneşer,
Mohd Nazri Mahmud and Cihat Şeker

Abstract

Next-generations of wireless communication systems (5G scheme & beyond) are rapidly evolving in the contemporary life. These schemes could propose vital solutions for many existing challenges in various aspects of our lives, eventually to ensure stable communications. Such challenges are even greater when it comes to address ubiquitous coverage and steady interconnection performance in fast mobile vehicles (i.e., trains or airplanes) where certainly blind spots exist. As an early initiative, the Third Generation Partnership Project (3GPP) has proposed a regulation for Long Term Evolution (LTE)-based Vehicle-to-Everything (V2X) network in order to offer solid solutions for V2X interconnections. V2X term should comprise the following terminologies: vehicle-to-vehicle (V2V), vehicle-to-network (V2N) communications, vehicle-to-infrastructure (V2I), and vehicle-to-pedestrian (V2P). Superior V2X communications have a promising potential to improve efficiency, road safety, security, the accessibility of infotainment services (any service of user-interface exists inside a vehicle). In this chapter, the aforementioned topics will be addressed. In addition, the chapter will open the door on investigating the role of wireless cooperative and automatic signal identification schemes in V2X networks, and shedding light on the machine learning techniques (i.e, Support Vector Machines (SVMs), Deep Neural Networks (DNNs)) when they meet with the next-generations of wireless networks.

Keywords: Next-Generations of Wireless Communication Systems, Long Term Evolution, 5G scheme, Vehicle-to-Vehicle Communication, Vehicle-to-Everything, Automatic Signal Identification, Deep Neural Networks

1. Introduction

Artificial intelligence (AI)-based communication applications have shown a tremendous upsurge in the late decade. It is triggering an exceptional attention from academia, governments and diverse industry sectors on the evolving generations of wireless networks. The imminent coming application of fifth generation (5G) wireless communications scheme has spurred the question what is next?. Research sectors have recently started to investigate what is beyond 5G and envisage the upcoming sixth generation (6G). The work in [1] has paved the way for a more detailed exploration of possible methodologies of AI-empowered 6G communication systems and their unprecedented makeover in their architectures compared to the preceding versions of
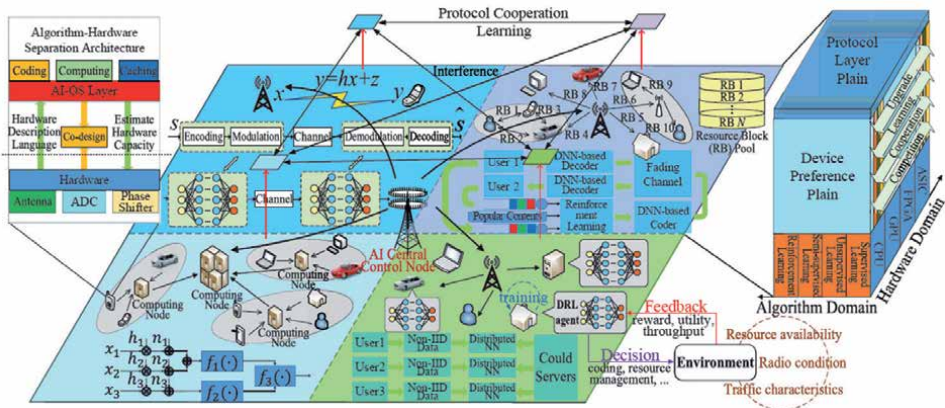
Figure 1.
Potential network design for future generation of wireless networks [1].

wireless networks. **Figure 1** illustrates a world of *connected things*, and the vision for the future generation wireless networks [1]. The future generation of wireless communication systems will unleash a remarkable advancement in wide range of applications such as, but not limited to, vehicles networking, wireless cooperative systems in drones, intelligent cities, etc. As connected things result in heterogeneous complicated networks, this in turn, necessitates the need of AI empowerment in the telecommunication sector.

Now, time has come for academia and manufacturing sectors to bring their focus on the potential applications of the coming generations of wireless communication systems in various aspects of our lives. It can be observed that multiple countries have been starting to apply the new generations of communications i.e., fifth generation (5G) wireless communications scheme. Today, the current promises in telecommunication sector for 5G tell that, firstly the deployment of 5G is ongoing now, prominent low levels of latency, significant increment in capacity, higher speeds of transmissions rate, device-to-device (D2D) communication and of course connected V2X networks, and internet of everything (IoE). Intensive progress is currently witnessed for the transition from the Long-Term Evolution (LTE) to 5G systems in the communication industry. With this momentum, V2X has garnered more considerable attraction today [2], it has the ultimate potential into the enhancement of transportation efficiency, road safety and security, forming a key platform for transportation systems. Such systems intend to be more efficient and intelligent when next-generation communication schemes (5G & beyond) are involved. 5G-based V2X communications can accelerate the advancement of the intelligent transportation systems and reduce traffic and road risks. In V2X schemes, the connected vehicles can aggregate more information about the road environment condition and communicate this valuable information with adjacent vehicles in a real-time scenario. This will lead to an accurate estimation of a risky event before its occurrence. Originally, before this collaboration among vehicles, an internal sensor unit like a global positioning system (GPS) or radar device was envisioned to generate and provide information about vehicle-surrounding environment. Today, the emergence of 5G & beyond communications schemes is promising to efficiently facilitate collaborative connections among vehicles. Back to LTE systems, the Third Generation Partnership Project (3GPP) worked on completing the standardization of LTE-based V2X in their Release 14 to support the automotive industry with LTE services [3]. In Release 16, 3GPP has developed the 5G New Radio (NR) to provide V2X services much more superior than the facilities provided by LTE networks earlier [4]. Normally, Mobile units in cellular networks are connected via one or more base stations but with 5G NR scheme, these unites are connected

directly by using what is called sidelink communication technology. Thus, 5G-assisted vehicles will be able to form their ad hoc systems, leaving the need of any extra radio access equipment as an interface among them. On the other hand, in contrast to LTE sidelink, plateau of services are offered by NR sidelink such as collision prevention, unicast and groupcast transmission, QoS administration, cooperative lane switching, compatibility in mm-wave frequency bands, etc. **Figure 2** illustrates V2X communication scenario. The figure depeicts various potential events that may occur among vehicles in real time, the roadside unit (RSU) can relay the received information and deliver them to a vehicle or a group of vehicles supporting V2I applications. This transportation system tends to be more intelligent when V2X scheme is applied as it enables less traffic, collision avoidance, real time data collection [5].
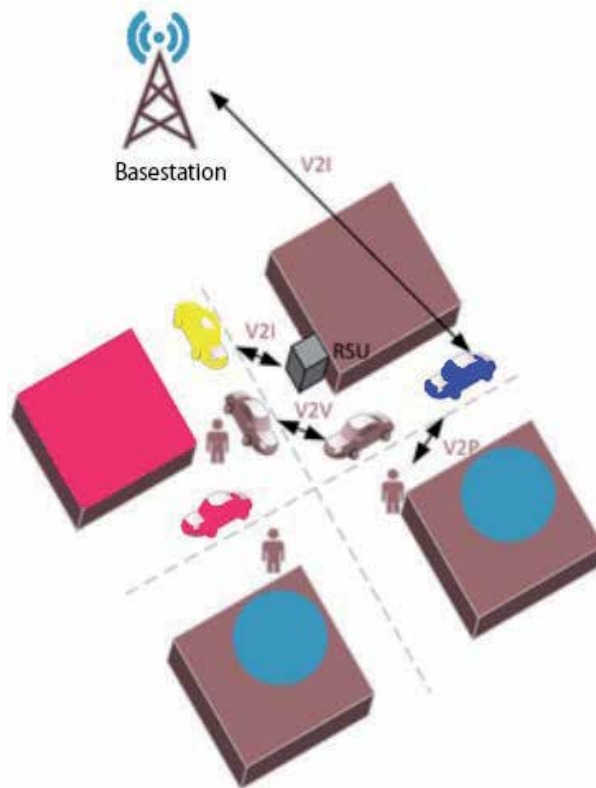
Figure 2.
V2X communication environment with roadside unit (RSU).

According to the European Telecommunications Standards Institute (ETSI), V2X communication messages are categorized into two groups: decentralized environmental notification messages (DENMs) [6] and cooperative awareness messages (CAMs) [7]. These messages convey information about the vehicle condition such as direction, position, velocity, and acceleration, etc. **Figure 3** portrays a scenario on how vehicles being instantly assisted by warning messages. In addition, LTE\5G NR enable exchanging these V2X-messages in unicast and broadcast carriers (bearers) whereas acknowledging the message delivery is executed, at the physical & MAC layers, by the network (i.e. base station). This acknowledgment feature can efficiently minimize the retransmission rate of V2X communication messages. Detected situations will generate DENMs to warn road drivers whereas the periodic CAMs to update the condition within up to 100 *ms* of latency.
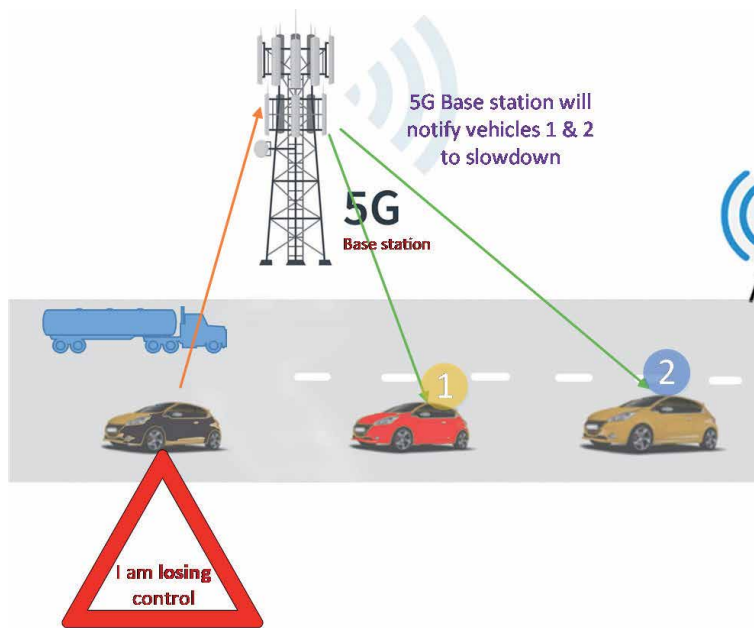
Figure 3.
The 5G base station broadcasting warning messages to vehicles on trajectory.

In June 2016, the use cases and related key requirements for enabling LTE network to serve V2X communications, were identified by Technical Specification Group (TSG) and System Aspects Working Group 1 (SA1). They classified the use cases in 3GPP into safety and non-safety use cases. The former focusing on securing life and objects, and collision avoidance, the latter use cases aiming the enhancement of environmental performance and transportation movement. Nevertheless, 3GPP has carried out a comprehensive revision of V2X service requirements and enhanced them by proposing NR Release 16 [8, 9]. There are four areas of V2X possible events, have been defined in [9] (i.e., platooning, advanced driving, extended sensor, and remote driving). The following **Table 1** maps these four areas into various 3GPP technologies.

Practically, most of the requirements mentioned in **Table 1** have been already attained by 5G Release 15 cellular downlink and uplink. On the other hand, remote driving demands optimal QoS requirements i.e., extremely small latency values and higher levels of reliability which are abbreviated as ultra-reliable low-latency communication (URLLC). In order to meet these demands, 3GPP has extensively worked on improving the reliability and reducing the latency of the cellular downlink and uplink [10] in Release 16, by considering the following procedures:

a. Enable more stable and solid transmissions by improving the downlink control channel information (CCI).

b. Enable prompt feedback of hybrid automatic repeat request (HARQ) by refining the uplink CCI.

c. Empower instant communication by enabling multiple configurations to the uplink and downlink scheduling.

d. Support the recurrence of short-range communications by improving the uplink data channel.

Use case field	Use cases	QoS necessities			Technical enablers
		Data rate [Mb/s]	Reliability [%]	Latency [ms]	
Driving group of vehicles together (platooning)	Sharing information among the vehicle group and with other groups	65	99.99	10	LTE or 5G broadcast (for limited cases), 5G groupcast or unicast
Advanced driving	Data sharing, Cooperative crash prevention, Vulnerable driver recognition, Emergency trajectory alignment	53	99.999	3	5G broadcast/ groupcast/unicast
Extended sensor	Collective perception of environment, Transparency	1000	99.999	3	LTE broadcast, 5G broadcast
Remote control	Drive a vehicle remotely	Uplink: 25, Downlink: 1	99.999	5	LTE or 5G unicast via cellular interface

Table 1.
3GPP considerations for V2X use cases [4].

e. Ease transmissions of critical packets at crucial levels of latency by prioritizing intra-vehicles and inter-vehicles packets

The above procedures will lead to the betterment of reliability and latency of V2X communications. Thus, 5G communication scheme (including LTE & NR Release 16) can increasingly enhance the V2X use cases covering those ones that require high levels of reliability and low latency.

2. Fifth generation (5G)-based V2X working situations

3GPP has been actively worked on specifying the 5G radio interface or as referred to as NR, aiming to achieve more flexible spectrum with higher frequency operations. This is due to the need of deploying radio access technologies and enlarging the spectrum range.

In order to ensure a reliable communication among vehicles and avoid any outage effect from the network, 3GPP, in its Release 16, proposed device-to-device link in NR called sidelink [11]. The proposed sidelink enjoys multiple advantages such as:

a. Flexible radio link benefiting from the exiting NR cellular interface.

b. Operates in unlicensed and licensed frequencies' ranges, hence, it can be allocated for V2X facilities and even shares with existing mobile network services.

c. Enables V2X use cases for unicast and broadcast transmission among vehicles themselves.
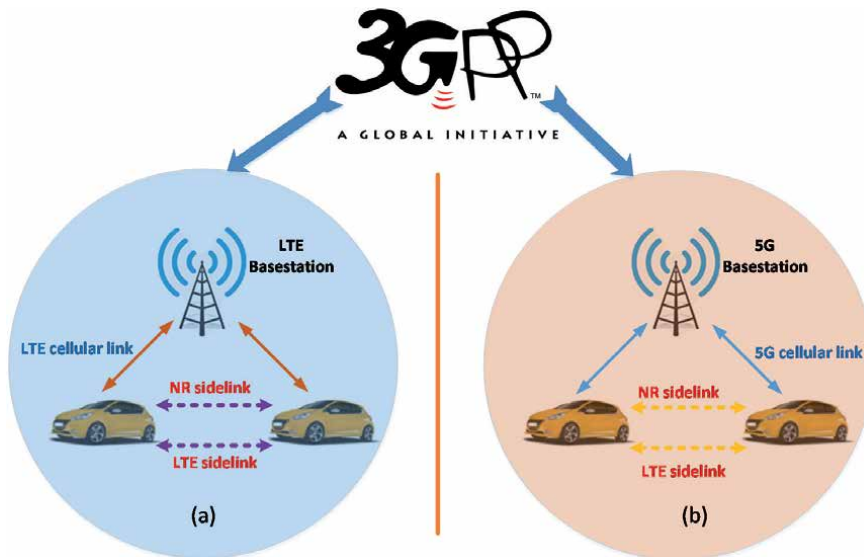
Figure 4.
Illustration of (a) LTE sidelink mechanism, and (b) 5G sidelink mechanism.

d. Gives a space to the network to allocate and control the sidelink resource.

e. Offers instant V2X services by the coexistence of NR and LTE sidelinks.

f. Operates in dual ranges of frequencies, lower (FR1) and higher (FR2) frequency bands i.e., 7.125 GHz and 52.6 GHz respectively.

g. Enables vehicles to connect with each other regardless the condition of the base stations in the network.

The design of NR inherently includes capabilities that support the user equipment to control the sidelink transmissions in the network. This, together with cellular transmissions, leads to share the existing available frequency bands. The aforementioned discussion can lead us to the fact that there are two transmission scenarios termed as mode 1 and mode 2. The former is active when decisions are given and centralized by the network. The latter operates in the case when base station system goes down.

Figure 4 shows potential scenarios of 5G (i.e., NR) and LTE with V2X networks. A base station can be classified into LTE or 5G station, depending on its connected core. As illustrated in the figure, the base station can configure all the cellular links and sidelinks over the network.

3. Wireless access in vehicular environment (WAVE)

WAVE is a group of wireless standards that are represented by the Dedicated Short Range Communications (DSRC) protocol such as IEEE 802.11p and IEEE 1609 standards [12]. This protocol, to support V2X networks, is being defined by IEEE and ETSI in collaboration with the automotive industry sector. The main idea behind DSRC protocol is the provision of road safety in V2X networks. Furthermore, academia, industries and governments have supported many projects to utilize DSRC in fulfilling V2X applications.

The IEEE 802.11p, which belongs to IEEE 802.11 family, is considered as a base to the V2X communication networks due to its high security levels. Moreover, road

safety applications such as crucial exchange of real-time data among fast-moving vehicles, and many more of Intelligent Transport System (ITS) platforms, are supported by IEEE 802.11p protocol.

Figure 5 portrays the WAVE stack, which has multiple layers and protocols. On the top WAVE stack, there is application layer (APPL) which is responsible for resource management and handling diversity of non-safety and safety applications. Under this layer, there are three essential sublayers, that is, user datagram protocol (UDP), transmission control protocol (TCP) and internet protocol version 6 (IPV6) sub-layers. They are part of the main WAVE short message protocol (WSMP) layer. Then, the logic link control (LLC) layer, WAVE MAC layer, and eventually the WAVE physical layer which essentially supports the higher layers [13–15].

It is crucial to mention that possessing a very flexible and reliable design of WAVE physical layer will ensure optimum throughput and extremely lower latency. This can be realized in the upcoming 5G communication scheme and its proposed NR sidelinks.

In fact, the structure of sidelink protocol between LTE and 5G is nearly common. However, as illustrated in **Table 1** before, the focus on quality of services' issues is much more vital in 5G sidelink than in LTE as enhancing the V2X use cases is an essential goal in this new cellular paradigm. In contrast to LTE, the 5G sidelinks are envisioned to provide more flexibility in efficient utilization of existing resources and superior adaptability to various mobility situations. These potentials are attributed to significant privileges of 5G sidelink, involving:

a. A power control procedure to alleviate interferences among V2V sidelink and base stations.

b. Radio link adaption based on sensing channel condition.

More details will be elaborated in subsequent sections on signal identification techniques in next-generations wireless communications.
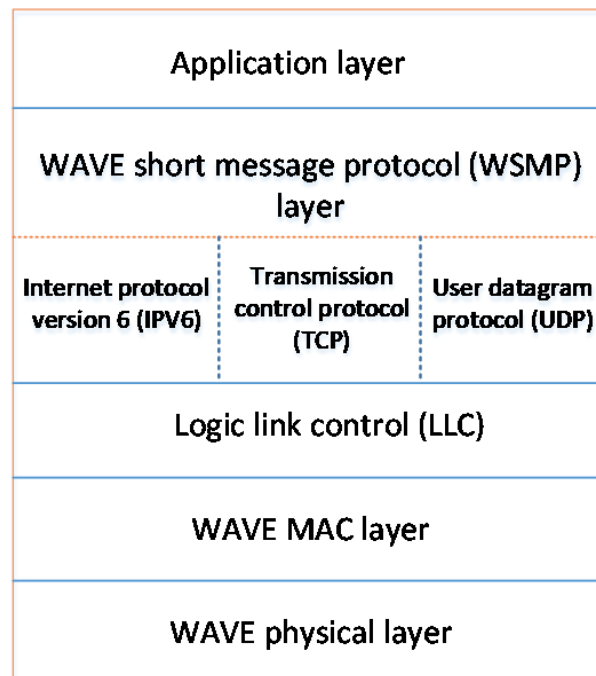
Figure 5.
Wireless access in vehicular environments (WAVE) stack.

4. Signal recognition in V2X using artificial intelligence (AI) techniques

Next-generation communication networks are envisioned to go more intelligent in the coming decade. Transmitters and receivers in any such networks are anticipated to work in adaptive mode when these devices are able to sense the communication medium (i.e., wireless channel) status between them. Based on the channel condition i.e., signal to noise ratio (SNR) value, the transmitter can decide the optimum transmitted signal parameters before the implementation of transmission process. For example, bit rates, modulation type, SNR level, transmitted power, and so on, can be adjusted by the transmitter, depends on the current environment status. It will monitor the channel condition, if it is good, then parameters such as less transmitted power, is required, or higher modulation schemes can be considered, hence higher transmission data rates can be achieved. This, in turn, requires the other receiving side to adapt to such unexpected changes and correctly estimate the parameters used to transmit the signal by the sender. Artificial intelligent (AI) tools can play a significant role to facilitate this estimation process [16]. On the other hand, it is promising that AI-based V2X communication systems will enable more safety, traffic efficiency, awareness & automotive driving, and security in the vehicular industry. When AI meets the emergence of 5G & beyond communication systems, the way is more paved to smart transport networks [17]. These networks will definitely bring a new concept of connectivity among vehicles and have a profound influence on our daily life. Furthermore, the deployment of 5G communication systems in V2X networks will bring this paradigm to higher efficiency and safety level.

As in traditional mobile networks, there are both transmitter and receiver nodes to exchange the data. Similarly in V2X communication networks, there are these nodes (i.e., vehicles) to exchange instant information. In the transmission process, a vehicular transmitter will modulate the data and send the modulated signal via the communication channel to the vehicular receiver side. A smart vehicle in 5G-based V2X network is anticipated to adapt to the channel condition and optimally adjust the modulation type or transmitted power suitable for transmission. This, in turn, will necessitate the vehicular receiver to adapt itself to these unexpected changes and recognize the signal parameter i.e., modulation being used at the transmitter side. Accurate recognition of V2V signal's parameters can be very beneficial to many use cases in the vehicular networks. In addition, it can be utilized as a source of information for the base stations to update many instant and vital data such as the position of moving vehicles, awareness messages, and information related to road environment.

For the purpose of meeting such demands, vehicular networks utilized indexed modulation (IM) techniques for data transmission [18]. IM method (i.e., spatial modulation) uses indices of the building modulated blocks (i.e., transmit antennas) in a communication scheme (i.e., MIMO systems). The following block diagram illustrates the key idea of IM technique as shown in **Figure 6**.

As illustrated in the figure, first, the input data is projected into a common vector before splitting it into two sub-vectors. They are dedicated to distinct transmit indices and then mapped to a digital modulation symbol such as phase shift keying (PSK) or quadrature amplitude modulation (QAM). Eventually, the common vector is mapped to IM vector for the purpose of transmission.

The decision of choosing which digital modulation type is suitable, can significantly affect the vehicular network throughput. In conventional transmission, the receiver will have a pre-knowledge about the selected modulation type, the channel condition, the transmitted power, the bit rates and so on. As mentioned earlier, a vehicle in advanced generations of vehicular communication systems is anticipated to go more intelligent in sensing the wireless channel condition and adjusting these parameters accordingly. In other words, to determine the optimal signal parameters (modulation type, bit rates, transmitted power, etc) before transmission takes a
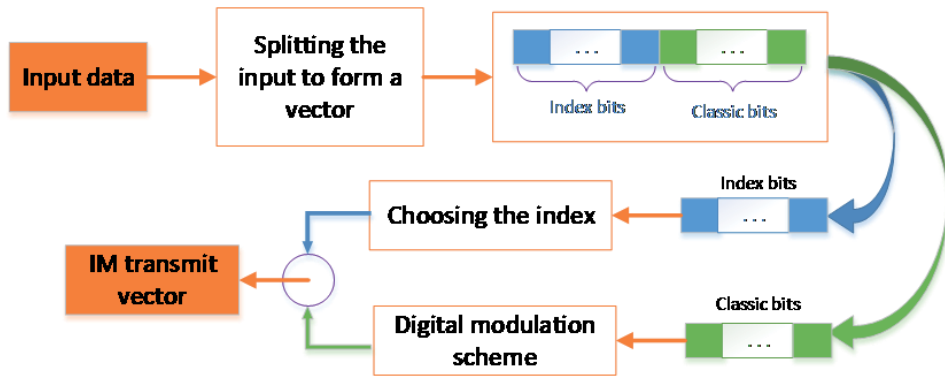
Figure 6.
The key principle of IM process.

place. In this scenario, the vehicular receiver has to track these possible changes and automatically recognize these signal parameters without any pre-communication with the transmitter. This capability at the receiver side, will exempt the vehicular transmitter to broadcast these valuable information over a wireless channel, and this means adding another good level of security to such information.

In order to enable the receiver with an accurate automatic recognition property of signal parameters i.e., automatic modulation recognition (AMR), two key approaches are used and have been reported in literature, that is, maximum likelihood (ML) approach and feature-based (FB) approach [19, 20]. The former provides optimal solution but suffers from higher computational complexity whereas the latter offers sub-optimal results but with lower complexity as illustrated in **Figure 7**. Hence, in this chapter, the FB approach is considered. After careful scanning of existing work in V2X networks, it is worth to mention that, to the best of our knowledge, the recognition of wireless signal parameters has not yet been addressed in the literature.

In ML approach, the values of likelihood functions are calculated and compared with a reference value to finalize the optimal modulation. On the other hand, in FB approach, the statistical characteristics of the received signal are extracted and utilized to estimate the intended signal parameters. There are numerous types of
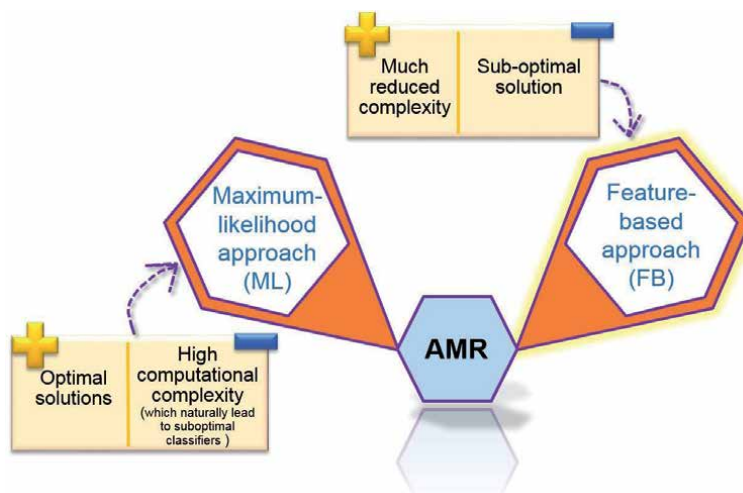
Figure 7.
ML and FB methods used for wireless signal parameter recognition.

features can be exploited to recognize the modulation type of a detected signal such as, instantaneous time-domain features, fourier and wavelet transforms, higher-order statistics, asynchronous amplitude histograms (AAHs), two-dimensional histogram of asynchronous sampled in-phase-quadrature amplitudes (2D-ASIQHs), and so on.

For instance, AAHs features have proved a prominent cost-effectiveness, flexibility and lower computational and implementation complexity. We have applied this type of features before in our work in [21] to estimate multiple signal parameters together using support vector machines (SVMs). It has shown a phenomenal performance to distinguish signals from each other in a realistic cellular wireless environment. Furthermore, SVM has proved its capability in processing small size of datasets compared to other machine learning tools. To clarify the conceptual meaning of AAHs features to the readers, the following **Figure 8** depicts the idea.
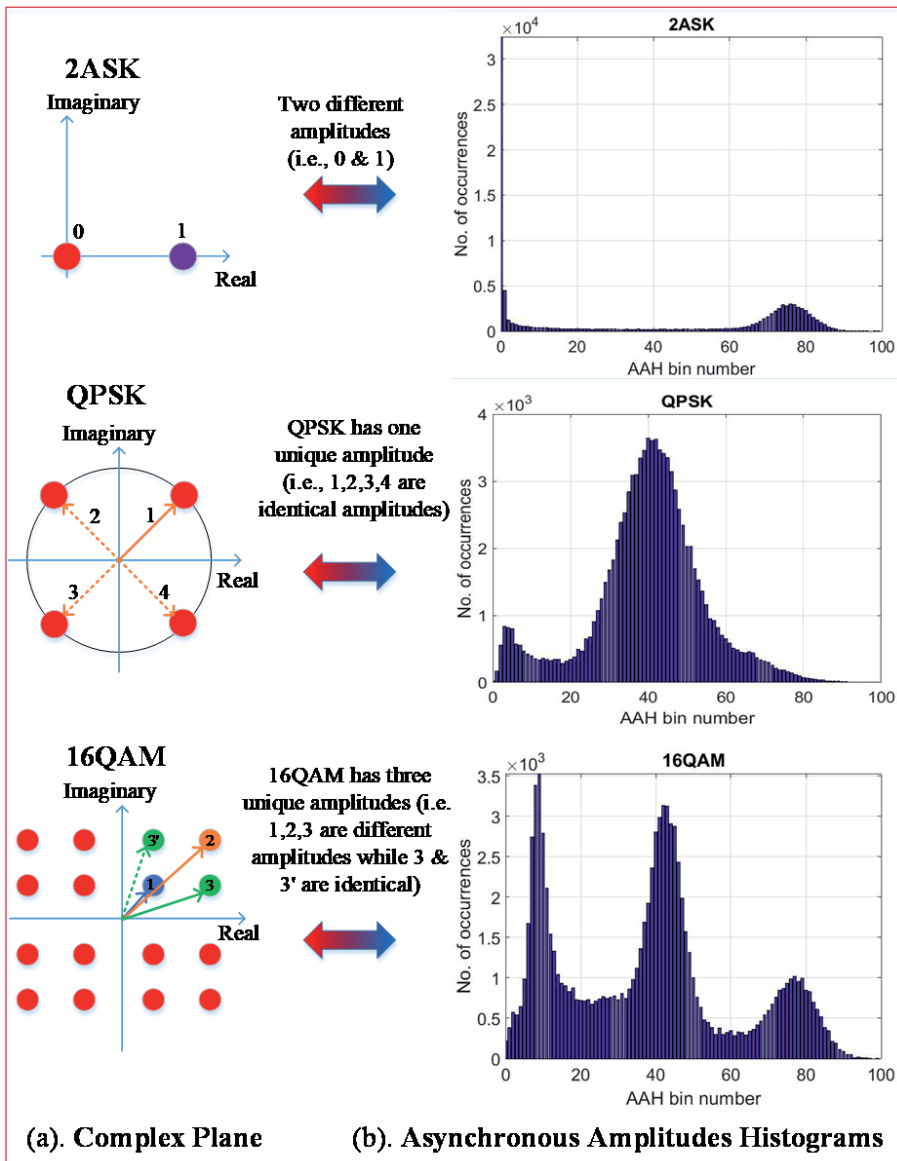
Figure 8.
The main idea of AAHs-based signals (three different modulations i.e., ASK, QPSK, and 16QAM) [21].

As illustrated in **Figure 8**, the main constellation diagrams of three different signals and the corresponding AAHs are shown. Asynchronous shift keying (ASK) has two constellation levels (0 and 1), therefore, two unique peaks appear in the corresponding histogram. But, the case is different in the second histogram for the quadrature-PSK, where one unique peak exists. This is due to the existence of single equal amplitude for the four constellation points in the related constellation diagram. In 16QAM modulation, AAHs show different shape than in the previous two signals. As portrayed in the complex plane for this type, there are 16 points of constellations but only three unique amplitude levels exist, and this interprets why we have three amplitude levels in the corresponding AAH for this signal. We can conclude that AAHs feature demonstrates distinctive signatures among various digital modulations of detected signals. This, in turn, will facilitate the job of the receiver node in the network to automatically recognize the type of modulation being used by the transmitter node leaving the necessity to obtain this information from the transmitter vehicle beforehand.

In the subsequent procedure, the aforementioned features will be fed into a machine learning tool as an input vector in order to enable autonomous recognition at the receiver terminal in the vehicular network. Machine learning tools have found a versatile deployment in different aspects of our lives. They construct smart systems to experience challenging environments. Moreover, they process large quantity of data generated from multiple resources, to extract useful and unique models that can be efficiently utilized in intelligent telecommunications terminals [17]. AI (i.e., machine & deep learning) techniques are still an attractive research direction in the vehicular communication to be more explored. They have the potential to enable data-driven decisions and offer exceptional services in the vehicular networks such as instant traffic control and estimation, position-based facilities, and of course, autonomous driving. Basically, machine learning tools can be broadly classified into two main groups. One called supervised learning machine, the second one is unsupervised machine. The former requires a training process for the classifier\ regressor whereas the latter does not use training subset and usually its task is for clustering and dimension reduction process.

Artificial intelligent (AI) tools have been regarded as a key solid solution to the challenges experienced by self-driving vehicles, such challenges are heavy rain, dense fog or snow, and any other difficult hostile weather conditions. For instance, authors in [22] have proposed a novel scheme to enable awareness and clear vision in automated cars of their surroundings. They deployed deep neural network in combination with the automatic white balance joined with laplacian pyramids (AWBLP) technique in order to enhance the contrast and resolution of the captured vehicle image. For a missed or wrong detection in the adverse condition of weather, they proposed an online tracking system and constructed a dataset which can serve as a benchmark called, detection in adverse weather nature (DAWN) aiming to examine their proposed system. Sample images of the DAWN dataset, before restoration, are shown in **Figure 9** where this dataset covers four challenging weather conditions for automatous vehicles.

The images in this dataset will be restored to enhance their resolution and then to be input into the deep learning tool. This is to perform an online detection of the vehicles and enable them to see each other in difficult weather conditions, and therefore to increase the road safety. However, we have enhanced the resolution of the sample images in **Figure 9** just to add more clarity and visibility for the reader as reflected in **Figure 10**. More challenges will be overcome in the industry domain with such current proposed panacea like DAWN and AWBLP. However, more investigations on other deep learning types, their parameters and their performance to serve cellular V2X networks are still demanded.

Figure 9.
Different groups of images that describe four challenging weather conditions in DAWN dataset.

Figure 10.
Samples from DAWN dataset after enhancing their resolution.

5. Conclusion

This chapter has offered an insight to the scientific community about the potential enhancement of V2X schemes by the deployment of 5G communication network. Let recap what have been addressed earlier, the 5G & beyond wireless systems will enable vehicles to talk to each other and to different infrastructures. Furthermore, the latest advancements in 3GPP enable deploying 5G as a great communication paradigm for V2X networks. In addition, the 5G sidelinks offer unicast, groupcast and broadcast transmission in vehicular communication networks. Furthermore, 5G & beyond systems can enhance the DSCR for collision-free and road safety. With the emergence of 5G technology, the cellular V2X networks will track the momentum and gain more capabilities and connectivity.

The chapter has also paved the way to a prospective research direction on signal recognition schemes (i.e., AMR & SNR) in V2X communication networks. Furthermore, it shed light on their potential techniques and the significance of their role in V2X networks in increasing security levels and enhancing V2V communication system throughput. However, further investigation on identifying many other parameters is required. For instance, a vehicular node in future intelligent V2V networks is envisaged to go adaptive and vary the transmitted power or transmission data rate when sensing the wireless channel.

On the other hand, simultaneous recognition of multiple signal parameters of a vehicle in V2X networks remains a future challenge in the V2X future development. Besides, issues related to wider coverage range utilizing wireless cooperative communication schemes; and matters concerned about higher levels of security in V2X networks with arising complexity of densely connected things will be attractive topics in the near future.

Abbreviations

V2X	Vehicle-to-Everything
V2V	Vehicle-to-Vehicle
5G	Fifth-Generation
SVM	Support Vector Machine
LTE	Long-Term Evolution
DNN	Deep Neural Network
IoE	Internet of Everything
6G	Six-Generation
3GPP	Third Generation Partnership Project
D2D	Device-to-Device
GPS	Global Positioning System
RSU	Roadside Unit
QoS	Quality of Service
ETSI	European Telecommunications Standards Institute
NR	New Radio
CAM	Cooperative Awareness Message
TSG	Technical Specification Group
SA1	System Aspects Working Group 1
CCI	Control Channel Information
HARQ	Hybrid Automatic Repeat Request
FR1	Lower Frequency Band
FR2	Higher Frequency Band
WAVE	Wireless Access in Vehicular Environment
ITS	Intelligent Transport System
UDP	User Datagram Protocol
IPV6	Internet Protocol Version 6
IM	Indexed Modulation
PSK	Phase Shift Keying
QAM	Quadrature Amplitude Modulation
AMR	Automatic Modulation Recognition
ML	Maximum Likelihood Approach
FB	Feature-Based Approach
AAH	Asynchronous Amplitude Histogram
2D-ASIQH	Two-dimensional Asynchronous Sampled In-phase-Quadrature Amplitude
AWBLP	Automatic White Balance Joined with Laplacian Pyramid
DAWN	Detection in Adverse Weather Nature

Author details

Tarik Adnan Almohamad[1*], Muhammet Tahir Güneşer[1], Mohd Nazri Mahmud[2] and Cihat Şeker[1]

1 Electrical-Electronics Engineering Department, Faculty of Engineering, Karabük University, 78050, Karabük, Turkey

2 School of Electrical and Electronic Engineering, Universiti Sains Malaysia, Seri Ampangan, 14300 Nibong Tebal, Pulau Pinang, Malaysia

*Address all correspondence to: tam_jami@hotmail.com; tarikalmohamad@karabuk.edu.tr

IntechOpen

References

[1] K. B. Letaief, W. Chen, Y. Shi, J. Zhang, and Y. A. Zhang, "The Roadmap to 6G: AI Empowered Wireless Networks," *IEEE Communications Magazine,* vol. 57, no. 8, pp. 84-90, 2019.

[2] J. Sang, T. Zhou, T. Xu, Y. Jin, and Z. Zhu, "Deep Learning Based Predictive Power Allocation for V2X Communication," *IEEE Access,* vol. 9, pp. 72881-72893, 2021.

[3] S. Chen *et al.*, "Vehicle-to-Everything (v2x) Services Supported by LTE-Based Systems and 5G," *IEEE Communications Standards Magazine,* vol. 1, no. 2, pp. 70-76, 2017.

[4] S. A. Ashraf, R. Blasco, H. Do, G. Fodor, C. Zhang, and W. Sun, "Supporting Vehicle-to-Everything Services by 5G New Radio Release-16 Systems," *IEEE Communications Standards Magazine,* vol. 4, no. 1, pp. 26-32, 2020.

[5] 5G Americas, "Cellular V2X Communications Towards 5G," *White Paper,* Mar. 2018.

[6] ETSI EN. 637-3, "Intelligent Transport Systems; Vehicular Communications; Basic Set of Applications; Part 3: Specification of Decentralized Environmental Notification Basic Service," no. v.1.2.2, Nov. 2014.

[7] ETSI EN 302 637-2, "Intelligent Transport Systems Vehicular Communications; Basic Set of Applications; Part 2: Specification of Cooperative Awareness Basic Service," no. v.1.3.2, Nov. 2014.

[8] 5G Automative Association, "C-V2X Use Cases, Methodology, Examples and Service Level Requirements," *White Paper,* June 2019.

[9] 3GPP TS 22.186 v16.2.0, "Enhancement of 3GPP Support for V2X Scenarios," June 2019.

[10] 3GPP RP-190726, "New WID: Physical Layer Enhancements for NR Ultra-Reliable and low Latency Communication (URLLC)," Mar. 2019.

[11] 3GPP RP-190766, "New WID on 5G V2X with NR Sidelink," Mar. 2019.

[12] B. S. Gukhool and S. Cherkaoui, "IEEE 802.11p modeling in NS-2," in *2008 33rd IEEE Conference on Local Computer Networks (LCN)*, 2008, pp. 622-626.

[13] S. Biswas, R. Tatchikou, and F. Dion, "Vehicle-to-vehicle wireless communication protocols for enhancing highway traffic safety," *IEEE Communications Magazine,* vol. 44, no. 1, pp. 74-82, 2006.

[14] T. L. Willke, P. Tientrakool, and N. F. Maxemchuk, "A survey of inter-vehicle communication protocols and their applications," *IEEE Communications Surveys & Tutorials,* vol. 11, no. 2, pp. 3-20, 2009.

[15] Y. He, M. A. Chowdhury, P. Pisu, X. Kang, and J. Johnson, "Vehicle-Infrastructure Integration-Enabled Plug-in Hybrid Electric Vehicles for Optimizing Energy Consumption," *In Meeting of the Transportation Research Board,* vol. Washington, DC,, 2011.

[16] T. A. Almohamad, M. F. M. Salleh, M. N. Mahmud, İ. R. Karaş, N. S. M. Shah, and S. A. Al-Gailani, "Dual-Determination of Modulation Types and Signal-to-Noise Ratios Using 2D-ASIQH Features for Next Generation of Wireless Communication Systems," *IEEE Access,* vol. 9, pp. 25843-25857, 2021.

[17] H. Ye, L. Liang, G. Y. Li, J. Kim, L. Lu, and M. Wu, "Machine Learning for Vehicular Networks: Recent Advances and Application Examples," *IEEE Vehicular Technology Magazine,* vol. 13, no. 2, pp. 94-101, 2018.

[18] P. Yang, Y. Xiao, Y. L. Guan, M. D. Renzo, S. Li, and L. Hanzo, "Multi-domain Index Modulation for Vehicular and Railway Communications: A Survey of Novel Techniques," *IEEE Vehicular Technology Magazine,* vol. 13, no. 3, pp. 124-134, 2018.

[19] T. A. Almohamad, M. F. M. Salleh, M. N. Mahmud, A. H. Y. Sa'd, and S. A. Al-Gailani, "Automatic Modulation Recognition in Wireless Communication Systems Using Feature-Based Approach," in *10th International Conference on Robotics, Vision, Signal Processing and Power Applications*, Singapore, 2019, pp. 403-409: Springer Singapore.

[20] O. A. Dobre, A. Abdi, Y. Bar-Ness, and W. Su, "Survey of automatic modulation classification techniques: classical approaches and new trends," *IET Communications,* vol. 1, no. 2, pp. 137-156, 2007.

[21] T. A. Almohamad, M. F. M. Salleh, M. N. Mahmud, and A. H. Y. Sa'D, "Simultaneous Determination of Modulation Types and Signal-to-Noise Ratios Using Feature-Based Approach," *IEEE Access,* vol. 6, pp. 9262-9271, 2018.

[22] M. Hassaballah, M. A. Kenk, K. Muhammad, and S. Minaee, "Vehicle Detection and Tracking in Adverse Weather Using a Deep Learning Framework," *IEEE Transactions on Intelligent Transportation Systems,* pp. 1-13, 2020.

Chapter 7

Advanced Driving Assistance System for an Electric Vehicle Based on Deep Learning

Abdelaziz Sahbani and Hela Mahersia

Abstract

This chapter deals with a design of a new speed control method using artificial intelligence techniques applied to an autonomous electric vehicle. In this research, we develop an Advanced Driver Assistance System (ADAS) which aims to enhance the driving manner and the safety, especially when traveling too fast. The proposed model is a complete end-to-end vehicle speed system controller that proceeds from a detected speed limit sign to the regulation of the motor's speed. It recognizes the speed limit signs before extracting from them, a speed information that will be sent, as reference, to a NARMA-L2 based controller. The study is developed specially for electric vehicle using Brushless Direct Current (BLDC) motor. The simulation results, implemented using Matlab-Simulink, show that the speed of the electric vehicle is controlled successfully with different speed references coming from the image processing unit.

Keywords: Brushless DC, Deep learning, Intelligent electrical vehicle, NARMA-L2 controller, Speed control, Traffic sign recognition

1. Introduction

Nowadays, internal combustion engine vehicles are the major source of air pollution and damage to our health. To solve these problems, electric vehicles are one of the most encouraging energy saving and environmental protection solutions. However, such solutions show luck of autonomy. The current trend in vehicle transportation is to implement solution where the driver and an intelligent system coexist and communicate to improve road safety and security. Advanced driver assistance systems (ADAS) are bridging the gap between traditional electric vehicles and the vehicles of tomorrow which are intelligent, autonomous and safe for the drivers, the passengers and everyone else on the road.

Generally, an autonomous electric vehicle consists of 4 main modules: the energy source module, the auxiliary module, the intelligent module composed of computers, sensors and actuators, and an electrical propulsion module [1], which consists of an electronic controller, a power converter, a mechanical transmission and an electric motor of either AC or DC, as shown in **Figure 1**. The motors convert the electrical energy that comes from the battery into a mechanical energy that allows the vehicle to move. They can also be considered as generators when sending energy back to the source of energy.
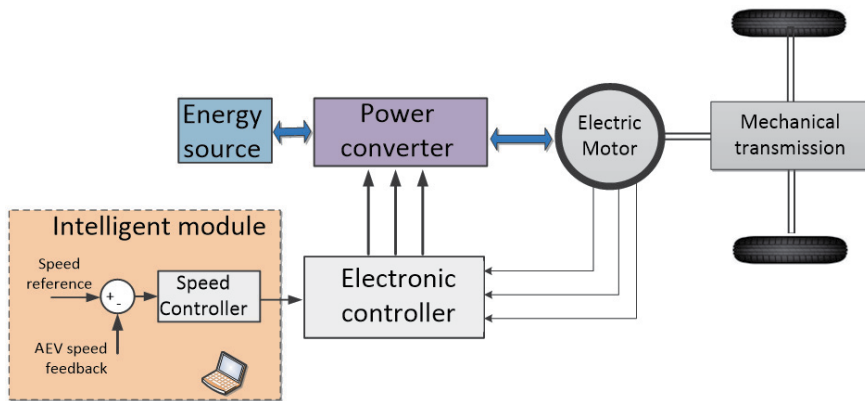
Figure 1.
Block of diagram of an Autonomous electric vehicle.

According to the specific requirements needed for autonomous electric vehicle's applications, such as, robustness, power, speed range and level of noise, the choice of motors can vary depending on their types. DC motors have been widely used since they fulfill some of the requirements mentioned before [2]. However, in recent years, in order to compensate for their electrical losses and mechanical friction, they have been replaced by Brushless DC Motors (BLDC), given their high efficiency and low noise [3–5]. Besides, BLDC are known to have a big initial torque with small size and low weight. They also can be built in the tires to reduce the complexity and weight of the driving mechanism.

Speed regulation is an important control challenge for any BLDC motor. In [6], the authors proposed an implementation of Space Vector Pulse Width Modulation (SVPWM) for the control of the power converter and the BLDC motor. They showed that using SVPWM methodology, offers the minimum switching losses, reduces harmonics compared with the other Pulse Width Modulation (PWM) methods.

In order to enhance and perfect the speed adaptation of the autonomous electric vehicle, while assisting at the same time the driver, and increasing its safety and security, ADAS has been developed, relying on inputs from multiple data sources, including automotive imaging, image processing, and in-vehicle networking.

In fact, It has been said that 80–90% of the driver's performance depends on visual information [2]. This is why, a huge number of collisions occur when the driver is not looking forward or unable to stop at an intersection due to excessive speed. It will be very important to automatically detect the speed limit sign and control the vehicle's speed when it is traveling too fast. Various ADAS are now designed with a large number of sensors and actuators to analyze the environment and take the appropriate actions. Among the existing ADAS systems, the traffic sign recognition holds a lot of potential as they enhance the driver's safety by notifying him about possible dangers related to speed.

The automatic recognition of these signs, however, is not easy to carry due to the weather's conditions, the blur resulting from moving vehicles and the lighting conditions. **Figure 2** shows some of these factors that make it difficult to identify the road signs.

To handle these challenges, researchers recommended the use of image processing and machine learning techniques. The automatic recognition of traffic signs includes, mainly, the traffic sign detection and the traffic sign classification.

Traffic signs have several distinctive features like colors, shapes and symbols. In the detection stage, the input images are preprocessed, enhanced and then, segmented according to their color or geometry. Color-based methods usually use

Figure 2.
Difficulties that affect the traffic sign recognition systems.

normalized RGB space [7–10] or HSV space [11–16] or YUV space [17] to distinguish between traffic and non traffic signs. However, these methods are generally affected by the weather conditions and the illumination variations.

Geometry-based methods are, on the contrary, robust to the illumination changes since they characterize the shape of the traffic sign. Mainly, authors used corner detection [11, 18], distance transform [19], Hough transform [20, 21] or radial geometry voting [22–24].

Recently, many researchers combined the color-based methods with the shape-based methods to achieve better results [10, 13, 16, 25, 26]. For instance, authors in [16], used color segmentation to roughly identify the sign before applying a matching technique based on the logical XOR operator using the shape extracted details. Similarly, authors in [10] used color segmentation to roughly locate the signs and then, used the shape information to eliminate the false candidates.

As for the classification stage, many methods have been used to identify the class of the traffic signs, such as, Support Vector Machine (SVM) [8, 13, 16], Viola-Jones detector [27, 28], neural networks [2, 15] and random forest [29, 30].

As we can see, all the presented researches focused only on recognizing traffic signs without trying to integrate and test them into a complete system controlling mechanical and electrical part. In [2], the authors designed an end-to-end system, where they proposed a NARMA-L2 neuro controller for speed regulation based on steerable decomposition and Bayesian neural networks. Despite the acceptable accuracy rate (about 0.975), it failed, unfortunately, to accurately recognize noisy signs.

In this chapter, we continue to design an end-to-end system, based on deep learning approaches, that enhances autonomous vehicle speed control and presents better performances in the presence of noisy inputs.

The rest of this chapter is organized as follows: in Section 2, we describe the proposed model. Section 3 will be reserved to the experimental results and finally, Section 4 will conclude the paper.

2. The proposed speed controller based on traffic sign recognition

The proposed speed control system comprises two main modules, an image processing module and a control module. The first module recognizes the speed limit signs before extracting from them, a speed information that will be sent to the control module. An overview of these units is shown in **Figure 3**.

2.1 The image processing module

This first module aims to recognize the speed limit traffic sign whatever the weather conditions are. **Figure 4** presents the proposed model of the speed limit sign recognition system. This system will perform two important tasks: detecting the sign and then identifying the speed. As it is shown in **Figure 4**, this unit receives an input
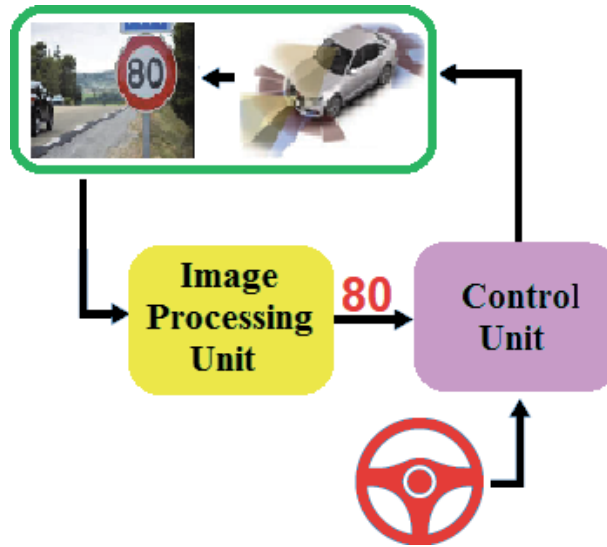
Figure 3.
The proposed speed control system.
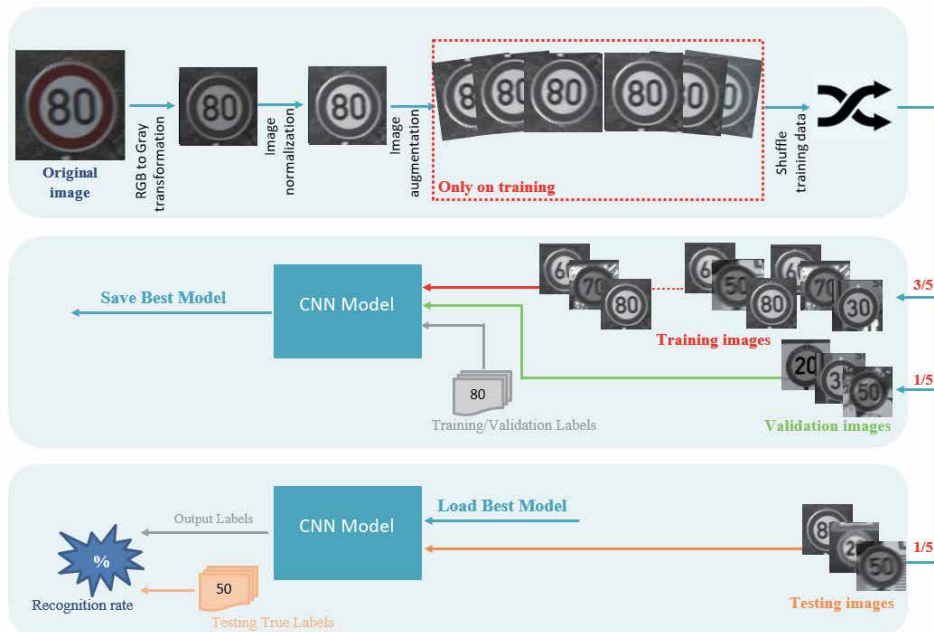
Figure 4.
The proposed speed limit sign recognition module.

image, performs grayscale transformation before normalization and noise removal. Lastly, each preprocessed image will be fed to a CNN unit for a classification process.

2.1.1 The preprocessing stage

In order to prepare the deep neural network to learn relevant features from speed-limit images, additional processing is required: first of all, we expand the training images, then, we normalize the augmented images, and finally, we filter them with a median filter.

- Data normalization:

  In this step, we normalized the gray scale images in order to reduce poor lighting variations observed in the database. Let $Im(i,j)$ denotes the grayscale value of pixel (i,j), Me and Std denote the estimated mean and standard deviation of Im, respectively, and $Nor(i,j)$ denotes the normalized grayscale value of pixel (i,j). The normalized image is defined using Eq. (1):

$$Nor(i,j) = \frac{(Im - Me) * Constant_1}{Std + Constant_2} \tag{1}$$

  $Constant_1$ and $Constant_2$ are two constants set experimentally to 50 and 100 respectively. **Figure 5** shows the images obtained by 1. Finally, a median filter is applied to the normalized input image to obtain an enhanced speed sign image.

- Data augmentation: Deep neural networks require a huge learning database to perform the speed limit recognition task. However, most publicly available databases suffer from lack of data. Increasing these databases is, therefore, a crucial step for an accurate sign recognition. Moreover, an augmentation on the training data makes the proposed model more robust to geometric changes. **Figure 6** shows a sample speed limit image with different augmentation techniques applied to it: vertical flipping, rotation with small angles $\in [-8°, 8°]$ and horizontal translation of 1 unit to both sides right and left.
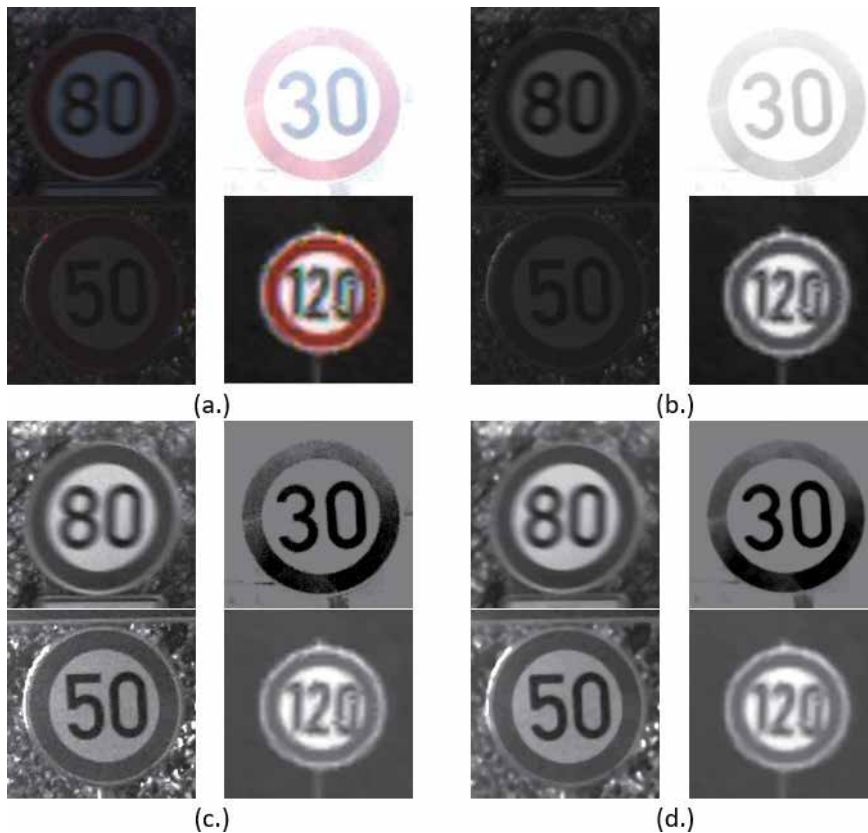
Figure 5.
Data normalization: a. Original images. b. After Grayscale transformation, c. After normalization by Eq. (1) and d. after median filtering.
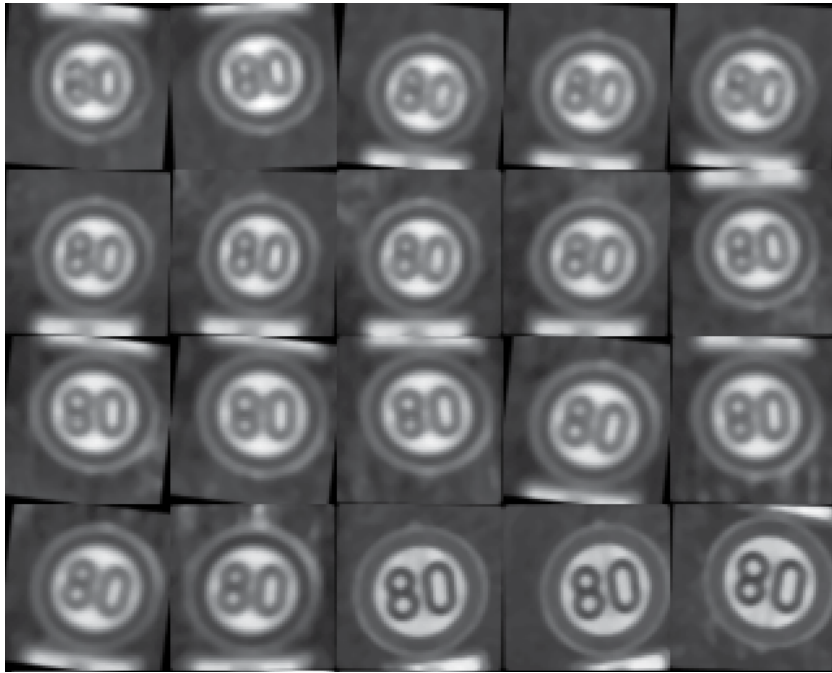
Figure 6.
Some of the transformations used for data augmentation.

2.1.2 The deep learning stage

In this chapter, in order to extract features and organize speed signs in categories, a Convolutional Neural Network was therefore used. The architecture of the proposed CNN, which has three convolution layers, and one output layer, is presented in **Figure** 7. The first, third and fifth layers are convolution layers with 8, 16 and 32 kernels, respectively, with a size of 5x5. The activation function in the CNN is a rectified linear unit (Relu) function. Sub-sampling is presented in the second, fourth and sixth layers. We used also a max pooling layer with a kernel size of 2x2 and a step size of 2. We flatted the sub-sampling to a 1152-dimensional vector and directly connected the output layer with a soft-max activation function.

2.2 The speed control module

The aim of this unit is to control the speed of the autonomous electric vehicle using information coming from the image processing unit as speed reference and then, input it to the control unit. The studied traction system is composed of BLDC motor, three phase Mosfets inverter, a gearbox bloc associated with mechanical differential used for speed adaptation for the shaft and the two wheels
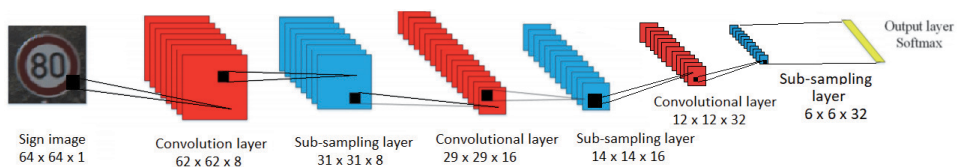
Figure 7.
Proposed CNN's structure.

(see **Figure 8**). The traction system can be changed by a single wheel [31] if we don't take in consideration the mechanical differential part.

Figure 8 shows the control strategy of the AEV using BLDC motor. The feedback signals are the motor speed signal measured by the speed sensor and the rotor's position taken from the three hall sensors. The speed controller unit receive the reference speed signal from the digital processing unit (detected from the trafic speed sign) and the actual speed of the motor (actual vehicle speed). Then, the generated PWM refers to the error between the reference speed and the measured speed as well as the commutation sequence of three hall sensor signals H_{sa}, H_{sb} and H_{sc} (**Figure 9**) in order to control the three phase inverter switches [32].

The three phase inverter consists of six Mosfet switches $Q_{i,i=1,..,6}$ and six freewheeling diode as shown in **Figure 10**. Considering that the motor is in clockwise
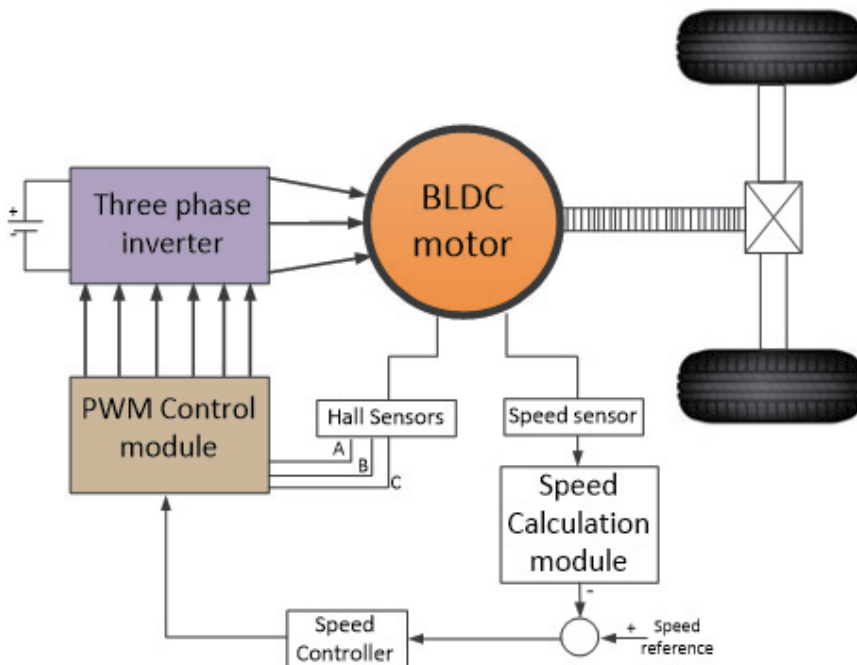
Figure 8.
Control strategy block diagram of the EV drive system using BLDC motor.
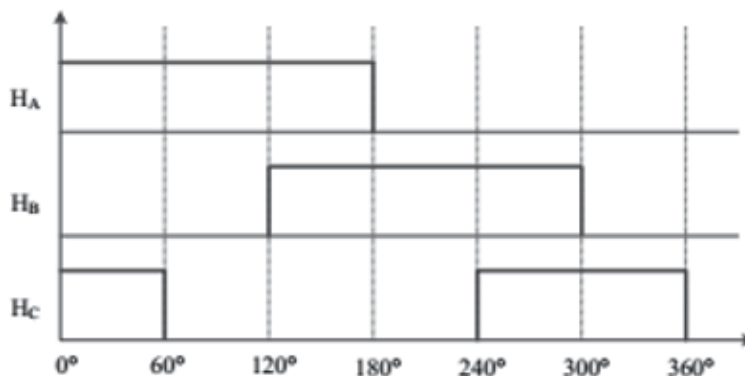
Figure 9.
Hall sensors output signals in a 360 electrical degrees cycle.
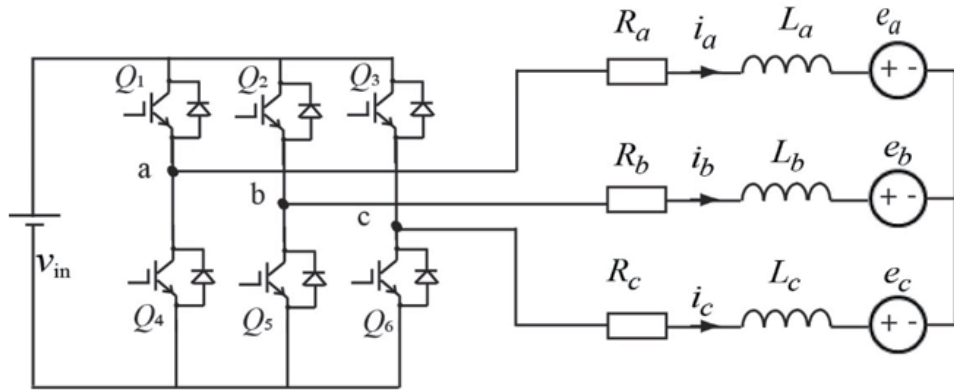
Figure 10.
Equivalent circuit of the BLDC motor associated with three-phase inverter.

Cycle	Hall Sensors			Switches State					
	H_a	H_b	H_c	S_{w1}	S_{w2}	S_{w3}	S_{w4}	S_{w5}	S_{w6}
1	1	0	1	1	0	0	1	0	0
2	1	0	0	1	0	0	0	0	1
3	1	1	0	0	0	1	0	0	1
4	0	1	0	0	1	1	0	0	0
5	0	1	1	0	1	0	0	1	0
6	0	0	1	0	0	0	1	1	0

Table 1.
Hall sensors output and the switch state.

revolution, the state of the six switches (S_{w1}, S_{w2}, S_{w3}, S_{w4}, S_{w5} and S_{w6}), depending to the three Hall sensors state (H_{as}, H_{sb} and H_{sc}), are shown in **Table 1**.

2.2.1 Mathematical model of the studied BLDC motor

The BLDC motor has three windings coupled in Y-connected on the stator with a permanent magnets rotor with. If we neglect any saturation effects with a constant parameters in the three phase.

The electrical equations of the BLDC motor are described by:

$$
\begin{bmatrix} V_{as} \\ V_{bs} \\ V_{cs} \end{bmatrix} = \begin{bmatrix} R_s & 0 & 0 \\ 0 & R_s & 0 \\ 0 & 0 & R_s \end{bmatrix} + \frac{d}{dt} \begin{bmatrix} L_{aa} & L_{ab} & L_{ac} \\ L_{ba} & L_{bb} & L_{bc} \\ L_{ca} & L_{cb} & L_{cc} \end{bmatrix} \begin{bmatrix} i_a \\ i_b \\ i_c \end{bmatrix} + \begin{bmatrix} e_a \\ e_b \\ e_c \end{bmatrix} \tag{2}
$$

Where:

- V_{as}, V_{bs} and V_{cs} are the Stator voltages,

- R_s is the stator resistance ($R_a = R_b = R_c = R_s$),

- i_a, i_b and i_c are the stator currents,

- L_{aa}, L_{bb} and L_{cc} are Self Inductances of phases a, b and c, respectively,

- L_{ab}, L_{ac} and L_{bc} are Mutual Inductances,

- e_a, e_b and e_c are back EMF's.

$$\text{If} \begin{cases} L_{aa} = L_{bb} = L_{cc} = L \\ L_{ab} = L_{ba} = L_{ac} = L_{ca} = L_{bc} = L_{cb} = M \end{cases} \tag{3}$$

The state space representation of motor becomes:

$$\begin{bmatrix} V_{as} \\ V_{bs} \\ V_{cs} \end{bmatrix} = \begin{bmatrix} R_s & 0 & 0 \\ 0 & R_s & 0 \\ 0 & 0 & R_s \end{bmatrix} + \frac{d}{dt} \begin{bmatrix} L & M & M \\ M & L & M \\ M & M & L \end{bmatrix} \begin{bmatrix} i_a \\ i_b \\ i_c \end{bmatrix} + \begin{bmatrix} e_a \\ e_b \\ e_c \end{bmatrix} \tag{4}$$

In addition, at balanced condition of motor phase, we have:

$$i_a + i_b + i_c = 0 \tag{5}$$

and

$$L_s = L - M \tag{6}$$

so the state space representation is:

$$\begin{bmatrix} V_{as} \\ V_{bs} \\ V_{cs} \end{bmatrix} = \begin{bmatrix} R_s & 0 & 0 \\ 0 & R_s & 0 \\ 0 & 0 & R_s \end{bmatrix} + \frac{d}{dt} \begin{bmatrix} L_s & 0 & 0 \\ 0 & L_s & 0 \\ 0 & 0 & L_s \end{bmatrix} \begin{bmatrix} i_a \\ i_b \\ i_c \end{bmatrix} + \begin{bmatrix} e_a \\ e_b \\ e_c \end{bmatrix} \tag{7}$$

The three back EMF (have trapezoidal form) are represented by:

$$\begin{bmatrix} e_a \\ e_b \\ e_c \end{bmatrix} = \omega_m . \lambda_m \begin{bmatrix} f_{as}(\theta_r) \\ f_{bs}(\theta_r) \\ f_{cs}(\theta_r) \end{bmatrix} \tag{8}$$

Where:

- ω_m is the rotor speed (rad/s),

- θ_m is the rotor position (rad),

- The functions $f_{as}(\theta_r)$, $f_{bs}(\theta_r)$ and $f_{cs}(\theta_r)$ are represented by **Table 2**.

2.2.2 Implementation of NARMA-L2 neuro controller for speed regulation

Many speed controllers have been frequently used in literature, such as PI (proportional integral) and PID (Proportional integral derivative) (PID), given their simple structure, rapid-reaction and reasonable cost. However, they exhibit a slow response when associated with dynamic loads. Recently, intelligent-based

θ_e	$f_{as}(\theta_r)$	$f_{bs}(\theta_r)$	$f_{cs}(\theta_r)$
0°-60°	1	−1	$1 - \frac{6\theta_e}{\pi}$
60°-120°	1	$\frac{6\theta_e}{\pi} - 3$	−1
120°-180°	$5 - \frac{6\theta_e}{\pi}$	1	−1
180°-240°	−1	1	$\frac{6\theta_e}{\pi} - 7$
240°-300°	−1	$9 - \frac{6\theta_e}{\pi}$	1
300°-360°	$\frac{6\theta_e}{\pi} - 11$	−1	1

Table 2.
Functions $f_{as}(\theta_r)$, $f_{bs}(\theta_r)$ and $f_{cs}(\theta_r)$.

controller, such as neural networks control (NNC), genetic algorithms and fuzzy logic control, were exploited in the speed control of BLDC [2]. Among these techniques, the neural networks are considered in this chapter, because they are the most suitable to handle the non-linearity of the BLDC system that contains uncertainties. Thus, an intelligent neuronal controller is proposed, based on Nonlinear Auto-regressive Moving Average Level-2 model (NARMA L2).

There are two steps involved in the control process. The first step is the feedback linearization to identify the system to be controlled, while the second step is the training of the system's dynamics. Generally, the NARMA L2 nonlinear description of the system is represented by a discrete-time n^{th} order equation (Eq. (9))

$$
\begin{aligned}
y(k + d) = &f(y(k), y(k - 1), \dots y(k - n + 1), u(k), u(k - 1), \\
&\dots, u(k - n + 1)) + g(y(k), y(k - 1), \dots y(k - n + 1), \\
&u(k), u(k - 1), \dots, u(k - n + 1)).u(k)
\end{aligned}
\tag{9}
$$

Where $u(k)$ is the system input, $y(k)$ the system output and d is the system delay. $f(.)$ and $g(.)$ are the additive and the multiplicative non-linear terms respectively, to be approximated in the training step. The **Figure 11** shows the structure of NARMA-L2 Model (**Figure 12**).
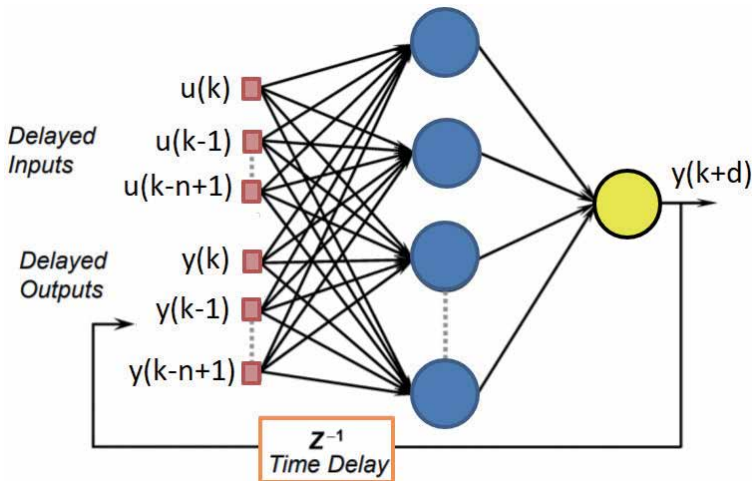
Figure 11.
NARMA-L2 Model.
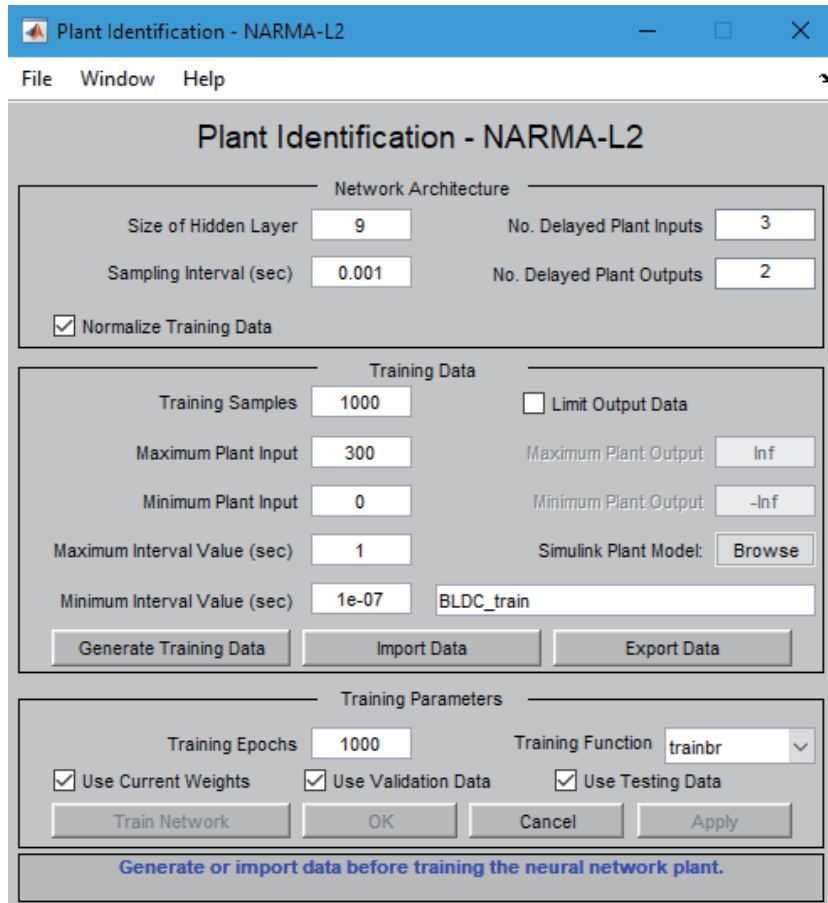
Figure 12.
Specifications of the plant model.

3. Experiments and discussion

In this section we present the dataset and the details of the experiments performed in this study. Experiments were performed to select the best number of folds, the best number of layers and the best optimization's function. The final proposed model was implemented using Matlab 2018 with an Intel Core i7 1.8 GHz CPU working in a windows 10 environment. The simulink model of the proposed algorithm is presented by **Figure 13**.

3.1 Used database

In order to validate the proposed method, we used the German traffic sign recognition benchmark (GTSRB). To solve the traffic sign recognition problem, this database has been made with different visual indications. The image qualities vary depending on the illumination, the contrast and the color. **Table 3** shows some details of the data-set used in our work.

3.2 Speed sign recognition result

The partitioning of the input data was performed randomly according to 10-folds cross-validation procedure: we divided the training database into ten folders.
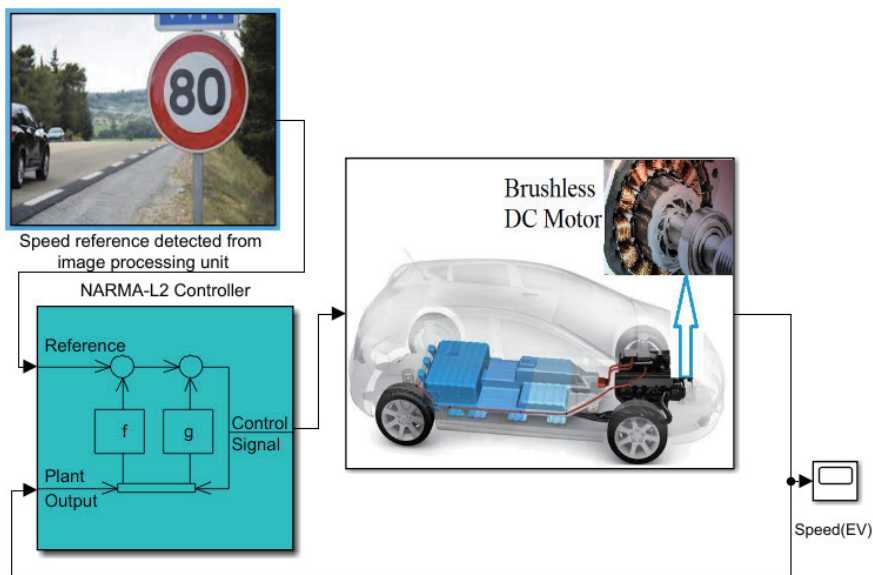
Figure 13.
Simulink model of our algorithm.

Speed limit sign	Class	Nb of Training image	Nb of Testing image
30	1	2220	17
50	2	2250	27
60	3	1410	229
70	4	1980	304
80	5	1858	573
100	6	1439	281
120	7	1410	450
Total images		**12567**	**1881**

Table 3.
Characteristics of the used database.

Each time, we used one folder as a validation set and we trained the nine remaining folders. The process will continue until the validation error starts increasing. At this moment, the training procedure will be stopped, and then saved. After running the 10-folds, we have selected the best neural network obtained with the best validation performances. An example can be shown in **Figure 14**. Concerning the final recognition rate, it will be calculated after trying the test database with the selected network that assigns the value of 1 for exact speed limit sign and 0 for all other signs (**Figure 15**). The average speed limit sign recognition rate obtained after several tries is 90.8% with a validation accuracy 0f 94.75% (**Table 4**).

As can be seen from **Figure 16**, 100 and 60 are two of the most difficult signs to classify, whereas 30 and 50 are the easiest to recognize. **Table 4** summarizes the recognition rates obtained with different folds: 3, 5, 8 and 10 as well as the Area-Under-Curve of the ROC curve. The best recognition rates were obtained with 10-folds. Besides, we show in **Table 5** that the *adam* function is a best choice for the optimization of the deep learning network.
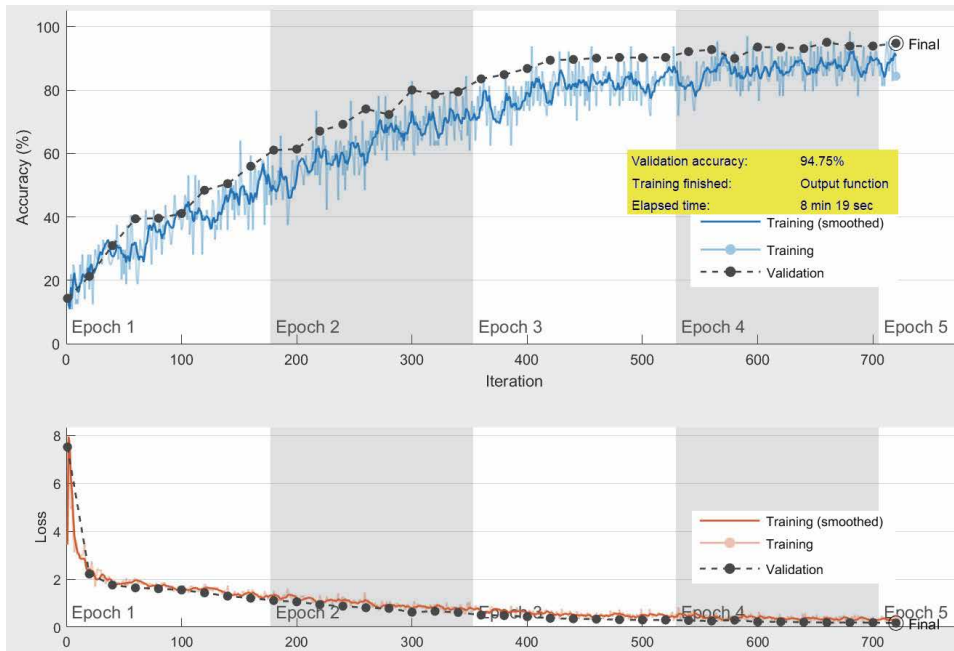
Figure 14.
Example of the best validation performance. The training stops when the validation error is increasing.

Figure 15.
Confusion matrix of the deep learning process.

K-Folds	Validation accuracy	Testing accuracy	AUC
3-folds	93.005 (%)	86.44 (%)	0.98
5-folds	93.95 (%)	87.9 (%)	0.998
8-folds	95.41 (%)	90.1 (%)	0.993
10-folds	**94.75 (%)**	**90.8 (%)**	**0.999**

Table 4.
Speed limit recognition accuracy with different k-folds.
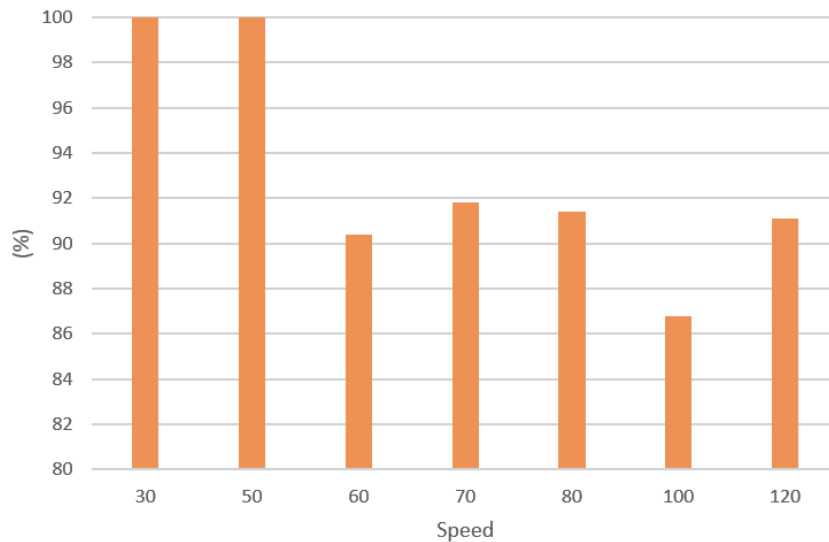
Figure 16.
Average recognition rates per speed limit sign.

Function	Testing accuracy
Sgdm	86.28 (%)
Rmsprop	84.68 (%)
adam	**90.8 (%)**

Table 5.
Speed limit recognition accuracy with different optimization function, K = 10 folds.

3.3 The NARMA L2 controller's result

The speed detected from the sign recognition process will be taken as a reference input to the NARMA L2 controller. Here, we must also train the controller to adjust the vehicle speed. The training data obtained from the NARMA-L2 controller are illustrated in **Figure 17**.

Figure 18, displays the speed response of the proposed system with both increase and decrease of speed reference. We notice that the speed reaches rapidly the desired value. The proposed controller presents a good behaviour upon disturbances, and thus it is stabilized after duration of 0.05 s with an almost no static error.
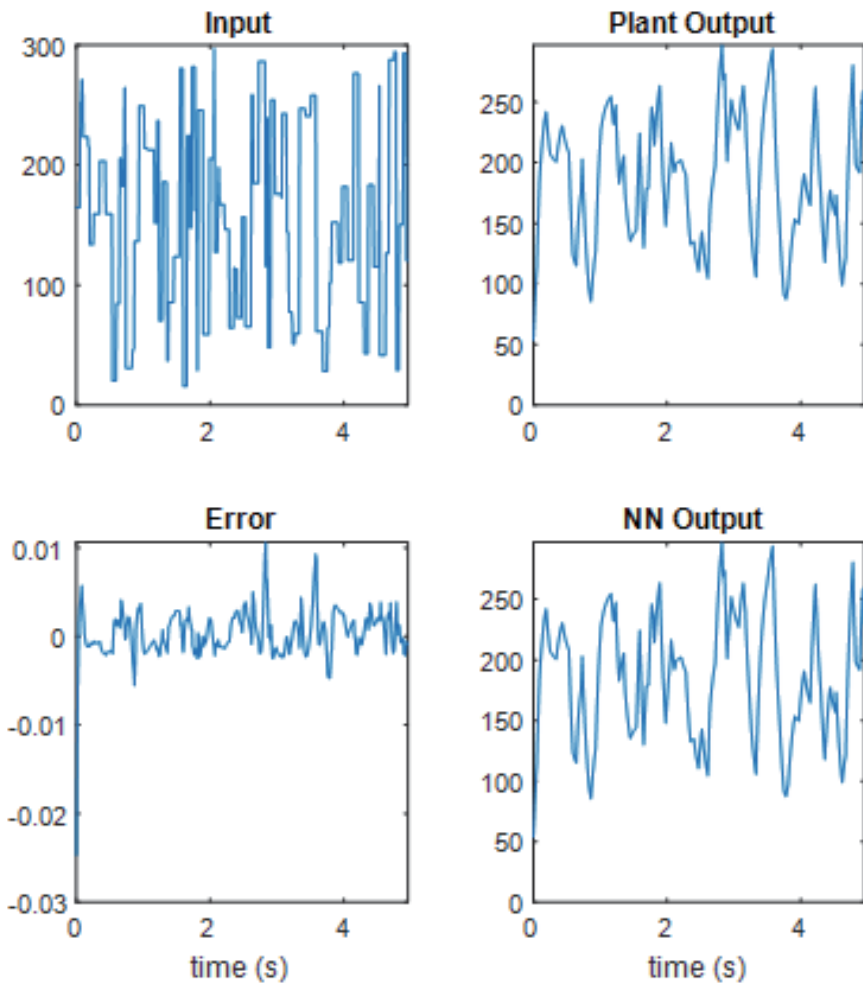
Figure 17.
Training data of NARMA L2 controller.
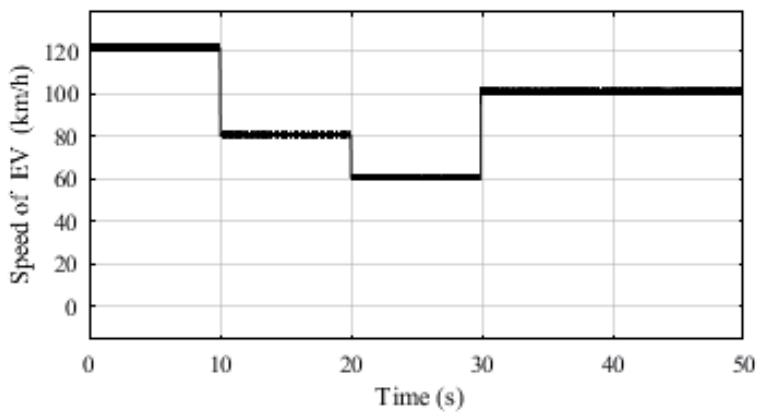
Figure 18.
Desired Speed curve with the NARMA L2 controller.

4. Conclusions

Deep learaning, image processing and NARMA-L2 controllers have been successfully developed and simulated using MATLAB to control the speed of a BLDC Motor by recognizing the traffic sign images. Simulation results show effectiveness of the proposed controllers for dealing with the motor system with nonlinearity under wide dynamic operation regimes.

Author details

Abdelaziz Sahbani[1,2*†] and Hela Mahersia[3†]

1 Medina College of Technology, Al-Madinah Al Munawwarah,
Kingdom of Saudi Arabia

2 Laboratory of Automatic (LARA), National Engineering School of Tunis, Tunis El Manar University, Tunisia

3 Signal, Image and Information Technology Laboratory (SITI), National Engineering School of Tunis, Tunis El Manar University, Tunisia

*Address all correspondence to: abdellazizsahbani@yahoo.fr

† These authors contributed equally.

IntechOpen

References

[1] K.-V. Singh, H.-O. Bansal, and D. Singh, A comprehensive review on hybrid electric vehicles: architectures and components, Journal of Modern Transportation, pp. 1-31, 2019.

[2] A. Sahbani, NARMA-L2 Neuro controller for speed regulation of an intelligent vehicle based on image processing techniques, In Proc. of the 21st IEEE Saudi Computer Society National Computer Conference (NCC 2018), 2018.

[3] A.-J. Godfrey and V. Sankaranarayanan, A new electric braking system with energy regeneration for a BLDC motor driven electric vehicle, Engineering Science and Technology, Vol. 21, pp. 704-713, 2018.

[4] M.-S. Kumar and S.-T. Revankar, Development scheme and key technology of an electric vehicle: an overview, Renew. Sustain. Energy Rev. Vol. 70, pp.1266-1285, 2017.

[5] C.-L. Jeong and J. Hur, A novel proposal to improve reliability of spoke-type BLDC motor using ferrite permanent magnet, IEEE Trans. Ind. Appl. Vol. 52, No. 5, pp. 3814-3821, 2016.

[6] F.-R. Yasien and R.-A. Mahmood, International Design New control System for Brushless DC motor Using SVPWM, Journal of Applied Engineering, Vol. 13, No. 1, pp. 582-589, 2018.

[7] H.Y. Yalic and A.B. Can, Automatic recognition of traffic signs in Turkey roads, In. Proc. of the 19 IEEE Signal Processing and Communications applications conference, 2011.

[8] X. Yuan, X.L. Hao, H.J. Chen and X. Y. Wei, Robust traffic sign recognition based on color global and local oriented edge magnitude patterns, IEEE Trans. on Intelligent Transportation Systems, Vol. 15, pp. 1466-1477, 2014.

[9] R. Timofte, K. Zimmermann, and L. Van Gool, Multi-view traffic sign detection, recognition, and 3D localisation, Mach. Vis. Appl., Vol. 25, No. 3, pp. 633-647, 2014.

[10] A. Alam and Z.-A. Jaffery, Indian Traffic Sign Detection and Recognition, International Journal of Intelligent Transportation Systems Research, pp. 1-15, 2019.

[11] A. Escalera, J.M. Armingol and M. Mata, Traffic sign recognition and analysis for intelligent vehicles, Image Vis. Comput., Vol. 21, No. 3, pp. 247-258, 2003.

[12] S. Maldonado, S. Arroyo, P. Jimenez, H. Moreno, and F. Ferreras, Road-sign detection and recognition based on support vector machines, IEEE. Trans. on Intelligent Transportation Systems, Vol. 8, pp. 264-278, 2007.

[13] J. Lillo-Castellano, I. Mora-Jimenez, C. Figuera-Pozuelo and J. Rojo-Alvarez, Traffic sign segmentation and classification using statistical learning methods, Neurocomputing, Vol. 153, pp. 286-299, 2015.

[14] A. Ellahyani, M. Ansari and I. Jaafari, Traffic sign detection and recognition based on random forests, Applied Soft Computing, Vol. 46, pp. 805-815, 2016.

[15] M.A. Sheikh, A. Kole and T. Maity, Traffic Sign Detection and Classification using Colour Feature and Neural Network, In proc. ot the International Conference on Intelligent Control Power and Instrumentation (ICICPI2016), 2016.

[16] A. Madani and R. Yusof, Traffic sign recognition based on color, shape, and pictogram classification using support vector machines, Neural Computing and Applications, V. 30, No. 9, pp 2807-2817, 2018.

[17] J. Miura, T. Kanda, S. Nakatani, and Y. Shirai, An active vision system for on-line traffic sign recognition, IEICE Trans. Inf. Syst., Vol. E85-D, No. 11, pp. 1784-1792, 2002.

[18] C.F. Paulo and P.L. Correia, Automatic detection and classification of traffic signs, In Proc. of the Eighth International Workshop on Image Analysis for Multimedia Interactive Services, WIAMIS'07, pp. 1-11, 2007.

[19] E. Moomivand and E. Abolfazli, A modified structural method for shape recognition, In. Proc. of IEEE symposium on industrial electronics and applications, Malaysia, 2001.

[20] A. Gonzalez, Automatic traffic signs and panels inspection system using computer vision, IEEE Trans. Intell. Transp. Syst., Vol. 12, No. 2, pp. 485? 499, Jun. 2011.

[21] W.-J. Kuo and C.-C. Lin, Two-stage road sign detection and recognition, In Proc. Int. Conf. Multimedia Expo, pp. 1427-1430, 2007.

[22] G.B. Loy and N.M. Barnes, Fast shape-based road sign detection for a driver assistance system, In Proc. Int. Conf. Intell. Robots Syst., pp. 70-75, 2004.

[23] N. Barnes, A. Zelinsky, and L.-S. Fletcher, Real-time speed sign detection using the radial symmetry detector, IEEE Trans. Intell. Transp. Syst., Vol. 9, No. 2, pp. 322-332, 2008.

[24] Y. Gu, T. Yendo, M. P. Tehrani, T. Fujii, and M. Tanimoto, Traffic sign detection in dual-focal active camera system, In Proc. IEEE Intell. Veh. Symp., pp. 1054-1059, 2011.

[25] C.S. Liu, F.L. Chang and Z.X. Chen, Rapid multiclass traffic sign detection in high-resolution images, IEEE Trans. on Intelligent Transportation Systems, Vol. 15, pp. 2394-2403, 2014.

[26] H.J. Li, F.M. Sun, L.J. Liu, and L. Wang, A novel traffic sign detection method via color segmentation and robust shape matching, Neurocomputing, Vol. 169, pp. 77-88, 2015.

[27] M. Mathias, R. Timofte, R. Benenson and L. V. Gool, Traffic sign recognition?How far are we from the solution?, In Proc. Int. Joint Conf. Neural Netw., pp. 1?8, 2013.

[28] S. Segvic, K. Brkic, Z. Kalafatic and A. Pinz, Exploiting temporal and spatial constraints in traffic sign detection from a moving vehicle, Mach. Vis. Appl., Vol. 25, No. 3, pp. 649-665, 2014.

[29] A. Kouzani, Road-sign identification using ensemble learning, In proc. of the IEEE Intelligent Vehicles Symposium, pp. 438-443, 2007.

[30] F. Zaklouta and B. Stanciulescu, Real-time traffic sign recognition in three stages, Robotics and Autonomous Systems, Vol. 62, pp. 16-24, 2014.

[31] W. Lhomme, A. Bouscayrol and P. Barrade, Simulation of series hybrid electric vehicles based on energetic macroscopic representation, Proc. of IEEE-ISIE'04, Ajaccio, 2004.

[32] A. Chen, B. Xie and E. Mao, Electric Tractor Motor Drive Control Based on FPGA, IFAC-PapersOnLine, 49-16, 271-27, 2016.

Chapter 8

Revisiting Olivine Phosphate and Blend Cathodes in Lithium Ion Batteries for Electric Vehicles

Yujing Bi and Deyu Wang

Abstract

As electric vehicle market growing fast, lithium ion batteries demand is increasing rapidly. Sufficient battery materials supplies including cathode, anode, electrolyte, additives, et al. are required accordingly. Although layered cathode is welcome in high energy density batteries, it is challenging to balance the high energy density and safety beside cost. As consequence, olivine phosphate cathode is coming to the stage center again along with battery technology development. It is important and necessary to revisit the olivine phosphate cathode to understand and support the development of electric vehicles utilized lithium ion batteries. In addition, blend cathode is a good strategy to tailor and balance cathode property and performance. In this chapter, blend cathode using olivine phosphate cathode will be discussed as well as olivine phosphate cathode.

Keywords: phosphate, phosphate composite, blend cathode, lithium ion battery, electric vehicles, stability, rate capability, safety

1. Introduction

Batteries are used as the power source in electric vehicles and take the critical role for driving milage improvement and transportation safety as well as cost control. Battery energy density is the important parameter related with the driving mileage. As battery material and technology development, energy density of lithium ion battery for electric vehicle has been increased to 300 Wh/kg at cell level, [1, 2] it has big progress compared with the lead acid battery at beginning period. Lithium ion battery is basically composed by cathode, anode, separator and electrolyte. Lithium ions move between cathode and anode to store and output energy through reversible chemical reaction. In present commercial lithium ion batteries, lithium ions are reserved in cathode side and the reversible lithium concentration in cathode mainly determine the battery energy density. Three type of cathodes have been widely utilized in commercial lithium ion batteries, layered oxide which has two-dimensional lithium ion diffusion pathway, spinel oxide that provides three-dimensional lithium ion transportation space, and olivine phosphate with one-dimensional lithium ion diffusion channels. Each of them has their merit and are servicing the specialized portable power source market.

Lithium ion battery utilized on electrical vehicles has high requirement on safety, long lifespan, high energy density, high power density as well as low cost.

Olivine phosphate cathode has stable crystal structure and present advantage on safety, long cycling stability and cost effective. In this chapter, lithium iron phosphate, lithium manganese phosphate and related composite cathodes are reviewed to understand material technology development. Blend cathode demonstrates the possibility to tailor and balance the cathode property and performance. Binary and ternary blend cathodes using olivine phosphate are summarized and discussed.

2. Olivine phosphate cathode

Iron source is abundant in earth, it is inexpensive and less toxic than cobalt and nickel, using iron redox in cathode is promising to reduce cathode material cost. Inspired and encouraged by the successful development of $LiCoO_2$ cathode, layered $LiFeO_2$ prepared by ion-exchange from α-$NaFeO_2$ presents iron redox activity [3]. But it is metastable and the performance was not attractive due to anion issues [4]. Comparing with other iron compounds, Fe^{3+}/Fe^{2+} redox energy and potential can be adjusted by different anion groups. As consequence, polyanions were considered to build stable framework structure and improve redox stability. Due to Fe^{3+}/Fe^{2+} redox potential is influenced by the corresponding anion group. A series of iron polyanion compounds were screened to search stable cathodes for lithium ion batteries [5]. In **Figure 1a**, Fe^{3+}/Fe^{2+} redox energy is compared in different phosphates. The lower redox energy below Fermi level can achieve higher voltage compared with lithium. Fe^{3+}/Fe^{2+} redox couple demonstrates the lower redox energy in $LiFePO_4$ and higher redox potential at 3.5 V (*vs*. Li^+/Li). This voltage matches with stable window of carbonate electrolytes very well and accelerate the development of lithium iron phosphate. It delivered 110 mAh/g capacity firstly reported by Nobel laureate J. B. Goodenough at 1997 and has been successfully commercialized with decades of research and development.

2.1 Lithium iron phosphate

The ordered olivine structure of $LiFePO_4$ is constructed by P-O framework with space group Pnma. Oxygen atoms are hexagonal-close-packed stacking order. Phosphorus atoms occupy tetrahedral sites, iron and lithium atoms locate at octahedral 4a and 4c position in Pnma space group. PO4 tetrahedral share one edge with FeO6 octahedron and two edges are shared with LiO6 octahedron. The FeO6
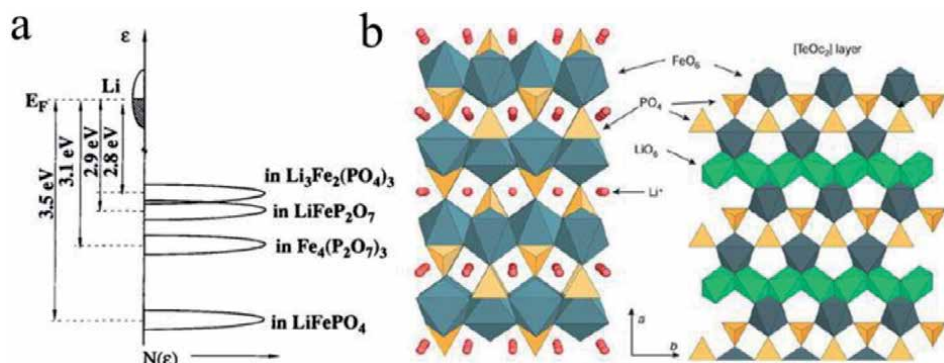
Figure 1.
(a) Iron redox energy and potential can be adjusted by polyanion groups [5]. (b) $LiFePO_4$ crystal structure [6].

octahedra are linked through corner in bc-plane and LiO6 octahedra form edge-sharing chains in b direction [6]. Li resides in chains of edge-shared octahedra and connecting as the Li diffusion channel. PO4 polyanion framework is very stable in thermal dynamics as P-O bonding energy is high. During heating up to 350°C in N_2 or O_2 atmosphere [7], $LiFePO_4$ and delithiated $FePO_4$ structure were not changed which contributes to the high safety performance.

Li diffusion pathway in olivine $LiFePO_4$ is one dimensional channel along [010] direction due to LiO6 octahedra is only continuous along b-axis. Although theoretical intrinsic ionic diffusion coefficient is 10^{-8}–10^{-7} cm^2/s for both $LiFePO_4$ and $FePO_4$ [8, 9] the tested lithium ion diffusion coefficient is lower than 10^{-12} cm^2/s. As structure defects existing, such as Li/Fe anti-site defect, stacking fault and impurities, one-dimensional channels would be block and the ionic diffusion coefficient will be dramatically decreased [10]. In ordered olivine structure, corner-shared FeO6 does not form a continuous 3D network, and transition metal-d-oxygen-p hybridization in phosphate is weak [11]. Accordingly, the electronic conductivity of $LiFePO_4$ at room temperature is only ~10^{-10} S/cm [12], which is usually thought as semiconductor [13]. Slow kinetics of lithium ion diffusion and low electronic conductivity lead to the poor rate capability of $LiFePO_4$. Thus, numerous works have been devoted to overcome this drawback. Such as reducing particle size, element substitution, surface coating et al.

2.2 Reaction mechanism

Phase transformation mechanism in cathode during delithiation and lithiation is critical for electrochemical performance in lithium ion battery. When lithium ion extracting from $LiFePO_4$, olivine $LiFePO_4$ host will transform to $FePO_4$ which have same structure. Even all active lithium ions are extracted out from $LiFePO_4$, lattice volume only vary 6.5–6.8%, which demonstrate high crystal structure stability. Although the two phases reaction mechanism in lithiation/delithiation is widely accepted, the specific transformation route is reported as several models, which are highly related with material morphology, particle size, even experimental conditions [14, 15].

Core-shell (shrinking-core) model was proposed when $LiFePO_4$ was initial reported by J. B. Goodenough at 1997 [7]. In lithiation process, lithium ions will be reserved from surface to particle core in FePO4 phase, two-phase boundary moves accordingly. In delithiation process, phase boundary will move reversibly from core to surface. In order to have deep and clear understanding on reaction mechanism, advanced operando/ex-situ characterization technologies are involved to study the structure changes furtherly. Beside two phases coexistence phenomenon (two phases distribution may be different), lithium deficient $Li_{1-x}FePO_4$ was seizing especially in nano size particle and high rate tests. Solid solution mechanism is reported to support the fast lithium transportation [16].

No matter phase transformation would undergo which mechanism in detail, the rigid P-O tetrahedral in structure provides rigid framework and contributes to highly reversible and stable delithiation/lithiation.

2.3 Carbon coating

Limited by the intrinsic low electronic conductivity, lithium utilization ratio in $LiFePO_4$ is low (~0.6) and decays fast. Carbon coating was developed to improve material conductivity. This approach can be achieved through simple process by mixing carbon precursors with active materials followed by calcination. However, the electrochemical performance is influenced by the carbon coating quality.

Numerous works were reported to study and optimize carbon coating for $LiFePO_4$ from different carbon sources, coating methods, carbon structure and carbon composite [17]. Beside enhancement of electronic conductivity, carbon coating can also be used to control $LiFePO_4$ particle growth in calcination.

Beside conventional carbon coating, advanced carbon materials such as carbon nanotube, graphene and carbon fibers are introduced to form composite for pursuing high performance. Benefitting by excellent electronic conductivity from carbon coating layer and carbon composite, $LiFePO_4$ material can be prepared into thick electrode without sacrifice performance [18].

2.4 Lithium manganese phosphate

Encouraged by well development of $LiFePO_4$, pure phase of lithium manganese olivine is expected to improve energy density due to the high redox potential (4.1 V *vs*. Li^+/Li) of Mn^{3+}/Mn^{2+} couple. However, lithium ion diffusion kinetics and electronic conductivity in $LiMnPO_4$ is even worse than $LiFePO_4$ and hard to prepare the pure phase with high performance [19, 20]. Morphology control and particle size reduction are effective solutions to improve the sluggish kinetics property referencing from $LiFePO_4$ development [21]. A facile polyol synthesis approach is developed to prepare well-crystallized $LiMnPO_4$ with ~30 nm thick nanoplates (as shown in **Figure 2**) [22]. High ratio of (020) plane which orientated in a-c plane and has short length along b-axis provides morphology to optimize kinetics property. Pure phase $LiMnPO_4$ prepared by polyol method can deliver 159 mAh/g reversible capacity at 50°C, and retained 95% over 200 cycles. Elemental substitution was applied on $LiMnPO_4$ to modify the olivine structure. Fe, Ni and Mg substitution made contribution to improve electronic conductivity, but only Fe substitution presents the positive function on electrochemical performance enhancement [24]. Poly synthesis method was further developed and cheap solvent DMSO was used to replace polyhydric alcohols in co-precipitation reaction. 50–100 nm Fe substituted $LiMn_{0.8}Fe_{0.2}PO_4$ presents promising capability and cycling stability as presented in **Figure 2** [23, 25]. Considering kinetics of $LiFePO_4$ is better than $LiMnPO_4$, a core-shell structure of $LiMn_{0.8}Fe_{0.2}PO_4/C$ which has Fe rich on surface is prepared by adjusting co-precipitation process. $LiFePO_4$ is controlled to grow on $LiMnPO_4$ shell [26]. Comparing with $LiMn_{0.8}Fe_{0.2}PO_4$ solid solution cathode, lithium ion diffusion kinetics is further enhanced due to the lower charge transfer resistance is achieved in this structure modification.
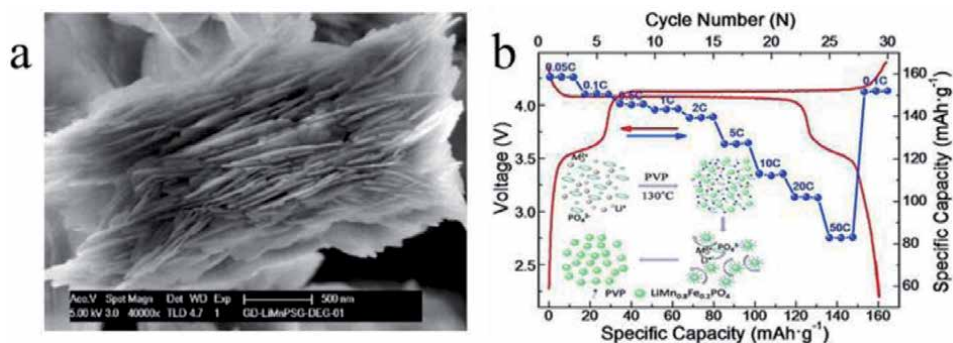
Figure 2.
(a) (020) Oriented LiMnPO$_4$ prepared by polyhydric alcohols approach [22]. (b) Developed co-precipitation method for synthesis of Fe substituted LiMnPO$_4$ [23].
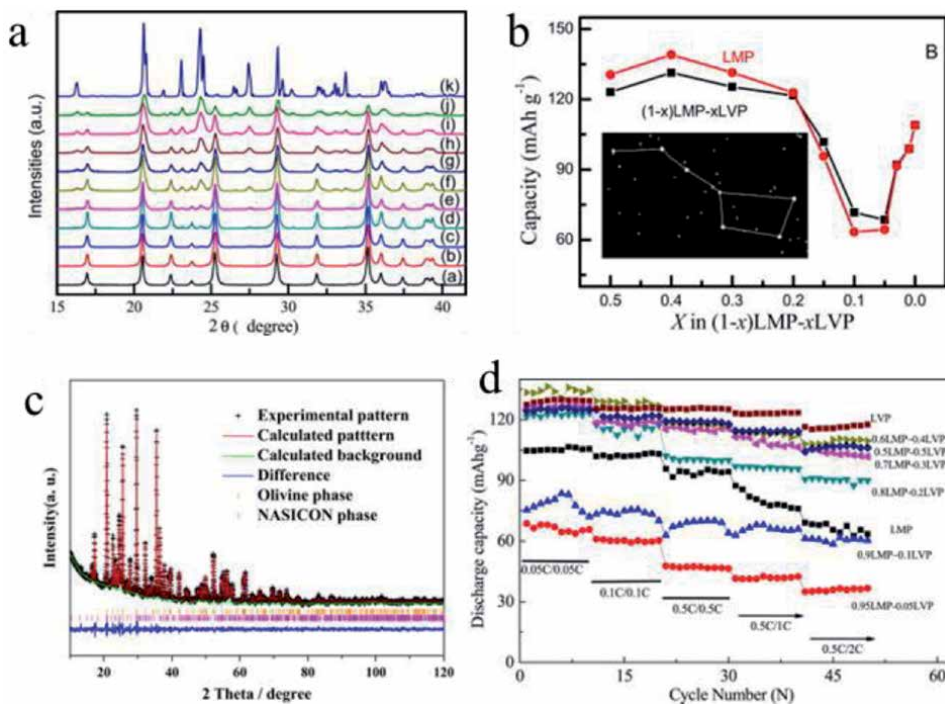
Figure 3.
(a) XRD patterns of the LMP and LVP sample prepared by different ratios. (b) Influence of LVP amount on reversible capacity of LMP-LVP composite [29]. (c) XRD pattern of LMFP and LVP composite cathode [30]. (d) Rate capability of LMP and LVP composite cathodes [29].

2.5 Composite cathode

Although the Mn doped $LiFe_{1-x}Mn_xPO_4$ can deliver higher energy density contributed by the higher redox potential of Mn^{3+}/Mn^{2+}, rate performance is geared down when increasing manganese ratio. NASICON structured phosphate $Li_3V_2(PO_4)_3$ has open lattice framework which guarantee the fast Li ion transportation in cathode bulk phase [27]. As consequence, high rate NISICON cathode is integrated with olivine phosphate to improve Li diffusion kinetics [28]. In $LiMnPO_4$-LVP composite cathode prepared by solid state approach, both the NISSCON and olivine phase diffraction peaks and plateau character could be identified even LVP ratio is below 3% [29]. As the composite LVP ratio is higher than 20%, the capacity contributed from Mn^{2+}/Mn^{3+} plateau is increased and indicates that LVP composite can improve activity of Mn redox in olivine phase. Checking the lattice paraments, olivine phase LiMnPO4 is substituted by a small amount of vanadium [30]. The composite cathode presents enhanced rate capacity (**Figure 3**).

3. Blend cathodes

The present commercial cathode layered oxide, spinel oxide and olivine phosphate have their own advantage and have already been successfully utilized in different lithium ion battery designs according to the application scenarios. The blend of different cathode is a facile method to tailor the properties and performance of electrodes for lithium ion batteries.

3.1 Blend cathode – olivine phosphate and layered oxide

Layered structure oxide contained nickel cobalt manganese (NMC) has much higher theoretical capacity (~270 mAh/g) than olivine phosphate cathodes (~170 mAh/g). Limited by the delithiated structure stability at high voltage and electrolyte decomposition window [31, 32], only <0.8 Li in layered oxide cathode will participate in charge–discharge process. Although NMC cathode can be used to prepare high energy density lithium ion batteries for electric vehicles, the safety concerns arise comparing with the one using olivine phosphate cathodes [33, 34]. Blend cathode including both olivine and layered oxide cathode would a moderate strategy to integrate.

$LiMn_{0.8}Fe_{0.2}PO_4/C$ was mixed directly with $LiNi_{0.88}Co_{0.09}Al_{0.03}O_2$ (NCA) to improve the comprehensive performance. The reasonable ratio of $LiMn_{0.8}Fe_{0.2}PO_4/C$ can extend cycling life of Ni rich cathode without sacrificing capacity at electrode level [35]. Adding 1% and 2% $LiMn_{0.8}Fe_{0.2}PO_4/C$, electrodes present similar discharge capacity. But the capacity retention ratio is increased from 77% using pristine NCA to 88% using 2% olivine addition. Using $LiNi_{0.5}Mn_{0.3}Co_{0.2}O_2$ (NMC532) and $LiFe_{0.15}Mn_{0.85}PO_4$ blend cathode, cycling stability is enhanced when LFMP/C ratio in blend cathode is less than 10% [36].

$LiCoO_2$ presents more stable structure stability with adding $LiFePO_4$, both the particle cracking and irreversible phase transformation are inhabited even cycling at high cutoff voltage. Mixing with 12 wt% $LiFePO_4$, discharge capacity of blend cathode is decreased to 177.9 mAh/g at 0.2C charging to 4.5 V (*vs.* Li^+/Li). However, overpotential of cobalt redox is reduced and presents enhanced cycling stability [37].

Redox dynamics in $LiFePO_4$ and $LiCoO_2$ blend cathode is different with individual component. At low C-rate, each components of the blend cathode can independently present their redox reaction. When working at high C-rate, the effective C-rate for each constituent is higher than nominal value. However, the rate performance of blend cathode is significantly improved [38]. Buffer effect is proposed that the internal pathway would be constructed by component with fast reaction kinetics as shown in **Figure 4**. Lithium is redistributed among the constituents to reach an equilibrium potential during relaxation.

Despite electrochemical performance is improved by blending, $LiFePO_4$ and layered oxide cathode blend cathode may have heterogeneity issue as material property such as particle size and density are different. 3D X-ray tomography technology is
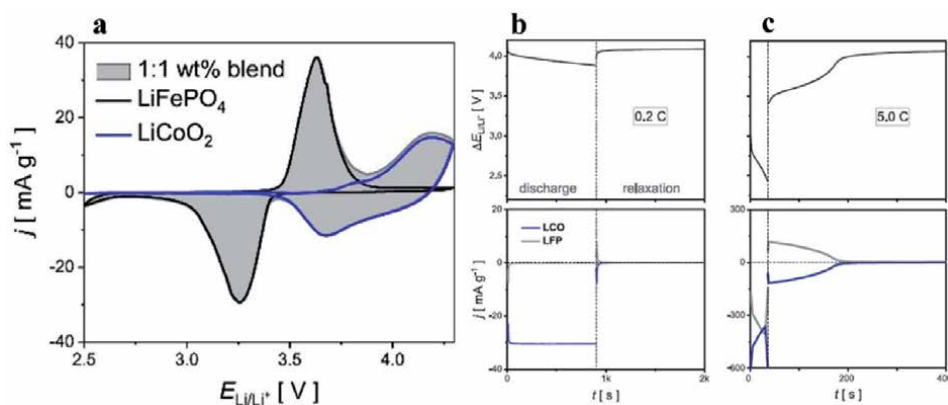
Figure 4.
a) Cyclic voltammetry of a blend electrode illustrating the contributions of LiFePO_4 and LiCoO_2. (scanning rate 25 μV/s). b) and c) potential profile and specific current during discharge and subsequent relaxation of a LiFePO_4 and LiCoO_2 blend at 0.2C and 5C [38].
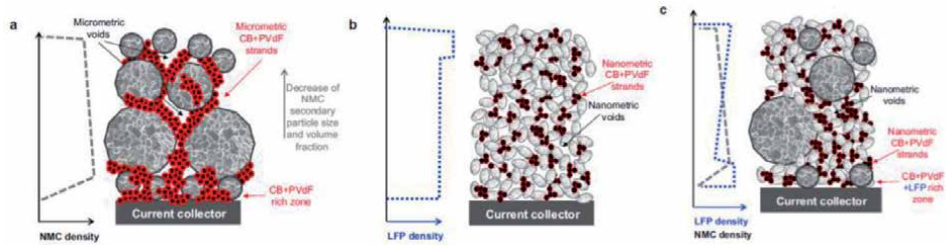
Figure 5.
Schematic figure of typical features in a) NMC, b) LFP, and c) NMC/LFP blend electrodes [39].

used to check the composition distribution in prepared blend electrodes [39, 40]. Small NMC, nano sized $LiFePO_4$ and carbon additives are enriched in layer close to current collector and large particle NMC is depleted in this region. Although electrode composition is close to design value above the NMC depleted layer, the mean NMC particle size presents gradient distribution toward top surface, as demonstrated in **Figure 5**. Beside local morphology heterogeneities, $LiFePO_4$ agglomeration and cavities are observed in NMC rich zones. The heterogeneity issue may can be resolved by technique and equipment optimization, but the reported results reveal that materials properties differences should be considered to prepare uniform electrodes with high quality especially for blend cathodes.

3.2 Blend cathode – olivine phosphate and spinel oxide

Spinel oxide cathode has advantage of low cost, high thermal stability and high rate capability. However, spinel oxide suffers from fast capacity fading in long cycling test, especially at high temperature. Olivine phosphate has excellent cycling stability and could blend with spinel to pursue the comprehensive performance.

$LiFe_xMn_{1-x}PO_4$ (LFMP) and spinel oxide blend cathode demonstrates linear changing on tap density, reversible capacity, energy density and power density at low C-rate by adjusting blend ratio between two components. However, synergetic effect was observed in blend cathode at high C-rate [41]. Discharge curves of blend cathode at 3C presents lower polarization for Mn^{3+}/Mn^{2+} plateau as shown in **Figure 6**. Structure change was studied by in-situ XRD characterization during 3C pulse discharge and the following relaxation. (004) diffraction peak of spinel cathode shifts toward lower angle during discharge and moves to high angle in relaxation period. This result indicates that spinel component is reoxidized in relaxation step. As lithium diffusion in LFMP is slower than spinel $LiMn_2O_4$, the higher delithiated state LFMP will provide lithium ions to spinel for reaching a common
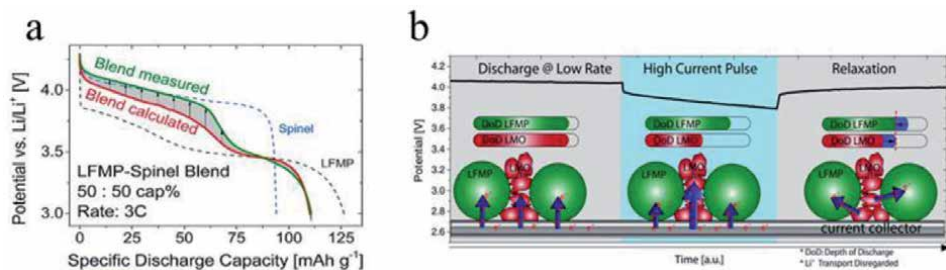
Figure 6.
(a) Discharge curve comparison of blend cathode and individual component [42]. (b) Schematic illustration of buffer effect in blend cathode during pulse power test [41].

Label	NMC/LMFP/LMO [wt%]	Areal capacity [mAh cm^{-2}]	Mass loading [mg cm^{-2}]	Specific capacity [mAh g$_{AM}$$^{-1}$]	Porosity [%]	Density [g cm^{-3}]	Conductivity [S cm^{-2}]
100%NMC	100:0:0	2.51 ± 0.02	15.86 ± 0.07	170.14 ± 0.67	33 ± 2	2.83 ± 0.05	0.68 ± 0.11
100%LMFP	0:100:0	2.53 ± 0.04	17.89 ± 0.25	151.27 ± 0.30	32 ± 2	2.13 ± 0.03	1.16 ± 0.03
100%LMO	0:0:100	2.58 ± 0.02	26.25 ± 0.01	105.41 ± 0.08	31 ± 1	2.73 ± 0.02	0.39 ± 0.20
75%NMC	75:12.5:12.5	2.48 ± 0.01	16.07 ± 0.02	165.57 ± 0.12	32 ± 2	2.72 ± 0.04	1.84 ± 0.19
75%LFMP	12.5:75:12.5	2.46 ± 0.08	17.70 ± 0.55	149.25 ± 0.29	32 ± 2	2.27 ± 0.03	1.89 ± 0.19
75%LMO	12.5:12.5:75	2.59 ± 0.07	23.20 ± 0.28	118.49 ± 3.72	30 ± 2	2.70 ± 0.03	1.52 ± 0.19
33%each	33.3:33.3:33.3	2.41 ± 0.2	18.79 ± 0.65	136.45 ± 11.95	32 ± 2	2.54 ± 0.04	2.04 ± 0.20

Table 1.
Characteristic properties of electrodes with an aerial capacity of approximately 2.5 mAh cm^{-2} and a porosity of 30% calculated from the electrodes' thickness. Mass loading includes active materials, binder, and conductive carbon. Specific capacity is based on 93% active material (AM) content. The proportions indicated in the second column are based on the total AM [45].

equibium potential state (demonstrated in **Figure 6**). This buffer effect reduce the electrode polarization and improves the power pulse capability. Energy density and power density at high C-rate are enhanced contributed by the reduction of electrode polarization by blend ratio optimization [42].

Manganese dissolution is notorious for lithium ion batteries using spinel $LiMn_2O_4$ cathodes [43]. Dissolution mechanism is generally ascribed to the presence of HF generated by the reaction between hexafluorophosphate anion and water impurity. Dissolved manganese will be reduced/deposited on anode side and involved in SEI formation in graphite surface. Spinel cathode will loss reversible capacity by manganese dissolution and anode impedance will be dramatically increased by manganese migration and deposition, as result spinel cathode performance in lithium ion battery is poor, especially calendar life and cycling stability at high temperature. This issue can be alleviated by using blend cathode design. Layered structure cathodes such as $LiCoO_2$ and NMC reported that can work as proton scavenger through Li ion and proton exchanging in blend cathodes [44]. In LFMP and spinel oxide cathodes, dissolved manganese may be precipitation on LFMP particle surface instead of migrating to anode side. This results is also approved in $LiFe_{0.3}Mn_{0.7}PO_4$ and $LiMn_{1.9}Al_{0.1}O_4$ blend cathode that manganese dissolution from spinel cathode is dramatically reduced [42].

3.3 Ternary blend cathodes

Based on the development of binary blend cathode, ternary blend cathode composited by olivine phosphate, layered oxide and spinel oxide are proposed to study. Mixing three components at even ratio (33% for each), the ternary blend electrode presents highest electronic conductivity when all the other electrode parameters are controlled at same level (as list in **Table 1**) [45]. Redox activities studies reveal that each components in blend cathode can work independently and contributes to reduce the over-potential [46]. This is consistent with other reports.

4. Safety

Along energy density of lithium ion battery increasing, safety concerns are serious raised. Safety performance and evaluation is one of the critical criteria for the practical utilization of novel battery materials/technologies. Although battery management systems (BMS) are equipped on electrical vehicles to monitor all the cells and ensure the safety operation, battery still has thermal runway risk and would cause disaster results. Many countries published the strict compulsory standards for battery safety tests before releasing to commercial utilization on EVs [47]. Therefore, it is important to pay attention on safety development as well as energy/power density improvement.

Lithium ion battery is a comprehensive system and sensitive to temperature. When battery temperature rising to the cathode decomposition triggering point, the exothermic reaction will abruptly release heat and accelerate thermal runaway which is the detrimental safety issue. Thermal studies of materials components in lithium ion batteries can be investigated by differential scanning calorimetry (DSC) or accelerating rate calorimetry (ARC) [48]. As cathode material property are different, the onset reaction temperature and released heat are varied. In brief, the onset temperature for cathodes follow the order: $LiFePO_4 > LiNi_xCo_yMn_zO_2 > LiCoO_2$ as compared in **Figure 7** [47]. Polyanionic phosphate cathodes have robust P-O covalent constructing stable three-dimensional framework, it reduces the reactivity between cathode and electrolyte.
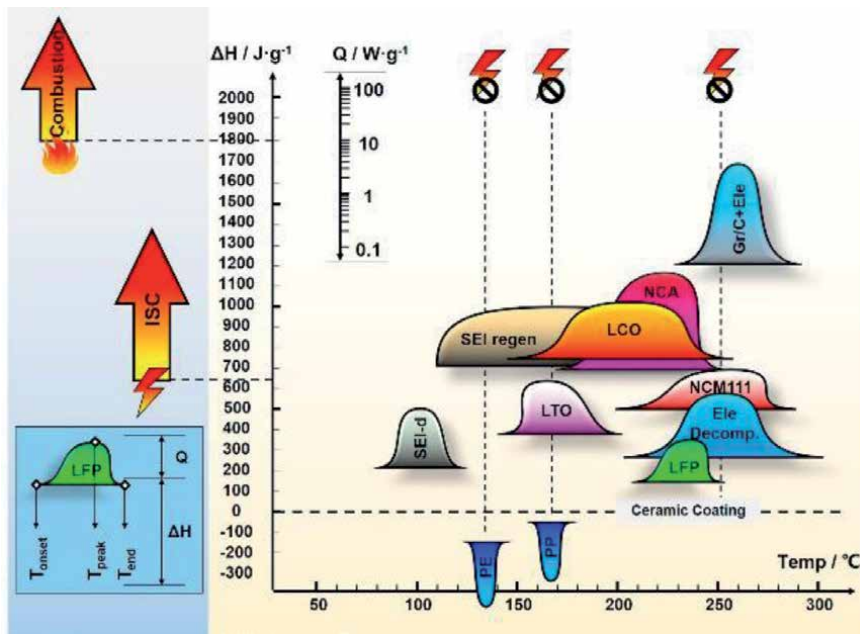
Figure 7.
The energy release diagram of different cathode in lithium ion batteries [47].
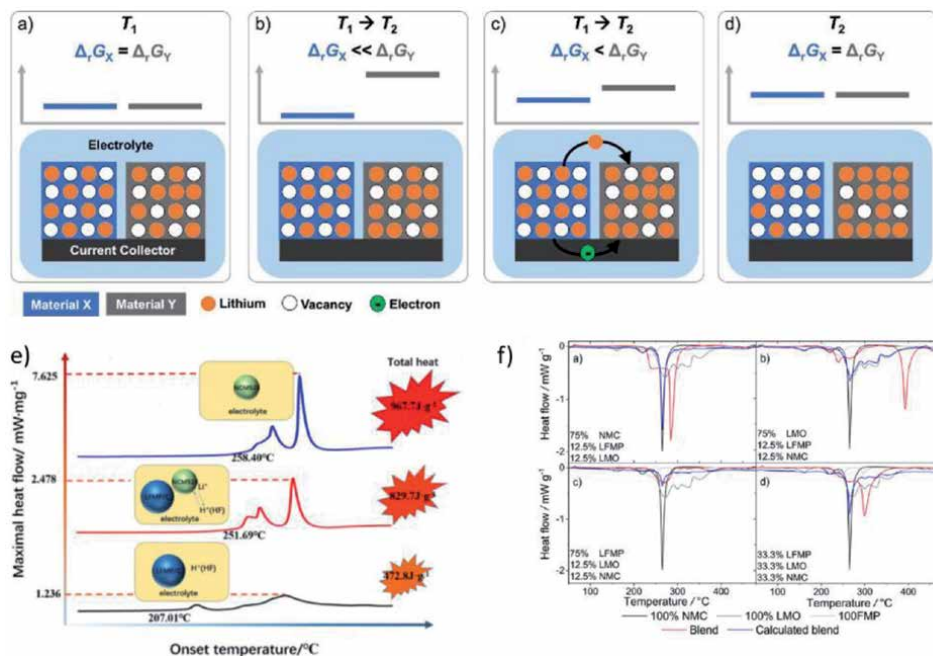

Figure 8.
(a–d) Schematic description of Li redistribution among the components induced by a temperature change [38]. (e) Thermal performance comparison in LFMP/C and NMC523 blend cathode [36]. (f) Differential scanning calorimetry of fully charged blend electrodes (red) comparing with individual cathode at different ratios [45].

Although spinel is reported that onset temperature is little higher than LiFePO$_4$ [49], but the exothermic reaction enthalpy is higher than LiFePO$_4$ and the peak shape is more sharp which means more heat will be generated in shorter time.

Although electrochemical performance of layered oxide cathodes have been improved a lot by material modification [33, 50, 51], they are still hard to compete with LiFePO$_4$ on safety performance evaluation. Blend cathode is a reasonable method to balance the comprehensive performance. By adding olivine phosphate cathode LiFe$_{0.15}$Mn0$_{.85}$PO$_4$/C in NMC523 cathode, the exothermic reaction enthalpy is significantly decreased [36]. But there is no linearly relationship between LFMP adding ratio and thermal performance (**Figure 8**).

5. Summary

Olivine phosphate has been successfully commercialized and used in lithium ion batteries to equip on electrical vehicles. Although energy density is not competitive comparing with using layered oxide cathode especially Ni rich cathode, olivine phosphate present excellent safety performance. Manganese substitution and composited with lithium vanadium phosphate is carried out to improve energy density and power density. Beside this, blend cathode is an effective strategy to improve energy density without sacrificing safety advantage. Binary and ternary blend cathode present the possibility to tailor cathode property and performance. Blend cathodes show synergetic effect on rate capability and thermal stability tests which is higher than nominal value. Structure and electrochemistry studies reveal that buffer effect in blended components is contributed to the improvement. This chapter provides opinions from material science and electrochemistry viewpoints to understand the requirement of lithium ion battery on cathode materials development.

Conflict of interest

The authors declare no conflict of interest.

Author details

Yujing Bi[1*] and Deyu Wang[1,2*]

1 Ningbo Institute of Materials Technology and Engineering, CAS, Ningbo, China

2 Jianghan University, Wuhan, Hubei, China

*Address all correspondence to: biyujing15@hotmail.com
and wangdeyu@jhun.edu.cn

IntechOpen

References

[1] Cao, W.Z., J.N. Zhang, and H. Li, *Batteries with high theoretical energy densities.* Energy Storage Materials, 2020. **26**: p. 46-55.

[2] Assat, G. and J.M. Tarascon, *Fundamental understanding and practical challenges of anionic redox activity in Li-ion batteries.* Nature Energy, 2018. **3**(5): p. 373-386.

[3] Nalbandyan, V.B. and I.L. Shukaev, *New Modification of Lithium Monoferrite and the Morphotropic Series AFeO2.* Russian Journal of Inorganic Chemistry, 1987. **32**(3): p. 453-454.

[4] YasuoTakeda, et al., *Sodium deintercalation from sodium iron oxide.* Materials Research Bulletin, 1994. **29**(6): p. 659-666.

[5] Padhi, A.K., et al., *Effect of Structure on the Fe^{3+}/Fe^{2+} Redox Couple in Iron Phosphates.* Journal of The Electrochemical Society, 1997. **144**: p. 1609-1613.

[6] Tarascon, J.M. and M. Armand, *Issues and challenges facing rechargeable lithium batteries.* Nature, 2001. **414**(6861): p. 359-367.

[7] Padhi, A.K., K.S. Nanjundaswamy, and J.B. Goodenough, *Phospho-olivines as positive-electrode materials for rechargeable lithium batteries.* Journal of the Electrochemical Society, 1997. **144**(4): p. 1188-1194.

[8] Ouyang, C.Y., et al., *First-principles study of Li ion diffusion in LiFePO4.* Physical Review B, 2004. **69**(10).

[9] Shi, S.Q., et al., *Enhancement of electronic conductivity of LiFePO4 by Cr doping and its identification by first-principles calculations.* Physical Review B, 2003. **68**(19).

[10] Yang, Z.G., et al., *How to make lithium iron phosphate better: a review exploring classical modification approaches in-depth and proposing future optimization methods.* Journal of Materials Chemistry A, 2016. **4**(47): p. 18210-18222.

[11] Zhou, F., et al., *The electronic structure and band gap of LiFePO4 and LiMnPO4.* Solid State Communications, 2004. **132**(3-4): p. 181-186.

[12] Chung, S.Y., J.T. Bloking, and Y.M. Chiang, *Electronically conductive phospho-olivines as lithium storage electrodes.* Nature Materials, 2002. **1**(2): p. 123-128.

[13] Guo, L.M., et al., *Unlocking the energy capabilities of micron-sized LiFePO4.* Nature Communications, 2015. **6**.

[14] Wang, J.J., et al., *Visualization of anisotropic-isotropic phase transformation dynamics in battery electrode particles.* Nature Communications, 2016. **7**.

[15] Wang, J.J., et al., *Size-dependent surface phase change of lithium iron phosphate during carbon coating.* Nature Communications, 2014. **5**.

[16] Liu, H., et al., *Capturing metastable structures during high-rate cycling of LiFePO4 nanoparticle electrodes.* Science, 2014. **344**(6191).

[17] Wang, J.J. and X.L. Sun, *Understanding and recent development of carbon coating on LiFePO4 cathode materials for lithium-ion batteries.* Energy & Environmental Science, 2012. **5**(1): p. 5163-5185.

[18] Li, H., et al., *Ultrahigh-Capacity and Fire-Resistant LiFePO4-Based Composite Cathodes for Advanced Lithium-Ion Batteries.* Advanced Energy Materials, 2019. **9**(10).

[19] Xiao, J., et al., *Synthesis and Characterization of Lithium Manganese*

Phosphate by a Precipitation Method. Journal of the Electrochemical Society, 2010. **157**(2): p. A142-A147.

[20] Xiao, J., et al., *Electrochemical performances of LiMnPO4 synthesized from non-stoichiometric Li/Mn ratio.* Phys Chem Chem Phys, 2011. **13**(40): p. 18099-18106.

[21] Guo, H., et al., *Performance Improvement of Lithium Manganese Phosphate by Controllable Morphology Tailoring with Acid-Engaged Nano Engineering.* Inorganic Chemistry, 2015. **54**(2): p. 667-674.

[22] Wang, D., et al., *High-performance, nano-structured LiMnPO4 synthesized via a polyol method.* Journal of Power Sources, 2009. **189**(1): p. 624-628.

[23] Yang, W., et al., *LiMn0.8Fe0.2PO4/C cathode material synthesized via co-precipitation method with superior high-rate and low-temperature performances for lithium-ion batteries.* Journal of Power Sources, 2015. **275**: p. 785-791.

[24] Wang, D., et al., *Improving the Electrochemical Activity of LiMnPO$_4$ Via Mn-Site Substitution.* Journal of The Electrochemical Society, 2010. **157**(2): p. A225-A229.

[25] Du, G., et al., *Additives to disturb LiMn0.8Fe0.2PO4 growth and their influence on performance.* Journal of Nanoparticle Research, 2015. **17**(6).

[26] Xu, X., et al., *Improvement of electrochemical activity of LiMnPO4-based cathode by surface iron enrichment.* Journal of Power Sources, 2017. **341**: p. 175-182.

[27] Tang, Y., et al., *Li2NaV2(PO4)3: A novel composite cathode material with high ratio of rhombohedral phase.* Journal of Power Sources, 2013. **227**: p. 199-203.

[28] Rui, X.H., et al., *Li3V2(PO4)(3) cathode materials for lithium-ion batteries: A review.* Journal of Power Sources, 2014. **258**: p. 19-38.

[29] Wang, C., et al., *Investigation of (1 − x)LiMnPO4·xLi3V2(PO4)3/C: Phase composition and electrochemical performance.* Journal of Power Sources, 2014. **263**: p. 332-337.

[30] Bi, Y., et al., *Influence of Li3V2(PO4)3 complexing on the performance of LiMnPO4 based materials utilized in lithium ion battery.* Ceramics International, 2014. **40**(5): p. 7637-7641.

[31] Bi, Y.J., et al., *Reversible planar gliding and microcracking in a single-crystalline Ni-rich cathode.* Science, 2020. **370**(6522): p. 1313-+.

[32] Xu, C., et al., *Phase Behavior during Electrochemical Cycling of Ni-Rich Cathode Materials for Li-Ion Batteries.* Advanced Energy Materials, 2021. **11**(7).

[33] Bi, Y., et al., *Highly stable Ni-rich layered oxide cathode enabled by a thick protective layer with bio-tissue structure.* Energy Storage Materials, 2020. **24**: p. 291-296.

[34] Noh, H.-J., et al., *Comparison of the structural and electrochemical properties of layered Li[NixCoyMnz]O2 (x = 1/3, 0.5, 0.6, 0.7, 0.8 and 0.85) cathode material for lithium-ion batteries.* Journal of Power Sources, 2013. **233**: p. 121-130.

[35] Liu, J., et al., *Re-considering the LiMn1-xFexPO4/C cathodes utilized in electric vehicles.* Ionics, 2020. **26**(7): p. 3215-3221.

[36] Sun, G., et al., *Synergistic Effect between LiNi0.5Co0.2Mn0.3O2 and LiFe0.15Mn0.85PO4/C on Rate and Thermal Performance for Lithium Ion Batteries.* ACS Appl Mater Interfaces, 2018. **10**(19): p. 16458-16466.

[37] Zhang, H.S., et al., *Olivine LiFePO4 as an additive into LiCoO2 electrodes for LIBs to improve high-voltage*

performances. Journal of Alloys and Compounds, 2021. **869**.

[38] Heubner, C., et al., *Internal dynamics of blended Li-insertion electrodes.* Journal of Energy Storage, 2018. **20**: p. 101-108.

[39] Etiemble, A., et al., *Multiscale morphological characterization of process induced heterogeneities in blended positive electrodes for lithium-ion batteries.* Journal of Materials Science, 2017. **52**(7): p. 3576-3596.

[40] Besnard, N., et al., *Multiscale Morphological and Electrical Characterization of Charge Transport Limitations to the Power Performance of Positive Electrode Blends for Lithium-Ion Batteries.* Advanced Energy Materials, 2017. 7(8).

[41] Klein, A., P. Axmann, and M. Wohlfahrt-Mehrens, *Origin of the Synergetic Effects of LiFe0.3Mn0.7PO4 - Spinel Blends via Dynamic In Situ X-ray Diffraction Measurements.* Journal of the Electrochemical Society, 2016. **163**(9): p. A1936-A1940.

[42] Klein, A., P. Axmann, and M. Wohlfahrt-Mehrens, *Synergetic effects of LiFe0.3Mn0.7PO4-LiMn1.9Al0.1O4 blend electrodes.* Journal of Power Sources, 2016. **309**: p. 169-177.

[43] Zhan, C., et al., *Mn(II) deposition on anodes and its effects on capacity fade in spinel lithium manganate-carbon systems.* Nat Commun, 2013. **4**: p. 2437.

[44] Tran, H.Y., et al., *LiMn2O4 Spinel/ LiNi0.8Co0.15Al0.05O2 Blends as Cathode Materials for Lithium-Ion Batteries.* Journal of The Electrochemical Society, 2011. **158**(5).

[45] Jobst, N.M., et al., *Ternary Cathode Blend Electrodes for Environmentally Friendly Lithium-Ion Batteries.* Chemsuschem, 2020. **13**(15): p. 3928-3936.

[46] Liebmann, T., et al., *Investigations on the Effective Electric Loads in Blended Insertion Electrodes for Lithium-Ion Batteries.* ChemElectroChem, 2019. **6**(22): p. 5728-5734.

[47] Feng, X.N., et al., *Thermal runaway mechanism of lithium ion battery for electric vehicles: A review.* Energy Storage Materials, 2018. **10**: p. 246-267.

[48] Chen, Y.Q., et al., *A review of lithium-ion battery safety concerns: The issues, strategies, and testing standards.* Journal of Energy Chemistry, 2021. **59**: p. 83-99.

[49] Zaghib, K., et al., *Enhanced thermal safety and high power performance of carbon-coated LiFePO4 olivine cathode for Li-ion batteries.* Journal of Power Sources, 2012. **219**: p. 36-44.

[50] Bak, S.M., et al., *Structural Changes and Thermal Stability of Charged LiNixMnyCozO2 Cathode Materials Studied by Combined In Situ Time-Resolved XRD and Mass Spectroscopy.* Acs Applied Materials & Interfaces, 2014. **6**(24): p. 22594-22601.

[51] Du, R., et al., *Improved cyclic stability of LiNi0.8Co0.1Mn0.1O2 via Ti substitution with a cut-off potential of 4.5 V.* Ceramics International, 2015. **41**(5): p. 7133-7139.

Section 4

Propulsion Systems

Chapter 9

Design, Simulation and Analysis of the Propulsion and Control System for an Electric Vehicle

Muhammet Tahir Guneser, Mohammed Ayad Alkhafaji and Cihat Seker

Abstract

The problems of global warming, a decrease of the available natural resources and many other problems in the world that happen recently become the major cause for increasing the demand for a new type of vehicle. That vehicle can be an environmental friend and so that a new generation of vehicles has been invented and tried to solve and avoid many problems. In this chapter, the proposed system is called the Multi-Converter/Multi-Machine system (MCMMS) which consists of two Synchronous Reluctance Motor (SynRM) that drive the two rear wheels of Pure Electric Vehicle (PEV). The SynRM speed and torque are controlled by using three different strategies of the PID controller. The PSO algorithm has been used as an optimization technique to find the optimal PID parameter to enhance the drive system performance of the PEV. In this system, the space vector pulse width modulation inverter for voltage source (VS-SVPWMI) has been employed to convert the DC battery voltage to three-phase AC voltage that feeds the SynRM motor in the PEV. The linear speed of the vehicle is controlled by an Electronic Differential Controller (EDC) which gives the reference speed for each driving wheel which depends on the driver reference speed and the steering angle. The specified driving route topology with three different road cases has been applied to acting and show the resistive forces that affected on the PEV during its moving on the road. In addition, to test the efficiency and stability of the PEV on the roads. Hence, this chapter has a full design, simulation and several comparison results for the propulsion electric vehicle system and it has tested implemented in the Matlab/Simulink environment version R2020a.

Keywords: SynRM, SVPWM, Inverters, d-q Transformation, Electric vehicle, EDC, PSO algorithm, Driving cycle, Matlab/Simulink

1. Introduction

Environmental pollution and global warming resulting from the combustion of petroleum products in mechanical vehicles have pushed many companies to use electric vehicles (EV) that rely on clean alternative energy instead of petroleum energy. Besides, customers' interest in the increasing demand for EV due to their efficiency and modernity [1–4]. This prompted several companies to develop their

products and expand their research studies on them so that they become as competitive as possible in mechanical vehicles. EVs are not only more efficient than their counterparts that operate on internal combustion engines, but they are also the best option to reduce pollution resulting from greenhouse gas emissions and noise, as they produce emissions at a rate less than half of what conventional cars produce.

EVs are environmentally friendly, as they do not emit carbon emissions of any kind and do not emit smoke or exhaust, and therefore, they protect the environment, especially in crowded cities [1–9]. It also works with recycled and reused batteries, to store energy in EVs, and finally it is suitable for cities where EVs are characterized by their quietness as they do not have an annoying engine sound, and suitable for crowded cities, due to the ease of controlling them from start and stop. Moreover, EV is not currently a detection; It was first proposed in the mid-nineteenth century. Although they have been around for a long time, they have not become as popular as Internal Combustion Engine (ICE) cars in the narrative of recent years [2, 4, 9–13], due to the main obstacles to electric vehicles as they are expensive, especially high-voltage batteries that are expensive, limited in range, and have little infrastructure. Charging stations as well [2]. The technological development of countries over the years, infrastructure and the EV of industries that led to the arising of environmental contaminate here then the need began to arise for the presence of vehicles that are concerned in that concern. The environmental side and from here began and the urgent need for EV to increase.

The market demand for EVs is expected to increase very shortly is anticipated to increase. Nowadays in many European and Eastern Asia countries and North America has a major interest in the development and the use of EVs [1–3]. They use EVs as taxis and as personal cars to move around within the city for the presence of trains and planes to move for the long distant places and a major concern now to make EVs move in the out-city range. Many EVs are used in cars as taxis Because EVs are a low cost compared to mechanical vehicles and charging stations are solar cells that transform solar energy into electrical energy [1, 2, 4–6]. It is one of the following sources of clean energy.

The manufacture and construction of electric vehicles vary from company to company, determined according to the needs and specifications required for the industry. There are many types that can be explained as follows: The first type is considered one of the oldest types which are still adopted in the industry and it contains one electric motor that is connected to the rear wheels and this type is called conventional electric vehicles or "classical EV system". The second type of system will be studied and analyzed in this chapter, which is based on two electric motors in the rear wheels of the EV, in which each engine operates separately from the other and is controlled by smart systems and this type is called " propulsion EV system ".The third type is the same design as the second type of electric vehicle, but the propulsion mechanism "electric motors" is attached to the front wheels of the vehicle and this type is called " traction EV system ".The fourth type of electric vehicle is a four-wheel drive using two electric motors. The first is on the axle of the rear wheels and the second is on the axle of the front wheels and each of them works separately with a specific control mechanism. This type is called a " four-wheel two motors EV system ". The last type of electric vehicle, which is four-wheel drive, using four electric motors, is distributed over the four tires of the vehicle and works separately, and this type is called "four-wheel EV system" [10]. In general, there are two types of electric vehicles which are Hydride Electric Vehicles (HEV) and Pure Electric Vehicle (PEV). These two types are considered as the major types of EV and minor types are divided from these two types depending on different aspects related to the driving system, configuration, costumers order, and other concerns depend on the designing specification.

The most current invention in the type of vehicle manufacturing EV [1–4]. The PEV are completely different from traditional "mechanical vehicles", although they operate on electrical energy starting from fuel and mechanical fuel engines, the internal structure of them depends on electronic circuits, transducers, and batteries. As well as the entry of artificial intelligence into the manufacturing process to control and control the electronic devices they contain [4, 13, 14]. Besides, in this type instead of using the gearbox, the Electronic Differential Controller (EDC) is designed and used to control the EV on the road. EVs that categorized according to the job of the drive system the many known electric drive systems that have been utilized in EV is induction motors (IM), brushless, DC motors (BLDC), permanent magnet synchronous motors (PMSM), switch reluctance motor (SRM) and other DC motors [15–20].

One of the most important things that must be considered when designing and simulating EVs is the method of controlling the electric vehicle on the road under different conditions to ensure the efficiency of the electric vehicle. As well as artificial intelligence and the application of new mathematical algorithms that help advance the manufacture of electric vehicles. The speed control of the electric motor in terms of rotation speed and torque is one of the most important factors that help in the success of electric vehicle design [2–4, 17–23]. As well as studying the forces affecting the vehicle on the street and applying artificial intelligence algorithms to get rid of them to make the electric vehicle compatible with all road conditions and the influence of external factors on it [13, 14].

The proposed EV system in this chapter called propulsion type EV which are consists of two motors that ensure the drive of the two rear driving wheels. Each motor is drive separately from the other by SynRM and the whole system is controlled by an electronic differential that guarantees the robustness of the vehicle. This vehicle system MCMMS. This type of EV is the most recommended type by the mechanical experts because of slipping issues in the curvature and high road in this type of vehicle **Figure 1** shows an EV with a rear-wheel drive system [4, 23]. Multiple intelligence theories and algorithms have been applied to control the vehicle's electric motor. Likewise, the design and analysis of EDC will be used to control the vehicle's speed during a bad road on road. In addition, a complete
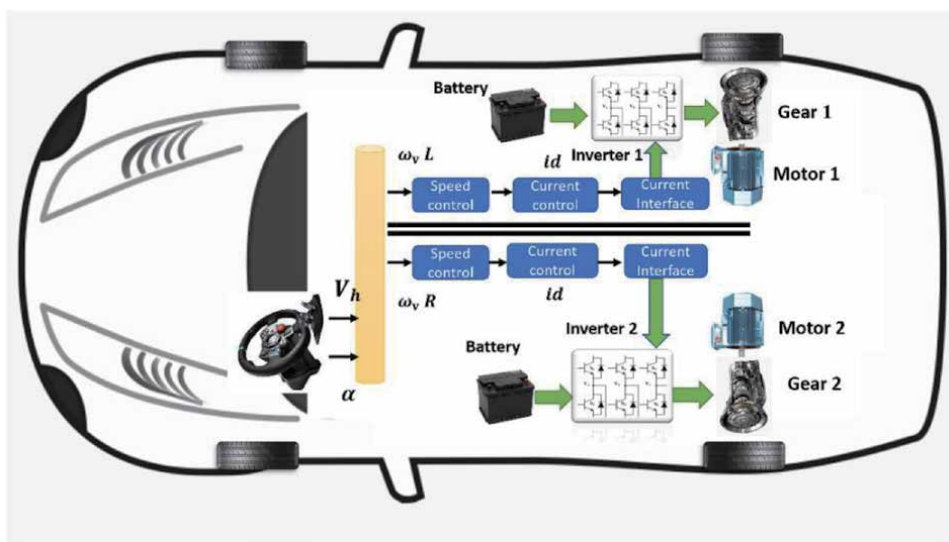
Figure 1.
The propulsion EV platform system.

simulation of the road with three different roofs to ensure the efficiency of the electric vehicle. The above will be explained in detail during this research with the scientific results and comparisons for each part designed in this EV [4–7, 24–31].

2. The mathematical modeling of the system

2.1 SynRM mathematical model

SynRM is one of several synchronous machines and it is one in every of numerous synchronous machines, the SynRM rotor structure has synthetic without winding or magnet fabric. As an evaluation among SynRM with other sorts of reluctance Electric Vehicles (EVs) like: IM, BLDC motor and switch reluctance motor SRM. The quit result suggests that SynRM is precise in production, easy form. In addition, it has an extraordinary residence like low torque average, larger torque pulsation and occasional energy factor [6, 7].

Undoubtedly, the SynRM may additionally moreover deliver an excessive solid performance in assessment with other AC drives compared with IM. As noted earlier, the SynRM is a type of synchronous machine that does not have any winding or permanent magnet at the rotor and salient poles, it has a fragmented rotor of several barriers. The cause for made the reluctance motor rotor form laminated axially metallic it has to dominate low torque response and incorrect electricity thing, notwithstanding the truth that older variations of reluctance motor have lacked this period of producing [5–7]. The stator-winding format of SynRM is quite much like the IM. Whereas the rotor shape of SynRM is quite precise from IM, it is not caged rotor or twisting and does not have any magnetic fabric, it has only laminated obstacles which designed in a complex manner, and an optimized to have a pinnacle quadrature axis compliments and non-direct axis jealousy, once the magnetic concern goes with the flow in the stator winding and in step with the rotor structure it's far a low and high hesitation vicinity and they represent almost the magnetic poles [5–16].

The rotor layout in SynRM is rotated to reach the low reluctance regions and drifting away of the immoderate reluctance areas inside the equational time of rotation, the purpose of this work method to acquire the magnetic location synchronous speed. The stator machine to each of SynRM and IM is the same signal in the rotating frame. The SynRM does no longer want any magnetic or winding substance at the rotor form which makes the motor rugged, introduction simplicity, the most inexpensive rate of manufacturing, better torque according to unit quantity possibility, working at most high speeds functionality which makes the SynRM, and the rotor windings Failing to end result from easy control strategies, and the decline's minimization create SynRM an appealing and famous desire for several business and care programs due to all of these awesome and splendid traits [7, 12].

The earliest variations of SynRMs are used immediately a caged rotor, the most crucial cause that pristine SynRMs do no longer have starting torque attributes, however now the modern-day SynRM and using the most updated styles of inverters, area orientation manage FOC generation at the side of using Pulse Width Modulation (PWM) method deliver a convenient approach for manage, so without any rotor cage that the tool may also be initiated. The velocity variable parameters have utilized in SynRM motor system layout to correct the motor speed strength because of numerous factors like electricity conservation, manage the situation, velocity, and enhancement of the brief response traits [6, 7–12, 28, 31].

The aim of a motor tempo controller is to take a sign representing the reference tempo and to strain the motor at that reference velocity. Although, the control

machine consists of velocity that been comments from the machine, a SynRM, a voltage supply location vector inverter, a controller, and a speed placing the device [6, 7, 22]. The fundamental reason for the use of comments in one's systems is with a purpose to gain a reference-thing irrespective of any variation or exclusive problem within the traits the tool decrease returned to the reference issue. **Figure 2** is displayed the SynRM rotor flux barrier and IM motor rotor cage. In addition, the SynRM motor can be located from its d-q stationary axis the same circuits as in **Figure 3**.

The SynRM version is pretty like the induction motor IM. The difference is by way of neglecting the rotor losses from the IM equations. The SynRM's version is described via (Eqs. (1)–(4)) [5–7, 16].

$$V_d = R_s I_d + \frac{d\lambda_d}{dt} - \omega_r \lambda_q \tag{1}$$

$$V_q = R_s I_q + \frac{d\lambda_q}{dt} + \omega_r \lambda_d \tag{2}$$

$$\lambda_d = L_d I_d \tag{3}$$
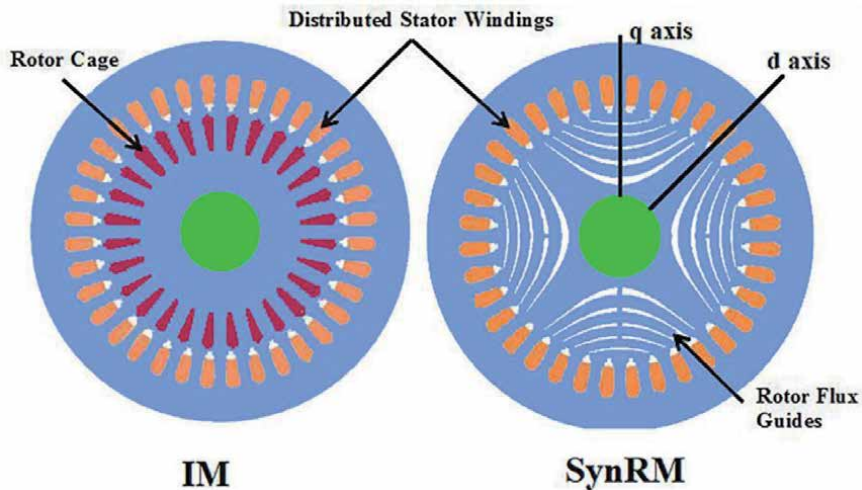
Figure 2.
The machinal contents of SynRM and IM.
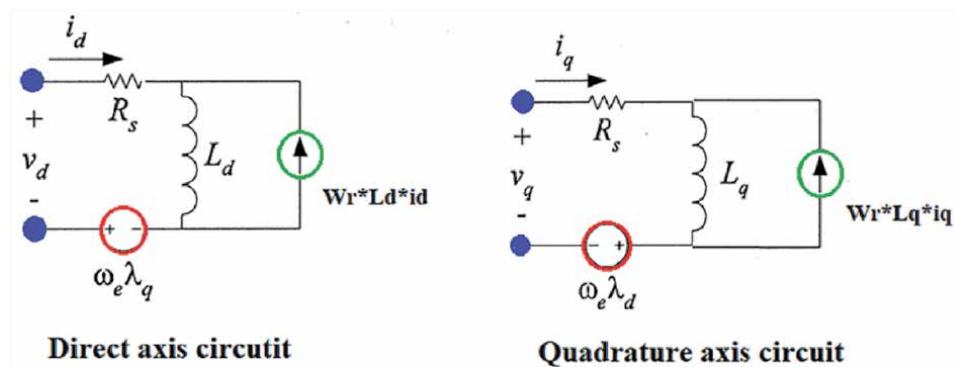
Figure 3.
The equivalent circuit of d axis and q axis for SynRM.

$$\lambda_q = L_q I_q \tag{4}$$

By both of each (Eqs. (3) and (4)) the over shift speed could be acquired as will detect in (Eqs. (5) and (6)) as following:

$$\frac{d\lambda_d}{dt} = V_d - R_s I_d + \omega_r \lambda_q \tag{5}$$

$$\frac{d\lambda_q}{dt} = V_q - R_s I_q - \omega_r \lambda_d \tag{6}$$

From (Eq. (5)) the change-speed rate of the direct axis current could be gained in (Eq. (7)).

$$\frac{dI_d}{dt} = \frac{1}{L_d}\left(V_d - R_s I_d + \omega_r L_q I_q\right) \tag{7}$$

And with (Eq. (6)) the change-speed rate of the quadratic axis current could be gained in (Eq. (8)).

$$\frac{dI_q}{dt} = \frac{1}{L_q}\left(V_q - R_s I_q + \omega_r L_d I_d\right) \tag{8}$$

Besides, to obtain the torque of SynRM we have used in (Eq. (9)).

$$T_e = \frac{3}{4}\frac{P}{2}\left(L_d - L_q\right)I_d I_q \tag{9}$$

The of speed rate can be acquired by (Eq. (10)).

$$\frac{d\omega_r}{dt} = \frac{P}{J}\left(T_e - T_L\right) \tag{10}$$

The Laplace transformation of the torque is given as follows by (Eq. (11)).

$$T = \frac{3}{2}P\left(L_d - L_q\right)i_d i_q - \left(B\omega_r + J\frac{d\omega r}{dt}\right) \tag{11}$$

Table 1 show the SynRM parameters that used in the design. These parameters are the same parameters for the IEv4 motor for the ABB company.

Parameter	Parameter value	Units
Ld	6.0645	mH
Lq	0.910	mH
Rs	0.0265	Ohm
J	0.245	Kgm^2
B	0.0000009	N.m.s
P	2	poles

Table 1.
The main parameters of the SynRM.

2.2 Voltage source inverter

Inverters are power electronics systems that turn the DC voltage from a battery or some other DC source into alternating current voltage, which may be single-phase, two-phase, or three-phase, depending on the inverter configure ratio. Inverters that feed synchronous motors are mainly used in variable voltage and variable frequency applications for high-performance variable speed [4, 6, 7]. SVPWM is the most widely used PWM technique due to its high output voltage, low harmonic distortion, and superior efficiency as compared to other types of inverters. The SVPWM inverter is a complex scheme that produces a high voltage fed to the generator, resulting in a low overall harmonic distortion [4, 6, 15, 16]. The aim of the various modulation schemes is to provide a variable output with a maximum fundamental factor that can generate as few harmonics as possible. The switching instants are calculated using the SVM scheme, which is based on the representation of the switching vectors in the rotating or stationary frame plane, based on the position of the output voltage vector in each sector of the space vector sectors. The mathematical model of SVPWM inverter is given as seen on (Eqs. (12) and (13)), where n represents the number of the space vector sectors.

$$T_a = \frac{\sqrt{3}T_z V_{ref}}{V_{dc}} * \left(\sin\left(\frac{n\pi}{3} - \alpha\right) \right) \tag{12}$$

$$T_b = \frac{\sqrt{3}T_z V_{ref}}{V_{dc}} \left(\sin\left(\alpha - \frac{n-1}{3}\pi\right) \right) \tag{13}$$

2.3 Mathematical model of stationary field transformation

The transformation from the mechanical model has completed by the usage of the d-q transformation, which is used for a vector manipulate approach of the synchronous motor machine. The base at the concept which is the windings of the stator are disbursed a d-q version is a powerful tool for simulation of all AC machines such as the SynRM [6, 7, 16]. When Three-segment balanced and altered windings and symmetry to two-segment Equation Equilibrium windings deliver rotating magnetic discipline speed Φ and cost are equatorial, the three-section windings are Equational with the two-segment windings. The d-q transformation is well-balanced three-phase V_d, V_b andV_c into balanced two-phase V_d and V_q as shown in **Figure 4**.

The transformation matrix "T" to transfer voltage or current vector from abc reference frame into dq reference frame as seen on (Eq. (14)):
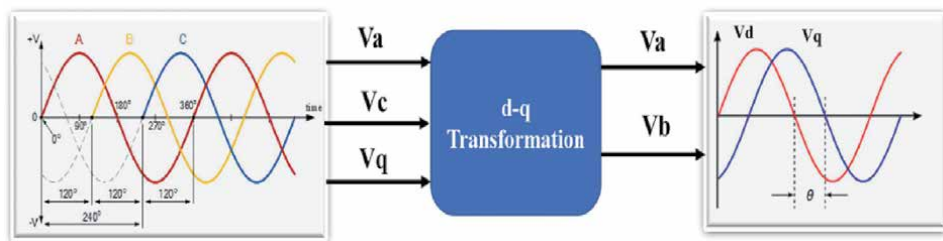
Figure 4.
The direct and quadratic voltage transformation.

$$\begin{bmatrix} V_d \\ V_q \\ V_o \end{bmatrix} = \mathbf{T} \begin{bmatrix} V_a \\ V_b \\ V_c \end{bmatrix} \tag{14}$$

The transformation matrix can be used in synchronous frame as explained in (Eqs. (15) and (16)),

$$\mathbf{T} = \sqrt{\frac{2}{3}} \begin{bmatrix} 1 & \dfrac{-1}{2} & \dfrac{-1}{2} \\ 0 & \dfrac{\sqrt{3}}{2} & \dfrac{-\sqrt{3}}{2} \\ \dfrac{1}{\sqrt{2}} & \dfrac{1}{\sqrt{2}} & \dfrac{1}{\sqrt{2}} \end{bmatrix} \tag{15}$$

$$\mathbf{T^{-1}} = \sqrt{\frac{2}{3}} \begin{bmatrix} 1 & 0 & \dfrac{1}{\sqrt{2}} \\ \dfrac{-1}{2} & \dfrac{\sqrt{3}}{2} & \dfrac{1}{\sqrt{2}} \\ \dfrac{-1}{2} & \dfrac{-\sqrt{3}}{2} & \dfrac{1}{\sqrt{2}} \end{bmatrix} \tag{16}$$

Where $\mathbf{T^{-1}}$ represents the inverse transformation matrix.

$$\begin{bmatrix} V_d \\ V_q \end{bmatrix} = \sqrt{\frac{2}{3}} \begin{bmatrix} 1 & \dfrac{-1}{2} & \dfrac{-1}{2} \\ 0 & \dfrac{\sqrt{3}}{2} & \dfrac{-\sqrt{3}}{2} \end{bmatrix} \begin{bmatrix} V_a \\ V_b \\ V_c \end{bmatrix} \tag{17}$$

The zero-axis voltage is neglected, and the power is the same in both the three phase and the two-phase transformation as seen on (Eq. (17)).

3. Motor control

3.1 Traditional cascade PID controller

Traditional PID controllers are considered the most largely used controllers in the control-process industry because of their simple structure and easy parameter settlement. The major cause of user feedback is a very substation in systems is to be able to attain a set-point regardless of disturbances, noise, or any variation in characteristics [5–16, 25]. A PID controller determines an "error" value as the difference between an obtained process variable and a reference setpoint. **Figure 5** shows the general cascade control system scheme. The controller tries to make the error signal as small as possible by manipulating the process control inputs. The calculation "algorithm" of the PID controller contains three separate constant parameters, and it is mainly called the proportional, integral, and derivative values [5–16, 29]. The differential equation of a PID controller is given by (Eq. (18)).

$$u(t) = k_p e(t) + k_i \int e(t)dt + k_d \frac{d}{dt} e(t) \tag{18}$$
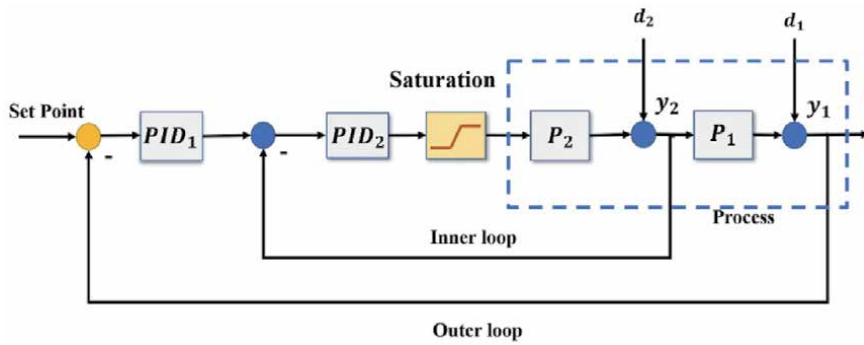
Figure 5.
The General Cascade control system scheme.
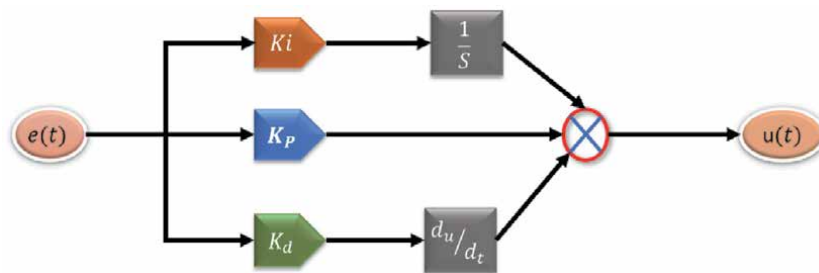
Figure 6.
Traditional PID controller.

Response parameter	Rise time	Overshoot	Settling time	Steady-state error
K_P	Decrease	Increase	Small change	Decrease
K_I	Decrease	Increase	Increase	Eliminate
K_d	Small change	Decrease	Decrease	Small change

Table 2.
The characteristics of the tradition controller.

Moreover, the transfer function is given by (Eq. (19)).

$$G_{PID}(s) = k_p + \frac{k_i}{S} + S.k_d \tag{19}$$

Figure 6 shows the block diagram with the parameters of the PID controller. The response to the error is connected to the proportional value, the sum of mistakes that were recent are the integral's assignment to determined and the reaction is being represented by the derivative to the rate at which the error has been shifting. The controller parameters K_P, K_I and K_d on traditional closed-loop systems as shown in **Table 2** give comprehensive effects of each parameter, in some control processing it may require only one or two parameters to present a suitable control system. Setting other parameters to zero is the method for correcting the PID controller to two or one activity. A PID controller will be named a PI, PD, P or I controller when neglecting one of the respective control actions [5, 6, 12]. PI controllers are common, since the activity is sensitive to sound change, whereas if there is absolutely no term that is integral the system may be avoided by it from reaching its target value due to the control activity [11–16].

3.2 Cascade control system

The procedures have more than one variable or factor at the output. That should be controlled is well known as a term multivariable or MIMO processes. Interactions usually exist or occasionally do not exist between the control loops of multivariable processes, which is famed by problems in control when compared with the Single Input/Single Output (SISO) control processes. Lead–lag compensators are utilized to provide a combines performance involving both lead and lag compensator and utilized as another phase following PI and PID controllers which allow the machine to have stabilized functionality [5, 6, 12, 26]. PI controller was utilized to control the guide axis current. This sort of control procedure is shown in **Figure 7**. The disadvantages of the type of control an ambiguity of control engineers' power SISO PID controller, flexibility for both interaction adjudication and compare it with overall multivariable control it is a couple of strong tools for its layout [6–9]. Therefore, there is one easy method to tune a multi-loop PID controller by tuning each loop one by induvial work, and completely discarding the loop connections and that is carried out by the (i) loop of cascade controller for the plant move. Then re-tuning all the loops together so the general system has stable functionality and supplies a suitable load disturbance response [5, 6, 12, 26–29].

3.3 Double-led compensation

The lead compensators are used to give advance phase margin, used in this chapter as a second stage after PID controller, and used to control quadrature axis current double-lead compensators to make the system have advanced stabilized performance because it is considered a cascaded lead compensator [6, 7–12]. The double lead compensator gives double of the phase advance that a simple lead compensator that gives. The double lead compensator mathematical description can be given in (Eq. (20)). The lead compensator is utilized to control the quadrature axis present of this SynRM.

$$G_{pd}(s) = K_p \frac{\left(1 + s/\omega_z\right)^2}{\left(1 + s/\omega_p\right)^2} \tag{20}$$
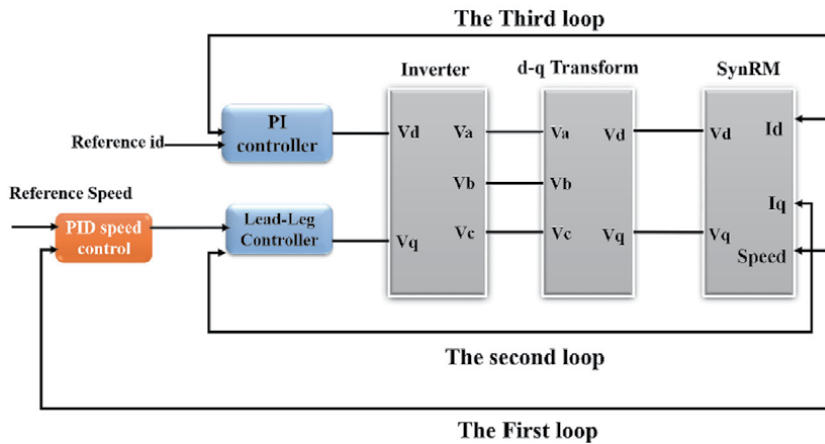
Figure 7.
Cascade controller block diagram.

3.4 Practical swam optimization tuning PID controller parameter

The Particle Swarm Optimization (PSO) is a public rely on computational approaches that the primary concept came in the simulation of social behavior "social-psychological methods" fish instruction, bird flocking and swarm concept. PSO was initially designed and evolved by Eberhart and Kennedy [4, 6, 12] This concept was designed to be effective in solving problems exhibiting non-linearity and non-differentiability. The scheme is obtained from research on swarms such as fish Instruction and bird flocking. Accommodation to the results of research for a flock of birds finds that bird's food by flocking (not by everyone). Instead of using the evolutionary proses such as mutation and crossover that been used for algorithm manipulation. In the PSO algorithm, none of these presses are used, the dynamics of the population simulates a "fish flocks" attitude, where sociably sharing of information takes a major part of work and individuals can profit from discovering and former experience of all the other escorts during the food searching process [4]. The fitness function is cast to maximize the constraints domain or to minimize the preference constraints. The most common performance criteria that depend on the error criterion are Integrated Absolute Error (IAE), Integrated of Time Weight Square Error (ITSE) and integrated of Square Error (ISE) which can be calculated analytically in the frequency domain. The criteria selection depends on the system and the controller [5, 6, 12–16]. In this chapter the fitness functions are used depend on the ISE criterion and the overshoot M_p criterion as seen on (Eqs. (21)–(24)).

$$\text{Fitness function} = \min(\text{ISE}) + \min(M_p) \quad (21)$$
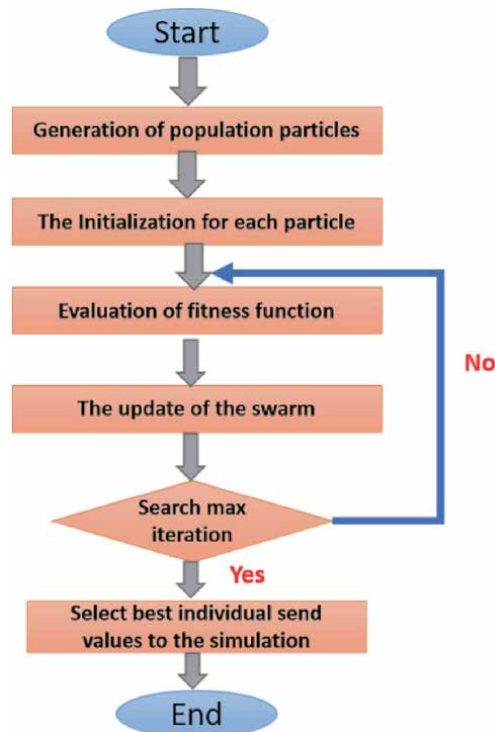
Figure 8.
The PSO algorithm steps.

$$ISE = \int e^2(t)dt \tag{22}$$

$$M_p = \max(n) - (n_{ref}) \tag{23}$$

$$e(i) = D(i) - y(i) \tag{24}$$

The $v_i(t)$ and $x_i(t)$ updating for each particle in the swarm are done depending on (Eqs. (25) and (26)). Then starting the main loop and the fitness function are calculated to update the positions of particles. If the new value is better than the quondam I_{best}, the new value is set to I_{best}. In the same way, g_{best} value is also updated like the I_{best}. The velocity of each agent can be updated by (Eq. (25)).

$$v_i^{k+1} = w * v_i^k + c_1 * R_1 * \left(lbest_i - x_i^k\right) + c_2 * R_2 * \left(gbest_i - x_i^k\right) \tag{25}$$

Moreover, the current position can be updated by (Eq. (26)):

$$x_i^{k+1} = x_i^k + v_i^{k+1} \tag{26}$$

$$w = w_{max} - \frac{(w_{max} - w_{min})}{iter_{max}} \tag{27}$$

The diagram below explains the order of PSO processes and steps that were adopted and implemented in this design as expend in **Figure 8**.

4. The design of the propulsion EV system

The proposed system is called the Multi-Converter/Multi-Machine System (MCMMS) which consists of two SynRM that drive the two rear wheels of PEV [6, 7, 12, 13]. The linear speed of the vehicle is controlled by an EDC which gives the reference speed for each driving wheel which depends on the driver reference speed and the steering angle. Different road conditions have been applied by the Drive cycle topology to test the stability of the EV under the EDC controller. The SynRM speed is controlled by using a PID controller and the PSO algorithm has been used as an optimization technique to find the optimal PID parameter to enhance the drive system performance [2–4, 24]. The VSSVI has been used to transform the DC voltage source to three-stage AC voltage [1, 2]. The EV system has tested implemented in the Matlab/Simulink environment. Moreover, the mechanical load that reflects the street state of the vehicle each one of these elements has been displayed in **Figure 9**. Which shows a succinct description to the suggested system the two-wheel driveway process is perceptible to everyone to grantee the equilibrium of the EV on various road state [1–12].

The inner construction system for this type of EV has controlled by an EDC system that ensures the robustness of the motor vehicle [1–5]. In addition, the propulsion electric vehicle system process has referred to as a MCMMS [18, 22]. Moreover, the pure-electric-vehicle is much simplified and like the traditional mechanical vehicle in the work way, because of slipping issues from the curvature or slope "inclined" angle roads [16, 17, 23].

4.1 The electronic differential controller (EDC)

The EDC is an electronic device that guarantees deliver a maximum value of the torque and control both driving wheels, so each wheel may turn at different speed
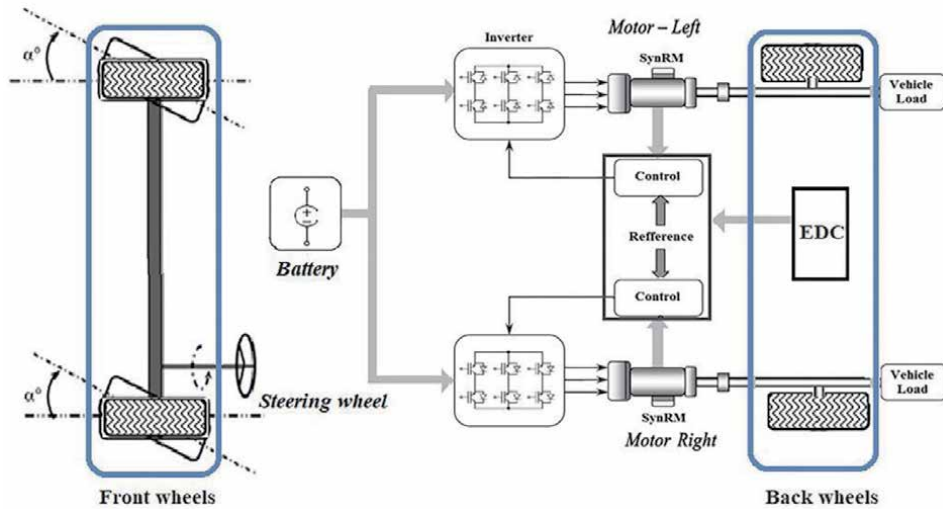
Figure 9.
Propulsion system control of the EV.

rates in virtually any curve or precisely the exact same rate of speed in the right line road. According to the road condition and especially the steering angle control of the vehicle, the electric power is distributed by EDC to each electric motor [4, 9–12, 27]. In addition, the most critical beholding in the plan of the EVs will be to make sure that the EV is secure when cornering' and under slippery road' conditions [9, 14, 15]. **Figure 10** shows the EV structure pushed at a curve road. The calculation of the speed rate of the vehicle is a task of EDC work, also is based mostly on; the driver, vehicle dimension and street condition. The linear speed rate as well as the steering angle that has awarded by the driver, which implies that both inputs regarded as the input reference to the EV system [9, 17–20, 27–30].

At the beginning of the vehicle's turn in the curve road, the driver utilizes the curve steering angle to the steering wheel to drive and control the vehicle. In this case, the EDC reacted quickly and calculate the benchmark speed of each wheel ought to be operating that appropriately and synchronous to ensure the equilibrium of the EV functionality within the curve street by increasing the speed rate of an outer motor and diminishing the speed rate of the Internal motor [4, 12, 17]. The mathematical model of this EDC signifies via (Eqs. (28) and (29)).

$$V_L = \omega_v \left(R + \frac{d_\omega}{2} \right) \tag{28}$$

$$V_R = \omega_v \left(R - \frac{d_\omega}{2} \right) \tag{29}$$

The curve road can be determined as (Eq. (30)).

$$R = \frac{L_\omega}{\tan \delta} \tag{30}$$

Moreover, the angular speed rate in a curve road for both wheels can obtain by the following in (Eqs. (31) and (32)) bellow:

$$\omega_L = \frac{L_\omega + \frac{d_\omega}{2} \tan \delta}{L_\omega} \omega_v \tag{31}$$
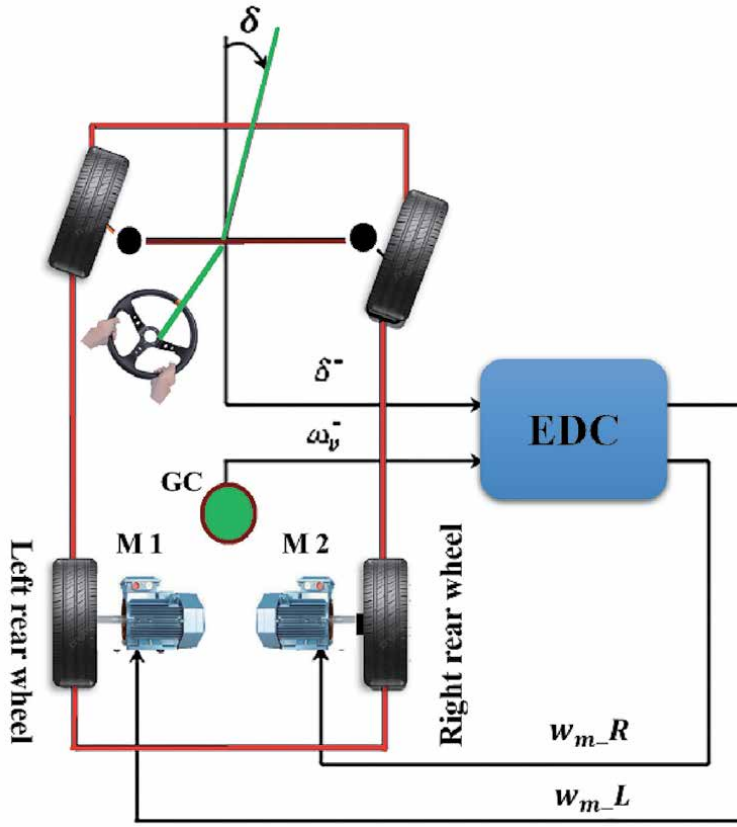
Figure 10.
The input and output of the EDC on the curve road.

$$\omega_R = \frac{L_\omega - \frac{d_\omega}{2}\tan\delta}{L_\omega}\omega_v \tag{32}$$

The difference in Rate between both of them (the left and right wheels) could be write as (Eq. (33)) bellow:

$$\Delta\omega = \omega_L - \omega_R = \frac{d_\omega.\tan\delta}{L_\omega}\omega_v \tag{33}$$

Besides, the mention of the speed rate for both Wheel engine can be described as (Eqs. (34) and (35)) bellow:

$$\omega_{Lr} = \omega_v + \frac{\Delta\omega}{2} \tag{34}$$

$$\omega_{Rr} = \omega_v - \frac{\Delta\omega}{2} \tag{35}$$

The Terms of the angle (δ) condition in both of straight or curve road are:

- First term: Turn right→ ($\delta > 0$)

- Second term: straight ahead→ ($\delta = 0$)

- Third term: Turn left→ ($\delta < 0$)
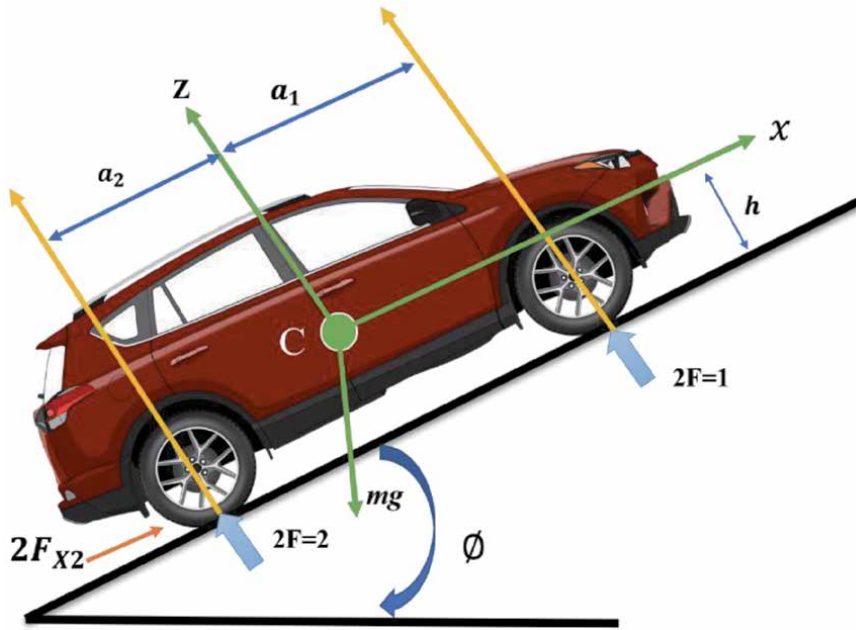
Figure 11.
The effective forces of the EV in an inclined road.

4.2 The resistive forces of EV

Typically, the EV regarded as a succession of heaps that described by numerous forces mainly or resistive torque. Anyway, the forces may include three components, which will be the rolling resistance, the aerodynamic resistance along with also the pitch "incline" resistance [4]. The forces acting in an EV moving across a likely road is displayed in **Figure 11**.

The resistive forces which influenced on the EV are described as seen on (Eq. (36)). And the effective rolling resistance can be described as seen on (Eq. (37)) [31].

$$T_r = T_{aero} + T_{slope} + T_{tire} \qquad (36)$$

$$T_{tire} = mgf_r \qquad (37)$$

The force of the aerodynamic resistance can be explained in (Eq. (38)):

$$T_{aero} = 1/2\rho_{air}A_fC_dV^2 \qquad (38)$$

Moreover, the force of the slope "incline" resistance describes in (Eq. (39)):

$$T_{slope} = mgsin\beta \qquad (39)$$

5. Simulation and results

5.1 Simulation and results of cascade-PI and lead-lag-controller

A single cascade controller with several control loops has been used in industrial processes. Since it provides an advantage in terms of ease of execution and the

ability to manually set the parameter of this managed kind. Furthermore, as compared to overall multivariable control, which has a few robust tools for its architecture, this control category has a high demand for interaction versatility modification. In this case, a system engineering team manually tunes the SISO for the PID controller to complete the control loop for this form of control. Even so, there is a single basic strategy for tuning a multi-loop PID control, which is to tune control loops step by step while refusing loop interaction completely. Furthermore, the install switch operation has been carried out by setting the I loop of the PID control. The machine would have steady functionality and a suitable load disruption response if the full loops are re-tuned together. To restrain the quadrature-axis (q) that exists in the SynRM, the lead–lag compensator was proposed.

Simultaneously, the procedure is depended on **Figure 6** that represents the SynRM cascaded control system. **Figure 12** explains the simulation for the cascaded PI controller model with the lead–lag compensator. **Table 3** reveals the cascaded controller parameters value of the cascaded controller system that has utilized by a strategy known as "trial and error". The **Figures 13–18** reveals the SynRM speed rate and torque due to different working condition.

5.2 Simulation and results of cascade-PI, PID and lead-lag-controller

The PI controller at the speed rate control has substituted via PID controller, which the metering activity gives to improve the motor speed and torque activity. As shown in **Table 4**, the cascaded PI and PID control parameters have utilized via trial-error strategy. Besides, **Figure 19** shows the Matlab/Simulink program has employed to simulate the PI and PID-cascaded controller. The **Figures 20–25** reveals the SynRM speed rate and the torque due to several working conditions.

5.3 Simulink and results for the cascaded controller with PSO

The cascaded PID, PI, and lead–lag compensator were used to simulate the SynRM model based on the results of the PSO algorithm discovered by using the
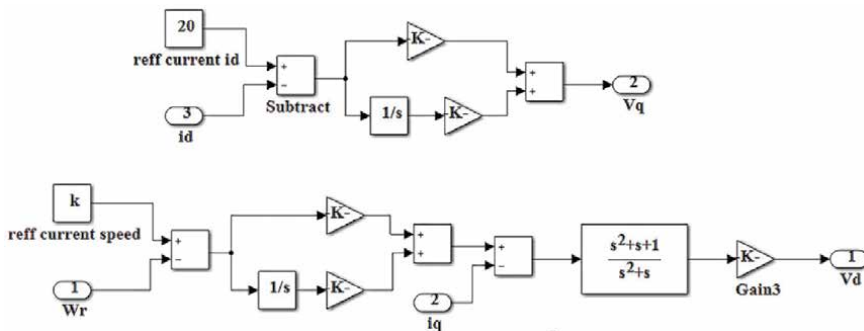
Figure 12.
Simulink model for cascade-PI and lead- lag controller.

The type of controller	Speed		Quadratic axis current		
The Parameters	K_P	K_I	K_3	K_P	K_I
The Result value	60.245	17.672	22	2130	9.8

Table 3.
The parameters and values of the cascade controller.
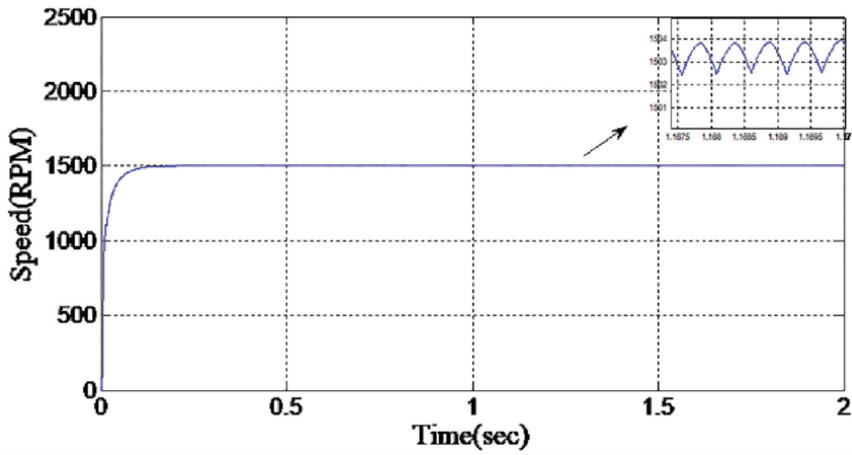
Figure 13.
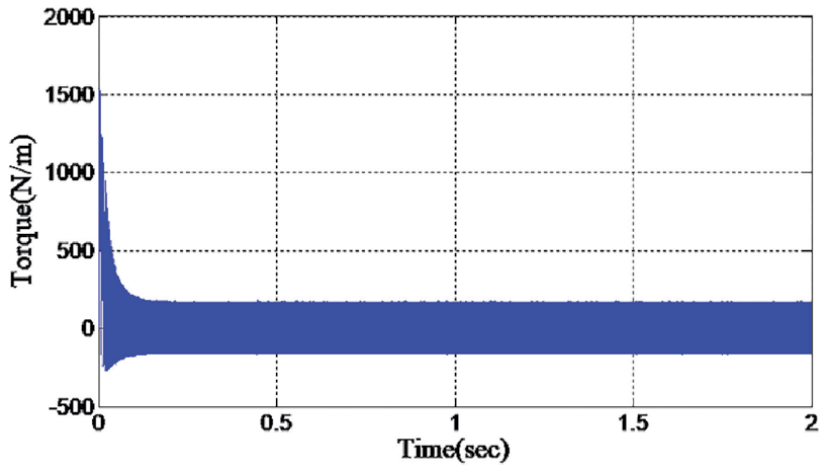*SynRM speed control at 1500 rpm with no load condition.*
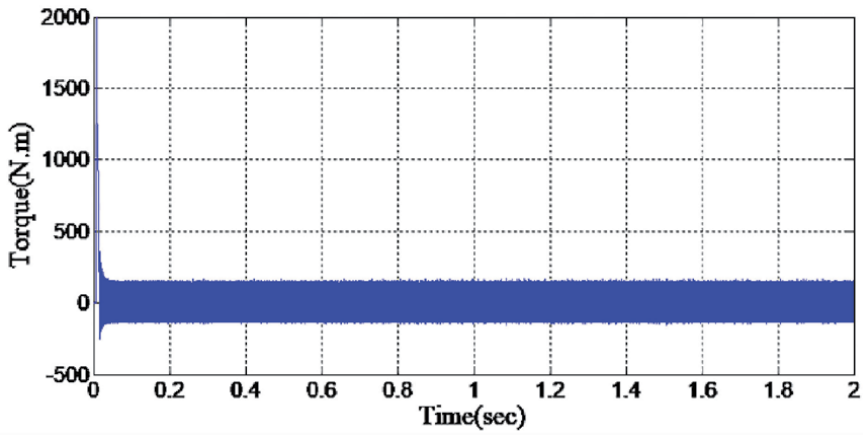
Figure 14.
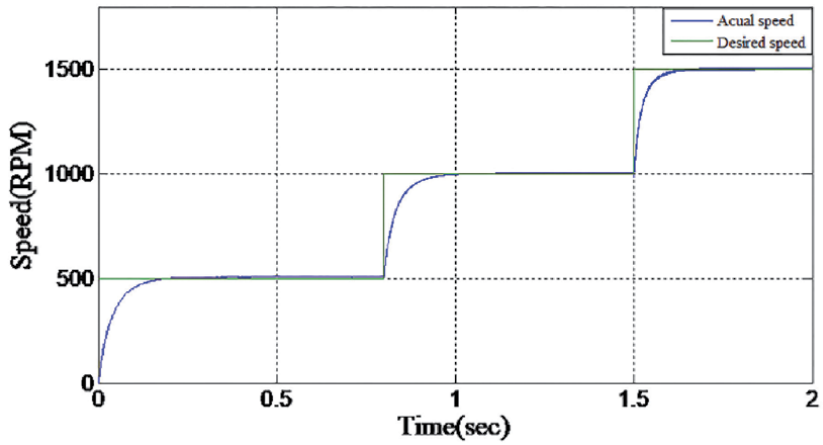*The SynRM torque control at1500 rpm with no load condition.*
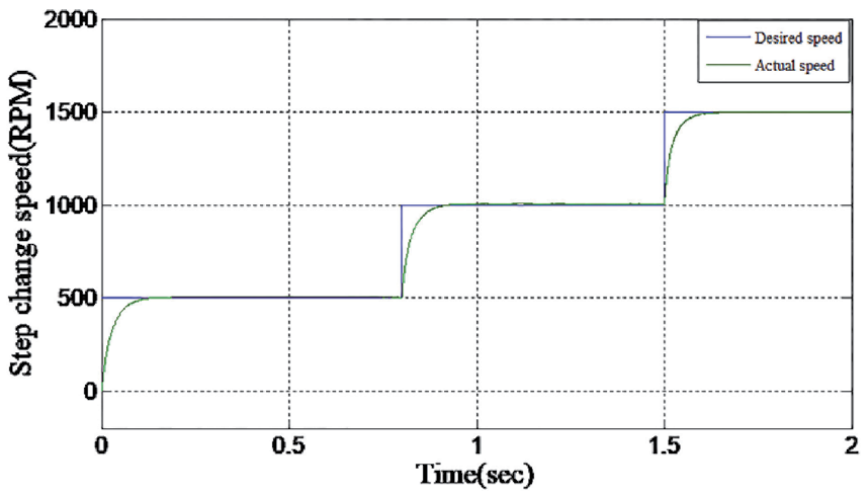
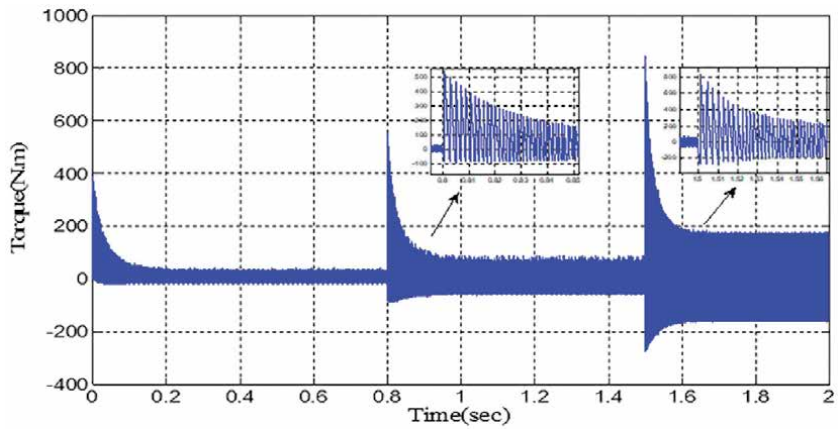**Figure 15.**
The SynRM speed control at steps of speed.
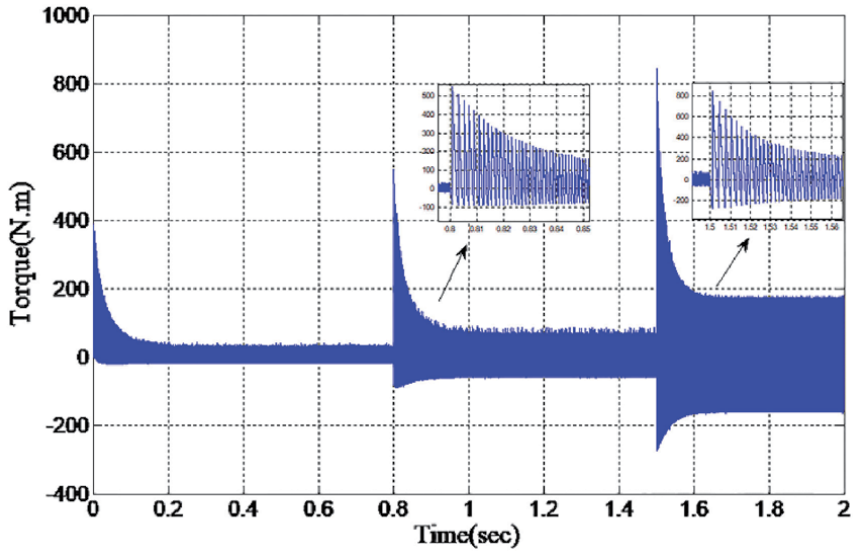
Figure 16.
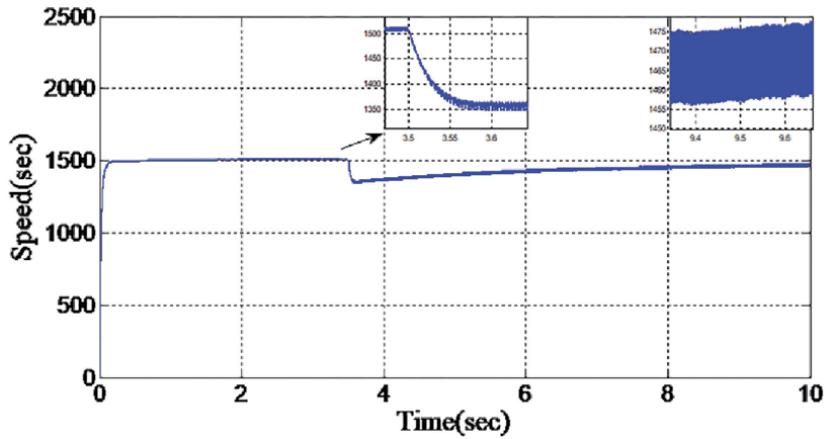*The SynRM torque control at steps of speed.*
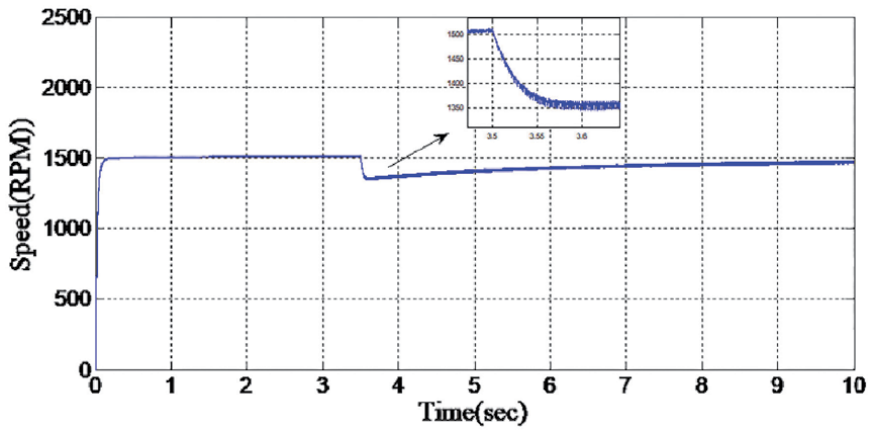
Figure 17.
The SynRM speed control with 1500 rpm and 50 N.m of load applied at 3.5 second.
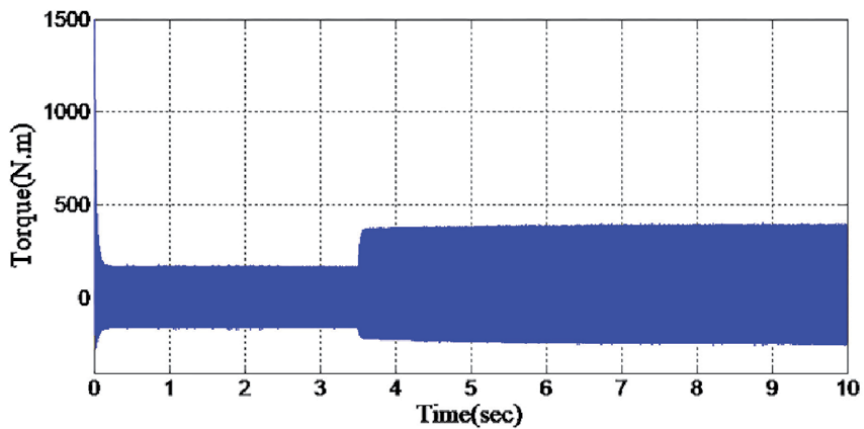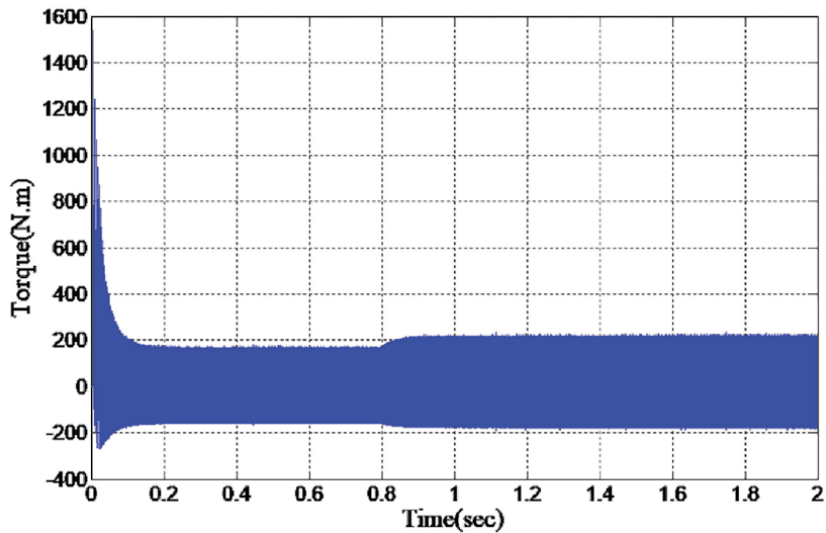

Figure 18.
The SynRM torque control at 1500 rpm with 50 N.m of load applied at 3.5 second.

'The type-of controller'	Speed-			Quadratic*Axis*Current		
The parameter	K_P-	K_{I-}	K_{d-}	K_{3-}	K_{P-}	K_I-
The value	40	10	1	22	1200	10

Table 4.
Manually tuned of the cascade controller.
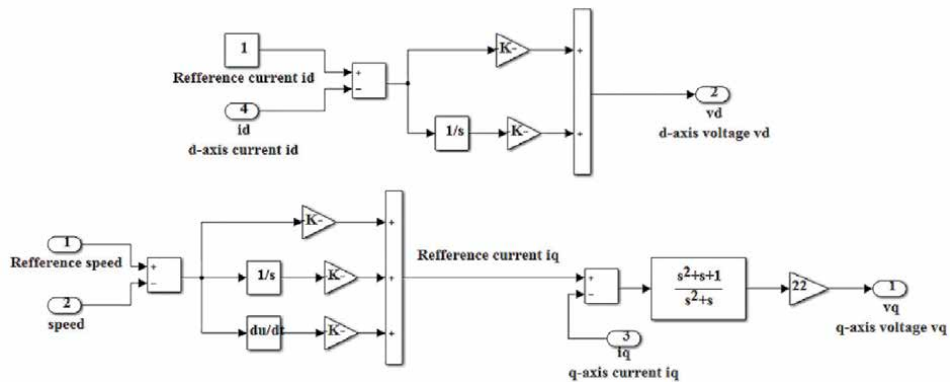
Figure 19.
Simulink model for PI, PID and lead–lag controllers.
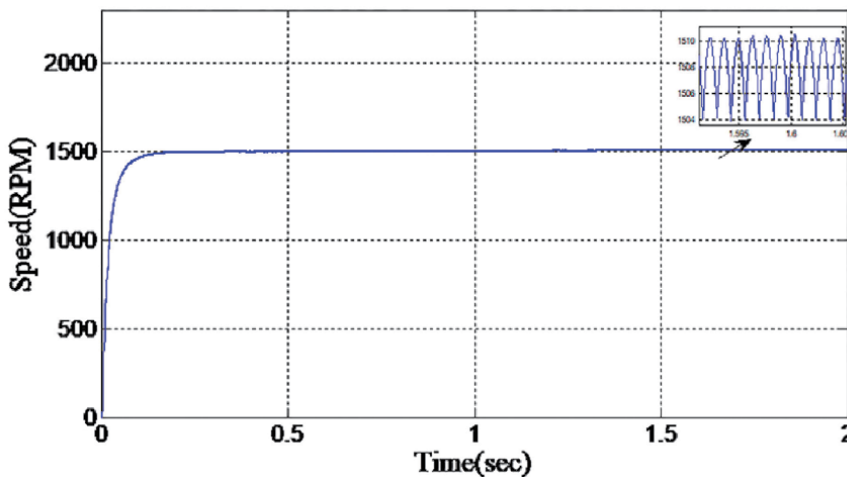
Figure 20.
The SynRM speed control at 1500 rpm with no load condition.

Simulink method with the PSO algorithm. The Simulink findings show characteristics and feature the PSO algorithm, which offers optimal PID, PI, and lead–lag-compensator parameter values to improve system functionality as shown in **Table 5**. Besides, **Table 6** shows the parameters of the PSO strategy tuned in cascade controller. **Figure 26** displays the technique parameters PID and PSO. Furthermore, the **Figures 27–32** show the SynRM speed control and torque control from PSO algorithm parameters of the cascaded control with approximately 50 integrations.
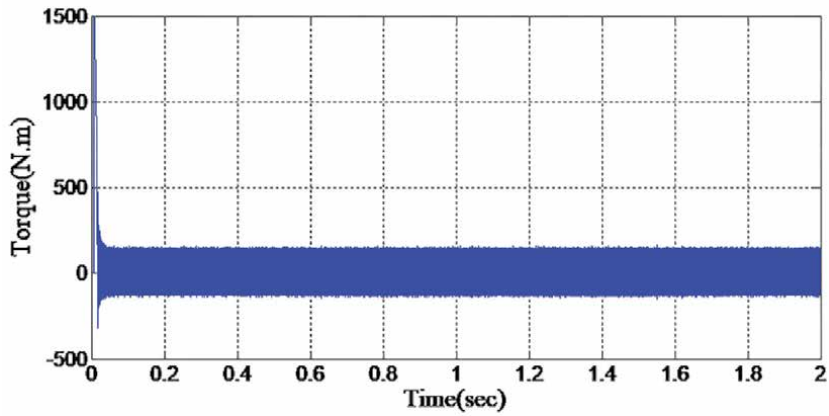
Figure 21.
The SynRM torque control at 1500 rpm with no load condition.
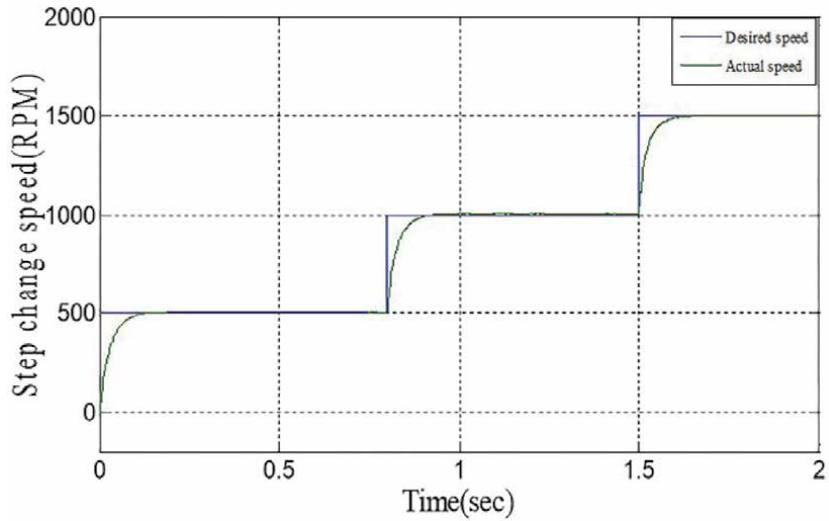

Figure 22.
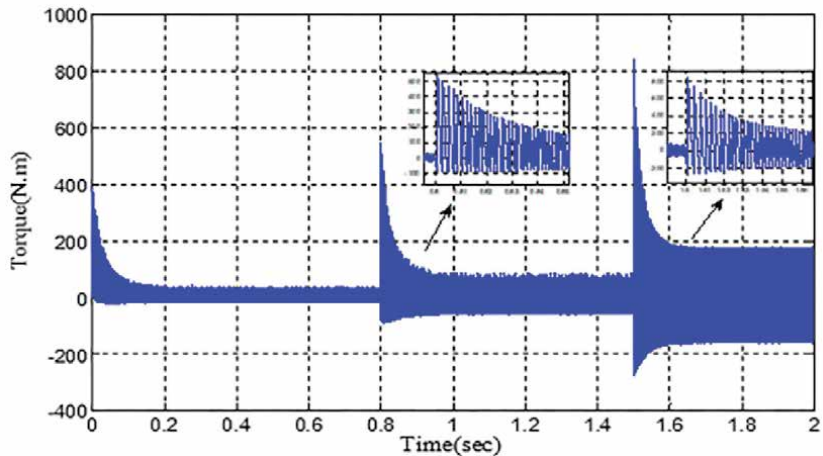*The SynRM speed control with steps of speed.*
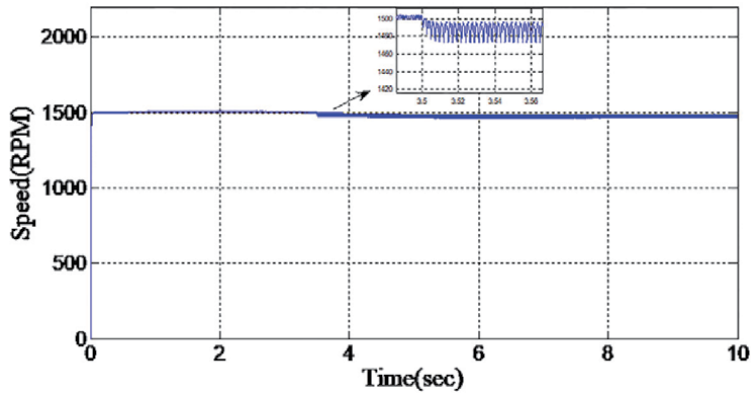

Figure 23.
The SynRM torque control with steps of speed.

Figure 24.
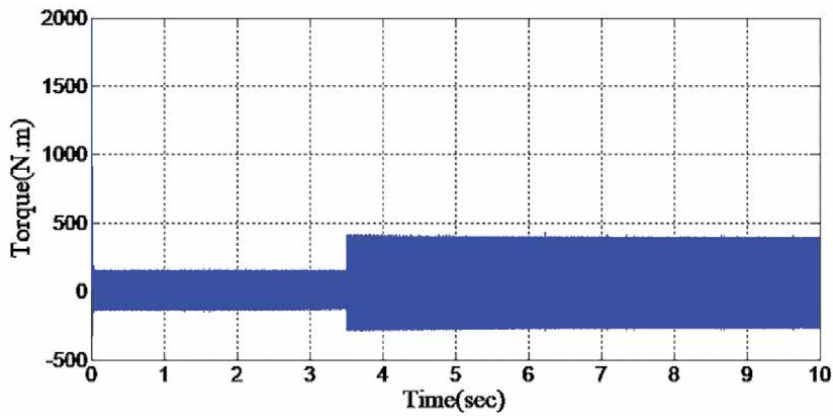*The SynRM speed control with 1500 rpm and 50 N.m step of load applied at 3.5 second.*

Figure 25.
The SynRM torque control with 1500 rpm and 50 N.m step of load applied at 3.5 second.

The PSO parameters	The value
The Size of the swarm.	50
Maximum iteration number.	50
The Swarm Dimension.	16
C_1 parameter.	1.3
C_2 parameter.	1.3
$W_{max.}$	0.8
$W_{min.}$	0.3

Table 5.
The characteristics of PSO algorithm.

175

The type of controller	Speed			Quadratic axis current		
Parameter	K_P	K_I	K_d	K_3	K_P	K_I
Value	200.64/	/8.8182/	/0.7914	/20.879	/2130	/9.8/

Table 6.
PSO strategy tuned.in-cascade-controller-parameters.
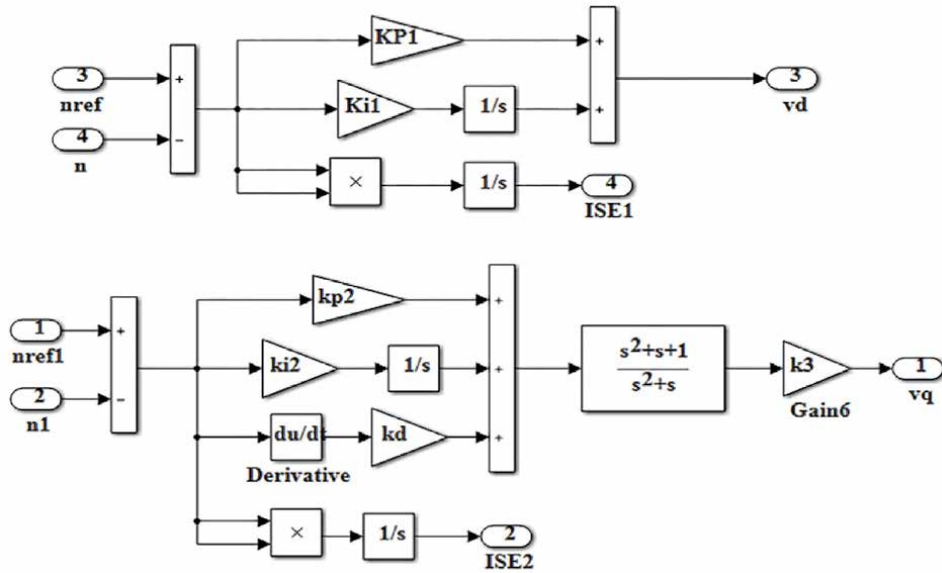
Figure 26.
Simulink for PSO fitness-function model.
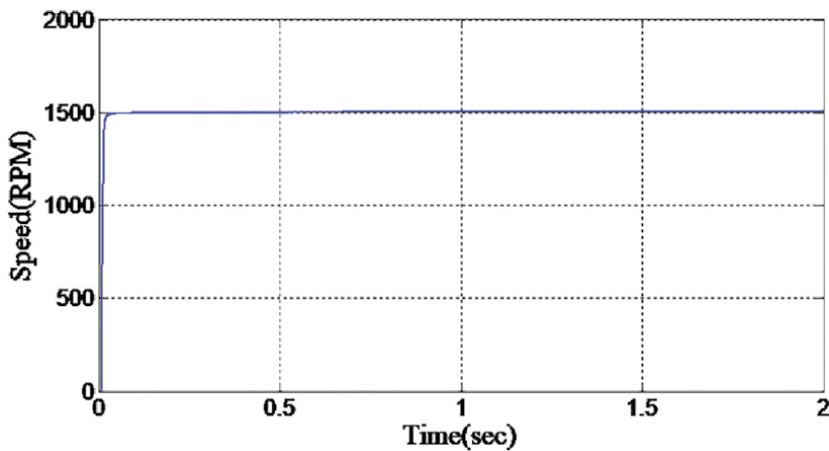
Figure 27.
The SynRM speed control with 1500 rpm and no-load condition.

5.4 Conclusion of SynRM controllers

The cascaded-PI and PID controls were used in conjunction with a lead–lag compensator to control the motor speed. Furthermore, the Simulink controls have been utilized to regulate the motor speed in a wide range and can provide adequate

Figure 28.
The SynRM torque control with 1500 rpm with no load condition.

Figure 29.
The SynRM speed control with steps of speed.

Figure 30.
The SynRM torque control with steps of speed.

177

Figure 31.
The SynRM speed control with 1500 rpm and 50 N.m steps of load at 3.5 second.

Figure 32.
The SynRM torque control with 1500 rpm and 50 N.m steps of load applied at 3.5 second.

speed and torque reaction or demonstrate their validity in regulating the motor speed rate in various operating conditions. Furthermore, the PSO algorithm simulated manipulating the parameters of their cascaded controls to achieve a more important output than traditional controllers. The simulation depicts the testing and study of each of the controller's structures under various circumstances. As a result, it is possible to infer that the proposed PSO strategy offers the best control parameters for improving system efficiency, especially in the loading state. The simulation depicts the testing and study of each of the controller's structures under various circumstances. As a result, it is possible to infer that the proposed PSO strategy offers the best control parameters for improving system efficiency, especially in the loading state.

6. The propulsion construction of EV

6.1 The simulation and design of the EV system

The simulation and design of the system have done via Matlab/Simulink depended on the above equations and the input parameters of these equations that have utilized in the design as showing in **Table 7** below:

d_ω	1.8 m
R_w	0.23 m
f_r	0.02
m	$710K_g$
ρ_{air}	$1.3K_g/m^3$
A_f	$2.8m^2$
C_d	0.34

Table 7.
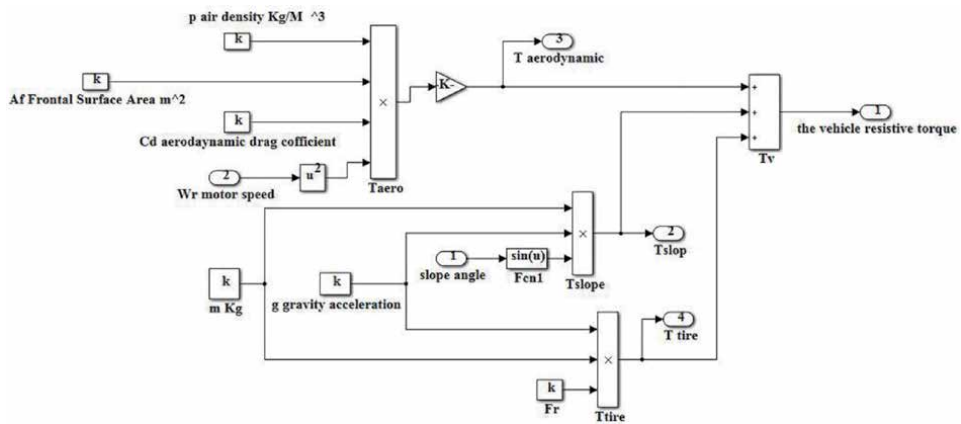*The design information of the EV.*

Figure 33.
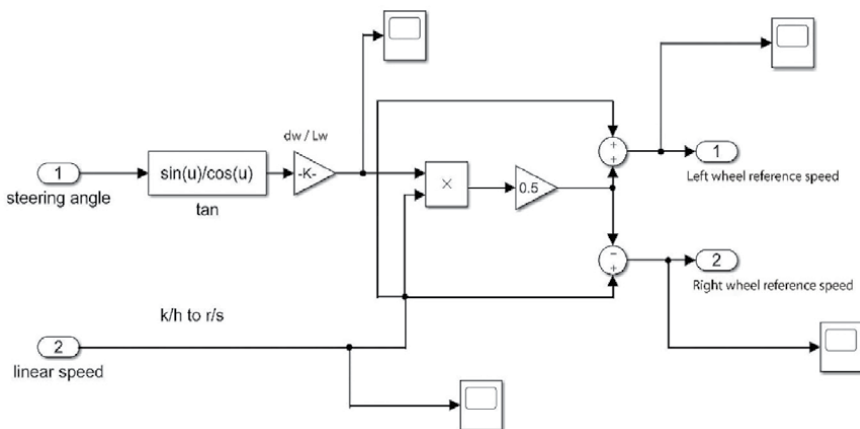*Modeling and simulation of the resistive force.*

Figure 34.
The simulation diagram of the EDC system model.

6.2 Simulink model of the resistive torque in EV

The important task for the EDC is the distribution of the torque, where the resistive forces are dispersed evenly on both electric motors in the case of a straight road. Besides, the complete resistive of the torque is divided into two parts

"two-halves", which are each half distributed on a single motor. The torques supply is the EDC assignment. The modulation and simulation of the resistive force are represented in **Figure 33**.
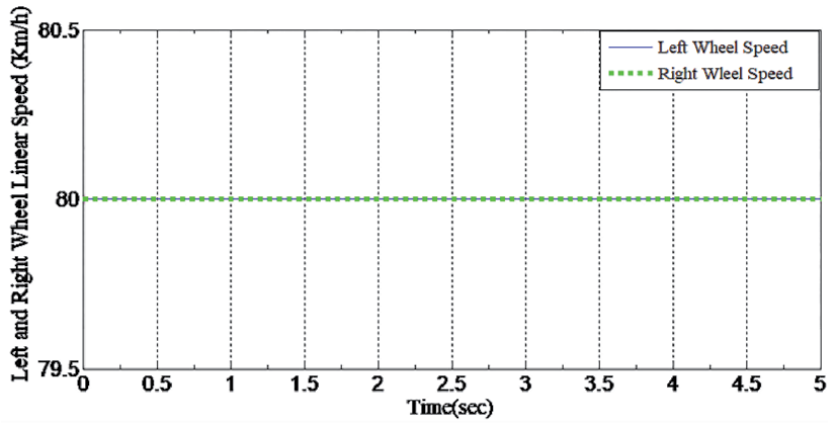
Figure 35.
The EV moving with 80 km/h speed rate at the straight road.
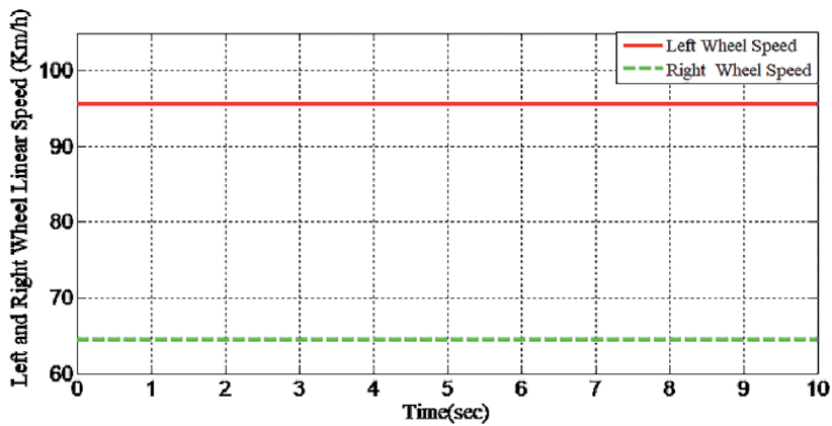
Figure 36.
The EV turn right with 80 km/h speed rate at the curve-road with +11-degree steering angle.
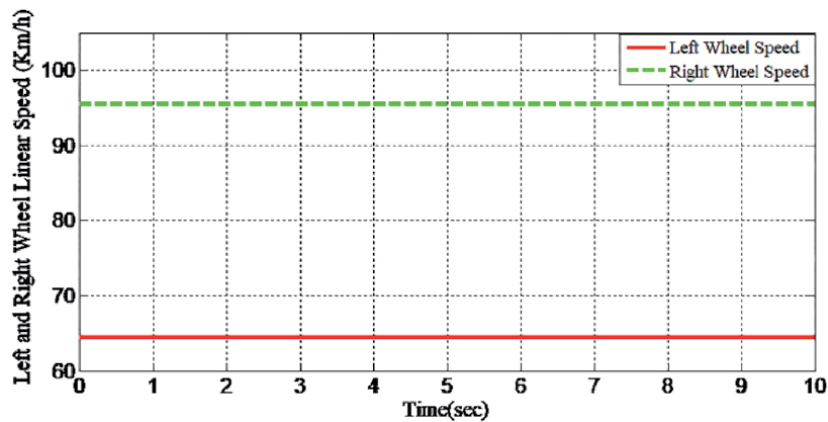

Figure 37.
The EV turn left with 80 km/h speed-rate at the curve-road with +11-degree steering angle.

6.3 The simulation and result of the EDC system

The simulation and result in this segment have applied using Matlab/Simulink software to describe and examine the validity of the EDC platform from the EV. Additionally, the simulation diagram of the EDC program version is displayed in **Figure 34**. The simulation model is designed based on the previously mentioned EDC equations. The simulation model represents two inputs to simulate the road conditions that the electric vehicle will travel: The first is the simulation of the inclined road with a different angle of inclination as needed in the simulations to test the vehicle on inclined roads. The second is the straight road, which has an angle of inclination of zero degrees. The model outputs represent the effect of different road conditions on the speed and stability of the electric vehicle, which is represented by the rear wheels of the vehicle that is connected to the EDC. Besides, the propulsion drive system layout at the EV includes two SynRMs that attached right on the wheels of the EV " right and left wheels" without decrease equipment, energy source signified by Lithium-Ion rechargeable battery power sours, EDC and VS-SVPWM inverter. In addition, **Figure 35** suggests the right road instance, where the two wheels in EV ought to be changed at precisely the exact same speed rate. Thus, once the EV turns directly from the curve street, the wheels proceed at a slow rate of speed when compared with the ideal wheels of the EV as shown in **Figure 36**. On the contrary, once the EV flip left from the curve street, the ideal wheels proceed at a higher rate of speed as compared with the wheels of their EV as shown in **Figure 37**.

6.4 The simulation result of driving cycles system

The EV **moving at 80 km/h of speed** as shown in **Figure 38** with comprise three stages. Moreover, the supply of this resistive force which impacts on the EV in these stages of the simulation differs from one point to another.

The supply of this resistive force that affects the EV in these stages of the simulation is somewhat different from one point to other. These stages are described as the points below:
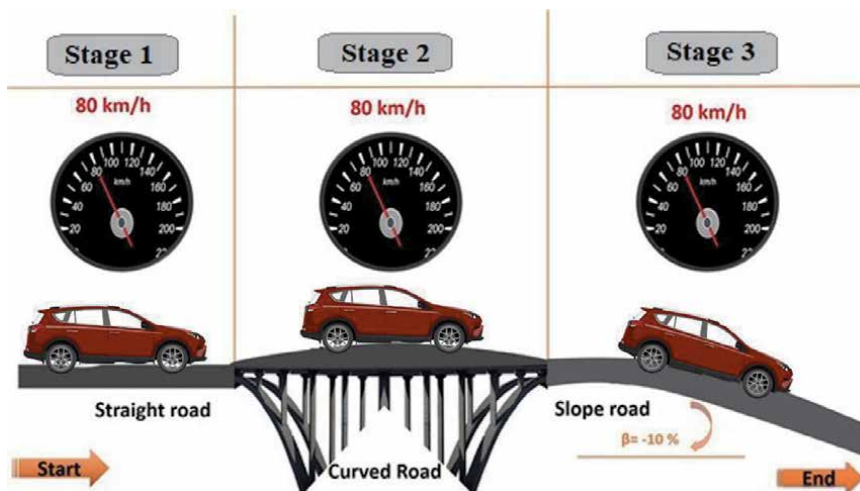

Figure 38.
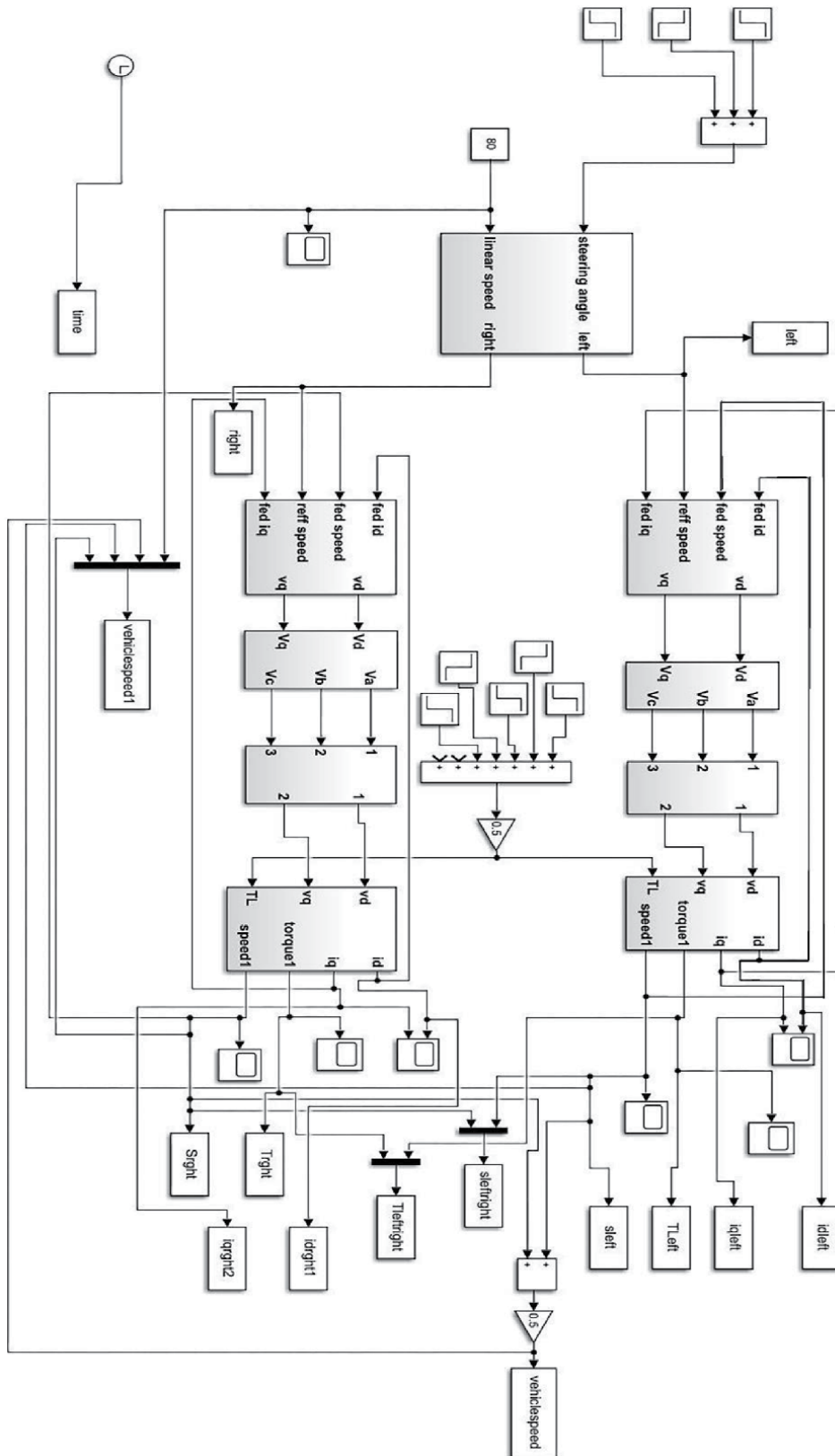*Driving cycle of the EV includes three stages.*

Figure 39.
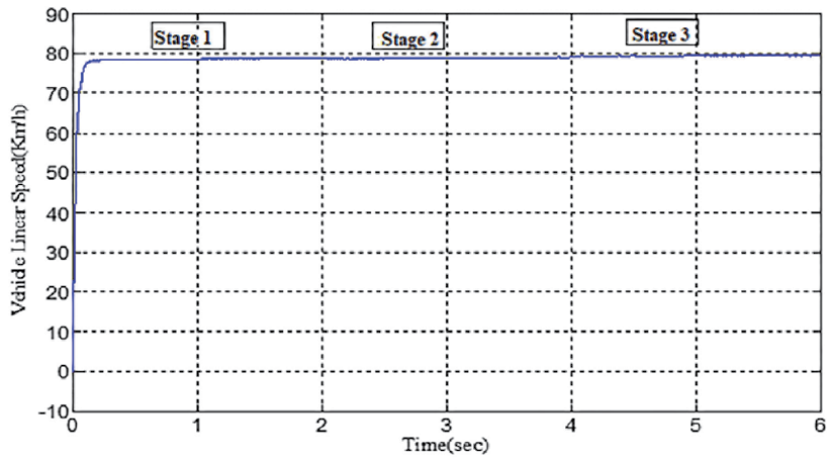*Modeling and simulation of PEV model.*
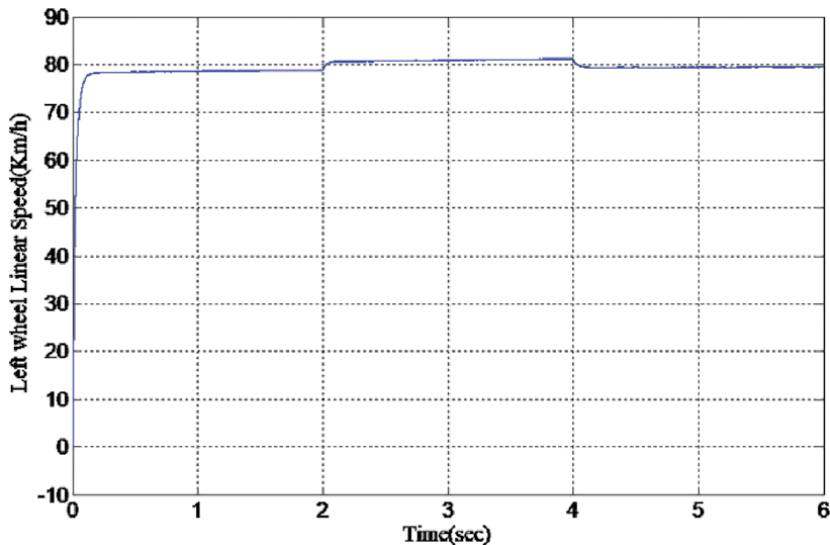
Figure 40.
The linear speed of the EV.

Figure 41.
The linear-speed at the left-wheel of the EV.

- The 1st stage: the EV moving in the straight road along with the moving beginning with the next zero and finish in the next two of the estimated time.

- The 2nd stage: that the EV turns directly from the curve street with 2.5 levels of the steering wheel along with the moving beginning from two minutes two and finish with the next four of the projected periods.

- The 3rd stage: that the EV descents in off-road street with 10 degrees of incline angle and the moving start from the next four and end with the next six of the estimated periods.

   Figure 39 shows the full design of the EV consists of all main parts in this chapter. Besides, it explained the connecting ways between them to get the full system simulation.
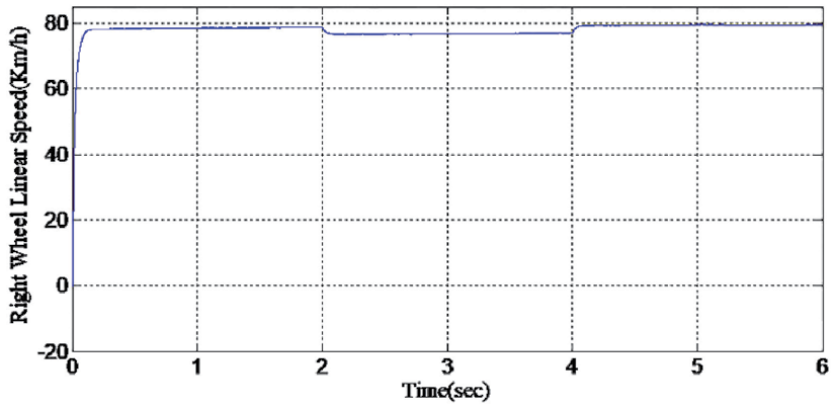
Figure 42.
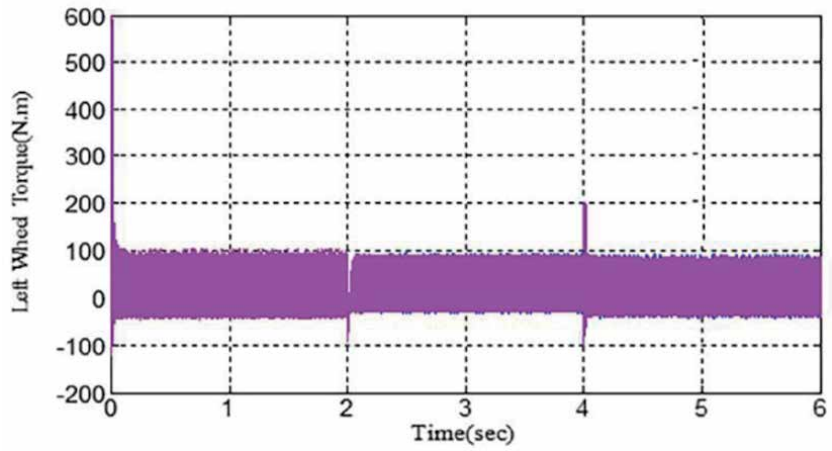*The linear-speed at the left-wheel of the EV.*
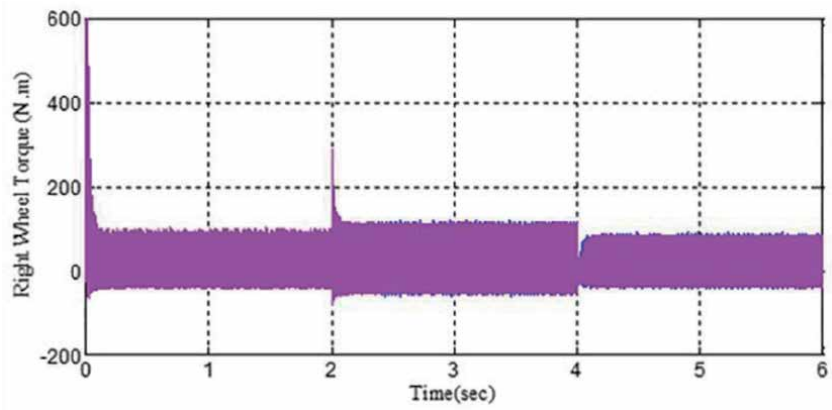

Figure 43.
The torque at the left-wheel of the EV.

Figure 44.
The torque at the right-wheel of the EV.

The time	From 0 to 4 second	From 4 to 6 second
The load	32.52 Nm	25 Nm

Table 8.
The load information's for the driving cycle.

The result of the simulation the first drive cycle that have referred to the **Figure 40** for each stage is explained in the points below:

Figure 41 represent the linear speed of the EV that is started from zero to reach the 77 km/h in stage1 in the next one and continued to reach at the 78.5 km/h at 2nd stage in the second two of the moving time also continue to reach the 80 km/h in the next four of the transferring time in the previous step of simulation in the slop road.

Figure 42 reflect the linear speed of the wheel of the EV that has started from zero to reach the 77 km/h in 1st stage in the next one and grow up to achieve the 83 km/h in the stage 2 since the EV has turned into and this point indicates the influence on the left wheel of this EV. The last point after the decease to reach the 80 km/h in simulation in the slop street.

Figure 43 reflect the linear speed of the right wheel of this EV that's started from zero to reach the 77 km/h in stage1 from the 2nd second and decease to 75 km/h at the 2nd stage since the EV has flipped directly which stage indicates the influence of the ideal wheel of the EV. In the 3rd stage after the decease to reach the 80 km/h at of simulation in the slop road.

Figure 44 represents the torque of the left wheel of the EV. The torque has already now reached 600 N.m at the first moment of the EV moving in stage1 then decease to be stable in 200 N.m throughout this stage. In the second two of those moving represent the 2nd stage of the simulation, the torque decease to 50 N.m due to the curve road then grew to become stable in 200 N.m in this stage. The second four reflect that the 3rd stage and the torque increase up to 600 N.m only at that second and then reduction to be stable in 188 N.m in the slop road.

The torque has already reached 600N.m at the very first moment of the EV moving-in stage1 after that decease to be stable in 145 N.m in this stage. At the next two of the moving represent that the 2nd stage of the simulator, the torque growth to 300 N.m due to this curve road after that increase to become stable at 180 N.m with this stage. The 3rd stage starts from the second four of their transferring periods and the torque decease to 50 N.m because of the curve road after that rise to attain and become stable at 150 N.m. The loaded that effect on the EV for each stage is represented in **Table 8**.

7. Conclusion

The EDC symbolizes the gearbox as positioned in electric vehicles which operate the transferring, the rate and transform the direction by the wheels into the fundamental engines accountable for providing the wheels of their EV using adequate torque for spinning along with forcing the EV. Besides this gadget controls the angle of the EV making it stable at the guide roads and alternative methods which have been mimicked by hypotheses in the research. Thus, the EDC-technology has really used to restrain the linear rate of their EV and confirm the vehicle equilibrium under several street states as exhibited in section.

The EDC topology has implemented in this simulation to test the stability and functionality of their EV under several street situations and road angles. Additionally, the simulator comprises three various drive-cycles each drive cycle includes many

stages with various road-condition. The linear rate of the EV might be computed by locating the result of the left and right wheel's linear rates. The driving cycle shows the EV balance across the whole cycle to make it to the close of the cycle.

According to the simulation result, the EV structure has stability and higher response in several distinct states with 80 km/h highest speed at the right road. Additionally, to guarantee the security of the function of the electric apparatus in the genuine electric vehicle must be analyzed separately on the simulators restrain the wheel of the EV along with also the angle of deviation of the vehicle by implementing different torque rates as shown in the simulator amounts.

Acronyms and abbreviations

T	The electromagnetic torque of SynRM in $\mathbf{N/m}$
P	The number of poles of SynRM
J	The moment of inertia coefficient of the motor in $\left(\mathbf{K_g M^2}\right)$
$\mathbf{T_L}$	The inside load torque of SynRM $(\mathbf{N/m})$
B	The viscous friction coefficient of SynRM
N	The number of the space vector sectors
$\mathbf{k_p}$	Proportional gain
$\mathbf{k_i}$	The integral gain
$\mathbf{k_d}$	The derivative gain
e(t)	The error
$\mathbf{M_p}$	The overshoot
$\mathbf{y(i)}$	The model output
$\mathbf{D(i)}$	The wanted output
n	The actual speed
$\mathbf{n_{ref}}$	The reference speeds
$\mathbf{v_i(t)}$	The velocity
$\mathbf{x_i(t)}$	The current position
x_i^k	The current position of particle (i) at iteration (k)
v_i^k	The velocity of particle(i) at iteration (k)
w	The inertia weight
c_1, c_2	The positive acceleration constants
R_1, R_2	are random variables distributed uniformly in the range [0; 1]
w_{min}	The inital weight
w_{max}	The final weight
$iter_{max}$	The maximum iteration numbers.
V_L ann V_R	The linear speed of the the left and right wheels of the EV in (km/h)
ω_v	The liner speed of the EV in (Km/h)
d_ω	The size width of EV in (meter). R the road curve
L_ω	The EV length and δ is the street angle
m	The total mass of the EV in(kg)
g	The gravity acceleration in (m/s)
f_r	The rolling resistance force constant.
ρ_{air}	The density of air in $\left(k_g/m^3\right)$
A_f	The frontal surface area in (m^2)
C_d	The aerodynamic drag coefficient
V	The linear speed of the vehicle in (km/h)
β	The slope angle of the street
ω_z	The zero of Led-leg compensator
ω_p	The pols of Led-leg compensator

Author details

Muhammet Tahir Guneser*, Mohammed Ayad Alkhafaji and Cihat Seker
Karabuk University, Karabuk, Turkiye

*Address all correspondence to: mtguneser@karabuk.edu.tr

IntechOpen

References

[1] İnci, Büyük M, Demir M H, İlbey G. Mint: A review and research on fuel cell electric vehicles: Topologies, power electronic converters, energy management methods, technical challenges, marketing and future aspects. ELSEVIER. 2021;36: 130-141. Doi: org/10.1016/j.egypro.2013.07.016

[2] Xu Y, Zheng Y, Yang Y. Mint: On the movement simulations of electric vehicles: A behavioral model-based approach. ELSEVIER. 2021; 283: 0306-2619. Doi: org/10.1016/j.apenergy.2020.116356.

[3] Agamloh E, von Jouanne A, Yokochi A. Mint: An Overview of Electric Machine Trends in Modern Electric Vehicles machines. MDPI AG. 2020; 8(2): 20. doi.org/10.3390/machines8020020

[4] AlKhafaji M A, Uzun, Y. Simulation and control of an electric vehicle by using PSO and specify driving route topology. In: Proceedings of the IEEE International Conference on Power Generation Systems and Renewable Energy Technologies (PGSRET); 1-6, August 2019; Istanbul. Turkey.

[5] Güneşer, M T, Dalcalı A, Özturk T, Ocak C. Influence of Rotor Slot Structure at Starting Torque and Efficiency on Urban Use EV Motor. IN: Proceedings of the IEEE International Conference on Power Generation Systems and Renewable Energy Technologies (PGSRET); 1-4, August 2019. Istanbul. Turkey IEEE.

[6] AlKhafaji M A, Uzun, Y. Design and Speed Control of SynRM Using Cascade PID Controller with PSO Algorithm. In: International Journal of Renewable Energy Development (IJRED); 69-76, February, 2020. Ispanya. Madrid.

[7] AlKhafaji M A, Uzun, Y. Design, simulation and analysis of synchronous reluctance motor, The International conference on innovative research in Science Engineering and Technology (IRSET). 2018, Belgrade, Serbia.

[8] Thounthong P, Sikkabut S, Poonnoy N, Mungporn P, Yodwong B. Kumam P, Bizon, Nahid-Mobarakeh B, Pierfederici S. Mint: Nonlinear differential flatness-based speed/torque control with state-observers of permanent magnet synchronous motor drives. IEEE Transactions. 2018; 2874-2884. DOI: 10.1109/TIA.2018.2800678.

[9] Tildirim M. and Kurum,H. Electronic Differential System for an Electric Vehicle with Four In-wheel PMSM. IN: Proceedings of the IEEE 91st Vehicular Technology Conference (VTC2020-Spring); 1-5. May 2020; Antwerp. Belgium.

[10] Yıldırım M. Öksüztepe E. Tanyeri B. Kürüm H. Electronic differential system for an electric vehicle with in-wheel motor. IN: Proceedings of the IEEE International Conference on Electrical and Electronics Engineering (ELECO); 1048-1052. November 2015; Bursa. Turkey.

[11] Zhang N, Xu C, Niu W, Lu X. The electronic differential control based on the slip ratio. IN: Proceedings of the IEEE 36th Chinese Control Conference (CCC); 9384-9389. July 2017. Dalian. China.

[12] Abdul-hassan, K M, Kahdum S A. Simulation of Speed Control for Synchronous Reluctance Motor Based on Tuning Cascaded PID Controller with PSO Algorithm. IN: Proceedings of University of Thi-Qar Journal for Engineering Sciences; 1-15. November 2016. Thi-Qar. Iraq.

[13] Gasbaoui B, & Nasri A. The uses of artificial intelligence for electric vehicle

control applications. In: Subhas Chakravarty, editors. Technology and Engineering Applications of Simulink. 2012. P. 239-256. DOI: 10.5772/36653.ch11

[14] AlKhafaji M A, Uzun, Y. Modeling and Simulation of A Photovoltaic Cell Module Controlled with Nonlinear Autoregressive Moving Average-L2 Controller. IN: Proceedings of the IEEE International Conference on Electrical, Communication, and Computer Engineering (ICECCE); 1-5. June 2020; Istanbul. Turkey.

[15] Hartani K, Bourahla M, Miloud Y, Sekour M. Mint: Electronic differential with direct torque fuzzy control for vehicle propulsion system. Turkish Journal of Electrical Engineering & Computer Sciences. 2009; 21-38. DOI: 10.3906/elk-0801-1

[16] Fellani, M A, Abaid E. Mint: Modeling and Simulation of Reluctance motor using digital computer. IJCSEE; 2013; 2:148-52. ISSN 2320–4028

[17] Roukas, M. Development of the control system for an electric vehicle [Thesis]. Göteborg, Sweden: Chalmers University of Technology; 2013

[18] Mebarki, B, Draoui B, Rahmani L, & Allaoua B. Mint: Electric automobile Ni-MH battery investigation in diverse situations. Energy Procedia, 2013; 36: 130-141. DOI: org/10.1016/j.egypro.2013.07.016

[19] Pesce, T, Lienkamp M. Mint: Definition and optimization of the drive train topology for electric vehicles. World Electric Vehicle Journal. 2012; 5: 24-35. Doi: org/10.3390/wevj5010024

[20] Daya J F, Sanjeevikumar P, Blaabjerg F, Wheeler P W, Ojo J O. Mint: Implementation of wavelet-based robust differential control for electric vehicle application. IEEE Transactions.

2015; 30: 6510-6513. DOI:10.1109/TPEL.2015.2440297.

[21] Jazar R N. Handbook of Forward Vehicle Dynamics. 2nd ed. Springer: Cham; 39-97 p. DOI: 10.1007/978-3-319-53441-1_2

[22] Roukas M. Development of the control system for an electric vehicle [thesis]. Göteborg, Sweden: Chalmers University of Technology; 2013.

[23] Sathyan S. Synchronous reluctance motor for household applications [thesis]. Espoo, Finland: AALTO University School of Electrical Engineering; 2013.

[24] Boyd S J, Nelson D. Hybrid electric vehicle control strategy based on power loss calculations hybrid electric vehicle control strategy based on power loss calculations [thesis]. Blacksburg, USA: Virginia Polytechnic Institute and State University; 2006.

[25] Kazmierkowski M P. Handbook of Automotive Power Electronics and Motor Drives. 2nd ed. Emadi, A: IEEE Industrial Electronics Magazine; 2006. 46-47 p. DOI: 10.1109/MIE.2008.926483.

[26] Rahimian M S, Raahemifar K. Mint: Optimal PID controller design for AVR system using particle swarm optimization algorithm. IEEE Ccece. 2011; 337-340. DOI: 10.1109/CCECE.2011.6030468.

[27] Ravi A, Palani S. Mint: Robust electronic differential controller for an electric vehicle. American Journal of Applied Sciences. 2013;10(11), 1356.

[28] Tran P H. Matlab/Simulink implementation and analysis of three pulse-width-modulation, [thesis]. Boise, Idaho: Boise State University; 2012.

[29] Salem, F A. Mint: Modeling and control solutions for electric vehicles.

ESJ. 2013; 9,15: 1857-7881. DOI:
10.19044/esj. 2013.v9n15p%25p

[30] Du J, Ouyang M, Chen J. Mint:
Prospects for Chinese electric vehicle
technologies in 2016–2020: Ambition
and rationality. ELSEIER Energy. 2017;
120: 584-596. DOI: 10.1016/j.
energy.2016.11.114.

[31] GÜNEŞER M T, Erdil E, Cernat M,
ÖZTÜRK T. Mint: Improving the energy
management of a solar electric vehicle.
AECE. 2015; 4: 53-62. DOI:10.4316/
AECE.2015.04007.

Chapter 10

Powerful Multilevel Simulation Tool for HiL Analysis of Urban Electric Vehicle's Propulsion Systems

Raul Octavian Nemeș, Mircea Ruba, Sorina Maria Ciornei and Raluca Maria Raia

Abstract

The general focus of the proposed chapter is to describe a complex yet transparent solution for advanced simulation analysis of urban electric vehicles propulsion unit. As general rule, precise and realistic results are obtained only when performing real-time simulations, engaging dedicated software for such applications. Hence, simulation of an electric vehicle as a complete solution can become rather difficult. The authors targeted advanced analysis of the propulsion unit, including the motor, the battery, the power converter, and its control. These are designed using multilevel models in Matlab/Simulink, referring to different complexity levels of each assembly. Another feature of the models is their organization, based on Energetic Macroscopic Representation (EMR), this easing the process of inter-connecting models correctly. Nevertheless, the mechanical, aerodynamical and road profile details are included using Amesim Software. All the simulations are performed on a real-time target, using a National Instruments PXIe embedded controller. The latter runs NI VeriStand software, allowing real-time communication between Amesim and Simulink offering in the same time possibility to read/write analog/digital IOs for external communication. This feature in fact is used when passing from modeling to Hardware in the Loop (HIL) analysis, replacing the simulated assembly with the actual one.

Keywords: real-time, Hardware in the Loop, EMR, multilevel, electric vehicle

1. Introduction

Electrification of urban transportation services, from high power solutions, such as busses and trains, to low power ones, such as small cargo delivery vehicles became highly important. The pressure of developing such solutions is continuously increasing due to the highly crowded urban scenarios in which merchandise and goods must be delivered as fast as possible. Investigating, researching and creating such solutions challenges many universities and OEM engineers. Nowadays, taking advantage of the achievements in the field of computer aided design, any serious study requires advanced simulations, fusing measured data, estimated

and computed ones into powerful computation models, able to replicate behavior of the actual hardware. It is important to mention that at a certain level of complexity, studies can become rather difficult by means of large required computation time, powerful computers to perform and many model's implementations time.

In order to achieve high precision and accurate phenomenon simulation, one must use several software interconnected, each performing analysis in their field of expertise. For example, when simulation of an urban electric vehicle (UEV), all the mechanical, aerodynamical and road conditioning factors can be simulated in Amesim Software, while all the power electronics, electrical drive assemblies and their advanced control can be simulated in Matlab/Simulink. Such a solution ensures high fidelity and correct analysis approach of each assembly of the UEV. However, a co-simulation of this magnitude becomes rather complicated, time and resource demanding, returning a non-real-time behavioral screening. Hence, one solution is to engage a third software, National Instruments VeriStand. This was created to integrate exported model from many simulation software and create one complex simulation solution. Another hands-on advantage is that using a PXIe embedded controller, VeriStand can upload the model and perform the simulation in real-time, allowing the user to observe the system behavior just like in the real life. The simulation time can be from seconds elongated to tens of hours. The data recording can be streamed and decimated as desired. Such a solution will be presented in this chapter.

Another important feature of this tool is given by the real-time target's nature. This allows external communication via analog and digital I/O s simplifying and facilitating the transition from model-based analysis to hardware in the loop (HIL) based analysis.

In order to offer the possibility of selecting the accuracy and the magnitude of the model, the authors considered developing multilevel complexity model, all organized in Energetic Macroscopic Representation (EMR). The latter ensures the user with the correct understanding of the system's power flow, creates a direct path when designing the control loops and facilitates the model exchange when passing from one level of complexity to another. It has to be mentioned that all the models presented in the following sections are designed in EMR philosophy. However, the interest of this chapter is not focused towards this special organization method, hence the reader is encouraged to lecture references [1–3].

2. Multilevel modeling of electric vehicle's propulsion unit

The multilevel approach for developing simulation models for an electric vehicle's propulsion system must be broken down into its main assemblies: the power supply (batteries), the electronic converter, the electrical machine and the general system controller (electronic control unit-ECU). To have a comprehensive analysis, each of these assemblies will be addressed separately in the following sub-sections. For each model, the corresponding energetic macroscopic representation (EMR) block will be presented, separately from its content. The latter will be in fact the modeling approach of each assembly. EMR is an energy flow based graphical organization philosophy easing the building process of complex electromechanical systems. The connection between blocks is always based on action-reaction principle according to the physical causality. In **Figure 1**, the basic elements used in EMR organization are depicted. These will be used in the following sections as some assemblies, for example, an electrical machine will include more than one such block in their graphical description.

Figure 1.
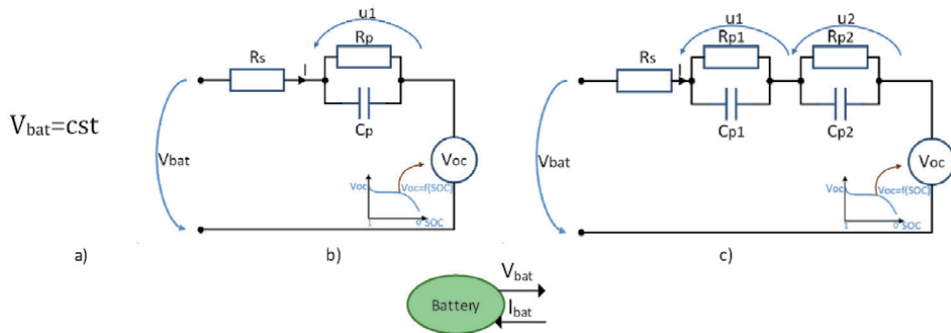*Main EMR pictograms.*

Figure 2.
First (a) and second (b) order equivalent battery circuits and their EMR pictogram (c).

Before diving in the presentation of the multilevel models, it is lucrative to explain the philosophy of building a control scheme using EMR. This is necessary because, in the present chapter, the control units will be also under discussion and their multilevel attribute will come from the level of compromises chosen when building its EMR representation. The control loop can be simply generated by inverting all the model blocks. Hence, the blue pictograms (the control) are a reversed model of the orange ones (the model). The main difference is that in the control loop, only the action path is reversed, while the reaction is neglected, as the latter one is necessary only for the model description and not for the control. In the above indicated references, more details about building EMR control loops are presented, hence the reader in encouraged to visit those.

2.1 Multilevel modeling of batteries

When it comes to model a power supply for an electric vehicle, one can choose between ideal or non-ideal approaches. The latter category can be divided into less or more complex mathematical description. In general, besides the ideal approach the non-ideal one include first and second order battery modeling [4, 5]. A source or a sink in EMR is represented by a green oval, outputting voltage, and inputting current or vice versa.

In **Figure 2** the pictogram used for the battery as electrical source in a simulation is depicted. The content of this block however, can be adjusted to the designer's

needs. In **Figure 2(a)–(c)**, the ideal battery model is depicted (where the voltage is imposed invariant of any changes in the system), the first and second order models (where the battery voltage is dependent on the sourced/sinked current and the state of charge (SOC)). The latter models are called first and second order ones due to the number of parallel RC branches that compound their circuit.

$$V_{bat} = V_{oc} - u_1 - R_s I_{bat}; \quad \frac{du_1}{dt} = -\frac{1}{R_p C_p} u_1 + \frac{1}{C_p} I_{bat} \tag{1}$$

The mathematical translation of the circuits is detailed in Eq. (1) and Eq. (2). It is important to mention that the circuits parameter's values for such models are identified using laboratory experiments and actual battery cells. Such approaches were carried out by the authors on a LG (LGABD11865) battery with a rated capacity of 3000 mAh, 3.75 V rated, 4.2 V maximum over charge voltage, 2.7 V minimum discharge voltage, 0.5–1 A charging current and 0.2–0.5 A discharging current.

$$V_{bat} = V_{oc} - u_1 - u_2 - R_s I_{bat}$$

$$\frac{du_1}{dt} = -\frac{1}{R_1 C_1} u_1 + \frac{1}{C_1} I_{bat}$$

$$\frac{du_2}{dt} = -\frac{1}{R_2 C_2} u_1 + \frac{1}{C_2} I_{bat} \tag{2}$$

The complete process described step-by-step to identify the parameters of the battery cell needed to run the correct model is presented in detail in [4]. Even more, not only the experimental process itself is presented, but also very important post processing steps mandatory to reach high accuracy results.

The open circuit voltage (V_{OC}) is identical for both models, being measured for the same conditions. The recorded function of the SOC is depicted in **Figure 3**.

To help the reader emphasize an image about the precision of these models, a comparative analysis was carried out, superimposing their results for the same testing conditions. After the parameter's identification process [5–8], both models
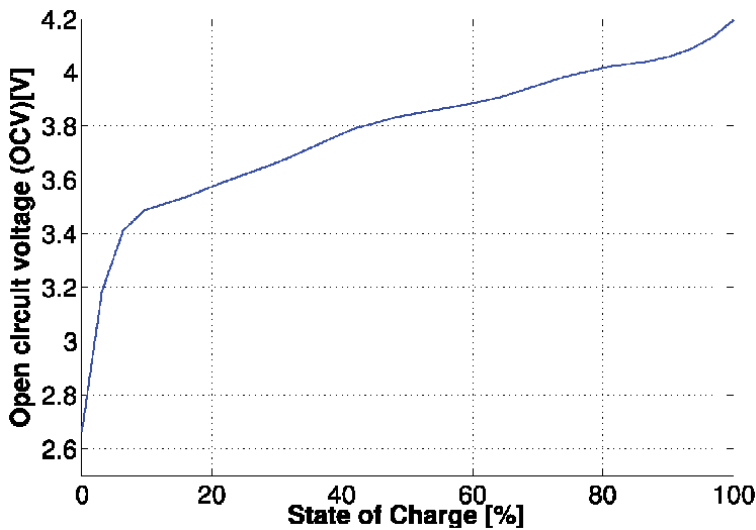

Figure 3.
The open circuit cell voltage vs. SOC.

presented in Eq. (1) and Eq. (2) were built in Matlab/Simulink, as depicted in **Figure 4**-left.

The considered test was to apply equal length current pulses with equal length relaxation time between them, discharging the cell from 100–10%. Initially, this test was applied to the actual cell, the results being also used to identify the necessary data for the simulation models. Imposing the same current variation to the two models, and comparing their voltage calculations with the measured one, one can conclude that the second order model reaches higher accuracy than the first order one. In the zoomed plot from **Figure 4**-right, it can be observed that the second order and measured voltages are in best agreement, while the first order's one marks a slight deviation.

To quantify this difference to a certain palpable value, the root mean square error (RMSE) is computed using Eq. (3) and the instantaneous error between the two signals.

$$RMSE = \sqrt{\frac{1}{T} \cdot \int_0^T [V_{measured}(t) - V_{model}(t)]^2 dt} \qquad (3)$$

The comparative results of the RMSE and the instantaneous error are depicted in **Figure 5** (left and right). In both cases one can observe that the second order model yells lower disturbance compared to the first order one. More, in **Figure 5**-left
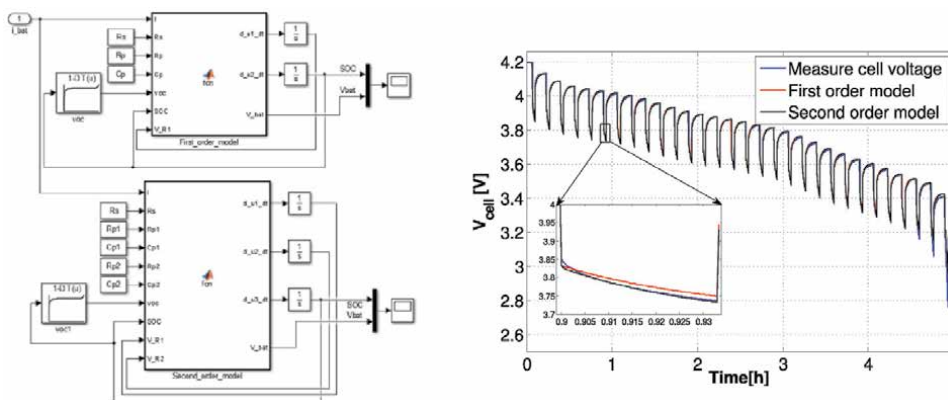

Figure 4.
The Matlab/Simulink cell models (left) and the comparative analysis (right).
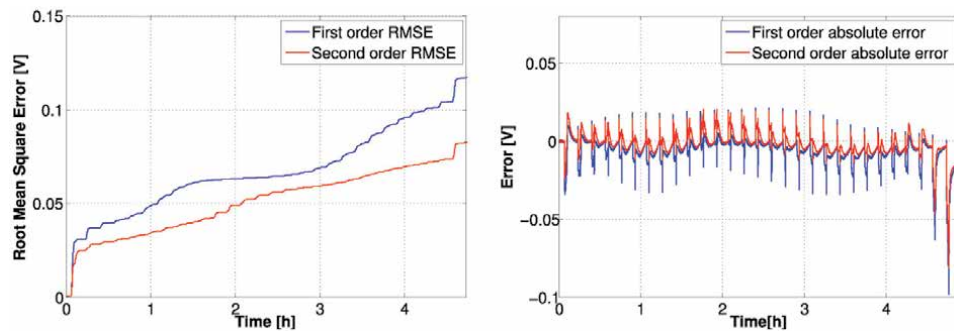

Figure 5.
The RMSE (left) and the instantaneous error (right) of the battery models.

shows that during the ongoing discharging process, the RMSE for the first order model increases gradually faster than the one of the second order one.

To conclude this section, one can understand that increasing the rank of the battery model, the gap between real and simulated results is mitigated. The cost of this is the increased complexity of models, time-consuming parameters identification and the necessity of more data post processing operations. On the contrary, the first order model is quite simple to design, its parameters are simple to identify with classical calculations and there is no need for values post processing. If the compromise of accepting a small error in the battery model with the gain of simplicity, the first order model is the hands-on solution.

2.2 Multilevel modeling of power electronics' losses

The general approach when dealing simulation approaches of electronic converters regard conventional ideal ones, with or without switching, so called smooth or switched models. However, none of these consider the losses that occur in a non-ideal converter. The largest losses are due to the switching components (power transistors and/or diodes), while the rest of the losses inside a converter can be neglected (those on the driver and measuring circuits). One reason why the losses are generally neglected overall is because their actual measurement is rather difficult and requires dedicated equipment. In doing so, one simple method is to consider a general efficiency of the converter and add it into its calculations. So, already some straightforward solutions for modeling electronic converters were mentioned, solutions that are available in nearly any reference the reader would search. To add value to the research and to the present chapter, the authors introduce 2 different approaches to compute the losses that occur on one MOSFET transistor. Of course, these can be then extrapolated towards the total number of power switches.

In **Figure 6**-bottom the EMR pictogram used for any electronic converter is presented. It inputs the DC link voltage (V_{dc}), the load currents (i_load) and the duty cycle (m_s). After the internal calculations, the converter outputs the resulting voltage (u) to be supplied to the load and its output currents (i_conv). The inputs and outputs do not change with the chosen method of internal calculations. Either is
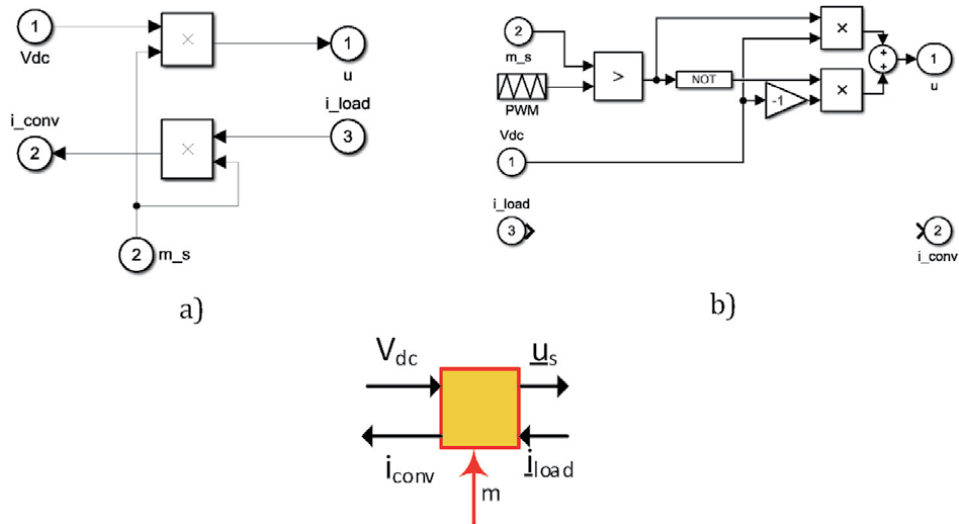

Figure 6.
Smooth (a) and switched (b) converter architectures and their EMR pictogram (c).

a smooth or switched model, these remain the same and valid even if we consider DC or AC converters.

In addition to the above depicted models, this block can include also the calculus for the converter losses. Even if in the standard pictogram there are no input/output ports considered for this, the information, being additional, can be manipulated to/from the block via wireless labels.

Taking into consideration of these losses is mandatory when one is interested in reaching optimal converter architectures [9, 10]. The following calculus can be adapted to any power transistor, the authors using the IRFP4668PBF MOSFET, having its specifications listed in **Table 1**.

The losses computed in any active switching electronic component can be broken down into: conduction losses, switching losses and blocking (leakage) losses, the later normally being neglected, as expressed in Eq. (4).

$$P_{lossT} = P_{condctionT} + P_{switchingT} \tag{4}$$

As mentioned before, two approaches will be presented in detail. The first one computes the power losses during conduction and switching the MOSFET while the second one computes losses during switch-on and switch-off transients.

In the first approach, the conduction and switching losses are computed based on Eqs. (5) and (6), with regards to the semiconductor's parameters and its operation. The latter is described via the duty cycle (D), the switching frequency (f_{sw}) and the transistor's output capacitance (C_{oss})

Parameter	Symbol	Value	Unit
Forward voltage	V	120	V
Drain to source resistance	Rds	0.008	Ω
Switching Frequency	fsw	10000	Hz
Output Capacitance	Coss	810e-12	F
Turn off time	Toff	64e-9	s
Turn on time	Ton	41e-9	s
Forward voltage drop	Vf	1.3	V
Reverse Leakage current	Ir	0.00025	A
Reverse Recovery Time	Trr	135e-9	**s**
Max Recovery Current	Irrm	8.7	A
Gate Resistance	Rg	11	Ω
Plateau Voltage	Uplateau	6.1	V
Gate Capacitance	CGD1	200e-12	F
Gate Capacitance	CGD2	1200e-12	F
Reverse recovery charge	Qrr	700e-9	C
Rise Time	tr	105e-9	s
Fall time	tf	74e-9	s
Reverse Recovery Current	IDoff	8.7	A
Average diode current	IFav	20	A
Diode on-state zero-current voltage	ud0	0.5	V

Table 1.
The main specifications for IRFP4668PbF MOSFET.

$$P_{conductionT} = I_d{}^2 R_{ds} D \tag{5}$$

$$P_{switchingT} = \frac{VI_d}{2}\left(T_{on} + T_{off}\right)f_{sw} + C_{oss}V^2 f_{sw} \tag{6}$$

On the other hand, the losses occurring in the diode attached to the transistor are broken down into conduction, reverse and switching ones. The total losses due to the diode's operation are:

$$P_{lossD} = P_{condctionD} + P_{reverseD} + P_{switchingD} \tag{7}$$

Each of the eq.'s (7) components are formulated in expressions (8)–(10), with parameters valued and explained in **Table 1**:

$$P_{condction} = I_f V_f D \tag{8}$$

$$P_{reverse} = I_r V(1 - D) \tag{9}$$

$$P_{switching} = \frac{T_{rr} I_{rrm} V_r f_{sw}}{2} \tag{10}$$

This model is quite simple and represents the hands-on solution for quantifying the converter losses without engaging too many mathematical tools.

The more complex model, the conduction losses are computed function of the on-state resistance (R_{ds}) and the current passing through the component (i_d):

$$P_{cond} = R_{ds}{}^2 i_d \tag{11}$$

The next component of the total losses, the switching one, is broken down into two states, according to the on and off transients. There are different opinions and mathematical interpretations on how to compute the voltage fall-time (tfu) to gain accuracy. Details are presented in Ref. [10]. Engaging a straight forward approach, the fall-time is considered to be composed of two parts in accordance with the variation of the gate capacitance:

$$tfu = \frac{tfu1 + tfu2}{2}$$

$$tfu1 = (U_{DD} - R_{DS}I_d)R_G \frac{C_{GD1}}{U_{drv} - U_{plateau}} \tag{12}$$

$$tfu2 = (U_{DD} - R_{DS}I_d)R_G \frac{C_{GD2}}{U_{drv} - U_{plateau}}$$

In Eq. (12), the terms (U_{drv}) and (U_{DD}) refer to the driver voltage that excites the transistor's gate and the converter's DC link voltage, respectively. The rest of the terms are to be found in **Table 1**.

The complementary model to compute the switch-off losses differ just by subtracting from Eq. (12) the driver voltage.

$$tru = \frac{tru1 + tru2}{2}$$

$$tru1 = (U_{DD} - R_{DS}I_d)R_G \frac{C_{GD1}}{U_{plateau}} \tag{13}$$

$$tru2 = (U_{DD} - R_{DS}I_d)R_G \frac{C_{GD2}}{U_{plateau}}$$

The required energy to turn on and off the transistor is calculated in Eq. (14) and (15).

$$E_{onT} = U_{DD}I_{Don}\frac{tru + tfu}{2} + Q_{rr}U_{DD} \tag{14}$$

$$E_{offT} = U_{DD}I_{Doff}\frac{tru + tf}{2} \tag{15}$$

With the above computed ingredients, one can calculate the power losses on the transistor, Eq. (16), and diode, Eq. (17).

$$P_{swT} = \left(E_{onT} + E_{offT}\right)f_{sw} \tag{16}$$

$$P_{swD} = \left(E_{onD} + E_{offD}\right)f_{sw} \approx E_{onD}f_{sw} \tag{17}$$

The losses in the MOSFET and the free-wheeling diode are computed as the sum of the conduction and switching losses.

$$P_{TotalT} = P_{conductionT} + P_{switchingT}$$

$$P_{TotalT} = R_{DSon}I^2_{Drms} + \left(E_{onM} + E_{offM}\right)f_{sw} \tag{18}$$

$$P_{TotalD} = P_{ConductionD} + P_{switchingD}$$

$$P_{TotalD} = u_{D0}I_{Fav} + R_DI^2_{Frms} + E_{onD}f_{sw} \tag{19}$$

It has to be mentioned that during operation, in one transistor or diode, the currents can be positive or negative. In an analytical approach, this would lead to decreased losses, hence, to correctly calculate those, the absolute current's value is used.

Comparing the results of the two approaches (**Figure 7**) one can conclude that the complex model reaches higher calculated values. This is more realistic as it contains more loss sources compared to the simple model. However, the simple model proves to offer a quite good quantification of the losses despite its ease in approach, reaching satisfactory results.
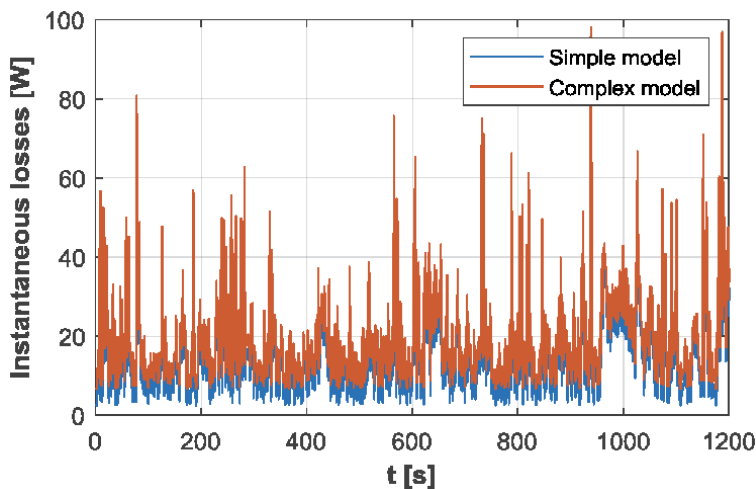

Figure 7.
The instantaneous converter losses for the simple and complex models.

2.3 Multilevel modeling of permanent magnet synchronous machines

The general approach when modeling a permanent magnet synchronous machine (PMSM) is to use its mathematical representation in dq0 reference frame, fixed to the rotor.

$$v_{sd} - R_s i_{sd} - e_{sd} = \frac{d}{dt}\psi_{ds}$$

$$v_{sq} - R_s i_{sq} - e_{sq} = \frac{d}{dt}\psi_{qs} \tag{20}$$

$$T_{pmsm} = \frac{3}{2}p\left(\Psi_{ds}i_{qs} - \Psi_{qs}i_{ds}\right)$$

$$e_{sd} = -\omega\Psi_{qs}, e_{sq} = \omega\Psi_{ds}$$

$$\Psi_{ds} = \Psi_{md} + L_d I_{ds} + L_{dq}I_{sq}$$

$$\Psi_{qs} = \Psi_{mqd} + L_q I_{qs} + L_{qd}I_{ds} \tag{21}$$

$$J\frac{d\Omega}{dt} = T_{pmsm} - T_{load} - B\Omega \tag{22}$$

The variables in Eqs. (20) and (21) are: the phase resistance (R_s), the direct and quadrature inductances (L_d and L_q) and the cross-coupling inductances (L_{dq} and L_{qd}). The number of pole pairs is denoted with (p), while the rotational speed is marked by (ω) and the friction coefficient in marked by (B). The dq currents (I_{ds} and I_{qs}) are computed by integration of the voltage expressions.

For a PMSM, the EMR model is constructed by coupling 3 pictograms, one accumulation element (for the windings) described by Eq. (20), one electrome-chanical conversion (for the torque generation), described by Eq. (21) and another accumulation element (for the mechanical equilibrium), described by Eq. (22), (visit **Table 1** for clarifications). Such a model is depicted in **Figure 8**.

Returning to Eq. (21), the dq magnetic flux equations give the opportunity to choose the level of modeling complexity. In this section, 3 different such levels will be detailed: based on constant dq inductances, based on variable dq inductances and a flux-linkage based model. The latter is the most complex and precise one.

To have a comprehensive analysis, like for the battery and the power inverter, for the PMSM the model's parameters are listed in **Table 2**.

The first level of complexity consists in using constant values for the d and q axes inductances. The identification of these is a very simple process. It can be carried out in finite element analysis (FEA) or on the real machine (or in both environments). It requires only fixing the rotor in 0 and 90 electrical degrees positions and applying in both one controlled voltage pulse. The time dependent slope of the current will return after some simple calculations the global machine inductance (L). Having this value, the d and q components are easy to be computed,
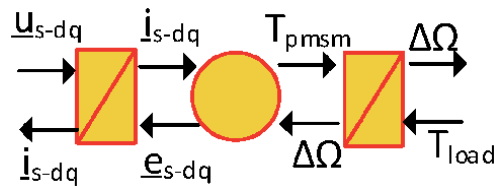

Figure 8.
The EMR for a PMSM.

Electric and geometric parameters			
	Dimension	Value	Unit
1	Pole pairs	3	—
2	Rotor speed	2000	[rot/min]
3	Rated torque	12	[Nm]
4	Rated current per phase	21	[A]
5	Mechanical power	2500	[W]
6	DC Voltage link	120	[V]

Table 2.
The PMSM under analysis.

using Eq. (23). Details about the identification process can be selected from references [11, 12].

$$L_d = \frac{2}{3} L \quad (\theta_{el} = 0°), L_q = \frac{2}{3} L \quad (\theta_{el} = 90°) \tag{23}$$

The second level model regards detailed information about the machine under testing. The latter needs to be simulated in a FEA environment in order to compute the dq inductance's variations function of the machine current. This is generally ranged from $\pm 10 \times$ In, where In is the machine's rated current. The method itself that allows preliminary identification of the 3-phase magnetic fluxes is the so called "frozen permeability" approach. Applying it demands to set to 0 the permanent magnet's remanent flux density, freezing its permeability. More details about this method are to be found in Ref.s [12, 13]. The resulted phase magnetic fluxes will be used to compute the dq inductances versus the machine current, applying Eq. (24).

$$\Psi_d = \frac{2}{3} \left(\Psi_a - \frac{1}{2} \Psi_b - \frac{1}{2} \Psi_c \right), \Psi_q = \frac{1}{\sqrt{3}} (\Psi_b - \Psi_c).$$

$$L_d = \frac{\Psi_d}{i_d}, L_{qd} = \frac{\Psi_q}{i_d}, L_q = \frac{\Psi_q}{i_q}, L_{dq} = \frac{\Psi_d}{i_q} \tag{24}$$

The outcome of these calculations is stored in look up tables (LUT) and introduced in the machine model. It is clear that such a procedure is impossible to be implemented in a real testbench or it would require complex and expensive hardware. One can observe that using the calculus from Eq. (23), the direct as well as the cross-coupling inductances are computed. Their variation function of the ranged current is depicted in **Figure 9**.

The last and altogether the most complex model is based on using instead of inductances, the variation of the d and q currents function of the d and q magnetic fluxes. These are 2D LUTs as depicted in **Figure 10**.

It is important to mention that building the 2D LUTs from **Figure 10** is a quite complex and challenging process. Here to the designer needs to have the FEA model of the machine under study. Several simulations need to be accomplished, fetching initially the Ψ_d (i_d, i_q) and Ψ_q (i_d, i_q). From this information mathematical inversion methods need to be applied to get $i_d(\Psi_d, \Psi_q)$ and $i_q(\Psi_d, \Psi_q)$. The complete process is explained in detail in [14].

In **Figure 11** a simple comparative analysis of the results obtained when simulating all the 3 models for the same conditions are depicted. Focusing the attention on the variation of the q axis magnetic flux, it can be noticed that flux linkage and
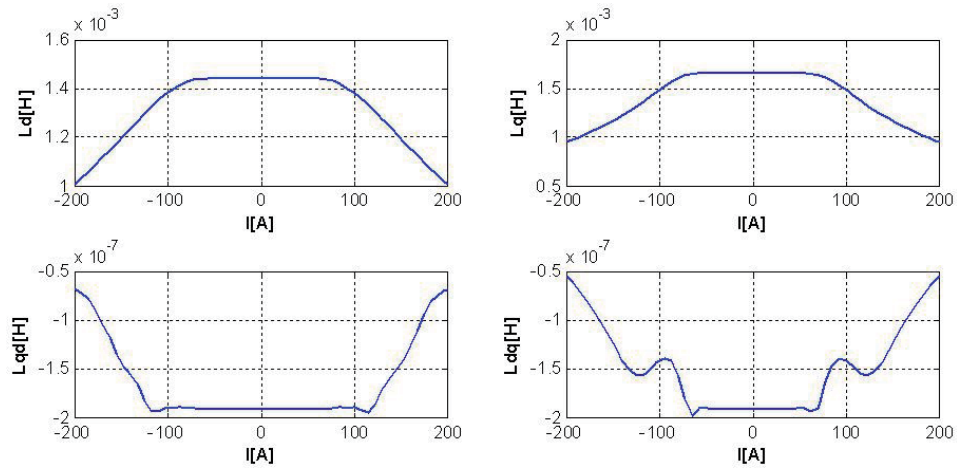
Figure 9.
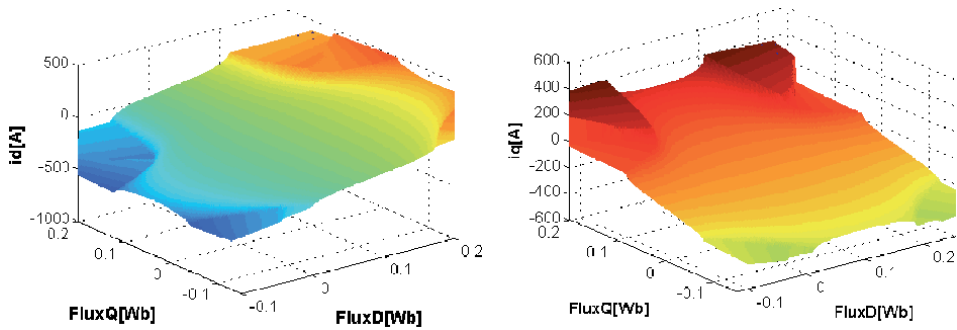*The direct and cross-coupling inductances calculated with frozen permeabilities.*

Figure 10.
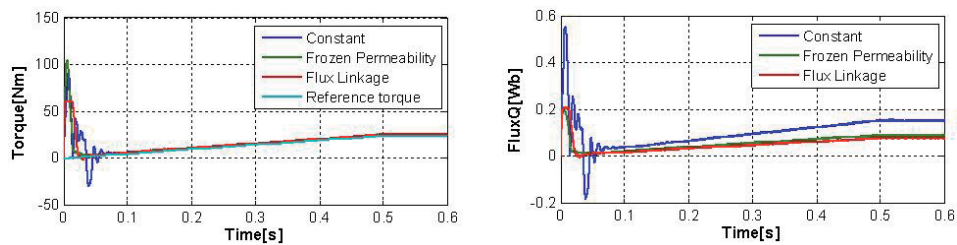*The 2D LUTs of $i_d(\Psi_d, \Psi_q)$ and $i_q(\Psi_d, \Psi_q)$.*

Figure 11.
The PMSM torque and Ψ_q during benchmarking the simulation levels.

frozen permeability models do saturate, while the one based on constant inductances reaches large values. The latter is ideal; hence the machine will never saturate. In this condition, one can perform simulations within rated operation. However, when attempting to go in overload region the results will not reflect the real machine operation.

The flux linkage and frozen permeabilities models are behaving quite in the same manner. However, the complexity of the flux linkage model is high, both in data post processing and design. The ultimate conclusion is that using the frozen

permeabilities model will lead to quite satisfactory results reflecting closely the actual machine behavior.

2.4 Designing the control loop

Energetic Macroscopic Representation is one organization concept that besides helping the designer to build simulation programs that reflect the actual power flow of a real testbench, it also proves to be a very lucrative solution when it comes to building control loops. To do so, one has just to inverse the simulation model and keep only the action path, discarding the reaction one.

In **Figure 12** the control loop can be observed being highlighted in light blue. Its inversed character compared to the model (in orange) is noticeable and each block contains the mathematical description of the inversed action.

The reversed accumulation block contains a regulator that outputs the reference torque to be developed function of the error between the actual and the imposed speed (see Eq. (25)).

$$\xi_{nPMSM} = n_{PMSM\_ref} - n_{PMSM}$$

$$\xi_{nPMSM} \rightarrow PI\left(k_{p\_n}, k_{i\_n}\right) \rightarrow T_{PMSM} \tag{25}$$

The inversed block without controller computes the reference q axis current function of the refence torque above expressed. In the same time, the d axis current is imposed to 0, this for torque maximization purposes.

$$i_{sq\_ref} = \frac{T_{PMSM}}{\frac{3}{2}p\left[\Psi_{PM} + \left(L_d - L_q\right)i_{sd}\right]}$$

$$i_{sd\_ref} = 0 \tag{26}$$

This reference d and q currents are compared with the actual ones. The resulting errors are sent to regulators that output the reference d and q voltages. This process is carried out in the third control block (see **Figure 12** from right to left).
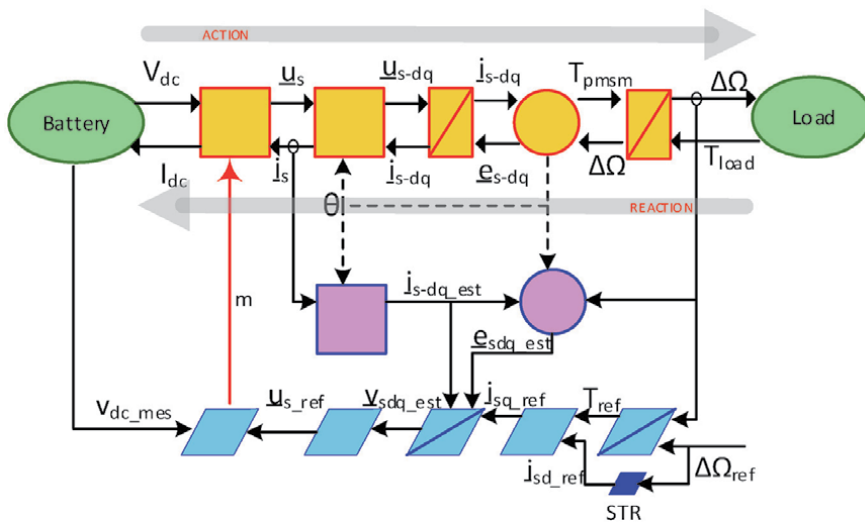

Figure 12.
The complete PMSM simulation model in EMR organization.

$$\xi_{iqd} = i_{sqd\_ref} - i_{sqd}$$

$$\xi_{iqd} \rightarrow PI\big(k_{p\_i}, k_{i\_i}\big) \rightarrow u_{sqd}$$

$$u_{sqd\_est} = u_{sqd} + e_{sqd\_est} \qquad (27)$$

The resulted d and q voltage refences are converter to 3-phase quantities and sent to the last control block, that computes the duty-cycle (m) for each phase. The duty-cycle is sent to the PWM generator (in orange) closing the model's loop. More details about generating the process model are indicated in Ref. [15].

3. Real-time model analysis

To develop an analysis tool able to replicate as close as possible the behavior of a real electric urban vehicle, it is clear that using complex simulation developments for the electrical assemblies will not be enough. However, building the mechanical models using advanced mathematical tools is highly time consuming and would require a lot of expertise and education in this direction. Hence, a wise solution is to engage a software created for such simulations, like Simcenter Amesim from Siemens.

In order to highlight the previously mentioned application with a practical example, an urban vehicle's mechanical model is developed. The vehicle is an electrical tricycle used for cargo delivery purposes. Its main specifications are presented in **Table 3**.

In **Figure 13**, the Amesim model is depicted, observing that none electrical assemblies are included in the model. Those are modeled in Matlab/Simulink as it will be presented in the following sections. The link between the two models will be performed using National Instruments VeriStand software, able to create an integrated project that runs a co-simulation on a real-time processor for the complete vehicle.

The Matlab/Simulink model for the electrical assemblies is built putting together all the components detailed in Section 2 based on the hierarchy depicted in **Figure 12**. It has to be mentioned that the pictograms cannot be exactly replicated in Simulink as the inputs are on the left and the outputs always on the right. However, the organization is the same as it can be observed in **Figure 14**.

Having all the models above presented, the goal is to create a virtual simulation platform that allows simple transition hardware in the loop (HiL) testing. The latter

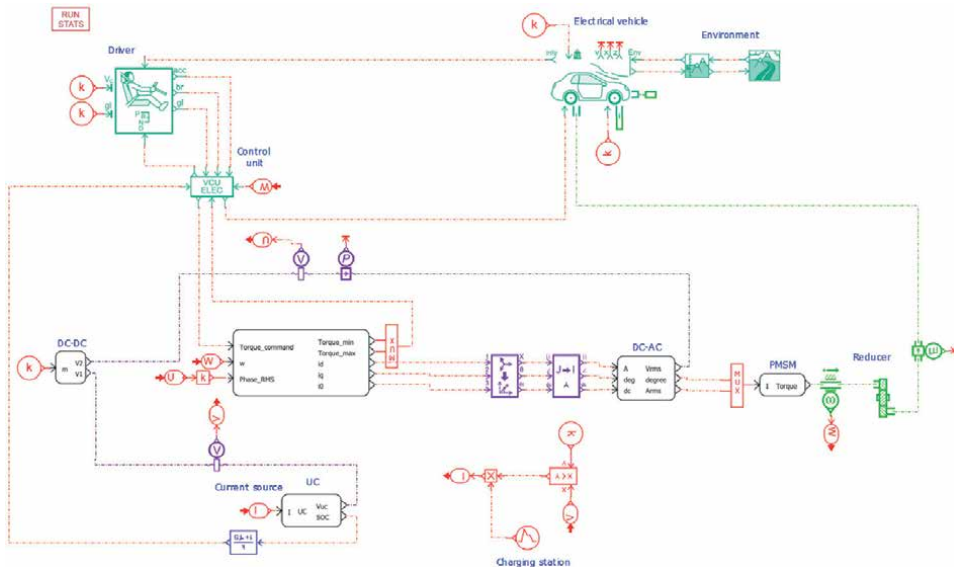| Parameter	Symbol	Value
Maximum mass	m	250 kg
Maximum speed	v	10 m/s
Wheel radius	Rw	12″
Maximum road slope	α	15%
Rolling resistance	f	0.017
Front area	A	1.2 m2
Air drag coefficient	Cs	0.36
Gear ratio	Gr	5

Table 3.
Tricycle specifications.

Figure 13.
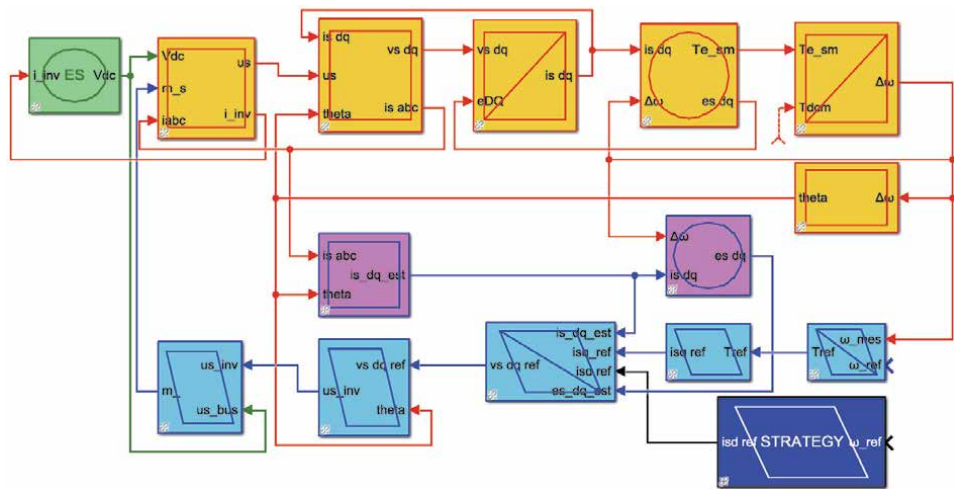*The mechanical assemblies' Amesim model.*

Figure 14.
The urban vehicle's EMR in Matlab/Simulink.

is the ultimate goal of testing any electromechanical system. It allows users to test certain physical assemblies while the rest of the system is virtual, running as simulation on a real-time target. This must ensure enough computation power and speed to cope with the demands of the actual hardware. National Instruments have in their portfolio hardware (NI PXIe embedded controller) and software (NI VeriStand) that are able to integrate into one real-time simulation all the above detailed models. The PXI computer, via its onboard field programable gate array (FPGA) enables the connection of the virtual model with the testbench using analog and digital IOs.

In **Figure 15**, the main components of the analysis platform are depicted. One can observe that VeriStand software that integrates the Amesim and Simulink models runs on the PXI and using the FPGA channels communicates with the actual
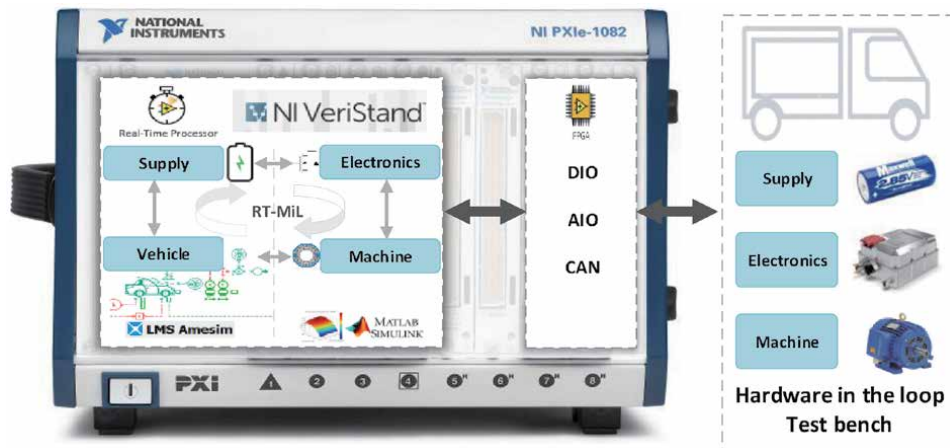
Figure 15.
The platform's hardware/software architecture.

hardware. The user has the possibility to run the virtual model and in parallel the actual hardware in a bidirectional communication network, performing as an entire entity. The real-time processor also features the possibility to run only the simulation of the entire vehicle, without any hardware connected to it. The difference between such a simulation and one running on a PC is that the latter would take tens of hours for a road cycle of 30 minutes while on the real-time computer it will take the elapsed 30 minutes.

Both scenarios will be presented in detail in the following section, comparing the results and discussing them.

4. System validation via urban scenario

Taking advantage of the flexibility of the above presented analysis platform one can perform a study using only simulation, hence a virtual vehicle or can combine virtual elements (mechanical assemblies) with real ones (the propulsion motor). For a robust simulation model, it is important to ensure that using it as reference will return results that mimic closely the actual hardware. In doing so, the platform depicted in **Figure 15** was initially tested only for simulation, the complete system being entirely virtual and running on the PXIe under VeriStand software. The latter ensured the continuous communication of the Simulink model (running all electrical assemblies) with Amesim (running all mechanical systems).

It has to be mentioned that the chosen simulation used the most complex model assemblies from those presented in Section 2. In order to avoid redundancy, results for the rest of the levels are not presented in the chapter, however during the presentations in Section 2, the main differences between the models were already presented.

The second step was to keep in the virtual level the mechanical assemblies (in Amesim) and the battery model (in Simulink). The rest of the virtual electrical assemblies (the inverter, the motor and the controller) were replaced with their laboratory homologs. These remained however connected to the simulator via the analog/digital IOs presented earlier.

The outcome of this comparative analysis was more than satisfactory. Firstly, the reference torque was plotted versus the simulated and the measured ones. It can be observed that the agreement is very good proving the accuracy of the simulator.
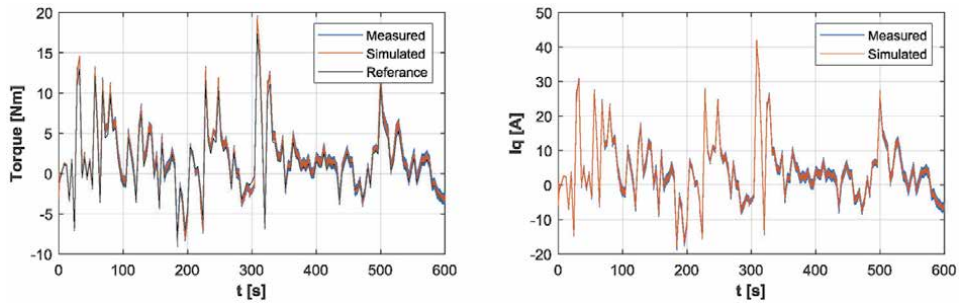
Figure 16.
The comparative analysis of the torque (right) and q current component (left).
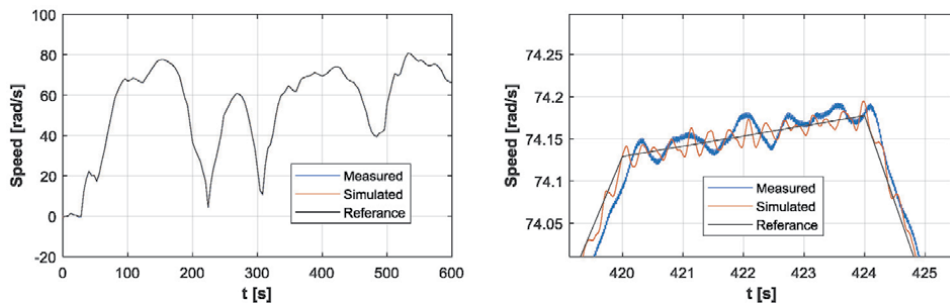

Figure 17.
The comparative analysis of the speed (right) and its zoomed section (left).

Knowing that in a PMSM the q current component is responsible for the torque production, for both measured and simulated cases this was recorded and depicted in **Figure 16**-right. The same conclusions as for the comparative analysis of the torque characteristics can be considered. In order to avoid redundancy, the d currents were not depicted as those values are forced to 0 at all times.

The slight differences between the values plotted in **Figure 16** are more due to measurements error and noise. No filtering was used what's so ever in order to avoid any unnecessary postprocessing (**Figure 17**).

The slight differences between the values plotted in **Figure 16** are more due to measurements error and noise. No filtering was used what's so ever in order to avoid any possible influence over the quality results.

Smoother results can be reached if certain data sampling time or other such procedure is considered. However, the interest in this entire work was to prove that one can reach very accurate results when building responsible simulation programs. Also using a real-time processor can benefit the study with fast analysis and reliable results as well.

5. Conclusions

When it comes to develop simulation tools wise enough to reach the expectations of the fast-growing industry in the field of engineering, one needs to consider solutions that become hands-on. These must be flexible to changes, simple to implement and accurate when it comes to results. Using real-time processors to run these simulations offers reduced analysis time, accurate results and close to real

study. The same processors when engaged, ease the transition from simulation to HiL testing, simply by replacing virtual components with real ones. Choosing between the complexity levels of the virtual models, allows the user to select the accuracy and the necessary time invested in the development. The system under analysis being compound of several assemblies, more complex models can be considered for those that are of interest, while the rest can be ideal ones.

In the present chapter the main assemblies of an electrical urban vehicle's traction system are presented, offering the choice of complexity, mathematical description and EMR organization. The latter is introduced as graphical method for representing the elements of any simulation program by respecting the actual action/reaction physical and natural laws.

It has to be mentioned that the nature of the present chapter is more towards a review than of an academic lecture, hence the reader is encouraged to consult the indicated references that are guidance and complementary information to the one described in the previous pages.

Acknowledgements

Author details

Raul Octavian Nemeş, Mircea Ruba*, Sorina Maria Ciornei and Raluca Maria Raia
Technical University of Cluj Napoca, Romania

*Address all correspondence to: mircea.ruba@emd.utcluj.ro

IntechOpen

References

[1] A. Bouscayrol, R. Schoenfeld, G. Dauphin-Tanguy, G.-H. Geitner, X. Guillaud, A. Pennamen, and J. Hautier, "Different Energetic Descriptions for Electromechanical Systems," in Proc. of the European Conference on Power Electronics and Applications (EPE), Sep. 2005, Dresden, Germany.

[2] K. Chen, A. Bouscayrol, and W. Lhomme, "Energetic macroscopic representation and inversion-based control: Application to an electric vehicle with an electrical differential," Journal of Asian Electric Vehicles, vol. 6, no. 1, pp. 1097–1102, Jun. 2008.

[3] A. Bouscayrol, X. Guillaud, P. Delarue, and B. Lemaire-Semail, "Energetic macroscopic representation and inversion-based control illustrated on a wind-energyconversion system using hardware-in-the-loop simulation," IEEE Transactions on Industrial Electronics, vol. 56, no. 12, pp. 4826–4835, Dec. 2009.

[4] Nemes, R.O., Maria Ciornei, S., Ruba, M., Martis, C., "Parameters Identification Using Experimental Measurements for Equivalent Circuit Lithium-Ion Cell Models", 11th International Symposium on Advanced Topics in Electrical Engineering, ATEE 2019; Bucharest; Romania; 28 March 2019 through 30 March 2019; DOI: 10.1109/ATEE.2019.8724878

[5] Ruba, M., Ciornei, S., Nemeş, R., Martis, C.,"Detailed Design of Second Order Model of Lithium-Ion Battery Simulator Based on Experimental Measurements", 11th International Symposium on Advanced Topics in Electrical Engineering, ATEE 2019; Bucharest; Romania; 28 March 2019 through 30 March 2019; DOI: 10.1109/ATEE.2019.8724878

[6] A. Nikolian, Firouz, Y. Gopalakrishnan, R. Timmermans, J. M. Timmermans, N. Omar, P. van den Bossche, J. van Mierlo, "Lithium ion batteriesDevelopment of advanced electrical equivalent circuit models for nickel manganese cobalt lithium-ion,", Energies 2016.

[7] X. Zhang, J. Lu, S. Yuan, J. Yang, X. Zhou, "A novel method for identification of lithium-ion battery equivalent circuit model parameters considering electrochemical properties," J. Power Sources 2017.

[8] M. Mathew, Q. H. Kong, J. McGrory, M. Fowler, Simulation of lithium ion battery replacement in a battery pack for application in electric vehicles, J. Power Sources 2017.

[9] D. Graovac and M. Pürschel, "MOSFET power losses calculation using the data- sheet Parameters," 2006. https://www.infineon.com.

[10] S. Shuvo, E. Hossain, T. Islam, A. Akib, S. Padmanaban and M. Z. R. Khan, "Design and hardware implementation considerations of modified multilevel cascaded H-bridge inverter for photovoltaic system," in IEEE Access, vol. 7, pp. 16504-16524, 2019, doi: 10.1109/ACCESS.2019.2894757.

[11] D. E. Pinto, A. C. Pop, J. Kempkes, J. Gyselinck, "dq0-modeling of interior permanent-magnet synchronous Machines for High-Fidelity Model Order Reduction, Optim & Intl Aegean Conference on Electrical Machines and Power Electronics, May, 2017.

[12] D. Zarko, D. Ban, R. Klaric, "Finite element approach to calculation of parameters of an interior permanent magnet motor", Automatika 46, 2005

[13] J. Wu, J. Wang, C. Gan, Q. Sun and W. Kong, "Efficiency optimization of

PMSM drives using field-circuit coupled FEM for EV/HEV applications," in IEEE Access, vol. 6, pp. 15192-15201, 2018, doi: 10.1109/ACCESS.2018.2813987.

[14] S. M. Ciornei, M. Ruba, R. O. Nemeş and C. Marţiş, "Multi-level models for a light electric vehicle propulsion system using EMR organisation," 2020 International Symposium on Power Electronics, Electrical Drives, Automation and Motion (SPEEDAM), 2020, pp. 357-362, doi: 10.1109/SPEEDAM48782.2020.9161855.

[15] M. Ruba, R. O. Nemes, S. M. Ciornei, C. Martis, A. Bouscayrol and H. Hedesiu, "Digital twin real-time FPGA implementation for light electric vehicle propulsion system using EMR organization," 2019 IEEE Vehicle Power and Propulsion Conference (VPPC), 2019, pp. 1-6, doi: 10.1109/VPPC46532.2019.8952428.

Edited by Marian Găiceanu

Modern transportation systems have adverse effects on the climate, emitting greenhouse gases and polluting the air. As such, new modes of non-polluting transportation, including electric vehicles and plug-in hybrids, are a major focus of current research and development. This book explores the future of transportation. It is divided into four sections: "Electric Vehicles Infrastructures," "Architectures of the Electric Vehicles," "Technologies of the Electric Vehicles," and "Propulsion Systems." The chapter authors share their research experience regarding the main barriers in electric vehicle implementation, their thoughts on electric vehicle modelling and control, and network communication challenges.

IntechOpen